Computational Fluid Dynamic Modeling of In-duct UV Air Sterilisation Systems.

Azael Jesus Cortes Capetillo

Submitted in accordance with the requirements for the degree of Doctor of Philosophy.

The University of Leeds
School of Civil Engineering

January, 2015

The candidate confirms that the work submitted is his own, except where work which has formed part of jointly authored publications has been included. The contribution of the candidate and the other authors to this work has been explicitly indicated below. The candidate confirms that appropriate credit has been given within the thesis where reference has been made to the work of others.

Three papers have been published. In all cases these are jointly authored with the supervisors. The candidate carried out the work and prepared the manuscripts for all three publications, with supervisors providing guidance and editorial input.

CAPETILLO, A., NOAKES, C. & SLEIGH, P. A. 2013. CFD Analysis to Assess Performance Variability of In-Duct UV-C Systems. ASHRAE IAQ conference 2013: Environmental Health in Low Energy Buildings, Vancouver, British Columbia, Canada, October 15-18. This paper contains part of the work in Chapter 5.

CAPETILLO, A., NOAKES, C. & SLEIGH, P. A. 2014. CFD Analysis to Assess Performance Variability of In-Duct UV-C Systems. HVAC&R Research, accepted for publication.Invited paper following the ASHRAE IAQ conference and is an extended version of the above conference paper. The paper contains part of the work in Chapter 5 and some elements from Chapter 3 and Chapter 4.

CAPETILLO, A., NOAKES, C. & SLEIGH, P. A. 2014. In-Duct UVGI air sterilisation: Optimisation study for high performance energy efficient systems. Indoor Air 2014. Hong Kong, July 7-12th. This paper contains part of the work in Chapter 6.

Acknowledgements

Agradecimientos

En primer lugar me gustaría agradecer a mi familia en especial a mi madre Mireya Capetillo que ha sido un apoyo constante a través de todos mis esfuerzos, y el modelo a seguir más importante en mi vida. Para mi abuelo, que ha sido un motivador constante y el mejor consejo en cada situación. Para mi tía Nina, que siempre me ha apoyado como una segunda madre. A mi amigo Javier González, que siempre me empuja a lograr metas más altas. A mis supervisores Cath Noakes and Andrew Sleigh que sobre el paso del programa se convirtieron más en amigos que en tutores, siempre tuvieron tiempo para mí y me dieron la confianza para hacer cualquier pregunta, sin importa lo simple que fueran, y me guiaron en la mejor dirección. Para Conacyt que patrocinó mis estudios y en más de una ocasión intervino para ayudarme a alcanzar mis metas. Por último, me gustaría agradecer a mi ahora esposa Alejandra Villarreal Treviño, quien es parte de mi vida y vivió parte de este viaje conmigo.

Abstract

In-duct UVC air sterilisation is a technology that can help in the reduction and control of airborne diseases. Nevertheless, improvements in sterilisation performance efficiency are required for the technology to succeed in an increasingly restricted energy society.

Computational fluid Dynamics (CFD) was used to systematically improve the performance of in-duct UVC air sterilisation systems. The Discrete Ordinates method (DO) was used to model lamp irradiation, and a user defined function (UDF) to model the injection of microorganisms inside the duct to then calculate the average UV dose of the system, with this it was possible to reproduce test results published by EPA. After the CFD model was validated, operation parameters such as wall reflectivity, lamp location, lamp position, air velocity and airflow patterns were analysed.

It was found that accurate information of UVC susceptibility for microorganisms in air was essential for the correct modeling of UVC air sterilisation systems using CFD, and current available data contain considerable variations that needed to be analysed and interpreted in an appropriate manner. It was also found that the DO method was appropriate to model lamp irradiation and could account for reflectivity, and that CFD was robust enough to reproduce lab tests results. Moreover it was found that airflow patterns, and lamp location and position influenced the sterilisation performance of a UVC system.

Results include a comprehensive list of microorganisms UVC susceptibilities in air (Chapter 3); a set of CFD models that can be used for validation or calibration for future studies and a confirmation that CFD is capable to model in-duct UVC air sterilisation systems (Chapter 5). Ultimately this research presents a series of conclusions that will help on the design of more efficient in-duct UVC air sterilisation systems.

Table of contents.

List of figures.

List of tables.

Chapter 1. Introduction

1.1 Background.

Pathogen and chemical air contamination is one of the top 5 health risks in the world according to the World Health Organization (WHO, 2005). Air pollution related risks range from indoor discomfort and mild health problems up to severe health risk and in serious cases death. Respiratory diseases are thought to be responsible for around 10% of all deaths worldwide (WHO, 2005), with infectious diseases such as tuberculosis a major contributor.

Clean indoor air is imperative in the modern civilization. New homes and offices often function with their own artificial environment, reducing fresh air intake and increasing recycled indoor air, modifying the chemical and biological environment inside buildings. People in industrialised nations spend more than 90% of the time indoors (Brown et al., 1996); Mendell et al. (2002) states that health problems related to the air quality in enclosed environments could be considered equivalent to health problems generated by ingestion of decayed food. Gustavsson (2000) puts this idea in perspective when stating that if an average person consumes around 1 kg of solid food, 3 kg of liquid food and breaths around 20 – 30 kg a day, we should expect our air to have a similar quality standard as our food and drink. Although this comparison might be somewhat extreme, it is a statement on the general underestimation of the importance of air quality in our lives.

Air quality is not the only concern; the current environmental situation has led the building industry to look for sustainable solutions and energy savings in every aspect possible. In the UK, the Climate Change Act 2008 established by the UK Government (2008) requires the nation to cut carbon emissions between 20% and 34% by 2020 and by 80% by 2050 in relation to a 1990 base line (HM Government, 2011).

Buildings account for around 40% of energy use in most countries (IEA, 2010). Mechanically ventilated building utilise fans, heating and cooling systems and air filters to keep indoor air quality to the required standards.

Particle air filters are responsible of up to 30% of the energy consumption in an air handling unit (Camfil Farr, 2011). It is crucial for air filtration and cleaning technologies to not only be effective, but also energy efficient. Some researchers consider ventilation as the responsible of up to 50% of problems related with indoor air quality, with microorganisms in the ventilation system being the most recurrent difficulty (Gustavsson, 2000). Documented evidence of bacteria, fungi and

protozoa in air-conditioning cooling coils, drip pans (Menzies et al., 1999), and air cooling units (Bernstein et al., 1983) suggests that microbial air contamination plays a part in indoor related illnesses (Menzies et al., 2003).

1.2 Air contaminants.

Breathable air is generally conceived to be composed by 78% Nitrogen, 21% Oxygen, 1% Argon and 0.04% Carbon dioxide; deviations from this composition are considered to be contaminated air (W.M. Haynes, 2011). Dangerous deviations include the reduction of oxygen under 12% and/or the increase of Carbon dioxide over 5%; both can cause loss of consciousness and/or asphyxia (ASHRAE, 2009a).

Air contaminants can be widely divided into two categories; (1) Particles, including aerosol, airborne particles and particulate contaminants and (2) Gases, referring to pure substances or mixtures that naturally exist in gaseous state during normal atmospheric conditions. Both having specific and well defined characteristics (ASHRAE, 2009a).

1.2.1 Particle contaminants.

Particle contaminants have a size be between 0.003 μm to 100 μm, and a greater mass and a lower diffusion rate than gases. A clean environment might contain up to 100 particles.cm^{-3}, while a polluted urban area can have up to millions particles.cm^{-3} (ASHRAE, 2009a). Particle contaminants can be divided mainly into three groups; (1) Dust, fumes and smoke, (2) Mist, fogs and smogs, and (3) Bioaerosol. Moreover, two subgroups can be included for further differentiation; A) Size and B) inhalable/breathable particle (ASHRAE, 2009a).

Dust, fumes and smoke: The particles are mostly solid, dust are smaller than 100 μm, fumes are the condensation of vapours of solid material and have a size between 1 μm – 2 μm, smokes can include ETS (environmental tobacco smoke) with an average size of 0.3 μm (ASHRAE, 2009a).

Mist, fogs and smogs; Are mostly suspended liquid particles.

Bioaerosol: includes virus, bacteria, fungal spores and animal allergens such as dust mite, cat dander, house dust and endotoxins with sizes ranging from 0.003 μm – 0.06 μm for some viruses, 0.4 μm – 5 μm for most bacteria, 2 μm – 10 μm for fungal and bacterial spores and up to 100μm for pollen (ASHRAE, 2009a).

The last two subgroups are a) Size, which is divided in; Coarse 1μm - 3μm, Fine 1 μm – 3 μm and Ultra fine 0.1 μm of less, and b) inhalable/respirable, including; inhalable particles 100 μm,

thoracic particle mass of 10 μm, respirable particles 4 μm and fine particles 2.5 μm (ASHRAE, 2009a).

1.2.2 Gaseous contaminants.

Gaseous contaminants are commonly found in three types; 1) Vapours, which can be solid or liquid under ambient conditions but evaporate quickly, 2) Gases, which are in gaseous state under ambient condition and 3) Chemical contaminants that exist as free molecules or atoms in air.

Gases are measured in parts per million (ppm), part per billion (ppb) or volumetric concentration $mg.cm^{-3}$ (ASHRAE, 2009a).The harmful effect of gases include; a) Toxicity, which effect is proportional to the exposure dose, b) Physical irritation, which does not carry continuous health effects, c) Undesirable odours, and d) Damage to materials such as corrosion or discoloration (ASHRAE, 2009a)Another harmful effect that could be included is asphyxiation, that happens when a gaseous contaminant displaces oxygen from the environment (ASHRAE, 2009a).

Gaseous contaminants can be organic and inorganic. An organic contaminant with a boiling point ranging between 48 - 249 °C is known as VOCs (Volatile Organic Compounds) (Brinkle et al., 1998). The sources of VOCs can be solvents, degreasers, furniture, walls, carpets, cleaning and maintenance products and some electric equipment.

It is known that the VOC concentration in home and buildings can be up to 2 – 5 times bigger than that of outdoor air (ASHRAE, 2009a). Inorganic gases includes Carbon dioxide (CO_2), Carbon monoxide (CO), Oxides of nitrogen (NO_X) of which Nitroxyl (NO) and Nitrogen dioxide (NO_2) are of main concern, Sulphur dioxide (SO_2), Ozone (O_3) and Ammonia (NH_3) (ASHRAE, 2009a). Gaseous contaminants are usually dealt with gas-phase filtration, using technology such as activated carbon.

1.3 Airborne transmission of infections.

Infections can spread easily through closed environments such as the home, schools, workplaces, transport systems, etc. Although many of the respiratory and gastrointestinal infections can be relatively mild (like coughs, colds or mild diarrhoea), they still represent a significant economic burden. Infections are caused by bacteria, viruses and other microscopic microorganisms, which can be found in the environment, and can be transmitted in a variety of ways. This includes through air, by direct or indirect contact of infected hosts, through soiled objects, through contact with skin or mucous membranes, body secretions, sexual contact,

contaminated water or food (Barker et al., 2001). In the hospital environment, there is growing awareness of the role of hand hygiene, surface decontamination and improved air quality standards for the control of infections (Barker et al., 2001).

It is estimated that infants suffer from about five to eight colds per year, while an adult can suffer between two to five colds per year associated with influenza viruses, rhinoviruses, corona viruses and respiratory syncytial viruses (RSVs) (Barker et al., 2001). Cold viruses can appear to be trivial; nevertheless, they can hold a considerable economic impact if it is considered the number of days lost from work and/or school, hospital admissions and the associated cost of treating the disease.

1.3.1 The airborne infectious route.

Only certain respiratory pathogens, known to be mainly transmitted by droplet nuclei containing microorganisms such as *Streptococcus pyogenes*, *Neisseria meningitidis*, *Corynebacterium diphtheriae*, *Mycobacterium tuberculosis* are fully accepted to be airborne transmitted (Schaal, 1991). The medical profession refers to airborne infection as the infections transmitted by particles transported by convective air currents, leaving close droplet transmission as a type of contact-spread instead of airborne-spread. This is based on the differences between the larger droplets that after expelled fall rapidly to the floor and the droplet nuclei that can remain in the air (Beggs, 2003). Nevertheless, many Gram-positive bacteria such as *Staphylococcus aureus*, and endospores of clostridia and bacilli, remain viable and infective in dry dust and have the possibility of infecting patients (Schaal, 1991).

Airborne infections can be divided into two groups: 1) Long-range airborne infection, happens when infected droplets are sufficiently small to remain airborne almost indefinitely allowing them to travel long distances (Tang et al., 2006); 2) Short-range airborne infections depend on the proximity of the infected source and susceptible host. Droplet size can be defined as large droplet having a diameter bigger than 60 μm, small droplet with diameters diameter equal or smaller than 60 μm and droplet nuclei with a diameter smaller than 10 μm (Tang et al., 2006). While small droplets can travel as clouds through the air, large droplets will drop to the floor.

 Cross infection from an infected person to a new host depends on a number of factors, including the number of virus particles shed by the infected person, their stability in the environment, in aerosols or on surfaces and the potential for spread within a closed environment (Barker et al., 2001). Respiratory secretions can become aerosolised after coughing, sneezing or spitting of the infected host, small respiratory droplets, smaller than 3μm evaporate instantly and remain in the air as their tendency to settle is almost negligible (Riley et al., 1976). These aerosolised

particles can then be inhaled by another uninfected host, or in some cases settle onto surfaces such as towels, doorknobs, food utensils etc. And continue the spread of infections. This route of infections has been implicated on the transmission of tuberculosis, measles, influenza and small pox (Riley, 1974). Diarrhoea increases the elimination of infectious microorganisms from the gut, and at the same time increases the potential for contamination of the environment. The more particles shed the greater the infectious microorganism survival and the greater the chance of reaching a new host (Barker et al., 2001). Vomiting can produce infectious aerosols; during a viral infection of SRSV (small round structured viruses), It is estimated that up to $3x10^7$ aerosolised particles are released into the environment during a vomiting attack, which then can be inhaled or deposit over surfaces, increasing the risk of spread of the infection (Caul, 1994). Skin shedding can also be a source of airborne contamination; Staphylococcus spp. can remain airborne for long periods of time after being aerosolised from skin shedding (Beggs, 2003).

1.3.2 Modern disease outbreaks.

Recent disease outbreaks including SARS, Bird Flu and Influenza A H1N1, are all associated with transmission through a droplet or airborne route (Weinstein et al., 2003, Yu et al., 2004). An example of the devastating social and economic effects of such a disease outbreak could be seen in Mexico during the epidemic season of the Influenza A H1N1. In the period from May 2009 to June 2009, health insurance companies paid on average £ 8,000 per person infected with the virus (Universal, 2009), and more than 4,900 persons were diagnosed with the Influenza A H1N1 virus (WHO, 2009a). Moreover, the epidemic alert forced closure of public and private areas for several days, stopping many productive activities.

Viruses are not the only reported problems, medical services worldwide are concerned by Health Care Associated Infections (HCAI), such as Methicillin-Resistant *Staphylococcus Aureus* (MRSA) and *Clostridium difficile* (*C. diff*) (NHS, 2008). In the UK it is believed that around 9% of patients acquire infections while being in a hospital (National Audit Office, 2004).

In the case of a patient being infected with MRSA, estimates suggest that he will spend 10 extra days in hospital, while a patient with *C. Diff* the number increases to up to 21 extra days; bringing an increased costs of £4,000 to £10,000 per patient (Department of Health, 2008). However, the most worrying aspect of MRSA is its mortality rate; figures suggest that about 15% of the reported cases result in death (Private Healthcare UK, 2005). Although the method of transmission of MRSA and *C. diff* is mainly by direct contact, there is evidence implicating airborne transmission. Rutala et al. (1983) ran a 10 week study in a Burn unit which had suffered an MRSA outbreak. The study aimed at defining the environmental epidemiology of the

pathogen, for this purpose, airborne and surface levels of contaminations were measured using volumetric air samples and Rodac plates. It was found that MRSA comprised between 16% to 40% of all bacteria growth from air samples. Moreover it was concluded that there was a chance for personal to be contaminated via the inanimate environment in the burn-unit. Kumari et al. (1998) related an outbreak of MRSA infections in an orthopaedic ward to the ventilation grilles of the University hospital in Leeds. In total six patients contracted the infection, two of the patients had been in direct contact, nevertheless the other four remained in different bays of the same ward. At the same time it was found that the ventilation grilles supplying the bays where the infected patients had been were harbouring MRSA and working at intermittent cycles. Research suggests that airborne contribution is likely to be greater than it is currently recognised (Beggs, 2003).

Another problematic infection is Tuberculosis (TB), a major concern in the world (Beggs et al., 2000, NTC, 2007, WHO, 2007). If untreated, a person with TB disease will infect between 10 – 15 persons in average (WHO, 2007). In 2009 9.27 million cases of TB were estimated globally, with Asia and Africa having about 55% and 31% respectively of the total cases in the world, and during the same year a total of £ 1.5 billion was allocated for the control of TB infections spread in 94 countries (WHO, 2009b).

The proof of the airborne infectiousness of TB is as peculiar as decisive, and included the use of a special TB ward, guinea pigs and a carefully controlled ventilation system. The original study dates back to Riley et al. (1957), and was later revised and extended in detail in (Riley, 1961). The details of the study ran as follows. The veterans' hospital in Baltimore with a special ward reserved for TB patients was studied to identify the probability of airborne transmission. The ventilation of a ward containing six single rooms that hosted patients with the disease was carefully controlled. Above the ward, in the "penthouse", was a chamber with guinea pigs. The air coming from the TB ward was directly discharged over the guinea pigs chamber. The guinea pigs thus served as biological samplers for TB. Each guinea pig was tuberculin tested every month, and over a period of four years 134 guinea pigs contracted tuberculosis. In many instances it was even possible to track the source of the TB colony within the infected guinea pig to a specific patient in the ward, thus leaving no doubts about the airborne transmission of the TB disease (Riley, 1974, Riley, 1961, Riley et al., 1957), this very same study was repeated in 2009 by Escombe et al. (2009), but with the inclusion of an UV air sterilisation system which helped to prevent up to 70% of TB infections .

1.3.3 Sick Building Syndrome.

Poor indoor air quality has also been linked with problems such as building related illnesses and the sick building syndrome.

Sick Building Syndrome (SBS) relates to acute health problems and/or discomfort experienced by building occupants in relation to the time spent in a building (Redlich et al., 1997), indoor air contamination can cause a building to get sick (Skov et al., 1990). SBS refers to the existence of persistent, non-specific symptoms (e.g., eye, nose, and throat irritation; fatigue; headaches) that occur in more than 25% of a building's occupants and that disappears once these inhabitants leave the building (Brown et al., 1996). In contrast, Building Related Illness (BRI) refers to clinically diagnosed disease(s) in building occupants that occur from exposure to indoor pollutants (Kowalski, 2009b). BRI cases are well documented and have a defined diagnostic criteria, recognizable causes, and treatments. In most of the cases individuals who suffer from a BRI require prolonged recovery times after leaving the suspected environment (Brown et al., 1996). BRI tend to have greater repercussions than SBI cases.

Records show that indoor air contamination has had social and financial impacts in the world. For example, in the United States alone, the EPA calculates that indoor air quality causes damages costing tens of billions of dollars each year (EPA, 1997). Airborne germs and fungi growing in ventilation systems can generate Sick Building conditions within indoor environments (Teeuw et al., 1994, Cooley et al., 1998). In fact, air quality and pollution in the environment have been directly related with Sick Building Symptoms (Table 1-1). Wargocki et al. (2000) highlighted the importance of the air quality on the effects of SBS. It is highly important to keep the air clean to reduce SBS effects as it has been found by numerous researchers (Finnegan et al., 1984, Wargocki et al., 1999, Cooley et al., 1998, Rostron, 1997).

Table 1-1 Illnesses known or suspected to be related to buildings from Menzies (1997).

Disease	Indoor source	Agent of exposure
Infectious Legionnaires disease and Pontiac fever	Cooling tower, air conditioning or humidifier, potable water	*Legionella pneumophillia*
Flu like illness and common cold	Human source	Respiratory virus
Tuberculosis	Human source	*Mycobacterium tuberculosis*
Hypersensitivity pneumonitis and humidifier fever	Humidifier	Multiple bacteria and fungus
Asthma	Surface dust, carpet, clothing	Dust mites, plant products, animal allergens, fungus

Epidemiological investigations have associated exposure to large concentration of airborne pathogens, a environment representative of SBS, with hypersensitivity diseases such as asthma (Pastuszka et al., 1999). For example hay fever has been linked with indoor concentration of *Cladosporium* fungi and Yeast and the concentration of *Aspergillus* has been found to be related with respiratory symptoms and/or asthma complaints in school age children (Li and Kuo, 1992). Even in the most hygiene sensitive environments, such as hospital rooms, it is possible to find microbial and fungal contamination (Curtisa et al., 2005). Kima and Kim (2006a) analysed the air quality in hospital environments founding that *Staphylococcus spp.*, *Micrococcus spp.*, *Corynebacterium spp.*, and *Bacillus spp.* were the dominant microorganisms and amounted over 95% of the total airborne bacteria. They also found that indoor air concentrations of *Staphylococcus spp.*, *Streptococcus spp.*, and *E. coli*, were higher than outdoors, implying indoor sources as the cause of increase (Kima and Kim, 2006b).

Approximately 50% of Sick Building Syndrome and Building Related Illness complaints can be attributed to microbiological agents (Brown et al., 1996). An improvement in air quality standards is estimated to bring between $ 5 to $ 75 billion annually in the USA alone (Mendell et al., 2002).

An option for enabling this increase in air quality standards, or say it in a different manner, reduce microbial contamination, is the use of Ultraviolet (UVC) sterilisation systems, which are easy to install and operate (Menzies et al., 2003).

1.4 Clean air supply.

Air filtration is the most commonly used approach to control the indoor air quality and remove contaminants from the environment. When first used, the main function of air filters was to keep heating, ventilation and air conditioning equipment free of deposited particles which diminished airflow rates and affected heat transfer (Fisk et al., 2002). Nowadays the use of air

filters has become mandatory for mechanically ventilated buildings, and with the pass of time, their main purpose has broadened the scope of application towards air quality for health benefits (Fisk et al., 2002).
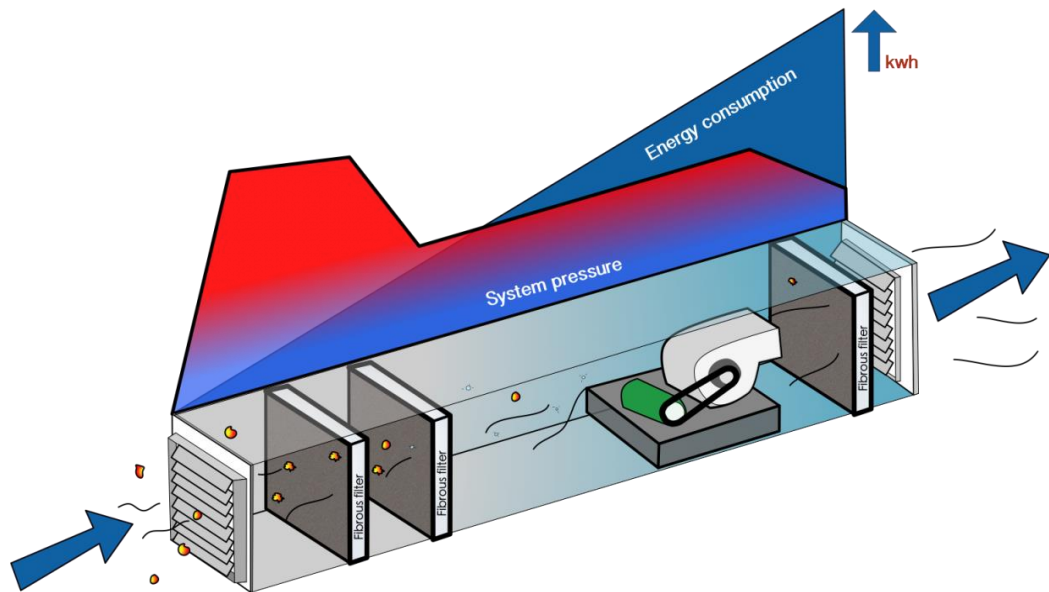
Figure 1.1 Fibrous filtration and energy consumption schematic.

Common in-duct air filtration relies on porous materials obstructing the air stream to trap contaminants as the air passes through; this slows down the air flow, increasing the in-duct pressure (Figure 1.1). The smaller the particles, the thicker the filter required, and the higher the air obstruction in the duct. Therefore bigger fans and higher amounts of energy are required to push the air through. Among the smallest particles that filters need to deal with are microorganisms and viruses (Figure 1.2). The development of technology that allows a more efficient control of the smallest contaminants (microorganisms and viruses) while reducing the energy consumption of the filtration process could bring energy savings in buildings.

Particle size μm

Viruses Bacteria Spores Pigments Aerosols Pollen

Blast furnace dust Refractory dusts

Zinc oxide dust Machining dust

Visible with electron microscope Visible with microscope Visible with human eye

Determinable by light scattering methods

Range of electrostatic precipitators Sieves

Range of membrane filters

Activated carbon Venturi scrubbers

Photochemical filter Cyclone separators

Range of wet scrubbers

Range of fabric dust collectors

ULPA and HEPA Paper and fabric filters

Figure 1.2 Contaminants and particle size vs filtration technologies. Adapted from Sutherland (2007b).

Depending on their size, particles can remain suspended in air for a given period of time. Larger contaminants such as human hair (100 μm to 150 μm) may settle quickly (five seconds approx.), viruses which are smaller than 0.1 μm can remain in the air for up to 10 days (ASHRAE, 2009a). Among small particles, viruses are the major problem, as they are very difficult to remove (Sutherland, 2007b). Typically around 90% (by weight) of airborne particles range from 0.1 μm to 10 μm in size.

The function of a particle filter is to remove contaminants from a fluid stream, either completely, or down to a specific size (Sutherland, 2007b). Air filters can be divided into three main categories (Sutherland, 2007b):

1) Ventilation systems filtration: Intended to deal with low concentration of contaminants in air and/or to remove contaminants to extremely low outlet concentrations. Mainly operating by depth filtration mechanisms, and are usually disposed when fully load.

2) Dust collection: Used for high inlet dust concentrations. They work through surface filtration, so they can be cleaned at frequent intervals, and remain in operation for long periods.

3) Demising: Deal with liquid droplets in a gas by a particular type of depth filtration, trapping the particles to then coalesce them.

Filtration operates entirely on particle or droplet size, providing a barrier where larger particles are retained and later removed (Sutherland, 2007b). Even though fibrous air filtration technology has continued its advance with the development of fine particle filters such as HEPA and ULPA, higher levels of filtration continue to present higher pressure drops, increasing the energy cost of the ventilation system (Fisk et al., 2002). Increasing filter efficiencies above ASHRAE Dust Spot 65% (MERV 11/F6/EU6) does not reduce significantly the contaminant concentration of dust-mite and cat allergens. For ETS (Environmental Tobacco Smoke) an ASHRAE Dust Spot efficiency of 85% (MERV 13/F7/EU7) could reduce the concentration in 61%, with further increases on filter efficiencies bringing only modest improvements i.e. up to 75% concentration reduction with a HEPA filter (MERV 16/H10/EU10) (Fisk et al., 2002). Viruses and bacteria rank even smaller in size, hence the same filtration efficiency could be expected.

1.4.1 UVC sterilisation.

Ultraviolet (UVC) air sterilisation is an alternative approach to dealing with biological and some chemical contaminants in air. UVC is a purification process and operates in a totally different manner to filtering. Particle size is not important but instead the process depends on the biological composition of the contaminant (microorganisms).The UVC light at 180 nm frequency generates ozone which can be used to oxidise VOCs and microorganisms. It is also known that UVC light at approximately 254 nm (Luckiesh, 1946) is capable of inactivating microorganisms by directly attacking their DNA, stopping their capacity to reproduce. Hence UVC light at this frequency is known as Ultraviolet Germicidal Irradiation UVGI (IUVA, 2005a). Special UV lamps designed to work at the germicidal frequency can be used to create a UV field, microorganisms passing through this field received a certain amount of UV dose, if this dose is sufficient to affect the DNA of the microorganism, it is inactivated. The effectiveness of the system depends on various factors including the interaction of the airflow, UV field and the microorganism susceptibility to UV light, Chapter 2 contains a detail explanation of the sterilisation mechanisms of UV light.

The sterilisation (disinfection) capacity of UVC light has been shown to be effective against airborne transmission of infection including the potential to reduce tuberculosis transmission risks by over 70% (Escombe et al., 2009). UVC sterilisation has proved to be capable of dealing with a range of contaminants in air, water and surfaces (Luckiesh et al., 1949, Bolton, 2000, Kowalski and Bahnfleth, 2000b, Fletcher et al., 2003). Notably, the water treatment industry has

had major acceptance of the UVC sterilisation technology, with disinfection systems being installed on waste water plants worldwide (Trojan, 2011), and recently used in domestic and commercial applications such as the treatment of swimming pool water (Leeds, 2010).

The main characteristics of UVC air sterilisation systems are their ability to clean the air from microorganisms (virus, bacteria and fungi), as opposed to fibrous filters that capture the microorganism within their fibres, allowing them to grow and in the worst case scenario turning the fibrous filter in to a source of infection. In contrast UVC air sterilisation destroys microorganisms by directly attacking their DNA rendering them unable to reproduce (Beggs, 2003). This technology has been mainly used by a small niche market primarily focused on clean rooms (e.g. hospitals). Moreover, if compared against fibrous filtration technologies (e.g. fine dust filters, HEPA, ULPA), photochemical filters are not capable of dealing with dust and other organic particles, however advances in the technology have shown that $UVC/TiO_2/O_3$ are capable of destroying VOCs (Volatile Organic Compounds) in the air stream e.g. phenol, formaldehyde and methane (Hodgson et al., 2008, Tompkins et al., 2005, Peral et al., 1997), thus widening the scope of application.

UVC air sterilisation technology has grown rapidly during the last decade, in part due to constant research and recent developments on its performance (Kowalski, 2009a, Beggs et al., 2003, Gilkeson and Noakes, 2013, Noakes et al., 2004), efficiency (Fletcher et al., 2004) and applications (Noakes et al., 2004, Escombe et al., 2009). Additional signs of this growth can be seen in the acceptance of major regulatory bodies of its use. Just in 2007, the ASHRAE HVAC Handbook stated that the use of UVC light for the control of viral infections had not proven reliable or effective enough to be recommended as a primary infection control measure (ASHRAE, 2007). However four years later, in 2011 ASHRAE included a full chapter (Chapter 60) on UV air and surface treatment, covering topics such as guidelines, standards, practices and energy use and economic considerations (ASHRAE, 2011).

1.5 Limitations of assessing in-duct UV systems.

The current state-of-the-art of the UVC sterilisation technology presents various limitations that have restricted the development of its full potential.

Although the mechanisms of UVC sterilisation are known, and research has shown that every microorganism has its very own susceptibility to UVC, considerable variations in the reported susceptibility of microorganisms make it difficult to establish values to carry out calculation of the performance of a UVC system. Moreover, current literature is limited to only a handful of

microorganisms that have been tested to identify their susceptibility to UVC irradiation in air. There are cases when there is only a small amount of data, not sufficient to conclude a reliable susceptibility value, or when multiple studies on the same microorganism do not correlate and a comprehensive evaluation is needed to create representative susceptibility curves.

The average UV dose of a system can be assessed by mathematical calculations (Bolton, 2001, Kowalski et al., 2001, Noakes et al., 2004). Nevertheless, these techniques do not account for particle trajectories, airflow patterns nor lamp position and/or the 3D UVC irradiation distribution. Moreover, the inclusion of reflections, refractions, absorption and shadowing can be extremely difficult and in some cases almost impossible to calculate. Such complexities in the operation of an in-duct UV sterilisation system generate variability in performance, which needs to be considered to ensure the right operation of an in-duct sterilisation system. Computational fluid dynamics CFD appears to be a good option to assess the performance of a UV system, and has been previously used for water (Ho, 2009a) and upper room sterilisation systems (Gilkeson and Noakes, 2013), yet it has had little application to in-duct systems. Nevertheless, the technique needs to be validated against reliable data to ensure its reliability and efficiency in the modelling of UVC sterilisation systems.

The performance of a UVC system can be measured in various ways, for example, the kill rate of a specific microorganism or by measuring the system average UV dose. However, without specific standards to express performance, the direct comparison between designs is difficult. This in turn, makes the selection of an UVC sterilisation system a rather troublesome process for both customer and designers; customers find it difficult to know what performance to ask for, and designers might have problems in what to design for. Therefore, for the improvement of designs of UVC sterilisation systems, it is necessary to have a common base line for direct comparison of performance between designs that standardises the use of units and operational parameters. More importantly there is a need for a specific rating value to measure and compare performance between designs. Such rating tool will help both designers and customers. Designers will be able to focus on the improvement of performance, while customers will be able to specify a required operation performance.

1.6 Aims and objectives

The aim of this research is to develop and validate a comprehensive and standard method to model in-duct UVC sterilisation systems with the use of computational fluid dynamics (CFD) techniques that can enable the design, improvement and future optimisation of in-duct UVC sterilisation systems.

The specific objectives of this research are to:

Objective 1.   Create a reliable set of microorganism susceptibility curves to UVC light in air.

Objective 2.   Establish an appropriate method for the modelling of UV fields for an in-duct UV system.

Objective 3.   Develop and validate a numerical CFD model capable of describing UVC irradiation, airflow patterns, wall reflections, particle trajectories and the UV dose received by microorganism injected into an in-duct UVC sterilisation system.

Objective 4.   Quantify the impact in performance of lamp position, multi-lamp configurations and airflow rates within an in-duct UVC sterilisation system.

Objective 5.   Identify the mechanisms that generate variability in the UV sterilisation performance of an in-duct system and quantify its impact.

Objective 6.   Develop a system performance rating that relates the UV dose of a system and operational airflow rates.

Objective 7.   Develop recommendations for the efficient design of in-duct UVC sterilisation systems.

1.7 Thesis overview.

Chapter 2 explains basic concepts of UV light, how the UVC sterilisation technology works, its important parameters, and operation.

Chapter 3 presents a study on microorganism UVC susceptibility and the current state of the research in this topic. The chapter highlights the variation in published results, and the limitation of information on microorganism UVC susceptibility in air. The chapter collates information from a wide range of published studies to develop a comprehensive table of UVC susceptibilities for microorganisms in air and introduces the use of a band-range susceptibility value.

Chapter 4 contains a detailed explanation of the mathematical model used for the calculation of UVC irradiation. Furthermore this chapter presents an analysis and a review of the various

models used in previous literature and explains the use of the Discrete Ordinates (DO) method to model lamp UVC irradiation.

Chapter 5 details the development of the Computational Fluid Dynamics (CFD) model used for the calculation of performance of UVC systems, and validates the model by reproducing the results of three experimental tests carried by the US Environmental Protection Agency (EPA) on UVC air sterilisation system. This chapter also considers the impact of reflectivity in the performance of a UVC air sterilisation system.

Chapter 6 presents a parametric study that explores the impact of lamp position, reflectivity and airflow patterns of an in-duct UVC air sterilisation system. Important results on the impact of turbulence, airflow patterns and microorganism susceptibilities are explained in this chapter.

Chapter 7 contains two studies. The first study explores the impact of lamp configuration on a multi-lamp set up and shows the impact of UV irradiation distribution on an in-duct system. The second study explores the impact of airflow rate on the performance of in-duct UV systems. This chapter introduces the concept of the performance constant R' for the rating of sterilisation performance and the calculation of performance of an in-duct system over a range of airflow rates. Also, this chapter sees the introduction of the performance efficiency rating (PER) for the rating of lamp position efficiency, and the use of the UV dose standard distribution for the rating of UV irradiation distribution.

Finally, Chapter 8 presents the conclusions of this thesis, summarising the findings of every chapter and the future work of the research.

Chapter 2. Air cleaning technology

2.1 Introduction.

UVC is becoming a mainstream air sterilisation technology, and is marketed in the form of energy saving and infection reduction devices. Understanding the basic concepts of the technology is imperative for its appropriate use and further design and development of new more efficient systems.

The performance of a UVC air sterilisation depends on airflow patterns, air velocity, lamp position among other parameters, therefore to quantify effectiveness and efficiency it is necessary to understand how these parameters relate to each other. This chapter provides further detail on the available methods for air cleaning and disinfection and their application, and outlines the principles of UVC air disinfection.

2.1.1 Particle filtration

Particle filters are rated according to their capacity to remove particles of a specific size from the airflow (Sutherland, 2007b). At least three different international classification exist (Table 2-1), the MERV classification using MERV 1 to MERV 20 (ASHRAE, 2003), the CEN classification using G1 to U17 from the Comite Europeen de Normalisation (CEN) and the Eurovent classification using EU1 to EU17 (Sutherland, 2007b). Based on rated performances a correlation between Eurovent/CEN and ASHRAE classifications can be made, nevertheless an official correlation table does not exist. Therefore, depending on the author the referred correlation can vary slightly, with variation being more common on high performance grade filters (e.g. HEPA/ULPA).

According to their performance particle air filters can be divided into at least three groups:

1) Coarse and fine dust (MERV 1 to 8 / G1 to F9 / EU1 to EU9),
2) HEPA (High Efficiency Particulate Air, MERV 9 to 14 / H10 to H14 / EU10 to EU14).
3) ULPA (Ultra Low Penetration Air, MERV 15 to 16 / U15 to U17 / EU15 to EU17).

Purchas and Sutherland (2002) argue that rather than classifying a filter in terms of its efficiency against a particle of a specific size, it would be more relevant to the user to know the efficiency of the most penetrating particle size (MPPS) which is the particle for which the filtration efficiency is the minimum (BSI EN 1822-1:2009). In practice, the performance of a filter will tend to be less than stated, this is due to the combined effect of the filter and the fluid flow bypassing

the filter through leaks and/or installation deficiencies, moreover the amount of particles penetrating through a filter depends on the operation parameters flow velocity, filter medium and particle size (Sutherland, 2007b). The following Table 2-1 of air particle filter classifications is an amalgamation of the various standards worldwide and their equivalent ratings made from information found in Purchas and Sutherland (2002), ASHRAE (2008b), Camfil Farr (2002) and Tronville (2006)

Table 2-1 Air particle filter classifications.

Type	MERV	*EN	*EU	Average efficiency in size range (%)			Arrestance %	Dust spot efficiency %	Minimum final resistance (Pa)	Particle size ranges	Typical air filter/cleaner type
				0.3-1.0 µm	1-3 µm	3-10 µm					
1	1	G1	EU1	-	-	E3 < 20	< 65	< 20	75	> 10.0 µm	Electrostatic Washable Throwaway
	2	G2	EU2	-	-	E3 < 20	65 - 70	< 20	75		
	3	G2	EU2	-	-	E3 < 20	70 - 75	< 20	75		
	4	G2	EU2	-	-	E3 < 20	75 - 80	< 20	75		
2	5	G3	EU3	-	-	20 ≤ E3 < 35	80 - 85	< 20	150	3.0 - 10.0 µm	Pleated filter Cartridge filter Throwaway
	6	G3	EU3	-	-	35 ≤ E3 < 50	85 - 90	< 20	150		
	7	G4	EU4	-	-	50 ≤ E3 < 70	> 90	25 - 30	150		
	8	G4	EU4	-	-	70 ≤ E3	> 90	30 - 35	150		
3	9	G4	EU4	-	E2 < 50	85 ≤ E3	> 90	40 - 45	150	1.0 - 3.0 µm	Bag filter Box filter
	10	F5	EU5	-	50 ≤ E2 < 65	85 ≤ E3	> 95	50 - 55	250		
	11	F6	EU6	-	65 ≤ E2 < 80	85 ≤ E3	> 95	60 - 65	250		
	12	F6	EU6	-	80 ≤ E2	90 ≤ E3	> 95	70 - 75	250		
4	13	F7	EU7	E1 < 75	90 ≤ E2	90 ≤ E3	> 98	80 - 90	350	0.3 - 1.0 µm	Bag filter Box filter
	14	F8	EU8	75 ≤ E1 ≤ 85	90 ≤ E2	90 ≤ E3	> 98	90 - 95	350		
	15	F9	EU9	85 ≤ E1 ≤ 95	90 ≤ E2	90 ≤ E3	-	> 95	350		
	16	H10	EU10	95 ≤ E1	95 ≤ E2	95 ≤ E3	-	-	350		
5	17	H13	EU13	-	-	-	-	-		≤ 0.3 µm	HEPA/ULPA
	18	H13	EU13	-	-	-	-	-			
	19	H14	EU14	-	-	-	-	-			
	20	H14	EU14	-	-	-	-	-			

2.1.2 Gas filtration

ASHRAE (2009b) provides a comprehensive review of the state-of-the-art of gas filtration techniques and technologies. The following is a summary of methods from "Chapter 29: Industrial Gas Cleaning and Air Pollution Control".

Odours and toxic gaseous contaminants are commonly removed by filtration technology different than that of particle filtration. Removal of gaseous contaminants is often achieved through absorption (into a liquid) or adsorption (onto a solid medium); in addition, incineration of the exhaust gas can also be employed for removing organic gases and vapours. Below are described a series of technologies and techniques for the removal or reduction of gaseous contaminants.

Spray dry scrubbing: This is used to absorb and neutralize acidic gaseous contaminants in hot gas streams. These systems make use of an alkali spray to react with the acid gases forming a salt. The process heat evaporates the liquid, creating dry particulates easily removable from the gas stream (ASHRAE, 2009b).

Wet-packed scrubbers: This is done by impingement of particulate matter and/or by absorption of soluble gas or vapour molecules on a liquid-wetted surface. During this process, the contaminant becomes a solute with a vapour pressure above that of the scrubbing liquid, which usually increases with a higher concentration of the solute in the liquid and/or with increasing liquid temperature. Scrubbing of the contaminant continues as long as the partial pressure of contaminant in the gas is above its vapour pressure with respect to the liquid (ASHRAE, 2009b).

Adsorption of gaseous contaminants: Freshly broken or heated solids are capable of physically or chemically adsorbing nearby molecules in a gas or liquid. The captured molecules form a thin surface layer on the solid, typically of one to three molecules thick. Commercial adsorbents can be solids with an enormous internal surface area, the large surface area makes possible the trapping and holding of a large numbers of molecules, e.g. a gram of a common activated carbon adsorbent might have an internal surface area of over 900 m^2. Adsorbents can be used for the removal of organic and water vapour, odours, and hazardous pollutants in an airstream. Activated carbon is a common adsorbent used in the HVAC industry; they can be derived from coal, wood, or coconut shells. The efficiency of a particular activated carbon to remove organic vapours from an airstream depends on the concentration and molecular weight of the organic compound and the temperature of the airstream (ASHRAE, 2009b).

Incineration of gases and vapours: Incineration is a process that can convert volatile organic compounds (VOCs), organic aerosols, and most odorous materials to carbon dioxide and water vapor using heat energy. Incineration is a proficient technology for the total elimination of VOCs. Thermal and catalytic are the types of incineration commonly used for air pollution control (ASHRAE, 2009b).

Thermal oxidizers: These are also known as afterburners or direct flame incinerators, consist of an insulated oxidation chamber where gas and/or oil burners are normally located. The contaminated airstream enters the chamber, getting in contact with the flame, thus gaining the heat energy necessary for oxidation (ASHRAE, 2009b).

Catalytic oxidizers: These generally consists of a preheat chamber followed by the catalyst bed, and operates under similar principles as thermal oxidizers, except for the use of a catalyst to promote oxidation. This technology allows oxidation at lower temperatures than thermal oxidation, thus less energy is required to preheat the contaminated airstream. Although residence time and turbulence are not as important as with thermal oxidizers, it is essential that the contaminated gas stream is heated uniformly to the required catalytic reaction temperature. A drawback of the technology includes catalyst poisoning or deactivation, caused by specific gas stream contaminants that chemically combine or alloy with the active catalyst material. Poisons frequently cited include phosphorus, bismuth, arsenic, antimony, lead, tin, and zinc (ASHRAE, 2009b).

Contaminant dilution: A different approach to filtration is by dilution. Cleaning a side stream and then mixing it back to the main flow at the correct ratio, the final contaminant composition can be made acceptable (Sutherland, 2007b).

Electrostatic precipitators: These are very effective at removing dust, smoke and other small particles. The basic principle of operation relies on electrically charging solid particles, and passing them between charged plates that work as electrodes. As particles pass, they move towards oppositely charged plates causing dust to agglomerate. Usually, the air is pre-filtered to trap large particles before it passes to an electrostatic precipitator (Sutherland, 2007a).

2.2 The UV light.

Ultraviolet (UV) light is a type of electromagnetic energy which is naturally emitted from the sun as part of the sunlight spectrum with a wavelength shorter than that of visible light. The UV light spectrum ranges from 100 to 400 nm. Within this spectrum there are three further

classifications of UV light; UVA (320 nm to 400 nm), UVB (280 nm to 320 nm) and UVC (100 nm to 280 nm) (Figure 2.1).
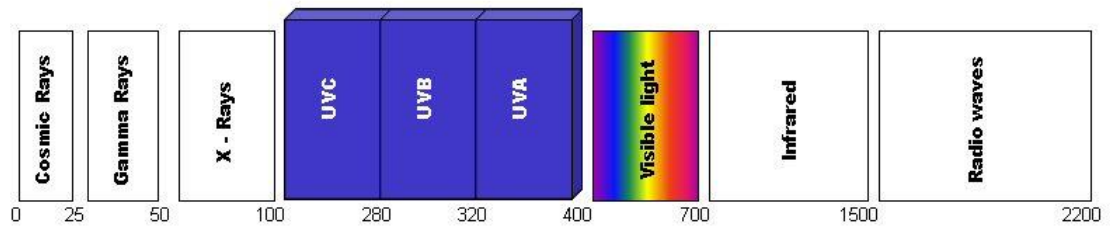
Figure 2.1 Light spectrum (wave length in nm).

UVC light has a peak germicidal effect at the approximately frequency range of 250 nm to 265 nm; this is reviewed in detail in chapter 3.1.2. It is thus that UV light at these wavelengths is referred as germicidal UV light (Luckiesh, 1946). Germicidal UV light is capable of directly damaging microorganisms DNA and thus stop their capacity of reproduction which, with sufficient irradiation, consequently renders the microorganism harmless (Beggs, 2003). As UVC light is harmful to microorganisms, it is also harmful to people, long exposures can create skin irritation and in some cases skin burning and if in direct contact with the eyes, UVC light can be a cause of photo conjunctivitis (Kowalski, 2009a), therefore, a careful design of UV air sterilisation system is required to prevent any dangers to the users.

2.2.1 UV lamps

Currently in the market there are various types of UVGI lamps. Most are discharge lamps which can be generally classified into two categories (IUVA, 2005e): 1) Medium pressure lamps, 2) Low pressure lamps. Medium pressure lamps work at broad spectrum of UV wavelengths, and are commonly referred as polychromatic. Low pressure lamps work exclusively in the of 254 nm and 180 nm wavelength commonly referred as germicidal lamps, moreover, at 180 nm wavelength, UV lamps have the capacity of generating ozone and are also known as germicidal (Figure 2.2) (Kowalski, 2009a).These categories are not exhaustive, other emerging technologies such as the microwave powered UV lamp (MPUVL) which can run for an indefinite amount of time as it has eliminated the need of electrodes (Gutierrez et al., 2006), and light emitting diodes (LED) working within UVC frequencies (Miller et al., 2013), are only just being introduced to the market and might open the possibility for new UVC system designs and applications.
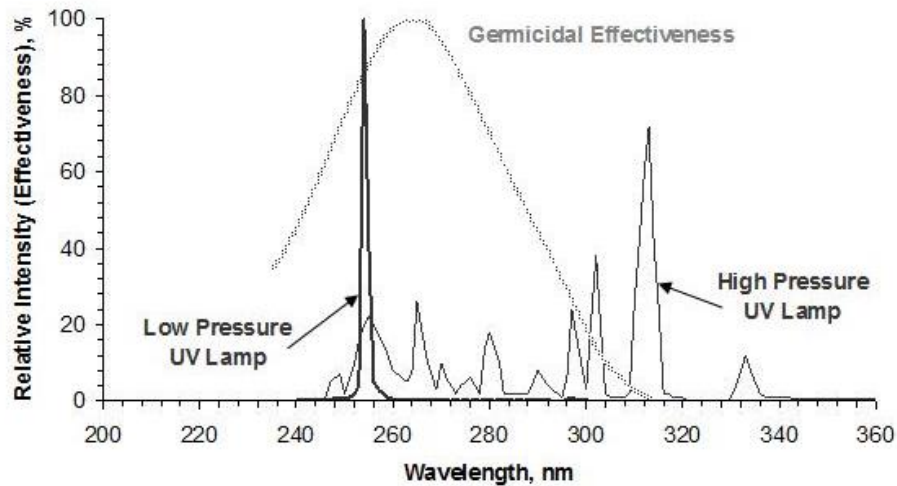
Figure 2.2 Medium Pressure and Low Pressure wave length spectrum (IUVA 2001).

Medium pressure lamps have a broad light spectrum in the ultraviolet and visible light range, much of their emitted radiation is at wavelengths outside the germicidal range (Gutierrez et al., 2006), spreading into the UVC/UVB wavelength (Kowalski, 2009b). Medium pressure lamps are inefficient in the production of UVC germicidal irradiation, and only 9% to 12% of its total power is converted into UVC light in the 250-280 nm wavelength (Gutierrez et al., 2006). In contrast, low-pressure UV lamps deliver a conversion of up to 40% from input Watts to UVGI Output Watts (IUVA, 2005e).

Low pressure lamps are highly efficient at generating UVC germicidal irradiation (IUVA, 2005e). They are essentially the same as fluorescent lamps emitting at 254nm and 185nm wavelength, the latter frequency used to generate ozone. Low pressure UV lamps offer high efficiency of up to 40 % of the electrical power turned into UVGI (IUVA, 2005e).

Low pressure - Amalgam lamps are called amalgam because they contain solid amalgam spots, an alloy of mercury with another element such as indium or gallium that controls the mercury vapour pressure (IUVA, 2005e). Amalgam lamps can be used at high ambient temperatures of up to 90∘c without affecting their performance (Hereaus Noblelight, 2007).

2.3 Basic concepts of UVC sterilisation.

It is important to know the basic concepts behind the UV sterilisation technology, and in this manner being able to differentiate terms such as fluence and dose, and UV irradiation and UV power.

Table 2-2 Terms and Definitions on UV irradiation.

Term	Symbol	Description	Definition	Units
Radiant Energy	Ev	Energy per unit time emitted by a radiant source.		J
Radiation power	Pv	Rate of radiant energy (Ev) per unit time emitted by a radiant source.	dEv/dt	W
Specific intensity	Iv	Rate of energy per unit area (dAcosθ) emitted over a solid angle (Ω).	$dEv.[dAcos\theta.dt.d\Omega]-1$	$W.m^{-2}.sr^{-1}$
Irradiance	qv	Total radiant power (Pv) incident from all directions over a surface area (dA)	$\int Pv\,dA$	$W.m^{-2}$
Fluence rate	Gv	Total radiant power (Pv) incindent from all directions over a sphere solid angle (dΩ)	$\int_{\Omega} Iv\,d\Omega$	$W.m^{-2}$
UV Dose (Fluence)	D	Fluence rate (Gv) over time (dT)	$Gv.dt$	$J.m^{-2}$

*Subscript v indicates germicidal frequency

The Radiant energy (Ev) is the watts per second emitted by a radiant source. When referring to UV power, it means Radiation power (Pv), which is the energy emitted by a power source simply stated as watts. The specific intensity (Iv) is the Radiation power emitted by a surface area (dA) about a solid angle (dΩ), therefore it is expressed as $W.m^{-2}.sr^{-1}$. Irradiance (qv) also referred sometimes as Radiative flux is the total Radiant power (Pv) from all direction received by a surface area (dA) and is expressed in $W.m^{-2}$, while the term Fluence rate (Gv) is the total Radiant power (Pv) from all directions received by the solid angle (dΩ) of a sphere and is also expressed in $W.m^{-2}$.

There are important fundamental aspect in the difference between Irradiance (qv) and Fluence rate (Gv). Irradiance (qv) is the Radiant power (Pv) received by a flat surface, meaning it works on a two dimensional domain, while Fluence rate (Gv) is the Radiant power (Pv) over a sphere, meaning it works on a three dimensional domain.

When using a collimated beam and UV is irradiated over a flat surface Irradiance (qv) and Fluence rate (Gv) become identical, as irradiation is coming from only one direction. Nevertheless, when UV is irradiated within an air duct from all directions, microorganisms receive UV irradiation from all directions, and in this case Fluence rate (Gv) is the appropriate term (Figure 2.3).
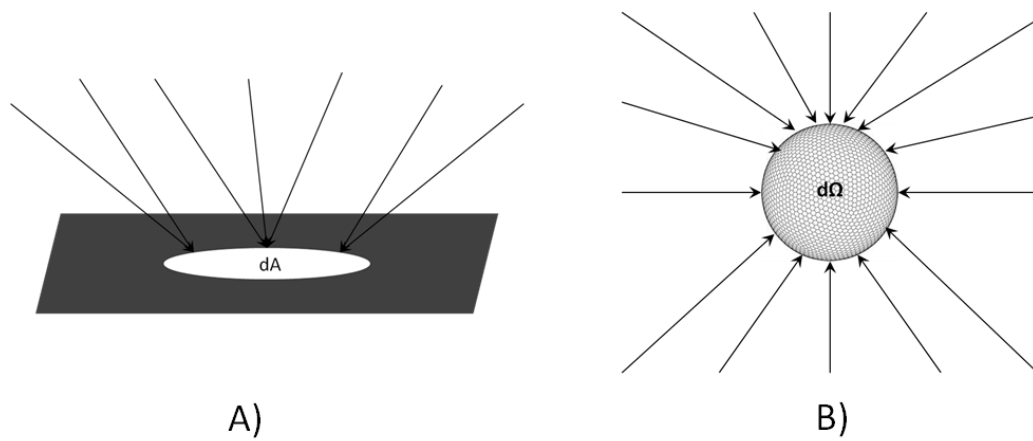
Figure 2.3 Difference between Irradiance (A) and Fluence rate (B).

The term UV Dose ($J.m^{-2}$) or Fluence, commonly used in quantifying UV sterilisation, refers to the Fluence rate (G_v) over a period of time (dt). In the most strict manner UV dose refers to total absorbed energy, while Fluence is the total energy received by a microorganism independently if it is absorbed or not (Bolton, 2001). However, the term UV dose is the most commonly used term for describing the technology.

2.4 UV sterilisation systems.

UVC air sterilisation systems aim to eliminate dangerous pathogens that compromise the health of room inhabitants. The technology relies on air carrying microorganisms and passing them through the field of UVC light. Therefore, pathogens on surfaces will not be affected by the UVC unless they are directly exposed to the light beam.

UVC air sterilisation refers to systems used to deal with indoor air, reducing indoor airborne levels of pathogens, toxins and particulates by the use of UVC irradiation (IUVA, 2005d). UVC air sterilisation systems can be classified into three main types, 1) In-duct systems, 2) upper-room irradiation systems and 3) recirculation stand-alone systems. Among the most popular in-duct system we find the designs for single pass or multi pass purposes (IUVA, 2005d) and the surface sterilisation for cooling coils (Shaughnessy et al., 1999). For the upper room irradiation, devices focus on irradiating UVC at the top areas of the room (Gilkeson and Noakes, 2013, Escombe et al., 2009, Xu et al., 2003, Beggs et al., 2005) and regarding recirculation stand-alone units we have the ceiling, wall and floor mounted units for the purpose of in-room sterilisation (Kowalski, 2003).

2.4.1 In-duct UVC sterilisation systems.

In-duct single pass or multi-pass UVC sterilisation systems.

These systems are designed to deal with the air within a mechanical ventilation system by the inclusion of UV lamps into the air stream (Figure 2.7). Most of the times these systems work on a single pass basis, and hence they are designed to provide high amounts of UV irradiation in a short period of time. Characteristically, these systems need to deal with high air velocities and low times of exposure (as explained in Chapter 5 and Chapter 6).

An in-duct system can be either of the retrofit or a stab-in type. Retrofitting systems consist of a UVC chamber containing one or more lamps replacing a portion of the original air duct, while the stab-in type consists of lamps inserted into the original air-duct (Figure 2.4).
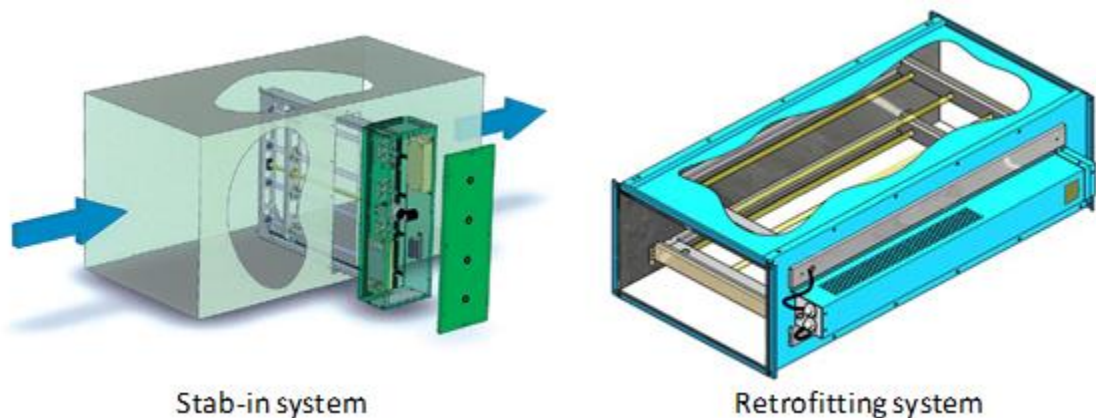
Figure 2.4 Stab-in system (left): AirGarde from GB environmental Ltd. And Retrofitting design (right) ASU 3000 from UVGI systems Ltd.

Cooling coil UVC sterilisation systems.

Cooling coil UVC sterilisation systems are mainly a surface sterilisation system where the lamp is mounted close to the cooling coil surface. As the installation is inside the air duct, it also provides air stream sterilisation, however as these systems are designed for surface sterilisation the operation parameters might not be the appropriate for in-duct air sterilisation. These systems are popular for providing reduced maintenance cost and energy savings on working cooling coils by irradiating them with UVC light in a permanent manner (Shaughnessy, Levetin et al. 1999), thus they can use relatively low UV wattage (Kowalski 2009).

UVC reduces the growth of microorganisms on HVAC coil surfaces, hence the coil pressure drop is reduced and the airflow is restored. To obtain these benefits the installation of UV germicidal lamps should be near the cooling coil, and spaced to allow an even distribution of the irradiation.

Fixtures must be designed to withstand moisture, and a wide range of temperatures. The ASHRAE guide also includes notes on safety, indicating maximum exposure times for different levels of irradiation, safety design guidance, training, and lamp breakage (ASHRAE, 2008a).

Cooling coil UVC sterilisation systems usually are installed before the cooling coil, an environment generally with high levels of relative humidity (RH) (over 70%) and high air temperatures (above 30c). High temperature benefits the performance of UV lamps, however, bacteria are generally more resistant to UV light at high RH (the effect of RH is discussed in Chapter 3). After the cooling coil, the conditions are even more challenging as cold air reduces the performance of UV lamps and levels of humidity still remain high most of times.

2.4.2 Upper room UVC sterilisation systems.

An upper room UVC system consists of UVC light being irradiated to the upper part of a room parallel to the ceiling (IUVA, 2005d). Upper room systems depend on the air passing through the UVC light beam, and the re-circulation of the air from the lower to the upper part of the room where the UVC field is in operation (ASHRAE, 2008a, Gilkeson and Noakes, 2013) (Figure 2.5). These systems have proved to be effective at reducing Tuberculosis infections (Escombe et al., 2009), many air pathogens including chickenpox, measles, mumps, varicella and cold viruses (Kowalski, 2009b) and even for reducing sick-day absenteeism (Menzies et al., 2003), although the specific mechanisms for this might still be difficult to prove.
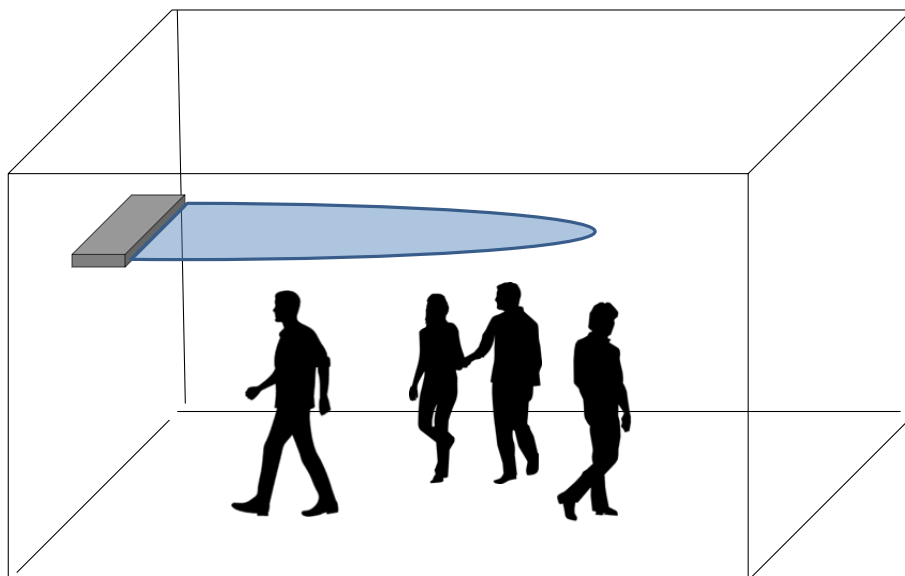
Figure 2.5 Schematic of an upper-room UVC system operation.

For health and safety reasons, upper-room systems must be design to work under the limits of UV exposure for inhabitants. OSHA limits a continuous UV irradiation not higher than 0.2 µW.cm⁻

^{2} for 8 hours, equivalent to a UVC dose of 58 J.m^{-2} (IUVA, 2005d). ACGIH (American Conference of Industrial Hygienists) limits the exposure to 30 J.m^{-2} (broadband UV) or 60 J.m^{-2} at 254 nm during 8 hours (Kowalski, 2009c).

2.4.3 Recirculation stand-alone UVC sterilisation systems.

These systems make use of a fan forcing the air to pass through a UVC chamber. Some of the benefits of these systems are their capacity to include reflective surfaces and in some cases to provide controlled and measurable performance. A great percentage of microbial contamination in a room comes from its inhabitants (Beggs et al., 2003). Room air patterns and the capacity of these types of systems to recirculate as much air as possible define their performance (Figure 2.6). Although they will not sterilise surfaces, they might reduce surface deposition of contaminants (Taylor et al., 1995).

Figure 2.6 Recirculation stand alone units. Ceiling unit (right) and floor unit (left) from IUVA Ltd.

2.4.4 UVC air sterilisation Guidelines

IUVA Guideline IUVA-G01A-2005: General Guideline for UVGI Air and Surface Disinfection Systems (IUVA, 2005a). Introduced in 2005, this guideline is intended for air disinfection of in-duct units, and surface disinfection aimed for cooling coil treatments. The document provides general information about UV technology and includes topics such as classifications of UV systems, types of UV lamps, UVC irradiation and safety issues among others. An important point of this document is the introduction of the URV (UVGI Rating Value) to classify the performance of a UVGI system.

Introduced by Kowalski (2009a), the URV classification originated from the need to measure the performance of the UV air sterilisation systems. The concept of the URV scale is similar to those

used for physical filters such as the MERV and the European H10 – H14 (ASHRAE, 2003), where a rating value is giving according to its sterilisation power. The URV level is based on the UV dose provided by a UV system and is expressed in $J.m^{-2}$. It is important to point out that URV levels relates only to average dose provided by the UV system, and this can change depending on the airflow rate of the system. Moreover the URV does not relate to a specific microorganism, although microorganisms react to a specific UV dose, it can vary at different levels of humidity. Therefore, a microorganism which is inactivated by a dose equivalent to a URV 13 in low humidity, might require a URV 15 in high humidity (above 70% humidity).

Table 2-3 URV rating (Kowalski, 2009a).

URV	Dose $J.m^{-2}$	Mean dose $J.m^{-2}$
1	0.01	0.055
2	0.1	0.15
3	0.2	0.25
4	0.3	0.4
5	0.5	0.63
6	0.75	0.88
7	1	1.25
8	1.5	2
9	2.5	3.75
10	5	7.5
11	10	12.5
12	15	17.5
13	20	25
14	30	35
15	40	45
16	50	55
17	60	70
18	80	90
19	100	150
20	200	250
21	300	350
22	400	450
23	500	750
24	1000	1500
25	2000	2500

IUVA Guideline IUVA-G02A-2005: Guideline for the Design and Installation of UVGI In-duct Air Disinfection Systems in New Building Construction (IUVA, 2005b). This standard was written to assist the installation of in-duct air treatment systems specially UV systems in new buildings. The document highlights the difference between retrofitting systems and new installation

designs. This guideline is intended for commercial office buildings and multi-stories facilities, broadening the previous scope of healthcare facilities only.

IUVA Guideline IUVA-G03A-2005: Guideline for the Design and Installation of UVGI In-duct Air Disinfection Systems (IUVA, 2005c). This guide focuses mainly on retrofitting systems, referring to the design and installation of UVC air treatment systems in existing buildings. The guide gives recommendation on location of UV systems, wiring, electrical connections, warning signs and general safety.

ASHRAE Handbook Chapter 16: Ultraviolet lamp systems (ASHRAE, 2008a). The document relates to three UVC technologies, in-duct disinfection, upper room disinfection and cooling coil surface disinfection. Also in this document there is information on UVGI fundamental concepts, lamp and ballasts specifications, maintenance and safety of the systems. For in-duct systems, where the irradiation is contained inside of the duct, it is recommended to make use of a safety interlock that will turn off the lights at the moment of accessing the duct. The document emphasises design factors to be considered including: duct dimensions, length of exposure to UVC light, air velocity, air temperature, lamp cooling effect, lamp fouling, bio contaminants and their susceptibility values, disinfection performance required, lamp age, power supply, reflectivity inside the duct, location of lamps inside the duct and humidity.

This guideline recommends the use of UVGI to complement system maintenance by keeping coils, drain pans and other surfaces free of microbial contamination.

2.5 UVC sterilisation: In-duct systems technology and operation.

In-duct devices typically comprise one or more UVC lamps mounted within the HVAC system to create a UV irradiation field inside an airflow duct (Figure 2.7). Microorganisms contained in the air passing through the UV field incur DNA damage proportional to the UV dose received and the microorganism UV susceptibility; with sufficient exposure the damage may be lethal rendering microorganisms inactive (this is explained in Chapter 3). Reduction on bacteria concentration on surfaces has been linked with the installation of in-duct UVC systems (Taylor et al., 1995). Moreover, in-duct UVC systems can also be used for reducing bio fouling of cooling coils, providing potential energy savings for the HVAC system (Blatt, 2006, Kowalski, 2009a, Lee et al., 2009).
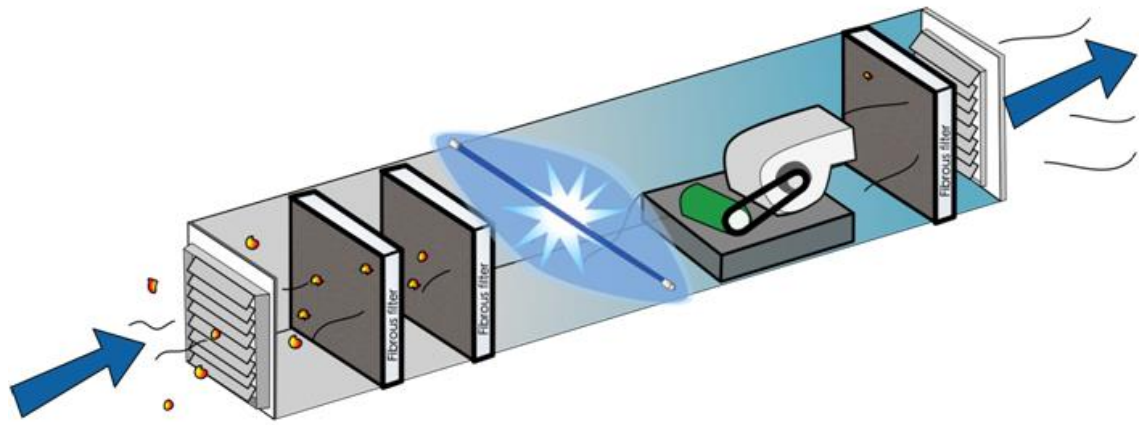
Figure 2.7 Schematic of an in-duct UV system.

With increasing application of in-duct UVC systems, it is important to accurately quantify the performance of the technology, for that reason appropriate analysis and test mechanisms must be set in place. For an in-duct air system, the efficiency of UVC sterilisation depends on many factors including UV irradiation intensity, dwell time (in the UV field within a duct or device), pathogen susceptibility to UV irradiation, air velocity, air temperature, humidity of air, reflectivity of duct or device internal surfaces, velocity profile, air mixing and lamp position.
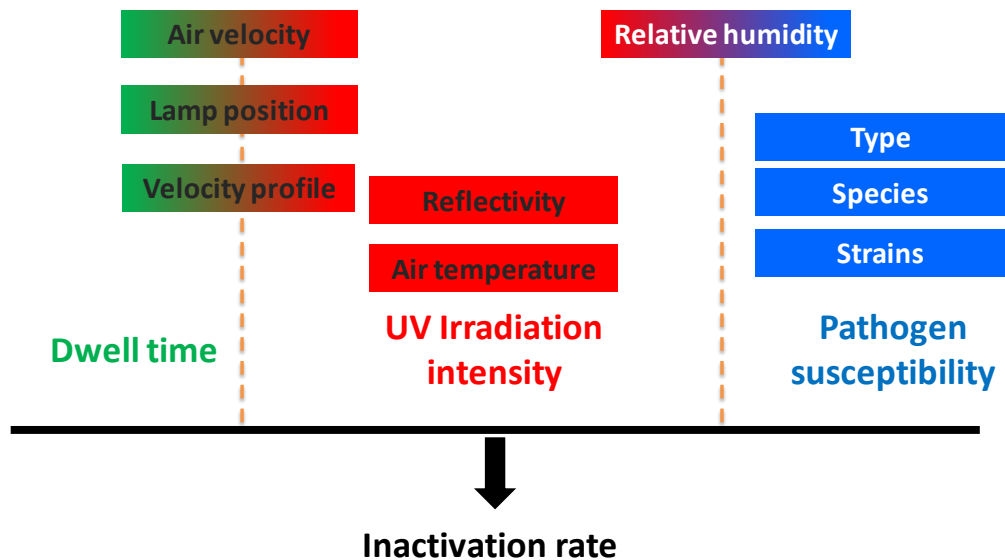
Figure 2.8 Factors affecting the performance of a UV system.

UV irradiation intensity is the UV power per unit area provided by the lamps, it is usually expressed in W.cm^{-2} and depends on the distance from the lamp at which it is measured, the closer to the lamp the higher the irradiation. Commonly UV lamp manufacturers will provide within their specification the UVC irradiation value at 1 metre from the lamp (Philips, 2007, LightSources, 2009). Inside the UV chamber, in this case the in-duct unit, the UV irradiation can

be affected by air velocity, air temperature and reflectivity. At velocities higher than 3.5 m.s^{-1} the lamp UVC power can be reduced up to 30% due to the cooling of the lamp surface and electrodes (Philips, 2005). In general, in-duct UVC sterilisation systems face operation velocities between 2 – 2.54 m.s^{-1} (Kowalski, 2003), however, in-duct ventilation systems might present velocities of up to 8 m.s^{-1} to 10 m.s^{-1} (Daly, 1992). The UVC output of a lamp is a function of the plasma temperature when the power input is constant (Kowalski and Bahnfleth, 2000b). UV lamps working at low air temperatures under 30 C and high air temperatures over 60 C (Lau, 2009) can suffer a shorter operational life (VanOsdell and Foarde, 2002), and up to a 70% reduction in UV power (Philips, 2007); only amalgam lamps are not affected by temperature (LightSources, 2009). Reflectivity of duct surface can improve the performance of a UV air sterilisation system by increasing the intensity field. If applied properly it can reduce the system cost, intensify the UVGI field and level the distribution of irradiation along the duct (Kowalski and Bahnfleth, 2000a). Reflectivity can be diffusive or specular. Commonly a UVGI system will use specular, or mirror like, reflective surfaces (Kowalski, 2003). Reflectivity is discussed in further detail in chapters 4, 5 and 6.

The impact of airflow profile and lamp position is considered in detail in chapter 6. Airflow profile affects the dwell time, and the particles path inside the duct, thus affecting the amount of UV irradiation that particles receive. For example airflow path lines close to the UV lamp will receive more UV dose than those far away from the UV lamp. The lamp configuration therefore has a direct impact in the sterilisation performance of the system.

Microorganisms have a natural susceptibility to UVC light. Their UVC susceptibility is basically the amount of UVC irradiation the microorganism needs to absorb to be inactivated. Microorganism susceptibility depends on the specific microorganism species and strain, as well as the environmental conditions. As it is a biological factor, variations are always present. Chapter 3 reviews in detail the importance of microorganism susceptibility.

2.6 UVC sterilisation: Performance evaluation methods.

The performance of a UVC air sterilisation system can be measured in various ways. A system can be tested in a laboratory to find the sterilisation performance against a specific microorganism with the use of a biodosimetry test, such as the ones carried by the US EPA (EPA, 2006a, EPA, 2006b, EPA, 2006c). The EPA tests series "Biological Inactivation Efficiency by HVAC In-Duct Ultraviolet Light Systems" (EPA, 2006a, 2006b, 2006c) presents experimental data on UV inactivation and are a popular reference for the performance of UVC in-duct sterilisation systems, Chapter 5 explains shows a detailed explanation of the tests results and procedures.

However such tests only show mean performances and give little insight into the mechanisms for airflow interaction with the UV field. After obtaining a specific kill rate of a microorganism, then it is possible to use data on the microorganism UVC susceptibility to calculate the energy of the UVC system. To accurately carry these types of tests it is necessary to control operational parameters such as air velocity, temperature, humidity and microorganism strain, as any of these could skew the calculated results. A further complication with biodosimetry testing is that results depend on the accuracy of the assumed microorganism UVC susceptibility, and currently in literature there is a great amount of data variation (Fletcher et al., 2003, Ke et al., 2009, Peccia and Hernandez, 2004).This is discussed in detail in Chapter 5.

Another option for the calculation of performance of a UVC sterilisation system is the mathematical modelling of the UVC irradiation of a lamp with the use of numerical methods (this is discussed in detail in Chapter 4). Among these methods are the Multiple point source summation (MPSS) which models the irradiation of a lamp as if coming from a finite number of points across the length of the lamp (Bolton, 2000). The Multiple segment source summation (MSSS), similar to the MPSS but instead of points assumes finite length differentials as the source of irradiation along the length of the lamp (Bolton and Cotton, 2001). The view factor used by Kowalski (2009a) to calculate the performance of predicted UV device performance with average irradiation fields. However these models assumed a fully mixed airflow, are incapable of accounting for particle trajectories and in most cases they do not consider the 3D flow-UV field interaction that happens in a real system.

Another option is the use of computational fluid dynamics (CFD) modelling, which is capable to account for sophisticated aspects of a UVC system such as wall reflections, shadowing, fluid absorption, UVC irradiation distribution, particle trajectories and flow development (this is discussed in detail in Chapter 5, Chapter 6 and Chapter 7). CFD modelling has been successfully applied to UV water systems, (Duran, 2010, Ho, 2009b) and upper-room UV (Gilkeson and Noakes, 2013). By using CFD in a parametric study, it is possible to look for lamp configurations that provide the highest sterilisation performance at the lowest energy use.

Although it has been long suspected that lamp position/configuration would have an impact on the performance of an induct UV sterilisation system, the information about the topic remains limited. Kowalski (2009a), presented a performance calculator table for induct UV systems based on fully mixed flow but this only considers total UV power within the duct and the duct measurements, neglecting lamp position/configuration. In most cases manufacturers' data are not specific on the sterilisation mechanisms and is difficult to establish a performance requirement from both users and customers. The EPA experiments do not describe the

sterilisation performance and are ambiguous on microorganism kill rate or average UV dose of the system (EPA, 2006a, EPA, 2006b, EPA, 2006c). Chapter 5, Chapter 6 and Chapter 7 of this thesis applies a CFD modelling approach to explore the influence of lamp location within a duct on the UV dose received by airborne particles.

Chapter 3. UV susceptibility of microorganisms.

3.1 Introduction.

Without entering into the complexities of the physical model of a working UV system, two essential parameters are necessary to calculate its performance. One is the UV dosage, which involves dwell time and most importantly light irradiation, and is determined by the engineering and flow parameters of the system. The second parameter is the UV susceptibility of microorganisms, which is a biological parameter.

This chapter commences with a brief introduction to UV susceptibility of microorganisms, explaining why is it that the DNA of microorganisms is disrupted with UV light at specific frequencies. Then it follows with the description of the decay models, this is the rate at which a microorganism population is decreased over time by the exposure to UV light. This chapter also considers the impact of relative humidity on the susceptibility of microorganisms.

After the explanation of UV susceptibility and its implication, the chapter continues with a review of UV susceptibility in air of various bacteria found in the literature.

Finally this chapter concludes by compiling a list of UV susceptibility data from a number of published studies to establish representative values for a series of microorganisms.

3.2 Microorganism UV susceptibility.

Microorganisms are inherently susceptible to UVC light, more specifically UVC light at the 254 nm frequency. The interaction of a microorganism with UV light is a complex process, and depends on biological and environmental factors (Rentschler, 1942), as a response to these mechanisms and for the means of practical calculations, researchers have developed what is known as the UV susceptibility (k) of microorganisms, this is the rate at which the microorganism population is generally affected by UV light, under controlled environmental parameters such as temperature, humidity and UV dose, and is represented with the units $m^2.J^{-1}$. The higher the susceptibility of the microorganism, the more reactive it is to UV light. In relation to resistance to UV light, in general fungi tend to be the most resistant against UV light, then bacteria spores, bacteria vegetative cells and at the end viruses tend to be the weakest microorganisms against UV light (Kowalski, 2009a).

Microorganisms are biological entities and their susceptibility under UV light is complex and variable. Factors such as relative humidity can change a microorganisms susceptibility (Fletcher, 2004), different strains of the same microorganisms, and even the same microorganisms cultivated in different batches might show variations in susceptibility. Different microorganisms decay under UVC light in different manners, e.g. some might show a single stage decay in which all the population its affected by UV light at a constant rate, some microorganisms might show a shoulder before they decay in a single stage, meaning that there is a UV dose threshold that needs to be achieved before a constant kill rate starts, and then we can have variations of different behaviours making the susceptibility of a microorganism to UV light a case specific value.

For these reasons a definitive susceptibility value for a specific microorganism might not be possible to determine. Nevertheless, quantifying a susceptibility value that accounts for variability and recognizes the type of survival decay could help to increase the accuracy of disinfection performance calculations.

3.2.1 The effect of UV light on DNA

The Deoxyribonucleic acid (DNA) is the molecule that encompasses all the genetic information of all known living organisms and some viruses, and is composed of nucleotides. Each nucleotide contains three parts: deoxyribose, phosphate, and one of the four nitrogenous bases or nucleic acid bases, which are thymine (t), adenine (a), cytosine (c), and guanine (g). These four subunits are the base of the double helix shaped structure found in the DNA, each helix terminates in a free hydroxyl group in one end and a free phosphate group in the other (Neidle, 1999)(Figure 3.1).

Figure 3.1 Structure of the DNA. Adapted from The Astrophysics & Astrochemistry Lab (2014).

Some viruses might contain RNA instead of DNA, the difference between them is that RNA has D-ribose as its main constituent and adenine, cytosine, guanine and uracil as bases, while DNA

has 2-deoxy-D-ribose as its main component with adenine, cytosine, guanine and thymine as bases (Casarett, 1968). UV light inactivate microorganisms mainly by causing cross-links between constituent nucleic acids (Figure 3.2), specifically the effect of UV light on DNA/RNA is the formation of dimers, being the creation thymine dimers the primary cause of lethal effect on DNA when exposed to UV light, and the secondary damage is also produced by cytosine dimers (Kowalski, 2009a), therefore viruses containing RNA which lack thymine are less susceptible to inactivation by UV light.
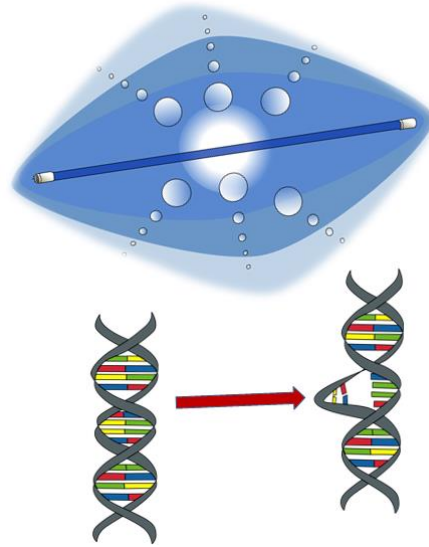
Figure 3.2 Damage to DNA by exposure to UV light.

The germicidal effectiveness of UV light is known to have its maximum in the region of 220 nm to 300 nm, with peaks of efficiency at 250 nm and 265 nm. Luckiesh (1946) reports that research prior to his found that *S. aureus* maximum kill rate efficiency was achieved at 253.7 nm and *E. coli* at 265 nm with the 253.7 nm frequency being nearly as effective, later in his own research Luckiesh (1946) found that the maximal germicidal effectiveness in the killing of *B. coli* in shallow depths of water by UV light is in the range of 253.7 nm to 257.5 nm (Figure 3.3).
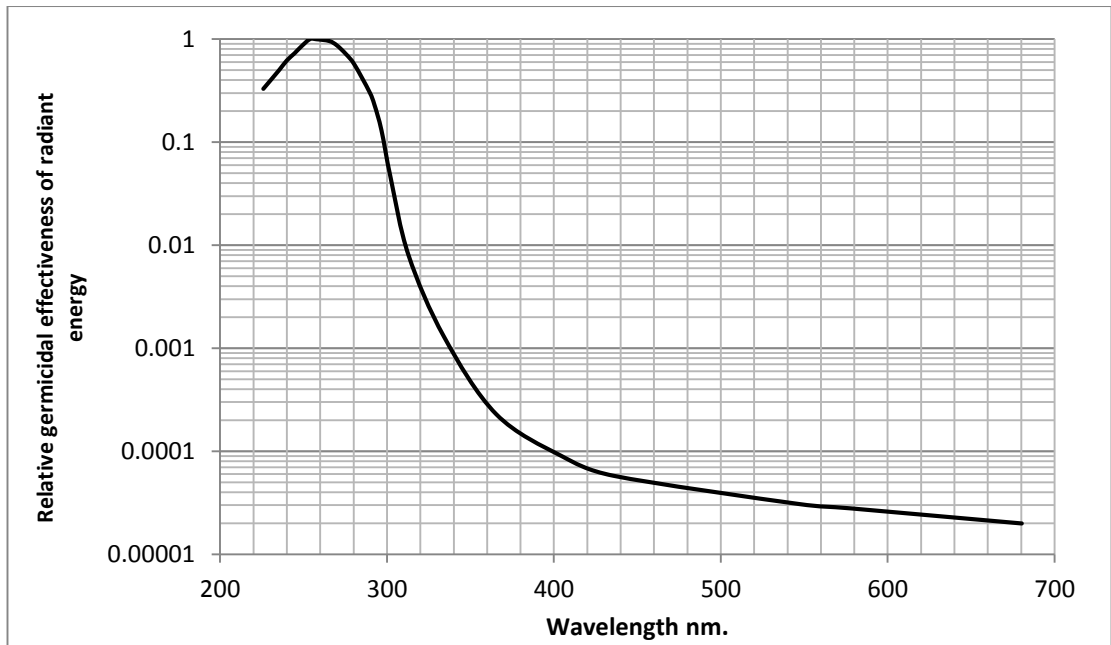
Figure 3.3 The relative germicidal effectiveness of UV light of various wavelengths as determines by the killing of B. coli. Adapted from Luckiesh (1946).

The effectiveness of germicidal irradiation rapidly decreases as it moves from 253.7 nm up to the region of 293 nm, with research suggesting that the energy to kill bacteria with wavelengths of 365 nm and above is 1000 to 10,000 greater than the energy required in wavelengths shorter than 300 nm (Luckiesh, 1946). It is important to highlight that such studies of germicidal effectiveness were run for *B. coli*, yet it is known that higher UV wavelengths also impact the survival of microorganisms (Munakata and Rupert, 1975, Kowalski, 2009a).

3.3 Microorganism UV decay models.

The microorganisms decay model represent the predictive effect UV germicidal irradiation will have on a specific microorganism, in this manner we can calculate how much UV power is required to achieve a certain level of sterilisation in a specific media such as air, water or a surface.

At least five decay models have been proposed depending on the microorganism type. These are single stage, single stage with shoulder, double stages, double stages with one shoulder, double stages with two shoulders, and then combinations of various (Kowalski, 2009a).

3.3.1 Single stage decay

Single stage or first order decay is a classical exponential decline (Equation 3.1).

$$S = e^{-kD}$$

Here k is the susceptibility value of the microorganism ($m^2.J^{-1}$) and D is the UV dosage ($J.m^{-2}$). This model is commonly used (Kowalski, 2009a, Beggs et al., 2003, Noakes et al., 2003) as the standard model unless a different decay model has been proven. The decay line would be as it appears on Figure 3.4.
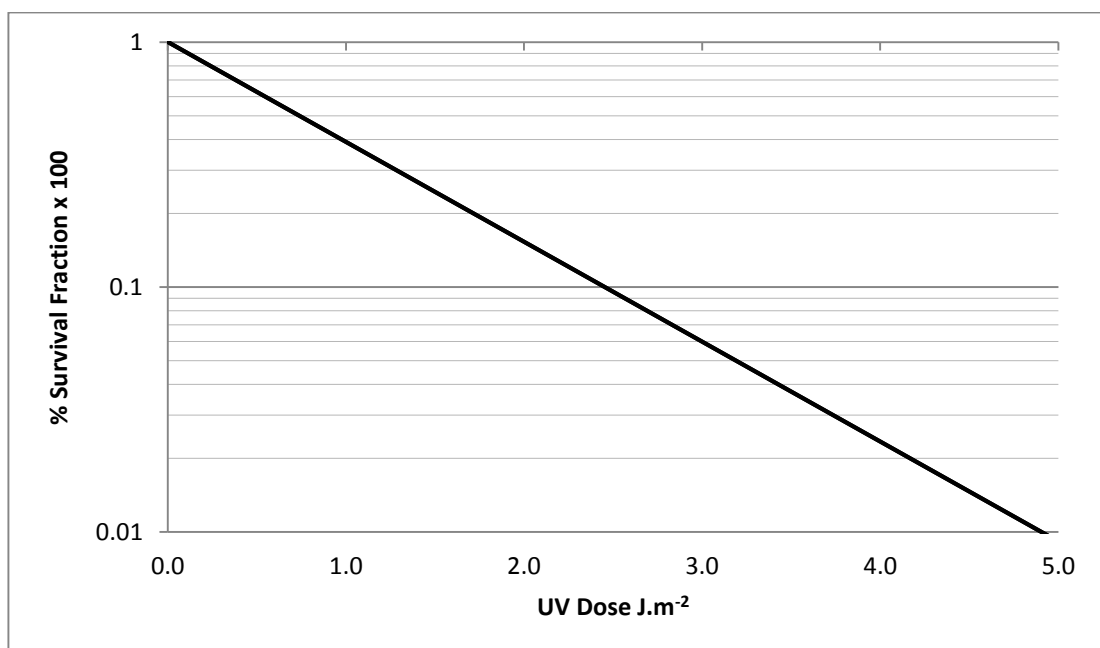
Figure 3.4 Example of single stage decay.

In many cases this will suffice for the calculations, yet some microorganisms can present a more complex behaviour.

3.3.2. Single stage with shoulder

It is known that some microorganisms, for example *B. subtilis* spores do not follow a first order decay model and are better represented with a shoulder (n) in their decay model (Kowalski, 2009a, Nicholson and Galeano, 2003) as shown in Equation 3.2.

$$S(t) = 1 - \left(1 - e^{-kD}\right)^n$$

Where the shoulder (n) is obtained by extrapolating the single stage line to the y-intercept. In a graphic a single stage shoulder looks like Figure 3.5. As commented before, there are various possible explanations for this phenomena, involving environmental and/or biological factor, in some cases a part of the population appears to be more resistant to UV light, and after a certain threshold the full population decays in a similar manner, this for example could be the case of a population with a mixture of vegetative cells and spores, sharing different susceptibilities to UV.
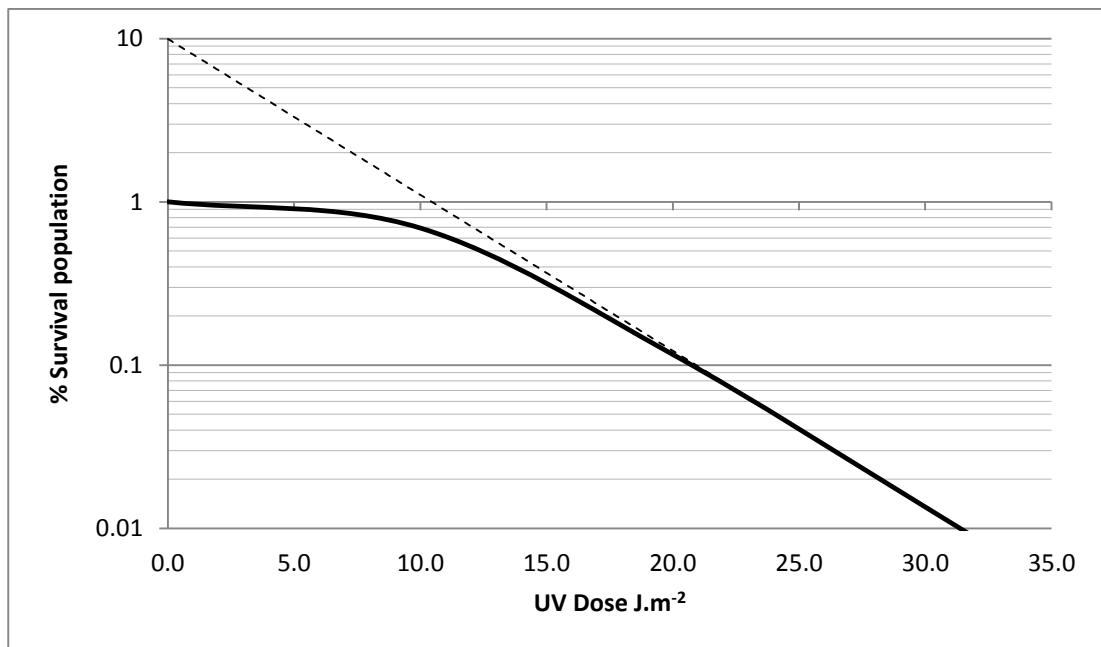
Figure 3.5 Single stage with shoulder decay.

3.3.3. Double stage decay models

Other variations include Double Stage Decay and Double Stage Decay with shoulder. When the UV dose is enough to produce several logs reduction of population, the survival population tend to be an order of magnitude more resistant to UVC (Kowalski, 2009a), this is common not only for UVC, it has also been observed in other methods of disinfection (Chick et al., 1963). The Double Stage Decay is when part of the population decays at a specific first order rate and then a second part of the population decays at a different order rate as represented by Equation 3.3.

$$S = (1 - f)e^{-k_1 D} + fe^{-k_2 D}$$

Where $k1$ is the highest susceptibility and $k2$ is the lowest, and the y-intercept is the value for population f. Figure 3.6 shows how a double stage decay would be represented on a graph.
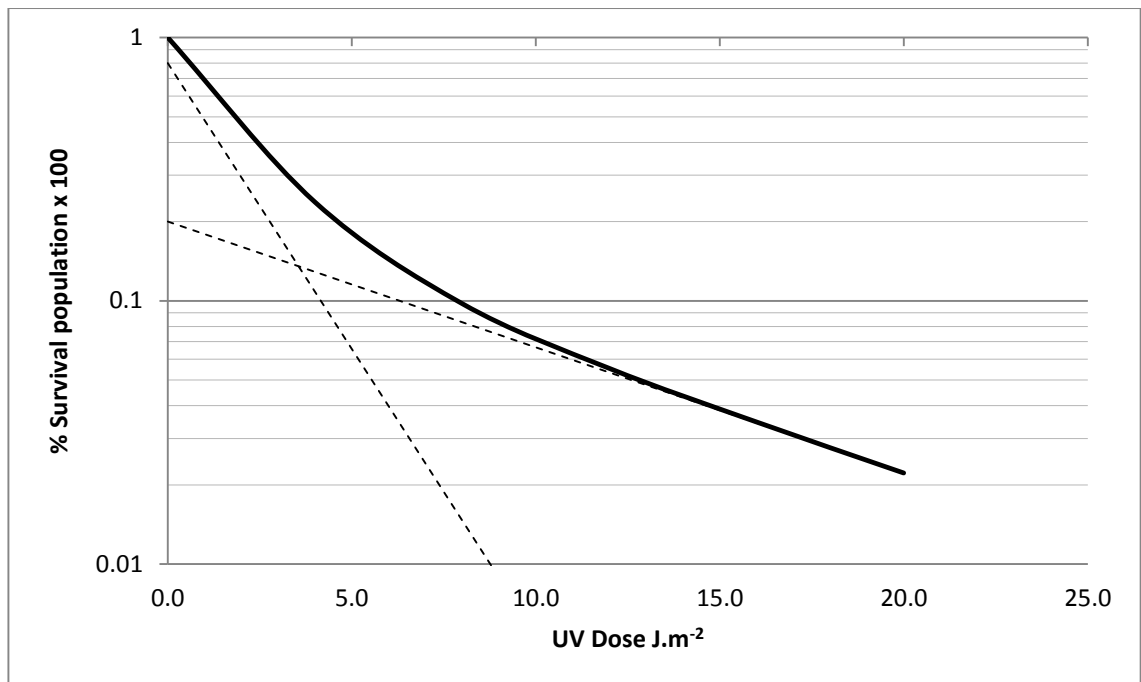
Figure 3.6 Double stage decay.

Finally the Double stage decay with shoulder is a combination of all the previous survival decays, and it can include either one or two shoulders for each of the stages of the decay (Equation 3.4).

$$S(t) = (1-f)\left[1 - \left(1 - e^{-k1D}\right)^{n1}\right] + f[1 - (1 - e^{-k2D})^{n2}]$$

Equation 3.4 Double stage with shoulders
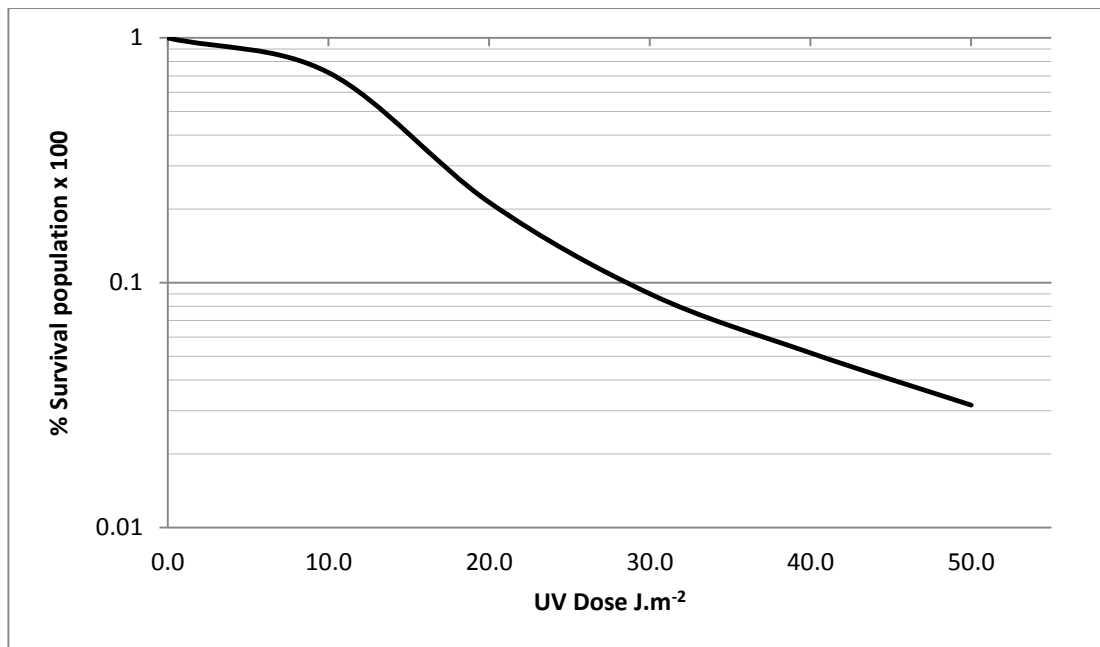
Figure 3.7 Double stage decay with shoulder.

Published data on susceptibility indicates that most microorganisms can be modelled using one of these five decay models, allowing prediction of the microorganism behaviour in a UV system. However selecting the appropriate model and coefficients is essential. Assigning the wrong susceptibility constant and/or model can result in either over powered systems which will incur in higher energy and running costs, or underpowered systems which could compromise the air quality of system. Current literature on UV susceptibility values of microorganisms in air is unfinished, nevertheless the information is sufficient as to have a practical performance calculation. Kowalski (2009a) provides a comprehensive list of microorganism susceptibility in air. Nevertheless the data it is based on shows considerable variations in test protocols, equipment and/or units. The following sections aim to carry out a comprehensive analysis of published experimental susceptibility constants for a number of microorganisms to provide a consistent susceptibility model to be used for air sterilisation.

3.4 Influence of relative humidity on UV susceptibility of microorganisms.

Relative humidity (RH) appears to have a direct relationship to microorganism's susceptibility to UV light. References to its effect date as back as the 1940's (Sharp, 1940, Rentschler and Nagy, 1942, Luckiesh, 1946) and several recent studies have explored the relationship (Peccia and Hernandez, 2004, Ko et al., 2000, Peccia et al., 2001, Fletcher, 2004).

There is no definitive theory on the mechanisms of RH and UV susceptibility, since the early studies of UVC as a technology for air sterilisation Rentschler and Nagy (1942), Luckiesh (1946) and others found that airborne bacteria are about ten times more resistant to radiation at high humidity levels than at low humidity levels. Rentschler and Nagy (1942) made an interesting observation, they referred the effect of RH on UV susceptibility to a selective sampling effect when using centrifugal devices as lighter particles are more easily diverted towards it, leaving heavier particles i.e. water droplets at high RH. Aside, in a similar note Ko et al. (2000) did not corroborate the selective sampling argument, but he did find that indeed at higher RH particle size increased for *Serratia marcescens* and BCG. For *S. marcescens* the increase in particle size was linear with RH increase, and for BCG the increase on particle size was more or less stepwise. His explanation was the type of bacteria as while *S. marcescens* is a gram negative bacteria and has a lipid-rich outer membrane, BCG is a gram positive bacteria with a waxy outer layer making it possible that this outer layer may increase its tendency to create clumps. VanOsdell and Foarde (2002) reported measurable differences in irradiation at different RH levels, meaning that RH may be having an effect on the lamp as well, nonetheless conclusive results on this issue are still needed.

Kowalski (2009) suggested the effect of RH is different between virus and bacteria. While high RH in bacteria can reduce their susceptibility by up to ten times (Luckiesh, 1946, Fletcher, 2004), in viruses the effect is less noticeable, with differences that are outside experimental accuracy (Kowalski 2009).

Leaving aside the discussion on the mechanisms of RH on UV susceptibility, it seems to be accepted that for bacteria, susceptibility to UV light decreases as RH increases. This has been constantly reported, i.e. by Rentschler and Nagy (1942) when dealing with *E. coli*, and later by Luckiesh (1946). Peccia et al. (2001) reported that for an increase in RH from 50% to 95%, *k* values decreased by a factor of 6.5 for *S. marcescens*, 1.5 for *Bacillus subtilis* and 3.2 for *Mycobacterium parafortuitum*. In further studies Peccia and Hernandez (2004) also reported a more than three times increase of UV susceptibility for various Mycobacterium strains when RH changed from 95% to 50%; these results were later corroborated by Xu et al. (2003). Fletcher (2004) also found that doubling the RH from 50% to 95% resulted in a decrease of UV susceptibility by a factor of 2 for *B. cepacia* and up to a factor of 10 for *S. marcescens*.

In conclusion, relative humidity has an impact on the susceptibility of bacteria to UV light (Ko et al., 2000), in some cases the difference in susceptibility can be up to ten times (Luckiesh, 1946, Fletcher, 2004), for viruses this effect is not clearly defined. In case that the RH is not known it is recommended to use the lowest susceptibility, that is the one at high RH or the ones recorded

in water, as this will ensure that sterilisation levels are achieved. UV susceptibilities used for microorganisms in water could be used as reference only for saturated air (95% RH) (Peccia and Hernandez, 2004). Understanding the impact of relative humidity is of great importance when designing integral UV systems as significant savings on energy could be achieved if the systems are located in areas where they deal with drier air.

3.5 UV susceptibility of airborne microorganisms: Reviewed and updated.

This section collates data from published studies carried on various microorganisms UV susceptibility, with the aim of achieving a commonality in results that are reliable for the purpose of sterilisation performance modelling. The end of section 3.5 presents a comprehensive UV susceptibility database of microorganism that can be used for such purpose.

3.5.1 Methodology.

There are numerous publications reporting on the sterilisation effect of UVC light on microorganisms suspended in air. Although not all microorganisms have been explored in the current literature, there is still enough information for the creation of a comprehensive database of microorganisms susceptibilities to UVC light in air. However, the expansion of the microorganisms susceptibility list is an important opportunity for future research.

Studies on the sterilisation capabilities of UVC light date as far back as 1939 or maybe even before. Some studies had the only purpose to prove the capability of UVC sterilisation (Koller, 1939), some others focused on sterilisation of microorganisms in air (Sharp, 1940, Nakamura, 1987, Jensen, 1964, Harstad et al., 1954, Rentschler and Nagy, 1942), and with the pass of time, the studies have moved to show the susceptibility of microorganisms to UVC light and the impact of relative humidity (Ke et al., 2009, Beggs et al., 2005, Peccia and Hernandez, 2004, Fletcher et al., 2003, Peccia et al., 2001).

To date, there are no standard tests or units to be used when referring to UVC sterilisation. Therefore it is possible to find information in the literature in a variety of units such as $\mu W.sec.m^{-2}$, $J.m^{-2}$, $\mu J.cm^{-2}$ or even $ergs.mm^{-2}$. This variation in units and procedures makes it difficult to filter the relevant data and give it meaningful results.

In order to calculate and consolidate the values of UVC susceptibilities in a meaningful manner from the current available literature it was needed to: a) Standardize units in the metric systems, and using $J.m^{-2}$. b) Consolidate the results by individual microorganism from the various

publications into a single data set. c) Calculate the UVC decay model for each microorganism, with the minimum and maximum ranges of UVC susceptibilities.

3.5.2 *B. atrophaeus, B. subtilis* spores, *B. subtilis* vegetative cells.

Bacillus atrophaeus is a reclassification of certain strains of *Bacillus subtilis* (Fritze and Pukall, 2001, Nakamura, 1989). *B. subtilis* is a rod-shapped, gram negative bacteria naturally found in soil and vegetation (Perez and Mello, 2000). It is known that *B. subtilis* spores do not follow a first order decay model and is better represented with a shoulder (n) decay model (Kowalski, 2009a, Nicholson and Galeano, 2003). Ke et al. (2009) reported a *k* value for *B. subtilis* spores to be 0.017 $m^2.J^{-1}$ with a shoulder (n) of 3 for relative humidity levels of 50 to 60% and 0.014 $m^2.J^{-1}$ with a shoulder (n) of 2 for relative humidity levels of 70 to 83%. The EPA (2006a) reported a susceptibility value to be 0.016 $m^2.J^{-1}$ referencing a study by VanOsdell and Foarde (2002) which presents only two UV dosages and resulting survival fractions for *B. subtilis* spores and a susceptibility that appears to be 0.02 $m^2.J^{-1}$; it is important to highlight that only two readings of UVC dose and survival are unlikely to be enough to accurately calculate the susceptibility of a microorganism.

Table 3-1 Reported susceptibility values for *B. subtilis* spores

Bacteria	Susceptibility value k $m^2.J^{-1}$	Relative humidity	Shoulder n value	Source
B. subtilis spores (*B. atrophaeus*)	0.014	70-83%	2	Ke et al. (2009)
	0.017	50-60%	3	Ke et al. (2009)
	0.020	unknown	-	VanOsdell (2002)
	0.017	-	1.66	Average
B. subtilis veg cells (*B. atrophaeus*)	0.044	95%	-	Peccia et al. (2001)
	0.063	20-40%	-	Peccia et al. (2001)
	0.053	-	-	Average

Peccia et al. (2001) worked with *B. subtilis* vegetative cells, reporting a *k* value of 0.063 $m^2.J^{-1}$ for low RH in the range of 20%-40% and stating that RH did not have any observable effect on susceptibility within that range. For RH above 95% Peccia et al. reported a *k* value of 0.044 $m^2.J^{-1}$. Vegetative cells tend to be more susceptible to UVC light as they do not have the outer cover found in spores.
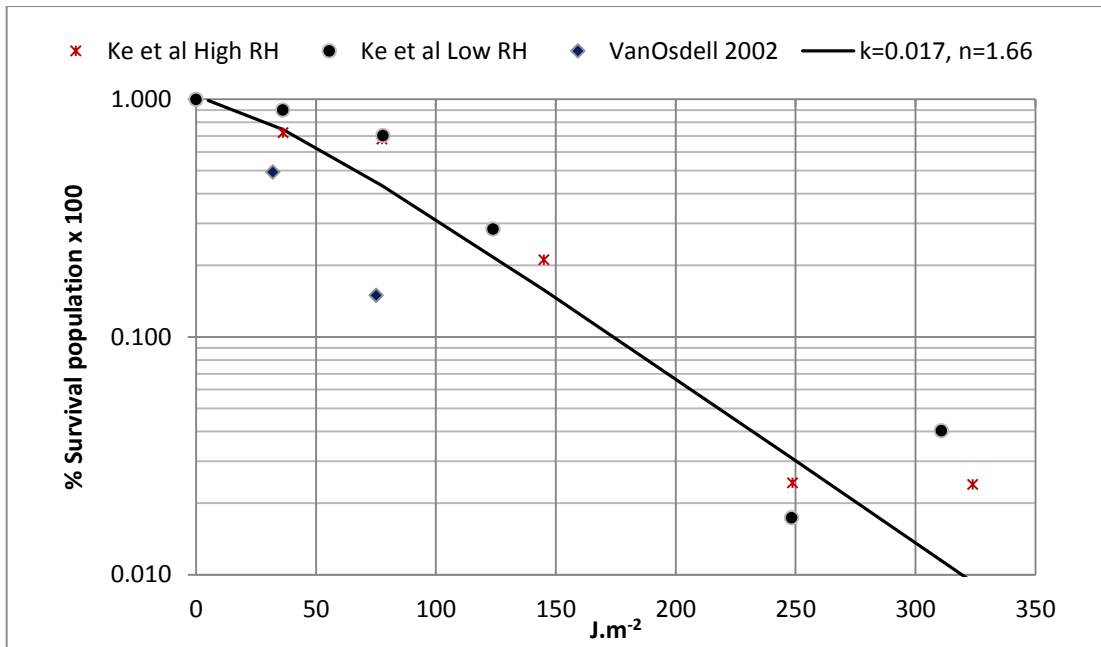
Figure 3.8 Survival of B. subtilis under UVC light.

Figure 3.8 shows the amalgamation of the studies referenced on Table 3-1 in a single graph, the average susceptibility value $k=0.017$ $m^2.j^{-1}$ was then plotted with an added fitted line. Independently of RH levels, for *B. subtilis* spores and *B. atrophaeus*, the average susceptibility value of $k=0.017$ $m^2.J^{-1}$ with a shoulder of n = 1.66 appears to be a practical approximation that can be used for modeling purposes with relatively good accuracy (Figure 3.8) and for *B. subtilis* vegetative cells the recommendation is to use the average $k=0.053$ $m^2.J^{-1}$ in a single stage decay calculated from results reported by Peccia et al. (2001).

3.5.3 *Burkholderia cepacia*

This is an opportunistic microorganism particularly dangerous for patients suffering from cystic fibrosis (cf) and compromised immune systems (Govan et al., 1996). *B. cepacia* was previously known as *Pseudomonas cepacia*, *P. multivorans* and *P. kingie*. It is a rod-shaped gram-negative, non-spore forming, aerobic bacillus ranging from 1.6-3.2 μm (Miller et al., 2002). As a side note and interesting fact, the term *cepacia* is derived from the latin word for onion; the term was allocated to the cepacia species due to their capacities to soft rot onions during harvesting (Govan et al., 1996). Fletcher (2004) conducted a comprehensive study to quantify the UV susceptibility and the influence of relative humidity of *B. cepacia* in air. At low RH of approximately 53% the UV susceptibility value was reported to be $k=0.2115$ $m^2.J^{-1}$, while at a high RH of 73% and above, the UV susceptibility was reported at 0.1052 $m^2.J^{-1}$ (Fletcher, 2004). The study highlights that increasing the RH by 15% produced a reduction on UV susceptibility by up to 50%.

For the high humidity sample, the susceptibility reported by Fletcher (2004) calculated using the last two values of the decay graph, and represented as a single stage decay brings a close correlation with the tests results. In the second case, the low humidity correlates with a double stage decay, with a population F=0.05 a $k1$=0.61 m^2.J^{-1} and a considerably stronger $k2$ = 0.05 m^2.J^{-1}.

Table 3-2 UV susceptibility for *B. cepacia*

Bacteria	Susceptibility value k m2.J-1	Relative humidity	Source
B. cepacia	0.211	53%	Fletcher (2004)
	0.105	73%	Fletcher (2004)
	k1 = 0.61 k2 = 0.05 *F=0.05	53%	This study

*F=survival population

The results from Fletcher (2004) and the fitted double stage curve are shown in Figure 3.9. In summary the average susceptibility value suggested for *B. cepacia* at 73% RH is 0.105 m^2.J^{-1} in a single stage decay, and at 50% a double stage decay is present with $k1$=0.61 m^2.J^{-1}, $K2$ = 0.05 m^2.J^{-1} and a population F=0.05 (Table 3-2).
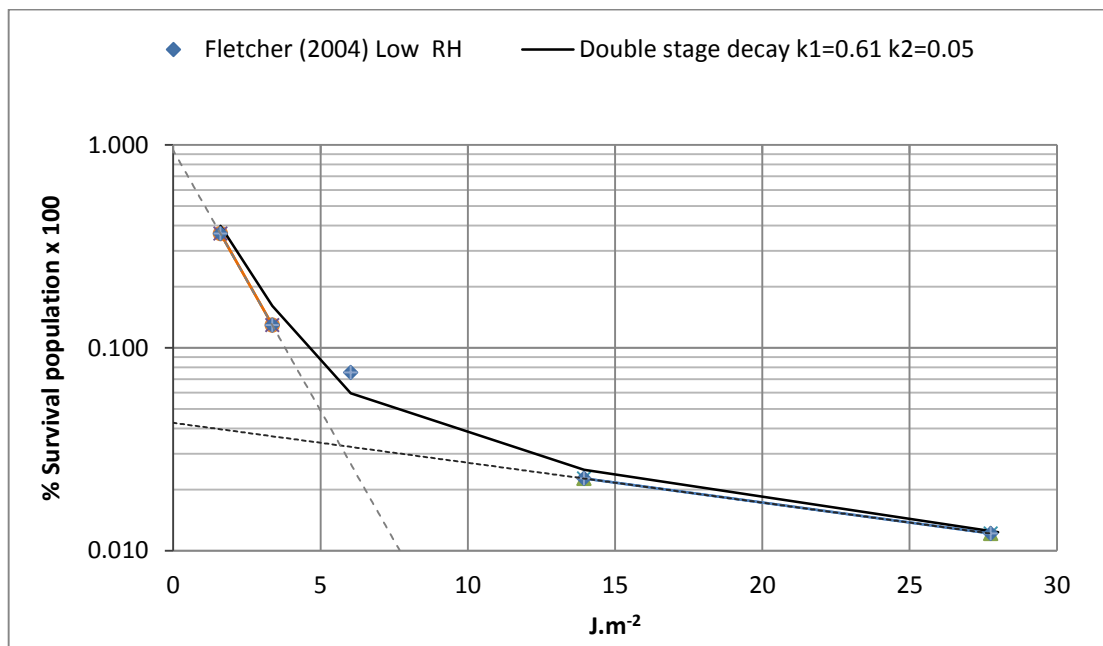
Figure 3.9 Survival of *B. cepacia* at 50% RH under UVC light.

3.5.4 *Ebola* virus

The *Ebola* virus is part of the *Filoviridae* family. This highly infectious virus can cause severe hemorrhagic fever with outbreaks of mortality of up to 80 – 90% (Sagripanti and Lytle, 2010). Research has shown that UVC is capable of sterilising the virus.

According to results from Sagripanti and Lytle (2010), Ebola virus suspended on a dried surface have a UVC susceptibility of 0.074 $m^2.J^{-1}$ and shows a single stage decay curve.
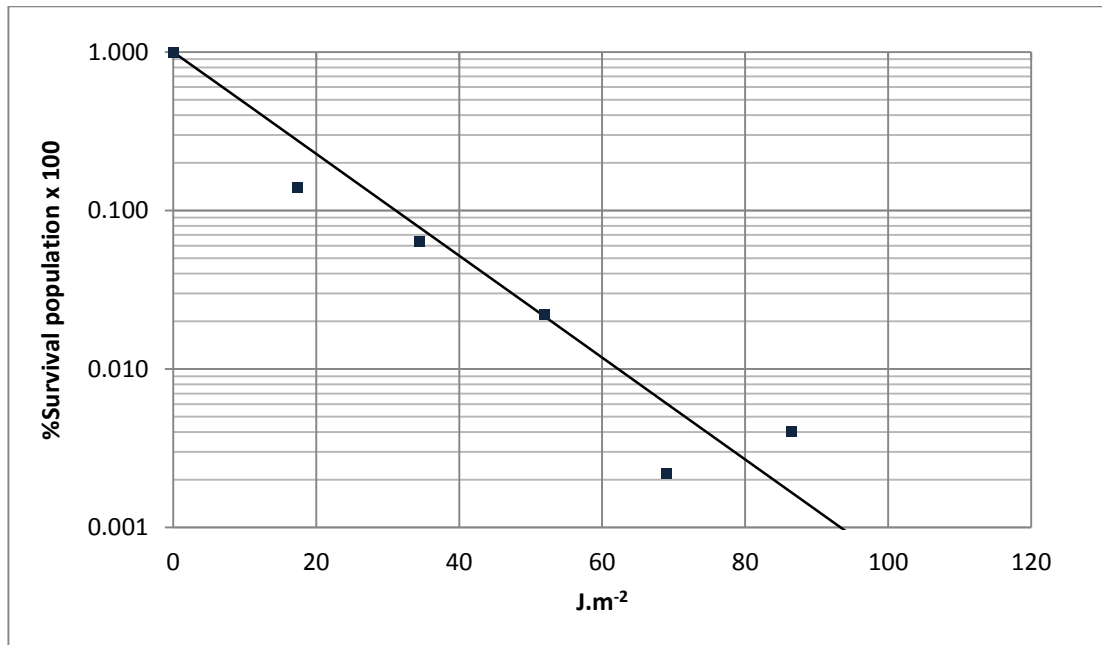
Figure 3.10 Survival of *Ebola* virus under UVC light.

3.5.5 *Escherichia coli*

Escherichia coli, commonly abbreviated as *E. coli* is an aerobic, rod-shaped, gram positive bacteria. Normally this microorganisms lives in the intestines of humans and animals alike, although most of them are harmless, some strains can cause diarrhoea and other problems in the intestinal tract (CDC, 2011). The current literature holds at least five different sources for laboratory tested susceptibility of *E. coli* in air under UV light. The most recent study is by Chang et al. (1985) preceded by Webb (1970), Luckiesh (1946), Rentschler and Nagy (1942) and Sharp (1940). In reviewing these studies it was found that at least four clusters of susceptibility were present with average *k* values ranging from 0.0676 $m^2.J^{-1}$ to 0.6475 $m^2.J^{-1}$ as seen in Table 3-3.

Table 3-3 UV susceptibility values for E. coli found in literature.

Bacteria	Susceptibility value k m^2.J^{-1}	Relative humidity	Source
E. coli	0.056	High (75%)	Webb 1970 *
	0.056	unknown	Rentschler et al. 1942^
	0.091	High	Chang et al. 1985
	0.0676		Average 1
	0.160	unknown	Rentschler et al. 1942^^
	0.178	High (75%)	Webb 1970 **
	0.182	High (90-95%)	Sharp (1940)
	0.173		Average 2
	0.327	Low	Luckiesh (1946)
	0.361	High (75%)	Webb (1970)***
	0.344		Average 3
	0.738	Low (30%)	Webb 1970 ****
	0.557	Low	Luckiesh (1949)
	0.6475		Average 4

*Br strain. **f strain. ***k strain, ****rh 75% no difference between strains.
^ resistant strain. ^^non-resistant strain.

There are some aspects to be discussed from the previous references, for example in the research by Webb (1970), results are expressed in a rather complex mixture of units i.e. "seconds of irradiation at 3.8 ergs.mm^{-2}" and "number of cells.(litre of air)$^{-1}$". This comment is to highlight how different measurements and standards are nowadays in comparisons with studies over 40 years old. He also presented experiments on the germicidal action of UVC at 320 – 400 nm, nowadays most germicidal lamps are tuned to work at 254nm with minimal leaks of energy at higher UVC frequencies (Kowalski, 2009a), yet it is known that higher UV wavelengths also impact the survival of microorganisms (Munakata and Rupert, 1975, Kowalski, 2009a).

Webb (1970) found that different strains of *E. coli* presented different susceptibility to UV light at 75% RH, as well as a confirmation that low RH resulted in higher susceptibilities to UV. Webb's findings are in agreement with those from Rentschler and Nagy (1942) and Luckiesh (1946).

The graph from Rentschler and Nagy (1942) in Figure 3.11, reproduced for clarity, illustrates how *E. coli*, exposed to various non-lethal pre-treatments appeared to be more susceptible to UV light. They found that it was possible to "injure" the microorganism i.e. making it easier to kill with UV light when it was pre-treated, highlighting that not only DNA photon absorption was present in the sterilisation process, and that further physical characteristics could impact the

susceptibility of the microorganism to UV light, therefore the UV susceptibility rate k might not be a constant as the kill rate does not depend only on the UV irradiation.
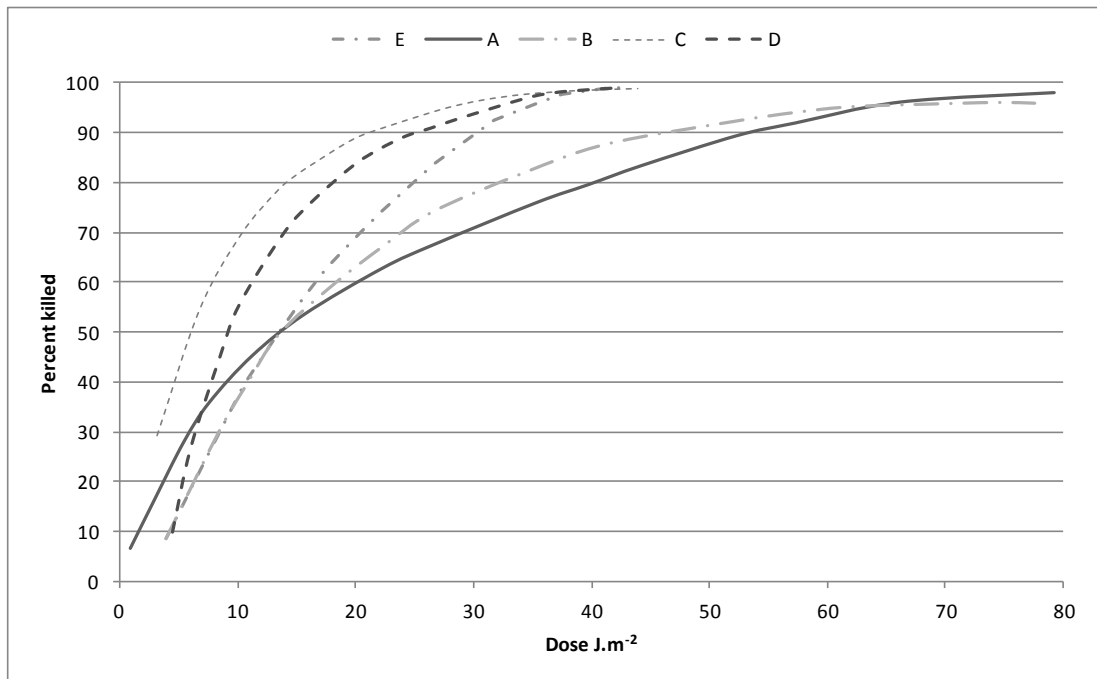
Figure 3.11 *E. coli* resistance to UVC at various pre-treatments. A) normal culture not Pre treated. B) Exponential curve 1-S=E(-ZD). C) Pre exposure to Grenz Rays. D) Pre-exposure to X-rays. E) Pre-exposure to heat, adapted from Rentschler and Nagy (1942).

The divergence on experimental results for the susceptibility of *E. coli* to UV light might be explained by a combination of factors, for example the microorganisms tested were of different strains, pre-treatments affecting the susceptibility of the microorganism and/or inaccurate measuring equipment. Figure 3.12 to Figure 3.15 show how the different clusters behave independently and how the average susceptibility predicts their survival decay.
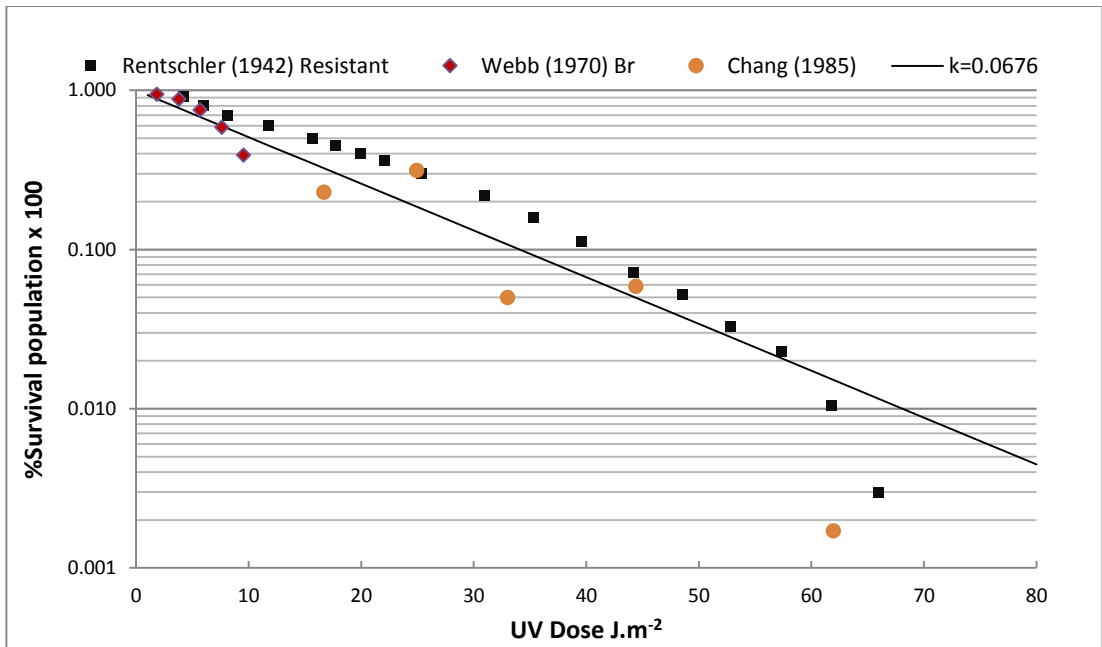
Figure 3.12 Survival E. coli fitted line at k=0.0676 m^2.J^{-1}.
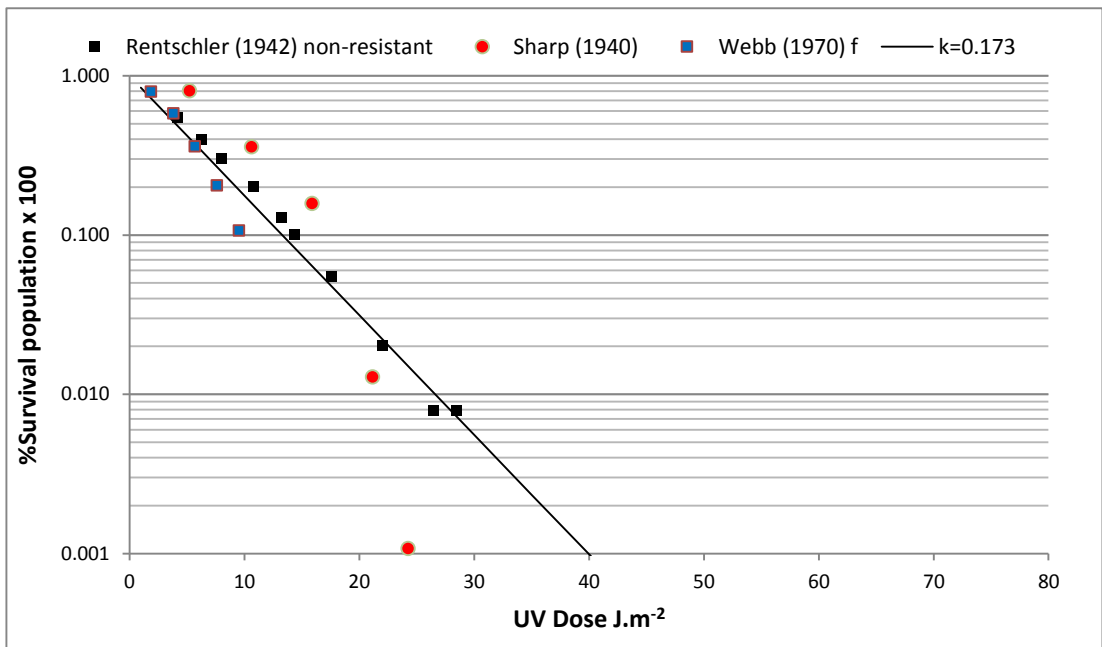
Figure 3.13 Survival E. coli fitted line at k=0.171 m^2.J^{-1}.
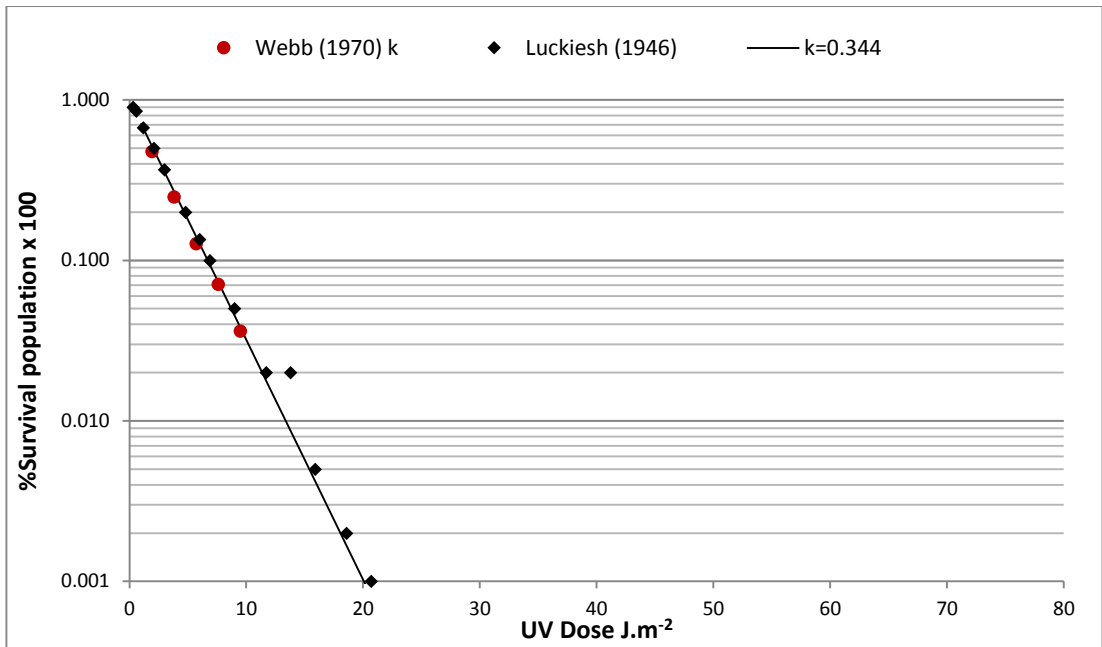
Figure 3.14 Survival E. coli fitted line at k=0.344 $m^2.J^{-1}$.
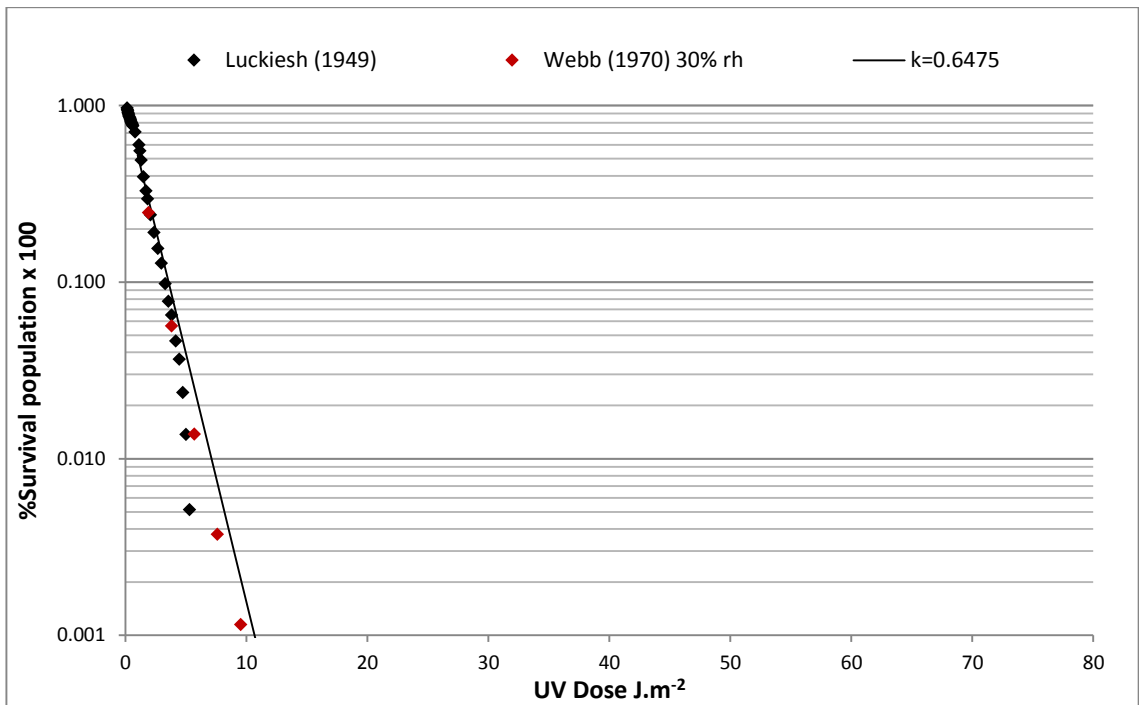
Figure 3.15 Survival E. coli fitted line at k=0.6475 $m^2.J^{-1}$.

In conclusion the susceptibility of *E. coli* to UV light appears to range from 0.0676 $m^2.J^{-1}$ at high humidity to 0.6475 $m^2.J^{-1}$ at low humidity. Though there is a difference between the two susceptibilities of up to 10 times in magnitude, this phenomena was previously noted by Luckiesh et al. (1949) who reported that *E. coli* in dry air was 10 times more susceptible than in highly humid environments. With no further information it is recommended to use the lowest

susceptibility of 0.0676 $m^2.J^{-1}$ for RH of 80-95% and a k=0.173 $m^2.J^{-1}$ for 50-70% RH in a single stage decay model to ensure that independently of the microorganism strain or humidity levels it is eradicated.

3.5.6 *Mycobacterium bovis* BCG

Mycobacteria is a type of Actinobacteria with its own family known as the Mycobacteriaceae (Ryan et al., 2010), the Greek prefix myco which means fungus refers to its ability to grow likewise mold when cultured on the surface of liquids (Kerr and Barret, 2010). *M. bovis* is a type of mycobacterium commonly associated with cattle, nevertheless it has the capability of causing tuberculosis in people (Grange et al., 1996). Sometimes used as an attenuated *M. bovis* strain for tuberculosis vaccination, *M. bovis* is genotypically closely related to *M. tuberculosis*, and appears to be an appropriate surrogate for it (Xu et al., 2003).

At least three studies on the susceptibility of *M. bovis* to UV light can be found in literature. Riley et al. (1976) reported two cultures with two slightly different k values 0.360 $m^2.J^{-1}$ and 0.255 $m^2.J^{-1}$ both values at a RH of 50%. Ko et al. (2000) reported susceptibility values of 0.270 $m^2.J^{-1}$ for Low RH, 0.170 $m^2.J^{-1}$ for Med RH and 0.02 $m^2.J^{-1}$ for High RH, this being the only k value reported at high RH, and Peccia and Hernandez (2004) which showed 0.19 $m^2.J^{-1}$ at 50% RH. Collins (1971) also reported inactivation values for *M. Bovis*, nevertheless the tests were conducted on surface deposition of plates and not airborne inactivation, obtaining a susceptibility value of 0.140 $m^2.J^{-1}$ in agreement with those reported by Ko et al (2000) and Peccia and Hernandez (2004).

The k values for a medium RH range (49 – 69%) reported by Ko et al. (2000) and Peccia and Hernandez (2004) appear to be in good agreement, however the values by Riley et al. (1976) for the same range of RH appear slightly higher, and appear closer to the k value reported by Ko et al. (2000) at lower RH in the range of 22-33%. Table 3-4 shows the complete range of k values for M. bovis BCG.

Table 3-4 Reported UV susceptibility for *M. bovis* BCG

Bacteria	Susceptibility value m².J⁻¹	Relative humidity	Source
M. bovis BCG	0.270	22-33%	Ko et al. (2000)
	0.170	49-60%	Ko et al. (2000)
	0.140	-	Collins (1971)
	0.190	50%	Peccia and Hernandez (2004)
	0.255	50%	Riley et al. (1976)
	0.360	50%	Riley et al (1976)
	0.249	50%	Average
	0.02	85-90%	Ko et al. (2000)

The studies found in literature used relatively low levels of UV dose (up to 10 J.m⁻²) and the survival rates reported where under 1 log reduction (Figure 3.16, Figure 3.17) (Ko et al., 2000, Peccia and Hernandez, 2004, Riley et al., 1976, Collins, 1971). Figure 3.16 shows a spread in the data points collected at 4 J.m⁻² and 8 J.m⁻² (approx.), and for high humidity, the UV susceptibility of *M. bovis* appears to be up to ten times lower (Figure 3.17), nevertheless, in both cases low RH and high RH there is not enough data to plot the complete spectrum of survival to show if there are any shoulders or double stages included. For the looks of Figure 3.17 It might be feasible that a high RH *M. bovis* presents a shoulder in the survival of the population, as a single stage decay if continued with the tendency would require a UV dose of over 300 J.m⁻² for a 3 log reduction, and this is a dosage comparable to those required to eradicate spores.
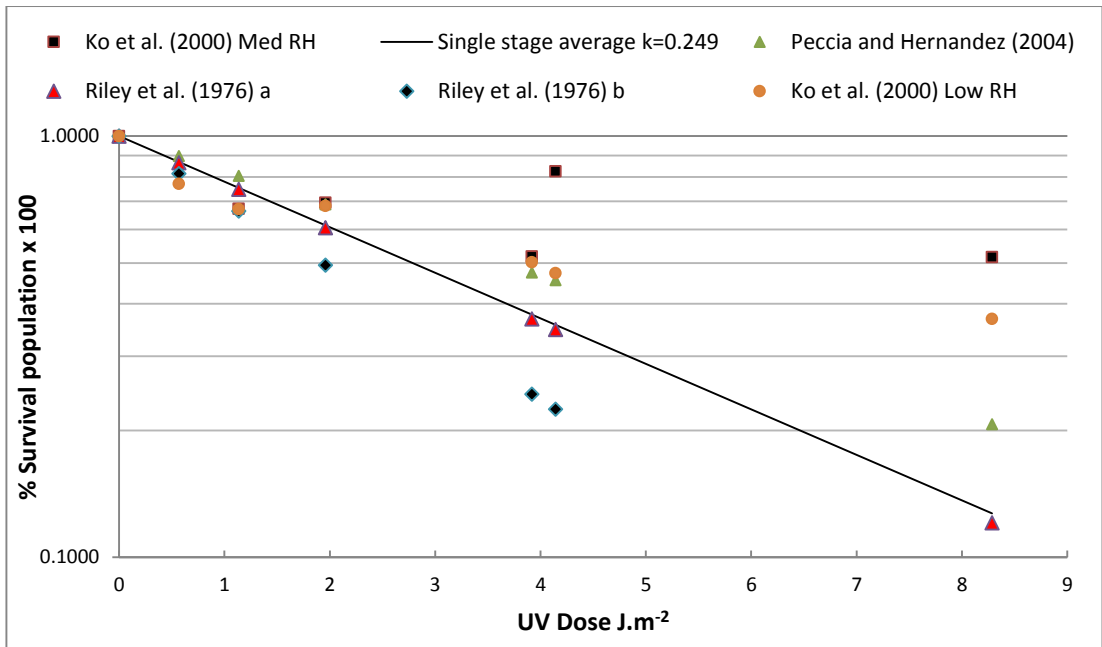
Figure 3.16 Survival of *M. bovis* BCG at 22-60 % RH under UVC light.
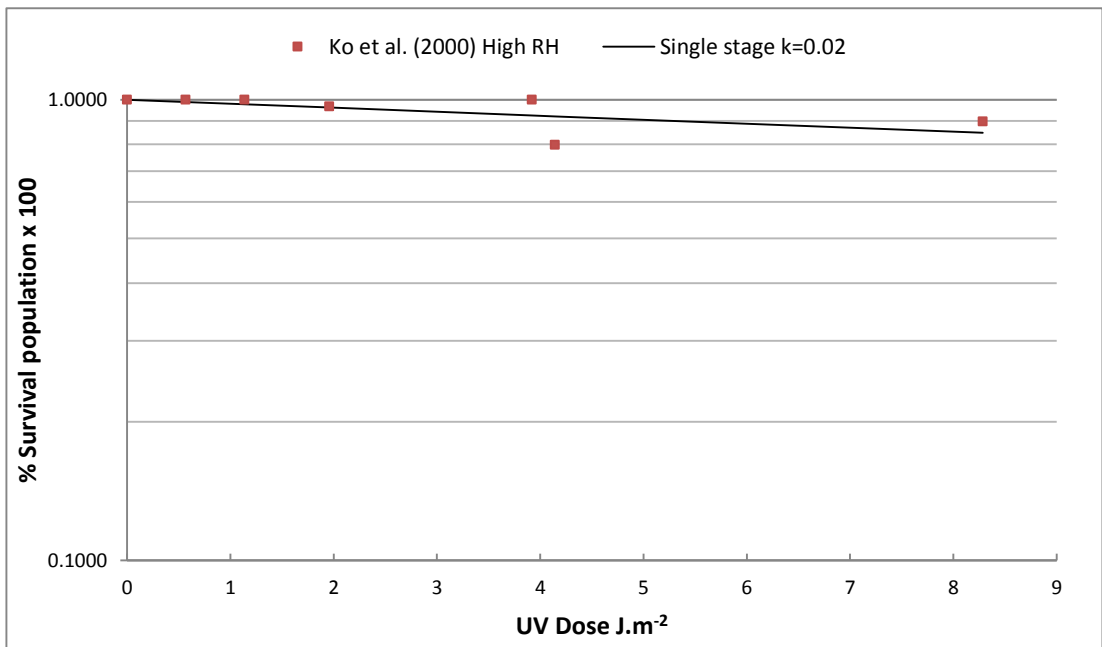
Figure 3.17 Survival of *M. bovis* at 85-90% RH under UVC light.

In conclusion for *M. bovis* BCG for a 22-60% RH it is recommended to use the susceptibility 0.249 $m^2.J^{-1}$ and for 85-90% RH a susceptibility of 0.02 $m^2.J^{-1}$ could be used although further research is needed to determine if a shoulder decay is present at high RH.

3.5.7 *Mycobacterium parafortuitum*

Part of the genus of the *Mycobacterium*, *M. parafortuitum* is gram positive, aerobic bacteria, and forms part of the non-tuberculosis mycobacterium (NTM) group that encompasses all the non *M. tuberculosis* complex. It can be found in water sources either natural or processed and in sewage and dirt (Ho et al., 2012).

In conjunction Peccia and Hernandez (2001), Peccia et al. (2001) and Xu et al. (2003) ran a series of studies where the susceptibility of *M. parafortuitum* for various RH was calculated, this is shown in Table 3-5.

Table 3-5 UV susceptibility values for *M. parafortuitum*

Bacteria	UV Susceptibility $m^2.J^{-1}$	RH	Source
M. parafortuitum	0.200	20-40%	Peccia et al. (2001)
	0.220	20-40%	Peccia et al. (2001)
	0.115	25	Peccia and Hernandez (2001)
	0.175	40	Peccia and Hernandez (2001)
	0.177	40%	Average
	0.120	50%	Xu et al. (2003)
	0.120	50%	Peccia et al. (2001)
	0.150	50%	Peccia et al (2001)
	0.162	50%	Peccia and Hernandez (2001)
	0.126	65%	Peccia and Hernandez (2001)
	0.135	50%	Average
	0.110	80%	Peccia and Hernandez (2001)
	0.100	95%	Peccia and Hernandez (2001)
	0.105	95%	Average

The difference of survival decay between low humidities (<40% RH) k=0.177 $m^2.J^{-1}$ and medium RH (50-65%) k=0.135 $m^2.J^{-1}$ is minimal, to avoid complications it would be better to use the medium RH (50-60%) value for both cases, and for high humidities of over 80% RH a susceptibility value of 0.105 $m^2.J^{-1}$ could be used, and both cases modelled as single stage decay.

3.5.8 *Mycobacterium phlei*

M. phlei is a gram positive rod-shaped, fast-growing, saprophytic bacterium widely distributed in soil and dust and on plants. *M. phlei* has occasionally been associated with disease in humans with a suppressed immune system (Abdallah et al., 2012). UV susceptibility values for *M. phlei* as reported Peccia et al. (2001) were taken from prior studies from Riley et al. (1976), Gillis (1973) and Kethley (1979).

It is important to highlight that Riley et al. (1976) did not used a collimated beam to calculate the UV susceptibility of *M. phlei*, instead it was used a fixture suspended 2 feet below de ceiling in a room where bacteria was injected, this can bring considerable variations as the airflow, dwell time and irradiation intensity cannot be calculated with accuracy, and could bring variations in results. Another reference to the UV susceptibility of *M. phlei* can be found in the study by Collins (1971), the study was ran on the deposition of bacteria on plates, however previous results also from the same study but of *M. bovis* deposited on plates showed good correlation with the results reported in airborne bacteria, this is the only study to show the decay spectrum of *M. phlei* as shown in Figure 3.18.
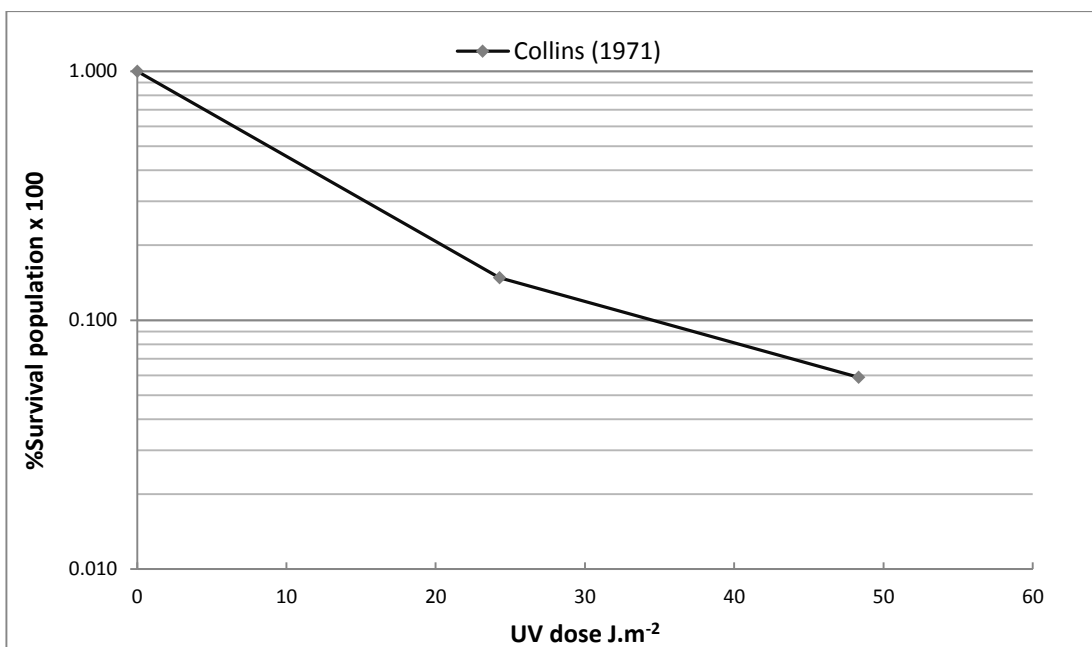
Figure 3.18 Survival population for *M. phlei*.

Table 3-6 shows the summary of susceptibility values found in literature, in conclusion, *M. phlei* at 50% RH shows a UV susceptibility of 0.076 $m^2.J^{-1}$ following a single stage decay.

Table 3-6 UV susceptibilities for *M. phlei*

Bacteria	UV Susceptibility m2.J-1	RH	Source
M. phlei	0.020	50%	Riley et al. (1976)
	0.053	50%	Riley et al. (1976)
	0.100	50%	Kethley (1979)
	0.140	50%	Gillis (1973)
	0.069	-	Collins (1971)
	0.076	50%	Average

3.5.9 *Mycobacterium tuberculosis*

Considered the main causative agent of tuberculosis (TB), *M. tuberculosis* infects the lungs as it requires oxygen to grow (Ryan et al., 2010), its responsible for the largest number of deaths attributable to a single microorganism and approximately one third of the population worldwide is estimated to be infected by it (Boshof et al., 2003).

Despite being one of the main microorganisms UVC devices are used against, information about its UV susceptibility is scarce, mainly due to the dangers involved in testing the bacteria. Peccia et al. (2001) reported a range of susceptibility values at 50% RH of two different strains Erdman strain and the 199RB strain previously published by Riley et al. (1976) which are in the range of 0.230 $m^2.J^{-1}$ to 0.550 $m^2.J^{-1}$. Collins (1971) ran various studies with *Mycobacterium* including *M. tuberculosis*, reporting susceptibilities slightly lower than those of (Peccia et al., 2001), although the studies were ran on surface inactivation, previous susceptibility values reported appear to be in good agreement with those reported in air (see susceptibility of *M. bovis* BCG and *M. phlei* in this study). David et al. (1971) ran studies in surface submerged in water, therefore its results can be considered as 95 - 100% RH, In the same manner, Boshof et al. (2003), ran tests in surface submerged in water for various strains of *M. tuberculosis* and obtaining similar results. Boshof et al. (2003) ran a series of experiments were of strains of *M. tuberculosis* (mc^2 155, pOmsmE2, dnaE2::aph, dnaE2::aph and attB::dnaE2) located on plates were exposed to a dose of up to 50 mJ.cm^{-2} of UVC light, with the main purpose of looking at the genetic mutation of the microorganism, nevertheless reduction rates can be inferred from his research, the summary of his results, and the results of Riley et al. (1976), David et al. (1971) and Collins (1971) are shown in Table Table 3-7.

Table 3-7 Susceptibility values for *M. tuberculosis*

Bacteria	UV Susceptibility m².J⁻¹	RH	Source
M. tuberculosis	0.230	50%	Riley et al. (1976)
	0.420	50%	Riley et al. (1976)
	0.440	50%	Riley et al. (1976)
	0.550	50%	Riley et al. (1976)
	0.107	-	Collins (1971)
	0.350	50%	Average
	0.051 *n=4	95 - 100%	David et al. (1971)
	0.056 *n=4	95 – 100%	Boshof et al. (2003)
	0.036 *n=4	95 – 100%	Boshof et al. (2003)
	0.033 *n=4	95 – 100%	Boshof et al. (2003)
	0.029 *n=4	95 – 100%	Boshof et al. (2003)
	0.041 *n=4	95 – 100%	Average

*n=shoulder value

Based on Boshof et al. (2003) it was noted the appearance of a shoulder of n=4 present at high RH (95-100%), There is the possibility that lower RH also present a shoulder, however results reported by Peccia et al. (2001) which are a reference of prior studies from Riley et al. (1976) only show the final *k* value missing the complete set of data for analysis.
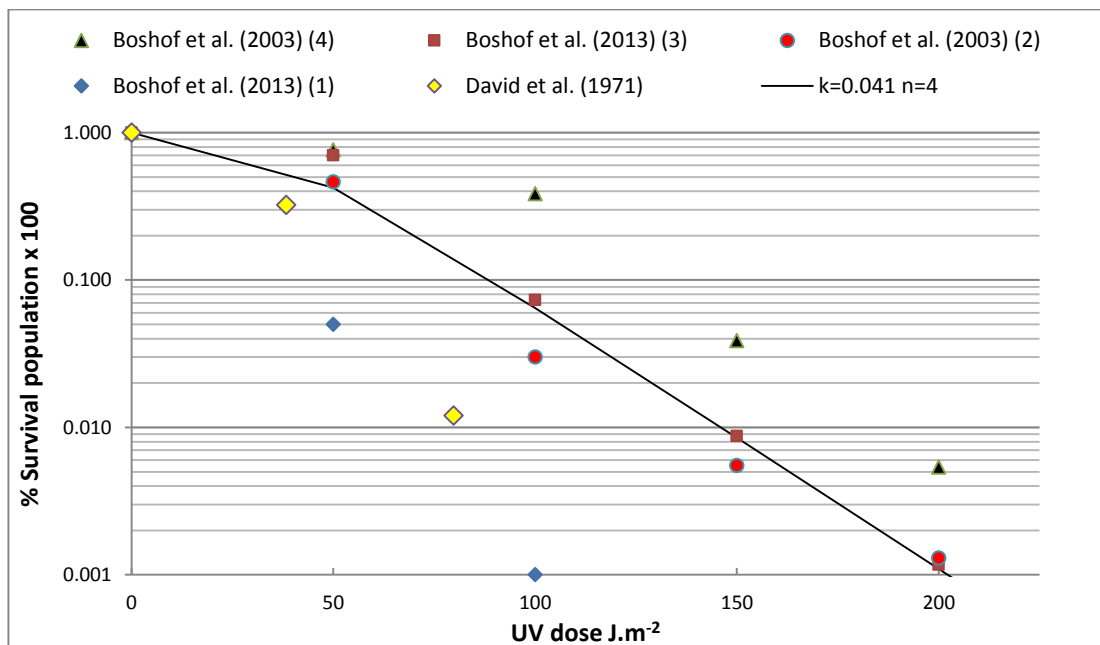
Figure 3.19 Survival of *M. tuberculosis* adapted from Boshof et al. (2003). *n is the shoulder value.

In general the different species of *Mycobacterium* show a relatively low susceptibility to UV light, research is needed to completely plot the population survival over a range of UV dosages to identify the presence of shoulders and the dosage value for a 3 log reduction. Boshof et al.

(2003) identified a shoulder value for *M. tuberculosis*, and results for *M. bovis* suggest the presence of a shoulder for high humidities, with this background it is not outside possibilities the presence of shoulder curves on other types of *Mycobacterium* species.

In conclusion, *M. tuberculosis* at low RH (50%) the value to use for UV susceptibility is 0.350 $m^2.J^{-1}$ to be used in a single stage decay, and for higher RH (95-100%) a susceptibility of 0.041 $m^2.J-1$ with a shoulder n=4 might be used.

3.5.10 *Pseudomonas aeruginosa*

P. aeruginosa is a Gram-negative bacteria commonly found in soil and ground water, *P. aeruginosa* is an opportunistic microorganism, it rarely affects healthy people, and most of times only affects when in prolonged contact with contaminated water. This microorganism is of medical importance as it has become a major cause of both healthcare-associated infections and chronic lung infections in people with cystic fibrosis (England, 2014). *P. aeruginosa* appears to be relatively susceptible to UVC irradiation, with reports of total 99.9% kill rate with a dose of 16 $J.m^{-2}$ (Sharp, 1940). Collins (1971) ran a more exhaustive study on the survival of *P. aeruginosa* to UVC irradiation, with UV dosages of up to 48 $J.m^{-2}$ reporting a kill rate of 99.9 % at 12 $J.m^{-2}$ in single stage decay, to complement the study, values reported by Noakes et al. (2003) also appear to fit within the same average susceptibility values.

Table 3-8 UV susceptibility of *P. aeruginosa*

Bacteria	UV Susceptibility $m^2.J^{-1}$	RH	Source
P. aeruginosa	0.432	95%	Sharp (1940)
	0.412	-	Collins (1971)
	0.550	48%	Noakes et al. (2003)
	0.464	-	Average

P. aeruginosa seems to follow a single stage decay in a relatively consistent manner as seen in Figure 3.20, a *k*=0.464 $m^2.J^{-1}$ in a single stage decay might be good predictor for its survival decay at high RH but also would ensure sterilization levels at low RH.
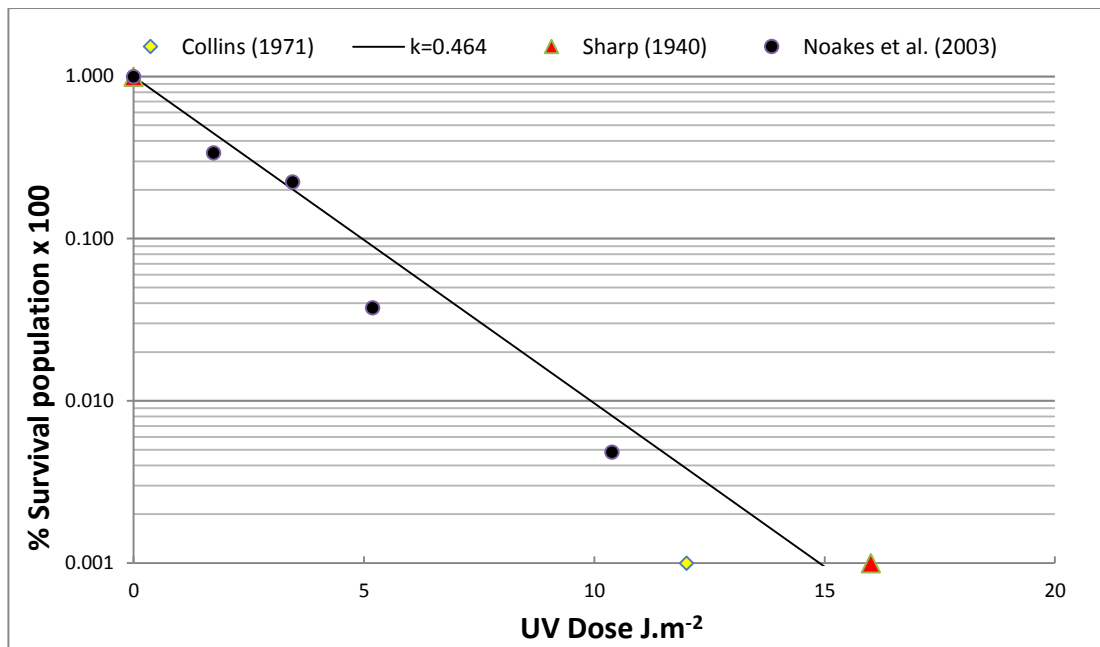
Figure 3.20 Survival of *P. aeruginosa* under UVC light.

3.5.11 *Serratia marcescens*

S. marcescens has been extensively tested for UV susceptibility in air, Kowalski (2009a) reports at least 12 sources which are here discussed and summarised in Table Table 3-9 . Fletcher et al. (2003) shows a comprehensive spectrum of survival rate for *S. marcescens* under various UV dosages at 48% and 78% RH with k=0.527 $m^2.J^{-1}$ and 0.071 m2.J^{-1}. Ko et al. (2000) reported values of dose and survival rates for high humidity (over 60%) and low humidity (under 50%), being k=0.575 $m^2.J^{-1}$ and k=0.02 $m^2.J^{-1}$ respectively, values at low levels of RH appear to follow a single stage decay with a 3 log reduction can obtained with a UV dose of 15 Joules.m^{-2} (Figure 3.21) .
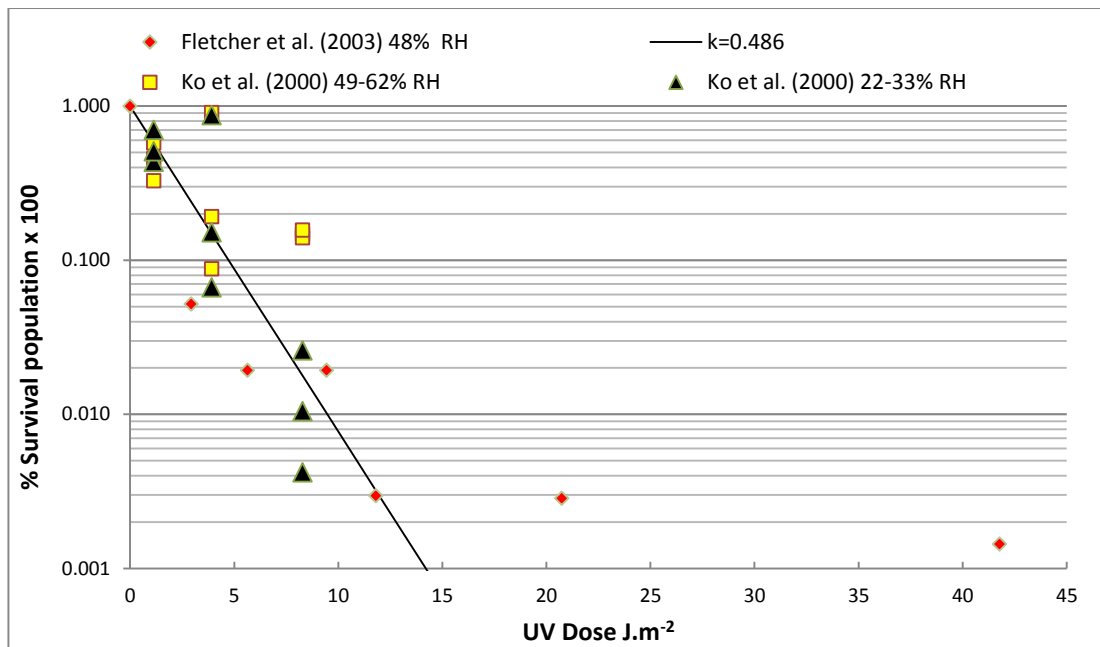
Figure 3.21 Survival for S. marcescens at low- medium humidity levels by Fletcher et al. (2003) and Ko et al. (2000).

Sharp (1940) reported values of k=0.4449 m^2.J^{-1}, based on a single value of the lethal dose of 20.7 J.m^{-2} (27,000 ergs.cm^2) that killed 99.99% of bacteria suspended in air. Peccia et al. (2001) reported a value of k=0.45 m^2.J^{-1} with a 50% relative humidity, in the same research an estimated dose 32.17 +/- 90 J.m^{-2} (3217 +/- 90 µw.cm^{-2}) is proposed for 90% inactivation at 95% relative humidity, regression of the estimated dose at high humidity gives a k=0.07 m^2.J^{-1}, never the less this is an estimated result, and is not supported by experimental data. Lai et al.(2004)reported the susceptibility of *S. marcescens* in various aerosolized media, including air with low and high relative humidity, PBS, serum and synthetic saliva, the susceptibility reported for aerosolised bacteria at 68% relative humidity is k=0.92 m^2.J^{-1}, this is more than twice the values reported by other researchers, for that reason this result will be considered as an outlier, but the record remains in case future research unveils relevant information. VanOsdell and Foarde (2002) used two dosages for the inactivation of 99% and 97% for *S. marcescens*, to be, 13.41 J.m^{-2} and 3.69 J.m^{-2} respectively, with susceptibilities of k=0.343 m^2.J^{-1} and k=0.95 m^2.J^{-1}, here the difference between the k values is more than double, this could be due to the inability to measure kill rates over 99%, after reaching the 99% reduction dosage, further increase on UV power will bring inefficient performance, therefore at 3.69 J.m^{-2} gives 97%, and higher dosages only bring a small amount of reduction, and is not because of the bacteria is resistant to UV light, is just that the reduction threshold has been reached and further reductions are only minimal, as the complete data of the inactivation at 99% is not shown, it seems reasonable to use the average of the two values which is k=0.6425 m^2.J^{-1}.

Table 3-9 UV susceptibilities for *S. marcescens* at different RH

Bacteria	Susceptibility value m²·J⁻¹	Relative humidity	Source
S. marcescens	0.920*	68%	Lai et al. (2004)
	0.575	22–62%	Ko et al. (2000)
	0.527	48%	Fletcher et al. (2003)
	0.45	50%	Peccia et al. (2001)
	0.449	-	Sharp (1940)
	0.430	50%	VanOsdell and Foarde (2002)
	0.486	50%	Average
	0.071	78%	Fletcher et al. (2003)
	0.070	90%	Peccia et al. (2001)
	0.020	85-91%	Ko et al. (2000)
	0.053	78-95%	Average
	Z1=0.25 Z2=0.045 F=0.18 n=5.5	78-95%	This study Two stage with shoulder

*not used in the average Z calculation

Fletcher et al. (2003) reported the full decay spectrum at 78% RH, calculating a k=0.071 m²·J⁻¹ accordingly assuming a single stage decay curve. However the data appears to follow a two stage shoulder decay with values of $k1$=0.25 m²·J⁻¹, $k2$=0.045 m²·J⁻¹, a survival fraction f=0.18 and a shoulder n=5.5. The results reported by Ko et al. (2000) might not be sufficient to account for the complete decay spectrum of *S. marcescens*.

In conclusion for RH up to 60% a k=0.486 m²·J⁻¹ in a single stage decay might be used and for higher RH 70-95% a double stage with shoulder model with values of $k1$=0.25 m²·J⁻¹, $k2$=0.045 m²·J⁻¹, a survival fraction f=0.18 and a shoulder n=5.5 are appropriate.
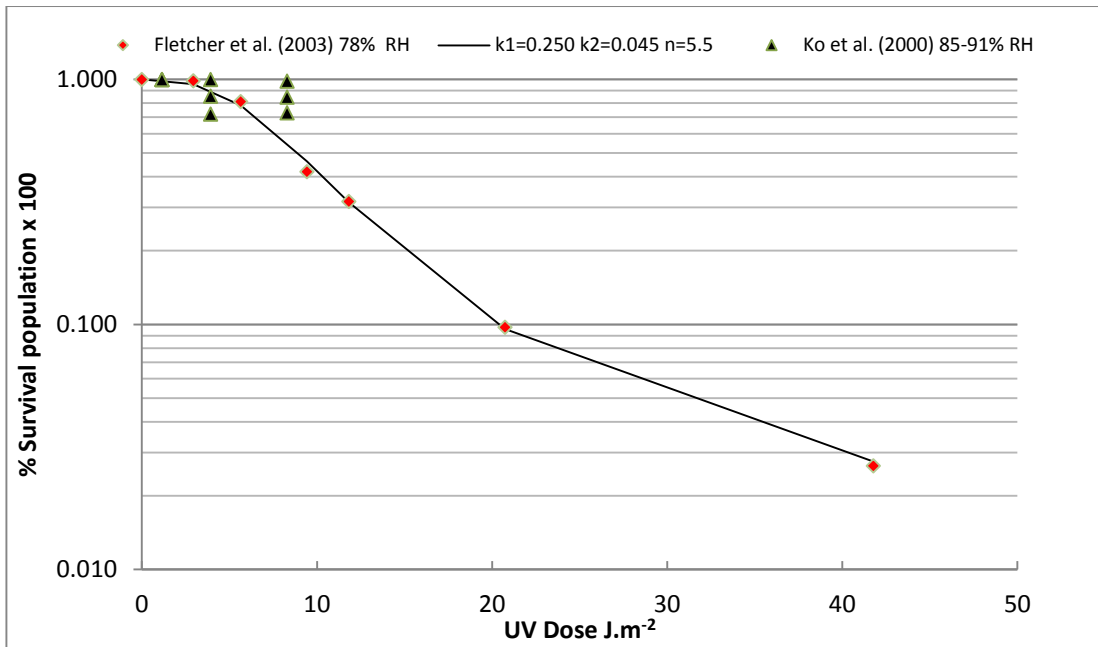
Figure 3.22 Fletcher et al. (2003) and Ko et al. (2000) survival fraction for *S. marcescens* vs calculated survival fractions.

3.5.12 *Staphylococcus aureus*

Usually *S. aureus* is not a problematic bacteria, it colonises human skin and mucosa without causing any problems. Nevertheless, If the bacteria enter the body, illnesses which range from mild to life-threatening may then develop, including skin and wound infections, infected eczema, abscesses or joint infections, infections of the heart valves, pneumonia and bacteraemia (England, 2014). A considerably more dangerous strain of the microorganism is becoming more and more common in hospital environment that is Methilicin resistant *Staphylococcus aureus* (MRSA), which in some cases can result lethal.

Table 3-10 UV Susceptibility for *S. aureus*

Bacteria	UV Susceptibility $m^2.J^{-1}$	RH	Source
S. aureus	1.188	Low	Luckiesh (1949)
	0.152	95%	Sharp (1940)
	0.071	High	Chang et al. (1985)
	0.112	-	Average High humidity

Susceptibility values reported by Sharp (1940) and Luckiesh et al. (1949), 0.152 $m^2.J^{-1}$ at 95% RH and 1.188 $m^2.J^{-1}$ at Low RH respectively differ up to 10 times, nevertheless this is not uncommon as the same phenomena was reported for *E. coli* at different RH (*E. coli* susceptibility in this document). Chang et al. (1985) ran experiments on petri dishes at high humidity levels with a calculated susceptibility of 0.071 $m^2.J^{-1}$ (referenced values can be seen in Table Table 3-10).
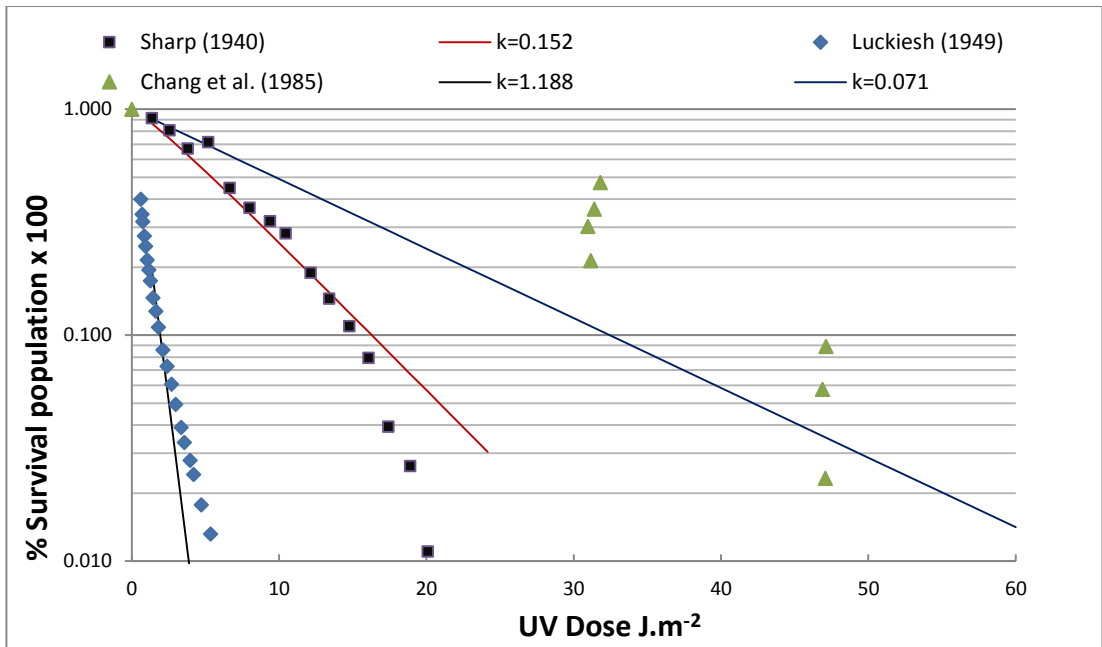
Figure 3.23 Survival for *S. aureus* under UVC light.

It is apparent that RH has a strong correlation with UV susceptibility of *S. aureus*. Figure Figure 3.23 shows that depending on RH (Sharp (1940) at 95% RH, Luckiesh (1949) at low RH, and Chang et al. (1985) at high RH), and while at low RH the susceptibility can be as high as 1.188 $m^2.J^{-1}$ (Luckiesh, 1946) at high RH (95%) the susceptibility decreases up to 10 times to a 0.071 $m^2.J^{-1}$ (Chang et al., 1985).

3.5.13 *Excluded microorganisms*

Francisella tularenss

The UV susceptibility of *Francisella tularensis* was reported by Beebe and Pirsch (1958) and Beebe (1959), in both studies the lamps used were adapted to filter light frequencies under 300 nm and in this manner simulate more close the spectrum of natural sun light, with the latter studies analyzing the effects of RH on bacterial decay. Correlating the reported results to obtain a susceptibility value to germicidal UVC (254 nm) might be difficult and prone to errors, therefore it would be better to run new experimental tests with a standard protocol to accurately calculate the susceptibility of the microorganism.

Pseudomonas fluorescens

The lack of data makes difficult the characterization of UV susceptibility of this microorganism. (VanOsdell and Foarde (2002)) reported a 98% microorganism reduction for a UV dose of 13.41 $J.m^{-2}$ and a 99.7% microorganism reduction for 3.69 $J.m^{-2}$. The fact that a lower UV dose provided a higher microorganism reduction might be the sign of over kill, i.e. the microorganism is been reduced to sterilisation levels and any further UV irradiation will not reduce the microorganism any further. In average the calculated UV susceptibility is 0.933 $m^2.J^{-1}$. The type of survival decay is unknown, the lack of data and more specifically the variation within the reported data makes it difficult to provide an accurate susceptibility value for *P. fluorescens*. In conclusion it is known that a UV dose 3.69 $J.m^{-2}$ might bring a 2-3 log reduction for *P. fluorescens*.

3.6 Conclusions.

Various reports on microorganism susceptibility to UV light were not included in the updated susceptibility review of airborne microorganisms. This is due to reported complex test methods, non-standard units, lack of data, non-reliable measurement techniques and/or age of the report which compromise the reliability of results. Some old reports dating back 50 years or more use methods or techniques too complex or non-standard to nowadays methods, making correlations and/or conversion of units prone to errors and miscalculations, therefore it would be better to run new test and obtain more accurate results.

Microorganism do not have static susceptibilities, instead the susceptibility of a microorganism consist of a range of values (minimum and maximum value) akin to a band width in the susceptibility spectrum.

Summary of results

It was found that most microorganisms in this study followed a single stage decay, the relative humidity of air has a considerably impact on the UV susceptibility of microorganisms and considerations should be taken when designing a UV system as in some cases the UV susceptibility of a microorganism can vary by up to ten times.

In some cases for easiness of results, when the difference on susceptibility is not that different between high and low RH it is preferably to use a single susceptibility value that being the lowest of both.

In real life, the performance of a system might be difficult to calculate, and small differences between single stage and two stage decay might be impractical to calculate, and difference of results between the two models might only be appreciated in lab test results, therefore if convenient calculations might be simplified by using a single stage decay.

Over 80 percent of the microorganisms in this study were sterilised to a 2 log reduction (99%) with a dose of 90 J.m^{-2}, to a 3 log reduction (99%) with a dose of 130 J.m^{-2}, Just for the case of *B. subtilis* and *M. tuberculosis* a UV dose of at least 200 J.m^{-2} might be required for sterilisation levels of more than 2 log reductions.

Table 3-11 UV susceptibility of microorganisms in air

Bacteria	*K m^2.J^{-1} Band width	k1 m^2.J^{-1} Average	k2 m^2.J^{-1} Average	*Shoulder n (width)	Shoulder n	F	% RH
B. subtilis spores / *B. atrophaeus*	0.014 – 0.020	0.017	-	1-3	1.66	-	General
B. subtilis veg cells	0.044 – 0.063	0.053	-	-	-	-	General
B. cepacia	-	0.105	-	-	-	-	>70
B. cepacia	0.05 – 0.61	0.61	0.05	-	-	0.05	50
Ebola	-	0.074	-	-	-	-	-
E. coli	0.056 – 0.091	0.067	-	-	-	-	>70
E. coli	0.160 – 0.182	0.173	-	-	-	-	50
M. bovis BCG	0.170 – 0.360	0.249	-	-	-	-	50
M.bovis BCG	-	0.020	-	-	-	-	>70
M. parafortuitum	0.115 – 0.220	0.135	-	-	-	-	50
M. parafortuitum	0.100 – 0.110	0.105	-	-	-	-	>70
M. phlei	0.020 – 0.140	0.076	-	-	-	-	50
M. tuberculosis	0.107 – 0.550	0.350	-	-	-	-	50
M. tuberculosis	0.029 – 0.056	0.041	-	4	4	-	>70
P. aeruginosa	0.412 – 0.550	0.464	-	-	-	-	>70
S. marcescens	0.430 – 0.575	0.486	-	-	-	-	50
S. marcescens	0.045 – 0.25	0.25	0.045	-	5.5	0.18	>70
S. aureus	-	1.18	-	-	-	-	50
S. aureus	0.071 – 0.152	0.112	-	-	-	-	95

*Used in Monte-Carlo analysis

When band width values are not available, use values of K1-K2
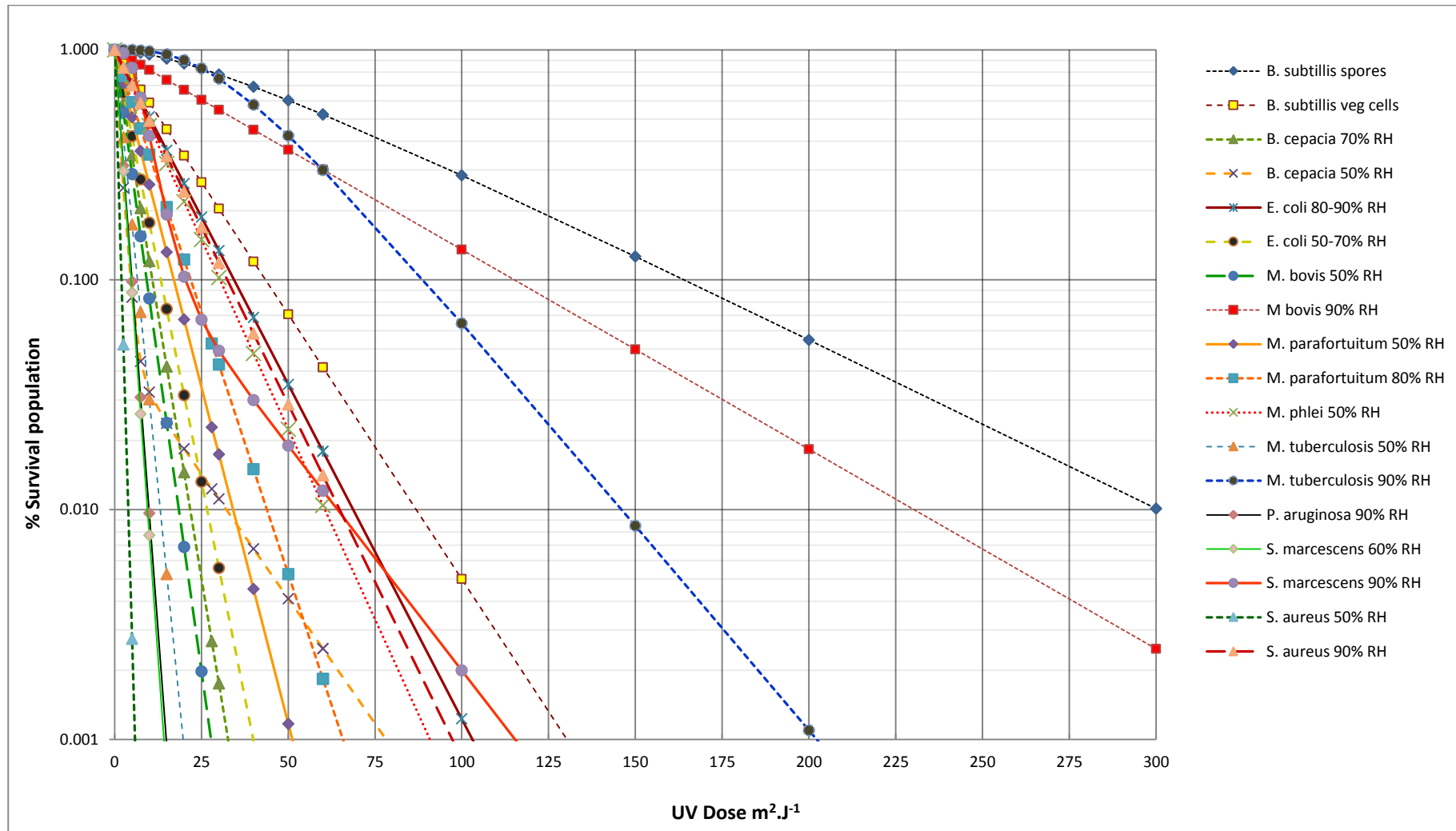
Figure 3.24 Summary of survival decays of airborne microorganisms under UVC light.

The figure legend lists the following:

- B. subtillis spores
- B. subtillis veg cells
- B. cepacia 70% RH
- B. cepacia 50% RH
- E. coli 80-90% RH
- E. coli 50-70% RH
- M. bovis 50% RH
- M bovis 90% RH
- M. parafortuitum 50% RH
- M. parafortuitum 80% RH
- M. phlei 50% RH
- M. tuberculosis 50% RH
- M. tuberculosis 90% RH
- P. aruginosa 90% RH
- S. marcescens 60% RH
- S. marcescens 90% RH
- S. aureus 50% RH
- S. aureus 90% RH

Axes: X-axis — UV Dose m².J⁻¹; Y-axis — % Survival population

Chapter 4. UV Irradiation Modelling.

4.1 Introduction.

Irradiation modelling has been considered by a number of researchers looking to quantify performance of UV disinfection in air and in water. Current literature lists a number of irradiation models, and each of them with specific characteristics that can appeal for the specific intended task. This ranges from a quick approximation, a simple design assuming constant characteristics to sophisticated models that account for airflow patterns and physical variations.

This chapter presents a review of the different irradiation models, starting by explaining basic concepts on irradiation, such as the inverse square law and the use of solid angles. The chapter then continues to explain the different types of irradiation models dividing them by Trigonometric methods and the Radiative Transfer Equation (RTE).

Finally this chapter explains the Discrete ordinates method which solves the RTE in a numerical simulation, and is used for the calculation of UV irradiation in the CFD commercial software ANSYS, described in Chapter 5.

4.2 The need for irradiance models.

Mathematical modeling of UV irradiation in a reactor is essential for its performance calculation and further optimization. UV Irradiation models attempt to represent a 3D light field in the UV-C wavelength, which is determined by the lamp and fixture geometry, the UV output of the lamp and the reflections from the surfaces in the vicinity of the lamp. It is essential for any UV irradiation model to capture the spatial distribution of UV light and the influence of all the different parameters that affect it. For that reason UV irradiation models have been widely debated in the literature, and yet, a definitive solution does not exist (Ho, 2009b, Lau, 2009, Wang et al., 2008, Liu et al., 2007, Kowalski et al., 2001, Bolton, 2000, Blatchley, 1997, Irazoqui et al., 1976). The debate continues, and various models have shown virtually the same level of accuracy. Nevertheless within a photoreactor, phenomena such as reflection, refraction, absorption, scattering and shadowing can have a great impact on final approximations (ANSYS, 2009, Kowalski et al., 2001, Bolton, 2000).

Irradiation models can be divided in two types, the trigonometric models and energy based models. Trigonometric models are based on the mathematical relationship of irradiation angles and surfaces and do not account for physical considerations such as light absorption, emission

or scattering. These models are based on the Inverse Square law and include Point Source models (Bolton, 2000, Irazoqui et al., 1976), Line Source model (Irazoqui et al., 1976) and view factor models (Kowalski, 2009). In general these types of models tend to be simpler and represented analytically.

Physical models such as the Radiative Transfer Equation (RTE) represent propagation of radiation through a media, and states that as a beam of radiation travels it loses energy to absorption, gains energy by emission, and redistribute energy by scattering (Cassano et al., 1995). The RTE also follows the inverse square law for energy transmission, with the difference from analytical model being that it accounts for reflection, refraction and absorption In general these methods are more physically realistic, but more complex requiring computational solutions.

Before reviewing the Irradiation models, it is important to revisit the concepts of Inverse Square Law (ISL) and Solid Angles as these themes will be widely used.

4.2.1 Inverse Square Law

The ISL based on Newton's law of universal gravitation. In simple terms it states that a specific physical quality or strength is inversely proportional to the square of the distance from the source (Figure 4.1) (Equation 4-1).

$$Intensity \propto \frac{1}{distance^2}$$

<div align="right">**Equation 4-1**</div>

ISL applies generally when a force or energy is radiated in a normal direction radially from a point source onto a three-dimensional space. It has been widely used on gravitational problems, electrostatic (Coulomb's law), lighting and telecommunications (Ryer, 1998).
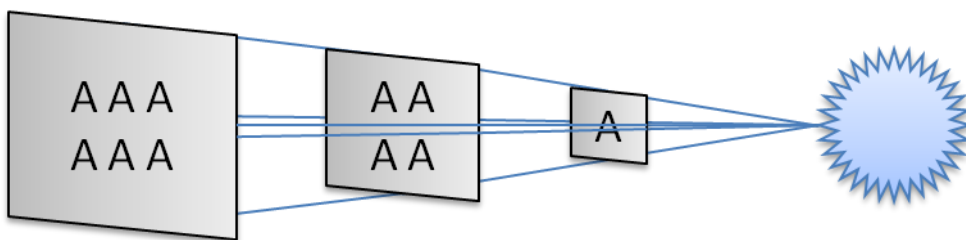
Figure 4.1 Propagation of energy according to the Inverse square law.

4.2.2 Solid angle

The solid angle, Ω, is the two-dimensional angle in three-dimensional space that an object subtends at a point. It is a measure of how large that object appears to an observer looking from that point and is expressed in steradian (sr). The solid angle, Ω, of a sphere in steradians, is equal to the spherical surface area, A, divided by the square of the radius, r (m).

$$\Omega = A/r^2$$

Steradians are dimensionless units, defined as the solid angle that has its vertex at the centre of a sphere which cuts out a spherical surface area equal to the square of the radius of the sphere; any sphere contains 4π steradians. (Ryer, 1998). A steradian of sr =1 is equivalent to a surface area of A=r² as shown in Figure 4.2.
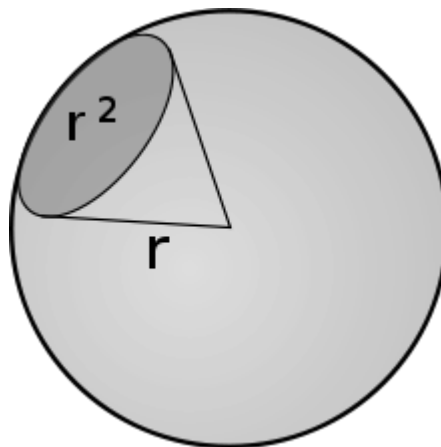
Figure 4.2 Graphical representation of 1 steradian (sr = 1).

4.3 Irradiation models.

This section outlines the trigonometric models used to calculate the irradiation of light at a single point including include a simple approximation of the irradiation field by the use of the inverse square law, and an irradiation model slightly different to the previous described which uses the view factor (VF), a revision on the Extense Source Radiation model (ESM), the Point Source model (PS) the Line Source model (LS) and the Three Dimensional Source model (TDS). Finally this section describes the use of the Radiative transfer model (RTE) which has become more popular, as it includes the possibility to account for particle Fluence, and if required, chemical reactions.

4.3.1 Inverse Square and View Factor Irradiation models in literature

Beggs (2000) used a geometrical representation of a two sectional lamp (Figure 4.3) to model the irradiance (E) of UV light as the inverse relation of irradiation and distance (Equation 4-3).
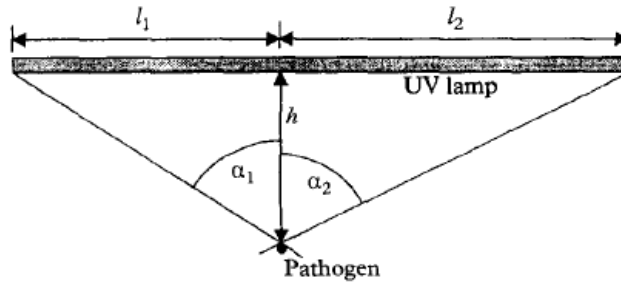
Figure 4.3 Plan view of a two sectional representation of a UV lamp (Beggs, 2000)

$$E = \frac{I_0(\sin\alpha_1 + \sin\alpha_2)}{(L_1 + L_2)h}$$

Equation 4-3

This model only considered direct irradiation and did not considered any reflections as they appeared difficult and unreliable to quantify. The model under-predicted the irradiation performance, but this favours a 'worse-case scenario' thus ensuring a safety margin that was integrally built in (Beggs et al., 2000). Moreover, the model considered particles as flat surfaces differentials, not as spherical bodies receiving a fluence of energy.

The view factor model was proposed by Kowalski et al. (2001) as it was found that the inverse square algorithm alone appeared to be insufficient to accurately calculate irradiation at close distances from the lamp; this is an important issue as most of the in-duct UV germicidal irradiation systems are designed to work at close proximity from the lamps (Beggs et al., 2000). To deal with this issue Kowalski, Bahnfleth et al. (2001) employed the view factor model for the transmission of thermal radiation. Such approach is based on thermal radiation view factors that define the amount of diffuse radiation transmitted from one surface to another (Kowalski et al., 2001). Figure 4.4 shows the comparison between the View factor (VF) calculation and the Inverse square law (ISL) for the UV irradiation power at different distances from the centre of the lamp. It can be seen that when close to the lamp, the ISL tends to over predict slightly the irradiation power, and as distance keeps increasing the same ISL tends to under predict the UV irradiation power. In the same manner the VF calculation slightly under predicts the measured

irradiation as the distance increases but it is evident that the accuracy is still better than that of the ISL.
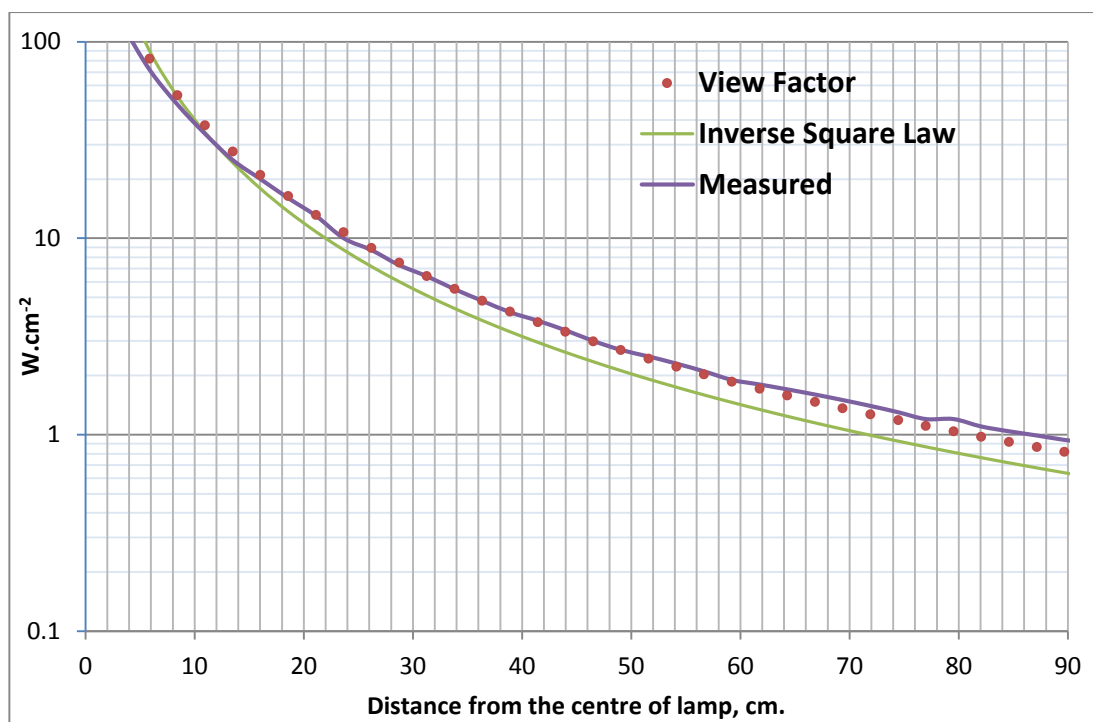
Figure 4.4 Comparison of View factor vs Inverse square law (Kowalski, 2009).

Almost at the same time, Bolton (2000) employed the multiple point source summation (MPSS) to model UV irradiation. The model principle assumes that the emission of a linear lamp is equivalent to that of n point sources spaced equally along the axis of the lamp, where the power output of each point source is F/n, with F being the total UV power output of the linear lamp. The overall value is then the sum of the values calculated for each of the n point sources. This model was then refined by the Multiple segment source summation (Bolton and Cotton, 2001) currently available as a stand-alone software UVCalc3D (Bolton Photoscience Inc., 2011).

4.3.2 Extense Source Radiation model (ESM)

Early records of UV irradiation models note the difficulties relating to lamp sizes, photoreactor design parameters and the need to develop a realistic consideration of the energy source (Irazoqui et al., 1973). After analyzing various Line Source models Irazoqui, Cerda et al. (1973) worked on the development of an Extense Source radiation model (ESM) . Line Source (LS) models assumed ideal lamps represented by a straight line projected as a point on perpendicular planes, and were attractive due to their simplicity and their relatively straight forward formulation; The Extense Source model (ESM) attempted to predict irradiation distribution in space as a function of the spatial coordinate system, this allowed the calculation of radiation

flux density values at any point inside the reactor and its optimisation if the characteristics of the lamp and reactor were known, something not possible with other Line Source models. Nevertheless Irazoqui, Cerda et al. model did not account for absorption and dispersion.

For the ESM the total energy per unit area and unit time over a differential of the area from all directions in space and from the whole volume of a lamp is represented in Equation 4-4

$$Q_{(z0,r)} = k \int_\theta d\theta \int_\phi d\phi \int_\rho \sin^2\theta \, \cos\phi \, d\rho$$

Where , ρ = radius (cm) or spherical coordinate (sr), ϕ = spherical coordinates in radians, θ = spherical coordinates in radians, k = lamp emissions.

The limits for ρ for any θ, ϕ directions are expressed in Equation 4-5.

$$\rho_{1\,2} = \frac{r\cos\theta \mp [r^2\cos^2\phi - r^2 + r_{l^2}]^{1/2}}{\sin\theta}$$

And the limits for θ in Equation 4-5 and Equation 4-6.

$$\theta_1(\phi) = tg^{-1}\left[\frac{r\cos\phi - [r^2(\cos^2\phi - 1) + r_{l^2}]^{1/2}}{(L - Z_0)}\right]$$

$$\theta_2(\phi) = tg^{-1}\left[\frac{r\cos\phi - [r^2(\cos^2\phi - 1) + r_{l^2}]^{1/2}}{-Z_0}\right]$$

The limits for ϕ in Equation 4-8

$$-\phi_1 = \phi_2 = \cos^{-1}\left[\frac{(r^2 - r_{l^2})^{1/2}}{r}\right]$$

The final radiant energy equation would be as follows:

$$Q = 2x \int_{\phi_1}^{\phi_2} [r^2\cos^2\phi - r^2 + r_{l^2}]^{1/2} \, [\cos\theta_1(\phi) - \cos\theta_2(\phi)] \cos\phi \; d\phi$$

<div align="right">**Equation 4-9**</div>

An important significance of this model was its ability to predict a finite flux density at the centre of the lamp.

Irazoqui, Cerda et al. (1976) advanced their research on the irradiation model and published a new analysis of radiation field properties where they showed that depending on the radiation model (point, line or spatial dimension) any property related to specific intensity will have a different definition and/or formulation. Their research presented three models for irradiation, the Point Source (PS) model, the Line Source with emission in parallel planes perpendicular to the lamp axis (LSPP), and the Three-dimensional source models (TDS). The development of these models was based upon dEv being constant in a diactinic medium, and the radiation flux density through a transverse area be given by:

$$dq_\nu = \frac{\partial q}{\partial \nu} d\nu = \frac{dE_\nu}{dA} = \frac{dE_\nu}{dA_T} = \frac{dE_\nu}{d\alpha_1 d\alpha_2 R_1 R_2}$$

<div align="right">**Equation 4-10**</div>

Where, E= differential flow rate, A= area in cm^2, q= radiation flux density in Einsteins cm^{-2} S^{-1}, ν=frequency, T= denotes transverse area and α= angle.

This is a brief introductory description of the basis for the PS, LSPP and the TDS models that will be explain in more detail below.

4.3.3 Point Source model (PS)

The Point Source (PS) model (Irazoqui et al., 1976) represents energy as being irradiated from a point (Figure 4.5) .
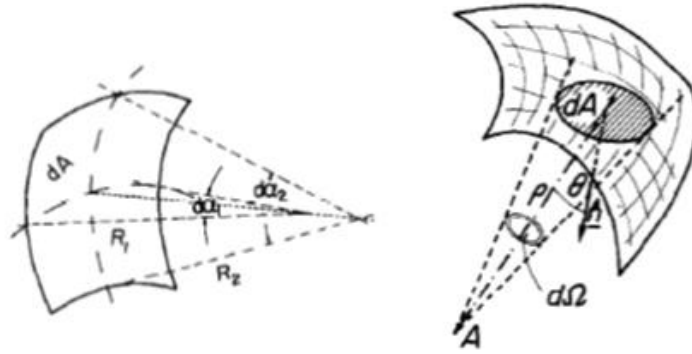
Figure 4.5 Point source irradiation diagram. Illustration from Irazoqui et al. (1976).

In such scenario R1=R2=ρ therefore from Equation 4-10 we obtain:

$$dq_v = \frac{dE_v}{d\alpha_1 d\alpha_2 \rho^2}$$

<div align="right">**Equation 4-11**</div>

Where, dq_v= Radiation flux density differential (W.mol^{-1}.cm^{-2}) and ρ = radius (cm) or spherical coordinate (sr). Equation 4-11 shows the factor $\frac{dE_v}{d\alpha_1 d\alpha_2}$ is independent of the distance travelled by light, for a spherical surface $d\alpha_1 d\alpha_2 = \sin\theta\, d\theta\, d\phi = d\Omega$ therefore by definition such factor represents the specific intensity (I), which leads to

$$I'_v d_v = \frac{dE_v}{d\Omega}$$

<div align="right">**Equation 4-12**</div>

Where, I'_v = Intensity at frequency v (W.cm^{-2}.mol^{-1}.sr^{-1}) for the PS model, d_v= Frequency differential, dE_v= Energy flow rate differential (W/mol), and $d\Omega$= Solid angle differential (sr).

Being the specific intensity the total energy irradiated by the point source, and the energy flow rate being the energy received by a particle in space through its solid angle. Finally the radiation density flux is defined by:

$$dq_v = \frac{I'_v dv}{\rho^2}$$

<div align="right">**Equation 4-13**</div>

For the PS model, It was concluded that it emits a finite amount of energy per unit time and the flux density at the centre of the lamp ($\rho \rightarrow 0$) is infinite.

4.3.4 Line Source with emission in parallel planes perpendicular to the lamp axis (LSPP)

The Line Source with emission in parallel planes perpendicular to the lamp axis (LSPP) model projects the irradiation as a line differential (Figure 4.6). The model is simple and attractive to use, nevertheless it has little physical meaning since every point of the source irradiates in perpendicular planes to the lamp axis (Irazoqui et al., 1976).
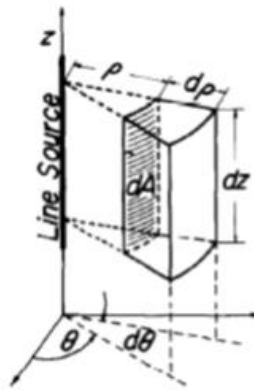
Figure 4.6 Geometry illustration of Line source in parallel planes. Image from Irazoqui et al. (1976).

In this model $d\alpha1 = d\theta$, $R1 = \rho$ and $R2d\alpha2 = dz$. From the interpretation of Equation 4-10 we obtain:

$$dq_\nu = dE_\nu/\rho \; d\theta \; dz$$

<div align="right">**Equation 4-14**</div>

The factor $dE_\nu / d\theta \; dz$ shown in Equation 4-14 is independent of the distance ρ, therefore the specific intensity (I) is described as

$$dE_\nu/d\theta dz = I''_\nu d\nu$$

<div align="right">**Equation 4-15**</div>

Where, I''_ν = Intensity at frequency ν (W.cm^{-2}.mol^{-1}.sr^{-1}) for the LS model, and d_ν = Frequency differential.

$$dq_\nu = \frac{I''_\nu d\nu}{\rho}$$

Finally the energy flow rate is represented as follows:

$$dE_\nu = I''_\nu d\nu \, d\theta \, dz = dq_\nu \, \rho \, d\theta \, dz = \left(\frac{I''_\nu d\nu}{\rho}\right) \rho \, d\theta \, dz$$

The conclusions for the LSPP model are similar to those of the PS, emits a finite amount of energy per unit time and the flux density at the centre of the lamp ($\rho \rightarrow 0$) is infinite. Blatchley (1997) worked on the development of a new Line Source Integration (LSI) model that was a continuous version of the Point Source Summation (PSS) model in which a lamp was simulated as a series of co-linear point sources of radiation. Basically the LSI model is a finite form of the LS model and both were mathematically identical in the limit as n $\rightarrow \infty$, and when finite solutions did not exist, numerical algorithms allowed convergence within specified limits.

4.3.5 Three-Dimensional Source model (TDS)

When three-dimensional emitting and receiving components are present, it is necessary to use two area differentials as part of the mathematical expression. The Three-dimensional source models in diactinic medium (TDS) considers a finite amount of radiation per unit time, thus the energy per unit time emitted by the radiation surface must be infinitesimal (Figure 4.7).
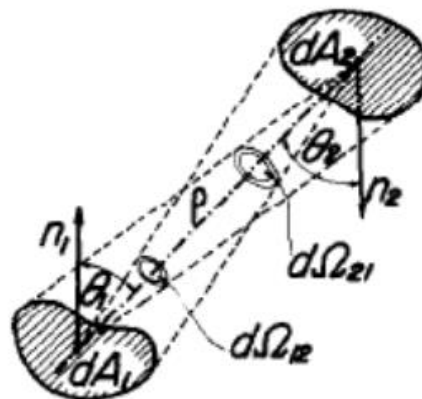
Figure 4.7 Illustration of the geometry of the TDS model. Image from Irazoqui et al. (1976).

This is one of the difference from the PS and LSPP model (Irazoqui et al., 1976). The equations related to the TDS are as follows:

$$dE_\nu = I_\nu d\nu \; dA_1 \cos\theta_1 \; \frac{dA_2 \cos\theta_2}{\rho^2}$$

<div align="right">**Equation 4-18**</div>

Where the term $I_\nu d\nu$ represents the specific intensity, $dA_1 \cos\theta_1$ is the area of the emitter and $\frac{dA_2 \cos\theta_2}{\rho^2}$ is the solid angle of the irradiated surface. Therefore Equation 4-18 can be rewritten as:

$$I_\nu d\nu = \frac{dE_\nu \rho^2}{dA_1 \cos\theta_1 \; dA_2 \cos\theta_2}$$

<div align="right">**Equation 4-19**</div>

And

$$dq_\nu = \frac{dE_\nu}{dA_2} = I_\nu d\nu \; \cos\theta_2 \; d\Omega_{2,1}$$

<div align="right">**Equation 4-20**</div>

The solid angle with origin in the receiving area sustained by the emission area at position ρ is represented by $d\Omega_{2,1}$.

As opposed to the PS and the LS models (infinite irradiation at the source) the TDS model did not introduce singularities in the prediction of radiation flux density at any point in space. Another characteristic of the TDS is the infinitesimal emission of energy in a manner in which the whole surface has a finite emission, as opposed to a finite emission by a point like in the PS model. Another interesting contribution from Irazoqui, Cerda et al. (1976) was the introduction of the local volumetric rate of energy absorption (LVREA) to consider the absorption of energy as a kinetic process and has units of Joules.mol^{-1}.cm^{-3}.sec^{-1} or Watts.mol^{-1}.cm^{-3}. For the PS, LSPP and TDS model the LVREA is represented by Equation 4-21.

$$de^a = \frac{dE_\nu^a}{dV} = \mu_\nu |dq_\nu|$$

<div align="right">**Equation 4-21**</div>

Where, de^a= Volumetric rate of energy absorption, dE^a_v= Absorbed energy flow rate, and dV= Volume differential.

4.3.6 Radiative Transfer Model (RTE)

Now, taking a jump a few years ahead, Cassano, Martin et al. (1995) used an alternative approach, the Radiative Transfer equation (RTE), to model the UV irradiation and chemical reactions in a photoreactor. When the smallest size characteristic, for example the diameter of the irradiated particle, is large compared with the wavelength and the range of times associated with frequencies, the radiation phenomena can be analysed from a macroscopic view. In this method the propagation of photons can be represented by a series of rays in which photons from all directions (not only normal to the surface) can be considered. Moreover, the RTE accounts for the energy transmitted through, emitted by, or reflected on the analysed surface. The final form of the equation employed by Cassano, Martin et al. (1995) integrates the irradiation over the whole solid angle of a particle in space and accounts for all the emissions, reflections and scattering (by wavelength).

To understand the extent of the RTE it is necessary to review the basic irradiation concepts in which it's built. In its simplest form the radiant energy E is represented by Equation 4-22

$$E = I.A.\Omega$$

<div align="right">**Equation 4-22**</div>

Where, I= Irradiation (W), A = Area (m^2), and Ω = Solid angle (sr). Irradiation (I_v) is the amount of radiative energy of frequency 'v' streaming through a unit area perpendicular to the direction of propagation Ω, per unit time and unit frequency (Equation 4-23)

$$I_v = \left(\frac{dE}{dA \; cos\theta \; d\Omega \; dt \; dv} \right)$$

<div align="right">**Equation 4-23**</div>

Where, dE= differential of Radiative energy, dA= Area differential, dΩ = Solid angle differential, dt= Time differential, and dv= Frequency differential.

When the irradiation is integrated through all the solid angles of a particle assuming a spherical shape we get the incident irradiation (G_v) (Equation 4-24).

$$G_v = \int_{\Omega} I_v \, d\Omega$$

$$G_v = \int_{\theta_1}^{\theta_2} \int_{\phi_1}^{\phi_2} I_v \sin\theta \, d\phi \, d\theta$$

The difference between I_v (irradiance) and G_v (fluence) is that the first considers only the irradiation about the direction of propagation, while the second considers the irradiation from all directions. In this manner LVREA is defined as the spectral absorbed incident irradiation as Equation 4-26.

$$e_v^a(\boldsymbol{x}, t) = \kappa_v(\boldsymbol{x}, t) G_v(\boldsymbol{x}, t)$$

Being κ_v the volumetric absorption coefficient, this is a function of the concentration of the absorbing species. Finally rearranging Equation 4-25 and Equation 4-26 we obtain Equation 4-27.

$$e^a = \int_{\theta_1}^{\theta_2} \int_{\phi_1}^{\phi_2} \kappa_v I_v \sin\theta \, d\phi \, d\theta$$

Considering the photons travelling within the same path of the solid angle of propagation dΩ in the direction $\boldsymbol{\Omega}$, within a surface area $\mathcal{A}$ that bounds the volume $\mathcal{V}$, the photon balance for the RTE would be as follows:

$$\begin{vmatrix} \text{time rate of change} \\ \text{of } \boldsymbol{\Omega}, v \text{ photons in} \\ \text{the volume } \mathcal{V} \end{vmatrix} + \begin{vmatrix} \text{net flux of } \boldsymbol{\Omega}, v \text{ photons} \\ \text{leaving the volume } \mathcal{V} \\ \text{across the surface } \mathcal{A} \end{vmatrix} = \begin{vmatrix} \text{net gain of } \boldsymbol{\Omega}, v \text{ photons owing to} \\ \text{emission, absorption, in} - \text{and} - \text{out} \\ \text{scttering in the volume } \mathcal{V} \end{vmatrix}$$

The general form of the radiation conservation is represented in Equation 4-28.

$$\frac{1}{c}\frac{\partial I_v}{\partial t} + \nabla \cdot \left(I_{\Omega, v} \boldsymbol{\Omega} \right) = -W_{\Omega, v}^a + W_{\Omega, v}^e + W_{\Omega, v}^{s-in} - W_{\Omega, v}^{s-out}$$

Where, c = speed of light, $W_{\Omega,v}^a$ = Change in energy due to absorption, $W_{\Omega,v}^e$ = Change in energy due to emission, $W_{\Omega,v}^{s-in}$ = Change in energy due to in-scattering and $W_{\Omega,v}^{s-out}$ = Change in energy due to out-scattering. With each of the terms having a constitutive equation, the first term in Equation 4-28 is usually neglected as the 1/c factor makes it very small to have any considerable effect (Cassano et al., 1995). For absorption we have that:

$$W_{\Omega,v}^a = \kappa_v(\boldsymbol{x},t) I_{\Omega,v}(\boldsymbol{x},t)$$

<div align="right">**Equation 4-29**</div>

Where, $\kappa_v(\boldsymbol{x},t)$=Linear or volumetric absorption coefficient.

The loss of energy due to change in direction (**Ω**) or frequency (v) by the interaction with matter is referred as out-scattering, and represented by Equation 4-30:

$$W_{\Omega,v}^{s-out} = \sigma_v(\boldsymbol{x},t) I_{\Omega,v}(\boldsymbol{x},t)$$

<div align="right">**Equation 4-30**</div>

Where, $\sigma_v(\boldsymbol{x},t)$= Linear volumetric scattering coefficient.

Emission of energy by a body external to the source of radiation can also be present, and is represented by Equation 4-31:

$$W_{\Omega,v}^e = j_v^e$$

<div align="right">**Equation 4-31**</div>

$$j_v^e = \kappa_v(\boldsymbol{x},t) I_{v,b}[\mathrm{T}(\boldsymbol{x},t)]$$

<div align="right">**Equation 4-32**</div>

Where $I_{v,b}[\mathrm{T}(\boldsymbol{x},t)]$, is obtained from the Planck equation for black body emission. Nevertheless for the case of UV air sterilisation reactors this term is eliminated due to no emission material present apart from the irradiation source.

Finally, in the same manner that out-scattering redirects photons in a direction or frequency different to that of (**Ω**,v) in-scattering accounts for photons redirected from their trajectories or frequencies to that of (**Ω**,v). When radiation arrives from all directions to the volume of interest we have

$$W_{\Omega,\nu}^{s-in} = \frac{1}{4\pi} \int_{\Omega'=4\pi} \int_{\nu'}^{\infty} \sigma_\nu(\boldsymbol{x},t)p(\nu' \to \nu, \boldsymbol{\Omega'}, \boldsymbol{\Omega})I_{\Omega',\nu'}(\boldsymbol{x'},t)d\nu'd\Omega'$$

<div align="right">**Equation 4-33**</div>

The RTE in homogeneous media can be rewritten as

$$\frac{dI_\nu(s,\boldsymbol{\Omega},t)}{ds} + \beta_\nu(s,t)I_\nu(s,\boldsymbol{\Omega},t) = j_\nu^e(s,t) + \frac{\sigma_\nu(s,t)}{4\pi} \int_{4\pi} I_\nu(s,\boldsymbol{\Omega'},t)p(\boldsymbol{\Omega'} \to \boldsymbol{\Omega})d\boldsymbol{\Omega'}$$

<div align="right">**Equation 4-34**</div>

Where, $\beta_\nu(s,t)$ = Extinction coefficient, which is the sum of absorption 'k' and scattering coefficient 'σ' ($k + \sigma$), $j_\nu^e(s,t)$ = Energy emission of frequency v, and $\sigma_\nu(s,t)$ = Volumetric scattering coefficient for frequency v (energy in-scattering).

For induct air UV reactors is no emission ($j_\nu^e(s,t) = 0$) apart from that of the lamp, and the medium is assumed homogeneous hence no scattering is present ($\sigma_\nu(s,t) = 0$) can be reduced to Equation 4-35.

$$\frac{dI(\vec{r},\vec{s})}{ds} = -\alpha\,I(\vec{r},\vec{s})$$

<div align="right">**Equation 4-35**</div>

Which can be rewritten as

$$\frac{dI_\nu(s,\boldsymbol{\Omega},t)}{ds} = -k_\nu(s,t)I_\nu(s,\boldsymbol{\Omega},t)$$

<div align="right">**Equation 4-36**</div>

The boundary condition for Equation 4-36 is given by integrating it from the point of entrance (s = sr) to the point under consideration (s = s) to obtain

$$\epsilon_\nu(x,t) = k_\nu(x,t) \int_{\phi 1}^{\phi 2} d\phi \int_{\theta 1}^{\theta 2} d\theta\,sin\theta I_\nu^0(\theta,\phi,t) \times exp\left[-\int_{s=s_r}^{s=s(x,\theta,\phi)} k_\nu(s,t)ds\right]$$

<div align="right">**Equation 4-37**</div>

Where, $\epsilon_\nu(x,t)$= local volumetric rate of radiant energy absorption and $k_\nu(x,t)$= volumetric absorption coefficient. In heterogeneous media, such as water UV reactors, where scattering and absorption have considerable impact, can be expressed as shown in Equation 4-38.

$$\frac{dI_v(s, \mathbf{\Omega}, t)}{ds} + \beta_v(s,t)I_v(s, \mathbf{\Omega}, t) = \frac{\sigma_v(s,t)}{4\pi}\int_{4\pi} I_v(s, \mathbf{\Omega}', t)p(\mathbf{\Omega}' \to \mathbf{\Omega})d\mathbf{\Omega}'$$

<div align="right">

Equation 4-38

</div>

Similar as in homogeneous, in heterogeneous media there is no emission present inside the reactor ($j_v^e(s,t) = 0$), nevertheless the scattering coefficient yields an impact on the calculation. The effect of photon scattering adds a considerable amount of complexity to the solving process. By integrating Equation 4-38 from the point of entrance (s = sr) to the point under consideration (s = s) we can obtain the boundary conditions given by Equation 4-39.

$$\epsilon_v(x,t)$$
$$= k_v(x,t)\int_{\phi 1}^{\phi 2} d\phi \int_{\theta 1(\phi)}^{\theta 2(\phi)} d\theta \, sin\theta \, I_v^0(\theta, \phi, t) \, exp\left\{-\int_{s_r}^{s(x,\theta,\phi)} [k_v(s,t) + \sigma_v(s,t)] \, ds\right\}$$
$$+ k_v(x,t)\int_{\phi=0}^{2\pi} d\phi \int_{\theta=0}^{\pi} sin\theta \, d\theta \left\{\iint_{s_r}^{s(x,\theta,\phi)} \frac{\sigma_v(s,t)}{4\pi}\left[\int_{\phi'=0}^{2\pi} d\phi' \int_{\theta'=0}^{\pi} sin\theta' d\theta' I_v(x, \theta', \phi', t) \, p(\theta', \phi'\right.\right.$$
$$\left.\left. \to \theta, \phi)\right] exp\left[-\int_{s(x,\theta,\phi)}^{s(x,\theta,\phi)} [k_v(s,t) + \sigma_v(s,t)]ds\right] ds\right\}$$

<div align="right">

Equation 4-39

</div>

For both equations (homogeneous and heterogeneous) it is necessary to obtain the boundary condition for the irradiance (Iv = I_v^0), which is provided by the modeling of the lamp radiation emission, two main lamps are usually employed in photoreactors, those of voluminal emission[1] and those of superficial emission.

Superficial emission is produced by radiation emitted by the surface of the lamp, this is the case of coated lamps, in which the radiation is actually produced by the lamp envelope. For these cases a three–dimensional Source with Superficial, diffuse emission (E-SDE model) can be used and the boundary condition is given by Equation 4-40.

$$I_v^0(\theta, \phi) = \frac{\Upsilon_{R,v}(\Omega)P_{v,s}}{2\pi^2 R_l L_l}$$

<div align="right">

Equation 4-40

</div>

Where, $I_v^0(\theta, \phi)$ = Irradiation at source, $\Upsilon_{R,v}$ = Transmission coefficient and $P_{v,s}$ = Radiant power.

Voluminal emission is produced by radiation emitted by the whole lamp volume, such is the case of arc lamps i.e. low, medium and high pressure mercury lamps. For these cases a three-

---

[1] Term appointed by Cassano, Martin et al. (1995)

dimensional Source with Voluminal, Isotropic Emission (E-VIE) can be used and the boundary condition is given by Equation 4-41.

$$I_v^0(x, \theta, \phi) = \frac{P_{v,s}\Upsilon_{R,v}(\Omega)}{2\pi^2(R_L)^2 L_L} \frac{[r^2(cos^2\phi - 1) + (R_L)^2]^{1/2}}{\sin\theta}$$

<div align="right">**Equation 4-41**</div>

The work of Cassano, Martin et al. (1995) is mathematically thorough and explicit, and it is a good source to understand the mechanisms of the RTE method. This method is also the basis of the Discrete Ordinates (DO) irradiation model used in CFD software ANSYS (ANSYS, 2009), as applied in Chapter 5.

Finally, there is also the case of empirical model derived from experimental measurements such as the one used by Gilkeson and Noakes (2013) to model an upper-room (open field) UV disinfection system, which appears to be a suitable approximation in cases where the field generated by the lamp is complex because of louvers, reflections and non-standard geometries.

4.4 The Discrete Ordinates method (DO) with CFD simulations.

The DO method have successfully been used for the modelling of UV photoreactors in the past. Ho (2009a) used DO model in a CFD computation to calculate the irradiation of a UV lamp within a water photoreactor and compared its result against measured data at different distances from the lamp, showing that in all cases the difference between measured data and the DO calculation was less than 10 percent.

The DO model is used to solve the Radiative Transfer Equation (RTE) for a finite number of solid angles Ω, each associated with a vector direction $\vec{s}$ in a fixed Cartesian system of coordinates (*x,y, z*) with the solution method being identical to the one used for fluid flow and energy equations (ANSYS, 2009). In the sections that follow is a description of the method, its use in previous literature, advantages and limitations.

4.4.1 The DO method.

As previously described, the RTE applied to photoreactors has been widely used as it is accurately enough to mathematically calculate their performance (Cassano et al., 1995).It is possible to track an early state of CFD solutions using the DO method to solve the RTE for photoreactor designs in 1998, although using "*reasonable computational effort*" for the time, the DO method allowed to a reliable angular distribution of the radiant intensity solution (Sgalari et al., 1998).

Fast forward a few years later, and in hand with enhanced computational power, CFD methods became increasingly popular. In his Doctoral dissertation Liu (2004) did a numerical simulation of a UV disinfection reactor for water using CFD Fluent 6.0, in his research he analysed fluence rate distribution and turbulence models. For the fluence analysis he compared various models including the Multiple Point Source Summation (MPSS), Multiple Segment Source Summation (MSSS), Line Source Integration (LSI), a modification of the LSI, the RTE solved through Discrete Ordinates (DO) method and the View factor. Liu selected the MSSS for further development and applied an attenuation factor to account for reflection, refraction and adsorption. His research suggested that the RTE solved through the DO method was inaccurate as it over predicted the irradiation close to the lamp and under predicted it far from the lamp, these conclusions were later corrected by Ho (2009b) who showed that the DO method could accurately reproduced the results reported by Liu (2004), and the reason for the inaccuracy of results of the latter researcher was that his DO model did not included refraction (Ho, 2009b).

Almost parallel to Liu (2004), Pareek (2004) published a research on light intensity distribution in a photovoltaic reactor, using CFD methods and with a slight variation on the DO calculation using the Finite Volume (FV) method, the difference being that this model allowed the RTE to be integrated over both, the control volume and the control angle, unlike the DO which only integrates the RTE over the control volume, the benefit of the FV method was to reduce star like irradiation fields, nowadays commercial CFD software ANSYS perform DO with the option of angular discretisation therefore simulating the FV method (Ho, 2009b, ANSYS, 2009).

Nowadays CFD methods are widely used for the modeling of photochemical reactions. Imoberdorf et al. (2008) used CFD methods to model the radiation field of a multi-lamp reactor, again using the DO method to solve the RTE equation and account for reflection, refraction and adsorption of a multi-lamp system, Their main aim was to calculate photochemical reactions using a Monte-carlo multi-lamp radiation model. Also in 2008 Alfano and Cassano (2008) published the paper "Photoreactor Modeling: Application to Advanced Oxidation Processes" on the International Journal of Chemical Reactor Engineering, in it they explain a general methodology for photoreactor analysis and design, which is based on the RTE, and applied to three specific cases one of them being on photocatalytic reactors for air purifications.

The DO method is used in this research to solve the RTE for the modeling of UV irradiation due to its practicality and reliability of results, indeed it requires reasonable computational efforts (Sgalari et al., 1998), but as time passes and technology advances, the computer power and computational resources stop being an impediment for DO method calculations.

4.4.2 The DO method: CFD modeling

Applying CFD to UV modeling is a challenging matter, it involves solving the irradiation of energy from a surface in this case a UV lamp, calculating the trajectories of particles and the UV irradiation received over the whole volume of the particle (Fluence).

The DO method in FLUENT uses the previously described finite volume (FV) variant of the RTE model (Pareek, 2004), which considers the RTE in the direction of $\vec{s}$ as a field equation, therefore Equation 4-34 is expressed as

$$\nabla.\left(I(\vec{r},\vec{s})\vec{s}\right) + (\alpha + \sigma_s)I(\vec{r},\vec{s}) = an^2\frac{\sigma T^4}{\pi} + \frac{\sigma_s}{4\pi}\int_0^{4\pi}I(\vec{r},\vec{s}')\Phi(\vec{s}.\vec{s}')d\Omega'$$

Equation 4-42

Where

$\vec{r} = position\ vector$
$\vec{s} = direction\ vector$
$\vec{s}' = scattering\ direction\ vector$
$s = path\ length$
$\alpha = absorption\ coefficient$
$n = refractive\ index$
$\sigma_s = scattering\ coefficient$
$\sigma = Stefan - Boltzman\ constant\ (5.672\ x\ \dfrac{10^{-8}W}{m^2} - K^4)$
$I = radiation\ intensity, which\ depends\ on\ position\ (\vec{r})and\ direction\ (\vec{s})$
$T = local\ temperature$
$\Phi = phase\ function$
$\Omega' = solid\ angle$

When modelling UV irradiation from a source (i.e. UV lamp), it is necessary to model the total irradiation intensity of such source (W.m^{-2}) therefore the total UV wattage of the lamp must be divided into the surface area, as in Equation 4-43.

$$\begin{matrix}Irradiation \\ intensity\end{matrix}(I) = \frac{Total\ Watts}{2\pi rl}$$

Equation 4-43

Where r is the radius of the lamp, and l is the length. The irradiation intensity must be considered as *Diffuse irradiation* this means the irradiation will be displayed in all directions, a limitation of this is that the irradiation is considered to be evenly distributed along the lamp, although in reality this might not be the case and small variations might be possible, such

variations might be beyond measuring capabilities. By solving the RTE in a discretised manner it is possible to calculate the irradiation profile around a UV lamp (W.m^{-2}) (Figure 4.8).
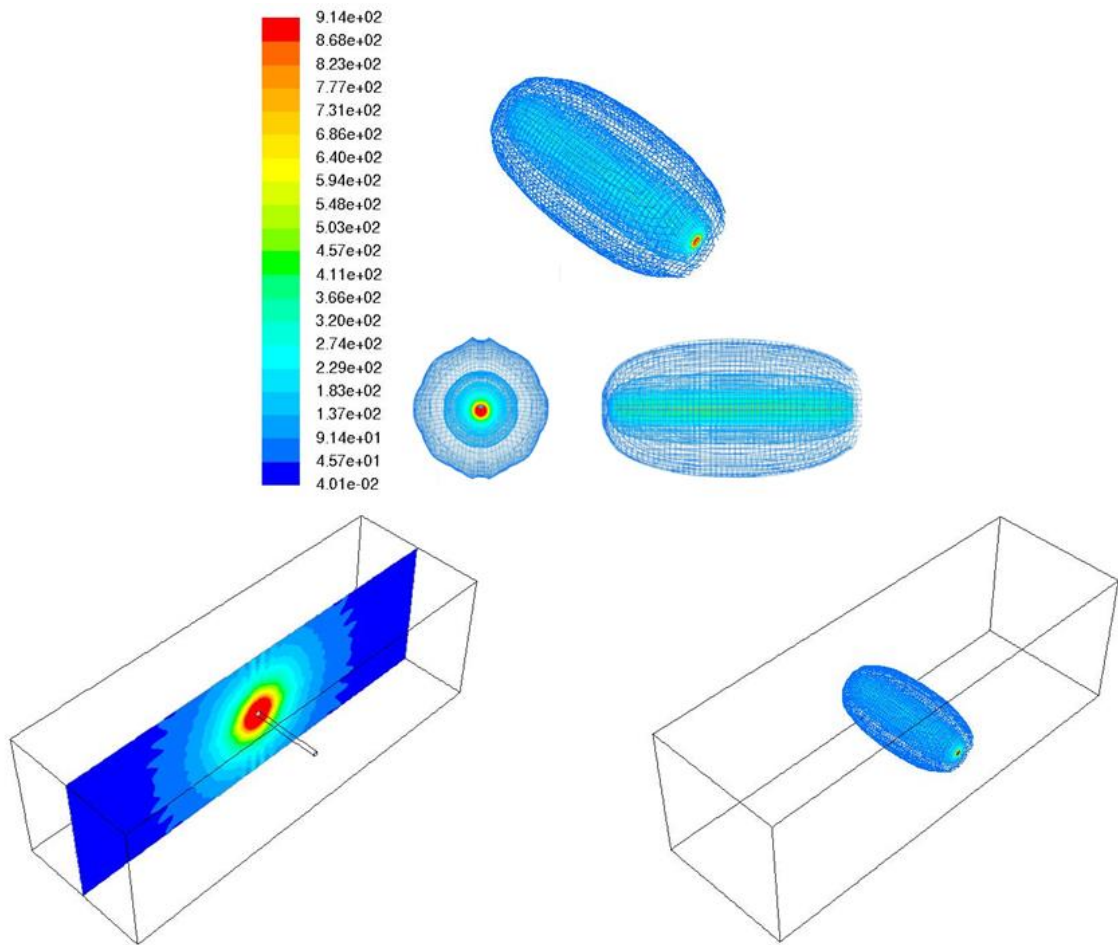
Figure 4.8 UV lamp irradiation as modeled with RTE in CFD, ANSYS. Grading in W.m-2.

Figure 4.9 shows a comparison of results for two UV lamps between the DO model used in this study, View factor and measured data previously published by Kowalski (2009a). In this case no reflections are included and the lamps characteristics used for the modeling are as shown on Table 4-1.

Table 4-1 Lamp modeling parameters

Lamp	UV power W	Arc length cm	Dia cm	Surface irradiation W.m^{-2}
GHO287T5L	3.2	20.6	1.6	309
AGHO287T5L	6.5	20.6	1.6	628

The results show that the DO irradiation model appears to be sufficiently accurate for modeling purposes, with very good agreement with experimental data
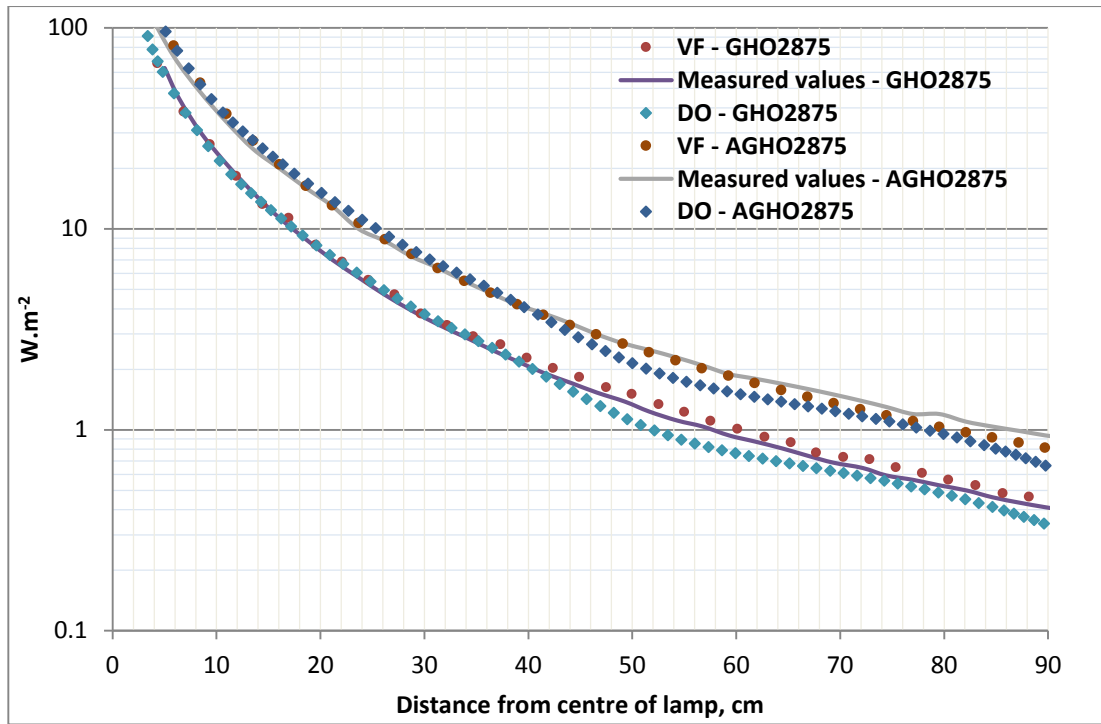
Figure 4.9 Irradiation values from centre of lamp. View factor, Discrete Ordinates and Measured values.

4.4.3 The DO method: Angular Discretization

Angular discretization, which is defined by the angles Theta and Phi, is used to avoid the star-shape irradiation problem (Versteeg and Malalasekera, 2007). Angular discretization defines the distribution of the irradiation within the model, as the irradiation intensities tend to concentrate towards the centre of the radiation source (Pareek, 2004). Although the average irradiation in the domain area might remain the same, the distribution of the irradiation will vary. The more divisions in the angular discretization in the model, the more even the irradiation field will be. Figure 4.10 shows the difference in the irradiation contour between a DO model solved with 3 divisions for angular discretization in Theta and Phi (left), a DO model solved with 10 divisions for angular discretization (centre) and a 15 divisions for angular discretization (right). The more angular divisions for discretization, the better the irradiation will be distributed within the control volume.
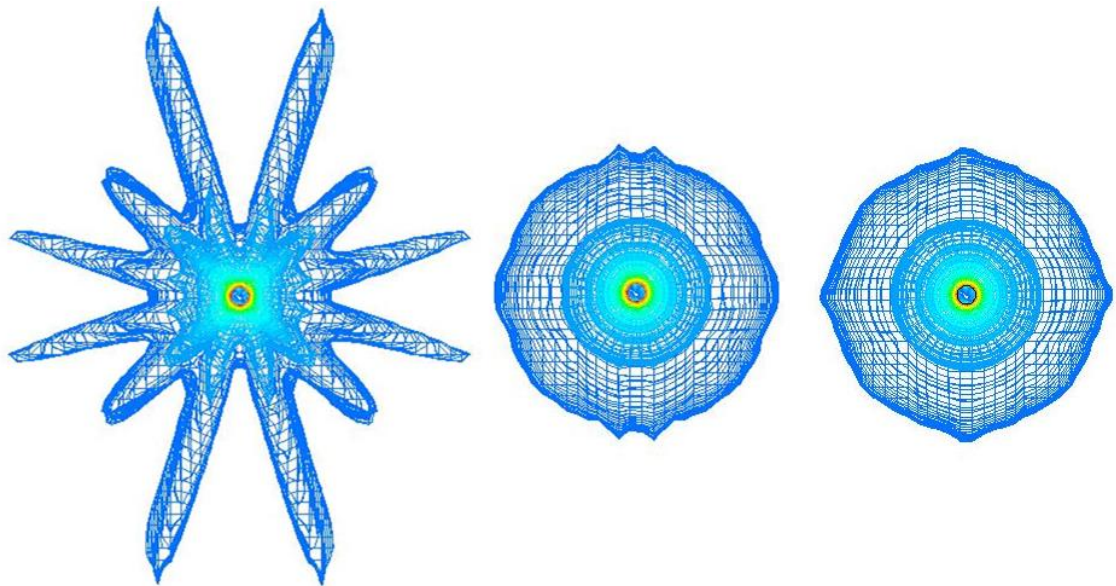
Figure 4.10 Left) DO model with 3 angular divisions on Theta and Phi, centre) DO model with 10 angular divisions on Theta and Phi, right) DO model with 15 angular divisions on Theta and Phi.

Figure 4.11 shows the irradiation values of the lamp model GHO2875T5L (LightSources, 2009) from published data (Kowalski, 2009a) taken at a range of distances from the centre of the lamp, the graph shows the difference between a solution wielding 15, 10 and 3 angular division in Theta and Phi.
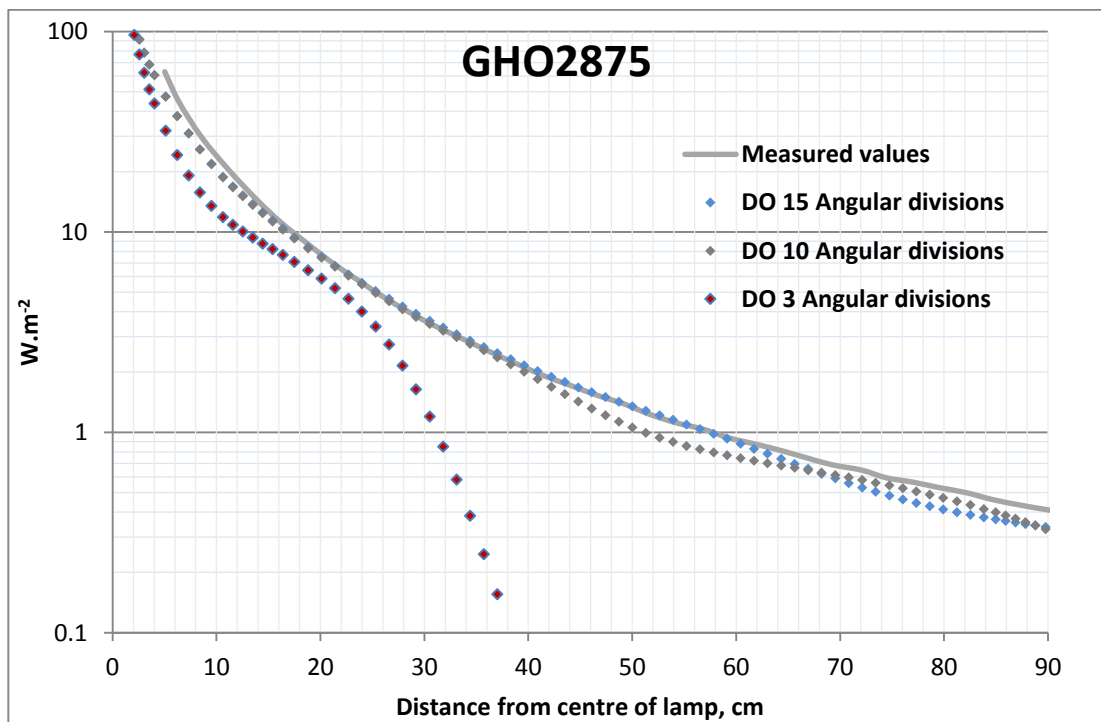
Figure 4.11 Comparison of the Irradiation calculation using the DO method with 15 Angular divisions and 10 Angular divisions.

4.4.4 The Do method: Reflections

One of the benefits of using the DO to solve the RTE is its capacity to account for the shadowing, reflection and refraction of the modelled geometry (Ho, 2009a), plus the CFD calculation can account for fluid characteristics of the model, making this a powerful tool for accurately calculate the effects of UV irradiation and airflow profiles in a photoreactor. This is a major difference from other modelling techniques such as the MPSS used by Bolton and Cotton (2001), the view factor used by Kowalski and Bahnfleth (2000a) and the inverse square model used by Beggs et al. (2000). None of those models had the capacity to account for the inherent shadowing and reflectivity of a system geometry. Moreover, fluid dynamic characteristics such as airflow profile, and temperatures could not be included in the calculations, instead such models calculated UV dose as an average from the system, and the airflow was merely used to calculate a dwell time of a particle assuming a straight line pathway, therefore the models could only work assuming a completely mix airflow.

Reflection is an integral part of the RTE model, and is accounted by the internal emissivity (or absorption) and the refractive index of the wall material when modelling opaque walls, while for semi-transparent walls transmittance is also accounted. Basically a surface producing reflections acts as a source of radiation emitting power in relation with the material emissivity and the energy it receives. Incident irradiation over the wall serving as reflector can be of two types diffuse or specular.

For the modelling of reflection we require the refractive index n which describes the manner in which light propagates through a medium (Equation 4-44) (Karlsson and Ribbing, 1982).

$$n = \frac{c}{v}$$

<div align="right">**Equation 4-44**</div>

Where c is the constant of speed of light and v is the speed of light in the substance. It is important to highlight that n is dependent on the energy wavelength, therefore the refractive index of UV light at 253 nm is different to that of visible light (Karlsson and Ribbing, 1982). Figure 4.12 shows the values for refractive index and the extinction coefficient of a generic type of stainless steel (393 M) (Karlsson and Ribbing, 1982).
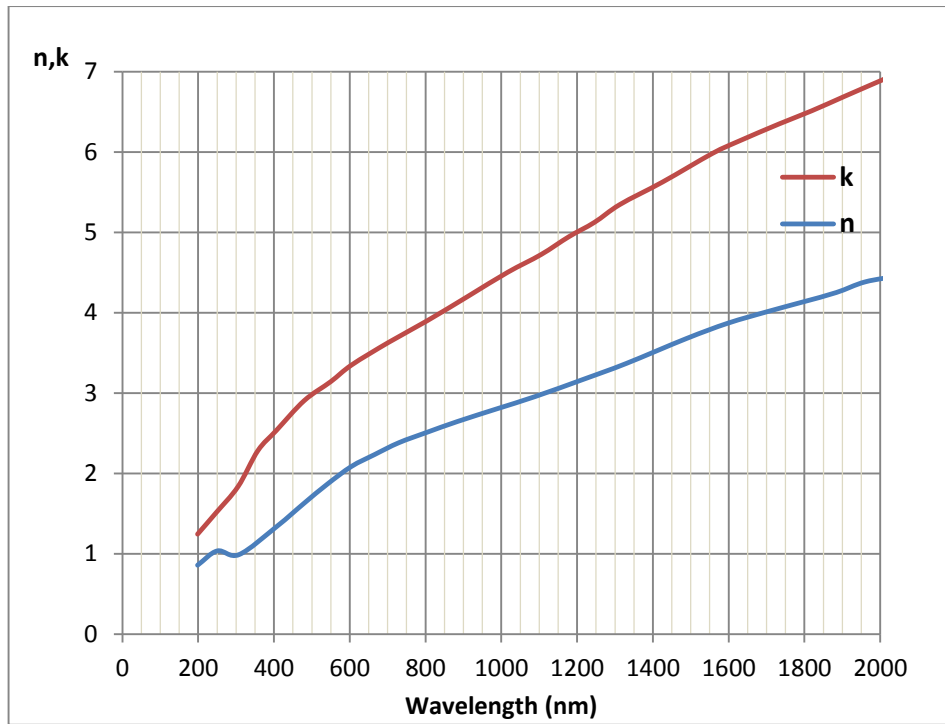
Figure 4.12 Refractive index (n) and extinction coefficient (k) of one ferritic stainless steel (393 M) adapted from (Karlsson and Ribbing, 1982)

The absorption coefficient α_c, although not required for the specific case of opaque wall reflections, is necessary for semi-transparent bodies as it determines how far light penetrates into the material before it is absorbed (Equation 4-45) (Karlsson and Ribbing, 1982).

$$\alpha_c = \frac{4\pi\kappa}{\lambda}$$

<div align="right">**Equation 4-45**</div>

Where κ is the extinction coefficient of the wall material, and λ the wavelength of the received energy by the wall. Finally, the emissivity (ε) of the material in a closed system is equal to its absorption (α), as explained in Equation 4-48 (Bartl and Baranek, 2004). The reflected (φ) and transmitted energy (τ) does not have any effect on the wall thermal energy, nevertheless absorption (α) does, and as energy is absorbed it needs to be radiated in order for the wall temperature to remain constant, therefore the energy absorbed is equal to the energy emitted.

$$\varphi + \tau + \alpha = 1$$

<div align="right">**Equation 4-46**</div>

For opaque bodies, as in the case of steel walls, there are no transmittance (τ=0) (Bartl and Baranek, 2004), therefore

$$\varphi = 1 - \alpha$$

In accordance to Kirchhoff's law for spectral emissivity (ε)

$$\varepsilon = \alpha = 1 - \varphi$$

In the case for stainless steel, the value for refractive index (n) at 254 nm appears to be 1 as per figure Figure 4.12 (Karlsson and Ribbing, 1982), and emissivity (absorption) according to the required reflectivity of the walls is shown in Figure 4.13.
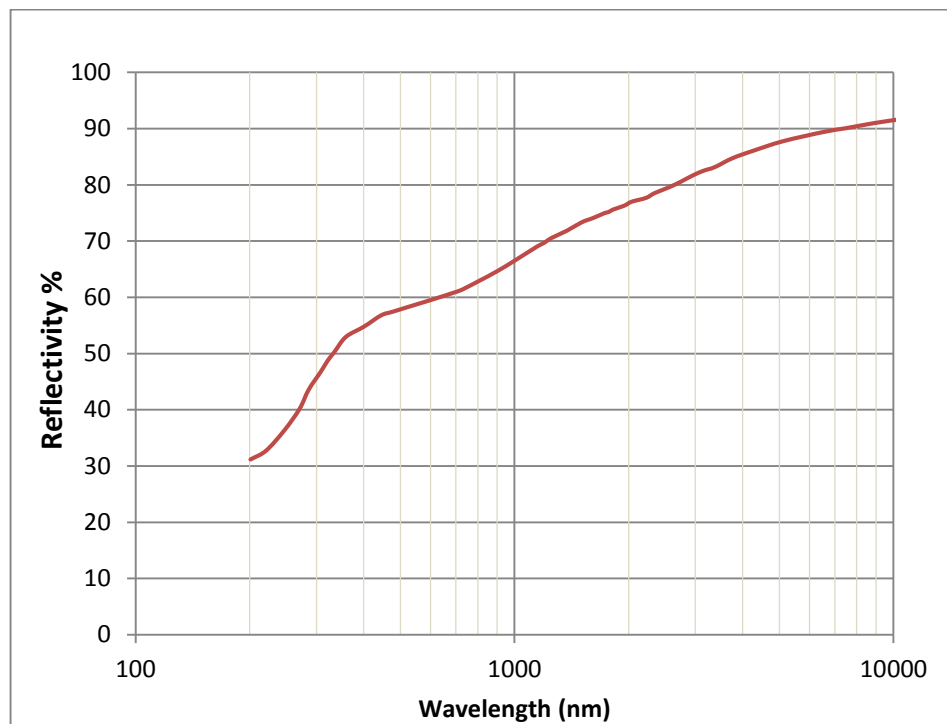
Figure 4.13 Reflectivity of a ferritic stainless steel (393 M) adapted from(Karlsson and Ribbing, 1982)

Basically, the reflective walls serve as a new irradiation source with its irradiation power defined by the incident radiation provided by the main source (the UV lamp), and the boundary condition of wall emissivity (Figure 4.14).
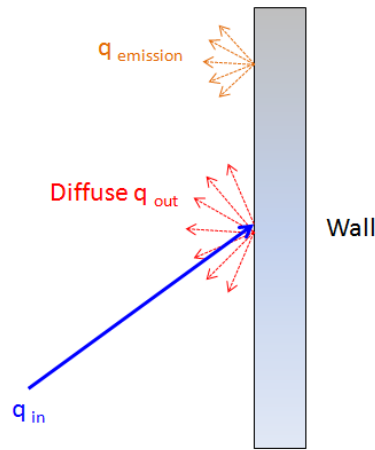
Figure 4.14 Reflected irradiation over a surface wall.

Energy Emission from the wall surface is defined within the CFD ANSYS software as:

$$Wall\ Emission\ = n^2\varepsilon_w\sigma T_w^4$$

$$Wall\ Diffuse\ reflected\ energy\ = f_d(1-\varepsilon_w)q_{in}$$

$$Wall\ Absorption\ = \varepsilon_w q_{in}$$

We have that f_d is set as the diffuse fraction that in the case of a fully diffuse irradiation is equal to 1, n is the refractive index of the wall at the specific wavelength, ε_w is the wall emissivity, σ is the Stefan-Boltzmann constant (σ = 5.670×10⁻⁸ J.K⁻⁴.m⁻².s⁻¹), T is the wall temperature, and q_{in} is the amount of incident radiation on the wall. Therefore as referred by previous equations, for a fully diffuse reflected irradiation, the total reflection by the walls is defined as:

$$q_{out} = (1-\varepsilon_w)q_{in} + n^2\varepsilon_w\sigma T_w^4$$

The impact of reflections in a configuration of a single lamp within a duct of 0.61 m x 0.61 m similar to the ones stated on the EPA tests reports can be seen in Figure 4.15, wall reflections enhanced the total Irradiance and the irradiance distribution of the system.
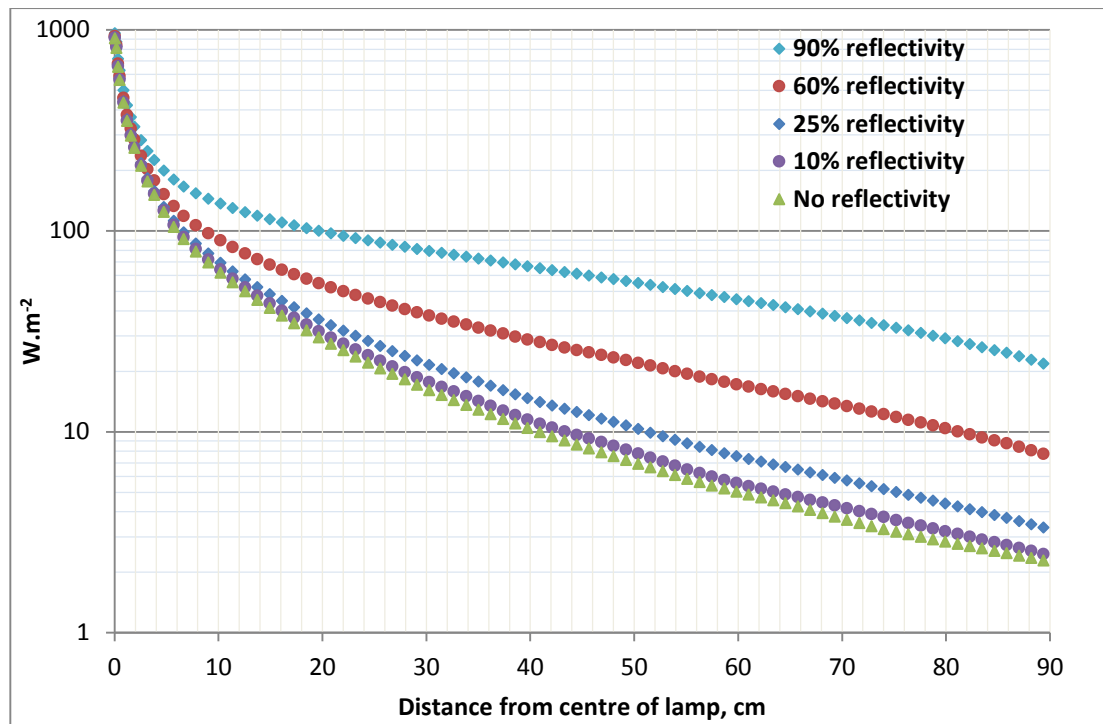
Figure 4.15 An example of the irradiation power from the centre of the lamp as modelled by DO method in a 0.61 x 0.61 m steel duct with various levels of reflectivity.

4.4.5 The DO method: UV dosage calculations.

Sandia National Laboratories (Ho, 2009b) made public a tutorial on CFD modeling and how to run a UV dose calculation with particle trajectories by using the DO method, the report described how to solve the RTE over a domain of discrete solid angles and how to calculate radiation intensity as a function of absorption, scattering, reflection and emissivity. Ho (2009a) evaluated the impact of reflection and refraction in a simulation of a UV disinfection reactor for water by using the same method as described by Sandia National Laboratories (Ho, 2009b). UV water reactors make use of quartz envelopes around the lamp to prevent cooling of the lamps and mercury contamination due to contact with the fluid, so the refraction and reflections from the envelopes needed to be included in the model. In this specific research, Ho (2009a) made a comparison of Liu (2004) MSSS models and the DO method, finding that the difference in accuracy on Liu (2004) results was due to wall reflections from the quartz envelope not being considered, and proved that DO could accurately calculate the irradiation performance of a photoreactor.

After modeling the UV irradiation field, it is then possible to calculate the UV dose. With the use of a user defined function (UDF) that approximates the integral by the use of a trapezoidal rule

(Equation 4-53), the cumulative UV dose ($J.m^{-2}$) received by a particle, represented by a scalar with physical characteristics as it passed through the UV field can be obtained.

$$UV \text{ dose} = dT * \sum_{i=1}^{i=n} \frac{UV_i + UV_{i+1}}{2}$$

Where *dT* is a time interval, *UV$_i$* and *UV$_{i+1}$* are the UV intensities in the computational cell at the beginning and end of the time step. Microorganism inactivation is calculated from the scalar received UV dose (fluence) at the end of the computational domain, using the model decay equations shown in Chapter 3 with the appropriate microorganism susceptibility constant. The average UV dose of the system is measured at the end of the duct by averaging the dose received by all the scalars tracked within the system (Equation 4-54).

$$System\ UV\ dose = \frac{\sum_i^n UV\ dose}{n}$$

At the end of the duct, the particle contains data of position in *X, Y* and *Z* and UV dose received (Figure 4.16). Under the idea that real life UV system deal with a wide range of microorganisms and a variety of susceptibilities which affects the performance of a UV system, the performance of a system can also be modelled in a multi-susceptibility arrangement by varying the susceptibility of each microorganism or in this case the susceptibility assigned to each scalar.
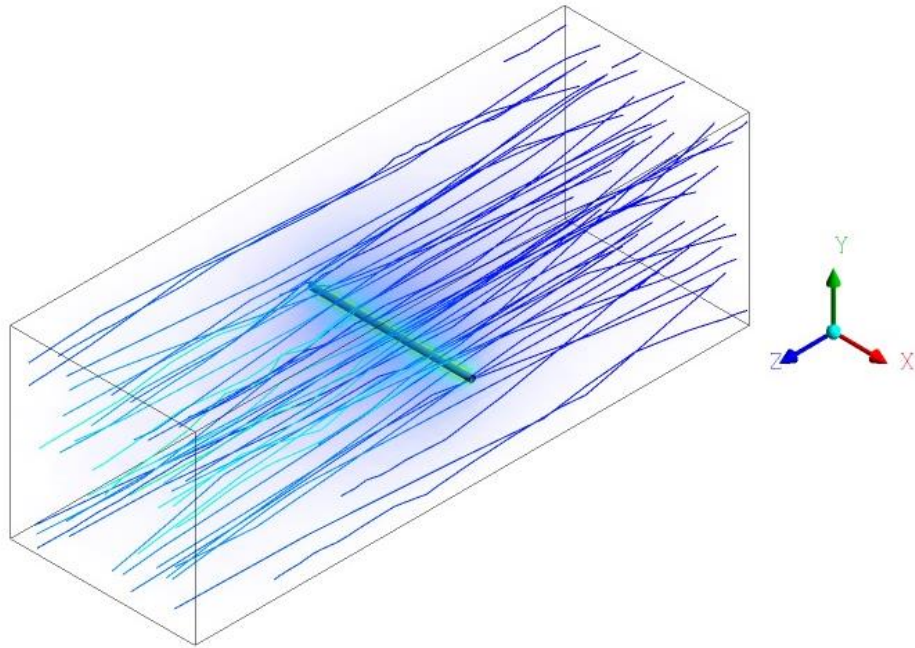
Figure 4.16 Particles trajectories and UV irradiation received.

Chapter 5 shows a detailed set up of the DO method on ANSYS fluent CFD, where the different set up parameters and its implications are explained.

4.5 Summary.

This chapter reviewed various irradiation models and their characteristics, and provided an introduction into the DO method, its use and its governing equations. Moreover this chapter described the process in which the CFD commercial software ANSYS Fluent deals with the DO method and it slight variation of the Finite volume technique, and how reflections are modelled within a UV chamber.

The DO model was used to calculate the irradiation performance of a single UV lamp which was then compared with measured results and previously published modeling results obtained with the View Factor method, results are a good agreement for the DO method against measured results, showing that the DO method is sufficiently accurate to be used for UV sterilisation modeling.

Chapter 5 will follow with an explanation of the CFD modeling process and the model validation by modeling of sterilisation performance of a series of in-duct UV air photoreactors and compare them against lab results.

Chapter 5. CFD Model Development and validation.

5.1 Introduction.

This chapter validates the use of CFD to assess performance of UV systems and demonstrates its potential benefits.

The first section of this chapter describes the main characteristics of the CFD technique including the governing equations, the definition of turbulence, how a model is meshed, the discretization process, and the solution methods employed. Section 5.3 aims to reproduce the results reported by the EPA tests EPA 600/R-06/050 which compasses a single lamp system, EPA 600/R-06/051 a four lamp system and EPA 600/R-06/055an eight lamp system, by the means of CFD modelling using discrete ordinate (DO) irradiation modelling and Lagrangian particle tracking as described in Chapter 4. To be able to compare inactivation results between the CFD model and EPA published results, it was necessary to reduce the uncertainty in microorganism UV susceptibility as discussed in Chapter 3.

The second part of the chapter focuses on the impact of lamp configuration and system designs. Moreover, the study explores the potential for CFD analysis to evaluate sterilisation performance and energy efficiency.

5.2 Computational Fluid Dynamics.

Computational fluid dynamics (CFD) is defined as "*the analysis of systems involving fluid flow, heat transfer and associated phenomena such as chemical reactions by means of computer-based simulation*" (Versteeg and Malalasekera, 2007).

Usually the characteristics of the fluid motion or dynamics can be represented in the manner of fundamental equations, most commonly in partial differential form. These are the equation governing the process, and thus they are referred as governing equations (Tu et al., 2007).

With the use of Computational Fluid Dynamics (CFD) it is possible to solve partial differential equations for fluid flows in a discretised manner. Governing equations are solved algebraically at determined number of points specified by a mesh. This consists of a series of points which in consequence form a grid.

The advantages of CFD are numerous. When used in engineering design, it can help in reducing design times and costly prototypes (Tu et al., 2007), when coupled with parametric studies CFD

can help in obtaining optimised solutions, and can help on predicting physical processes which otherwise are impossible to measure (Young et al., 2010). In the case of UV disinfection, it allows an understanding of the mechanisms of disinfection by modeling the interaction between a flow field and a UV lamp (Gilkeson and Noakes, 2013).

CFD is capable of mathematically solving complex and sophisticated models that are otherwise impossible to solve analytically. Prior literature on UV air sterilisation modelling made use of finite integral solutions and assumptions of completely mixed airflows as it was impossible to solve particle trajectories and complex airflow without the use of CFD. This is reviewed in Chapter 4.

5.2.1 Governing equations

The governing equations of fluid dynamics, which mathematically represent the conservation laws of physics are the fundamental base of CFD. The basic physical laws that are adopted include (Tu et al., 2007):

- Mass conservation for the fluid,
- The momentum rate of change equals the sum of forces acting on a fluid (Newton's second law)
- First law of thermodynamics, the rate of change of energy equals the sum of rate of heat addition to and the rate of work done on the fluid.

Mass conservation.

The general form of the mass conservation equation can be represented as follows (Tu et al., 2007):

$$\frac{\partial \rho}{\partial t} + \nabla . (\rho \vec{v}) = 0$$

Equation 5-1

This is valid for incompressible as well as compressible flows (ANSYS, 2011). The partial derivative form of the continuity equation (Tu et al., 2007) can be represented in the Cartesian coordinate systems as

$$\frac{\partial \rho}{\partial t} + \frac{\partial (\rho u)}{\partial x} + \frac{\partial (\rho v)}{\partial y} + \frac{\partial (\rho w)}{\partial z} = 0$$

In this case the velocity $\vec{v}$ at any point in the flow field is described by the local velocities u, v, and w which are functions of locations (x, y, z) and time (t). Expressed in the differential form, the continuity equation is said to be in the conservation form.

Momentum equation.

The conservation of momentum is described by the Navier-Stokes equations (ANSYS, 2011):

$$\frac{\partial}{\partial t}(\rho \vec{v}) + \nabla \cdot (\rho \vec{v} \, \vec{v}) = -\nabla \rho + \nabla \cdot (\bar{\bar{\tau}}) + \rho \vec{g} + \vec{F}$$

With ρ as the static pressure, $\rho \vec{g}$ and $\vec{F}$ as gravitational body force and external forces and the $\bar{\bar{\tau}}$ as the stress tensor given by:

$$\bar{\bar{\tau}} = \mu \left[\left(\nabla \vec{v} + \nabla \vec{v^{\tau}} \right) - \frac{2}{3} \nabla \cdot \vec{v} I \right]$$

Here μ is molecular viscosity, I is the unit tensor, and the second term on the right represents the effect of dilution (ANSYS, 2011).

Energy equation

The equation for the energy conservation comes from the statements of the first law of thermodynamics (Tu et al., 2007):

$$\begin{array}{l} Time\ rate\ of \\ change\ of\ energy \end{array} = \begin{array}{l} Net\ rate\ of \\ heat\ added \end{array} \left(\sum \dot{Q} \right) + \begin{array}{l} Net\ rate\ of \\ work\ done \end{array} \left(\sum \dot{W} \right)$$

Keeping up with the Navier-Stokes equations (momentum equations) the energy conservation can be described as (ANSYS, 2011):

$$\frac{\partial}{\partial t}(\rho E) + \nabla.\left(\vec{v}(\rho E + p)\right) = -\nabla.\left(\sum_j h_j J_j\right) + S_h$$

<div align="right">**Equation 5-6**</div>

These three equations of Mass conservation, Momentum equation and the Energy equations are the governing calculations performed for CFD modelling and are valid for any given flow. The DO method is an addition for the calculation of irradiation and is solved following the governing equations here described. Further equations are required to model contaminants, particles and other parameters such as irradiation fields which are model specific.

5.2.2 Turbulence

Turbulence is a chaotic and random motion, usually created by disturbances in a flow stream. The presence of turbulence can be associated with the ratio of inertia force and viscous force, i.e. the Reynolds number (Re).

$$Re = \frac{inertia\ force}{friction\ force} = \frac{\rho v_{in} H}{\mu}$$

<div align="right">**Equation 5-7**</div>

Here ρ is fluid density, v_{in} is the initial velocity, H is the pipe radius (or duct height) and μ is the dynamic viscosity of the fluid.

Low Re is associated with laminar flow while high Re, usually above 1400 suggest turbulent flow in an in-duct system. This is because at low Re inertia forces are higher than viscous force, while at high Re the opposite is true and inertia forces start to amplify the disturbances in the flow, generating thus a turbulent state (Tu et al., 2007).

Within a turbulent flow exists rotational flow structures, also known as eddies, which in turn contain a range of length and velocity scales known as turbulent scales (Tu et al., 2007). Turbulence can be described as random fluctuations in the fluid (Figure 5.1).
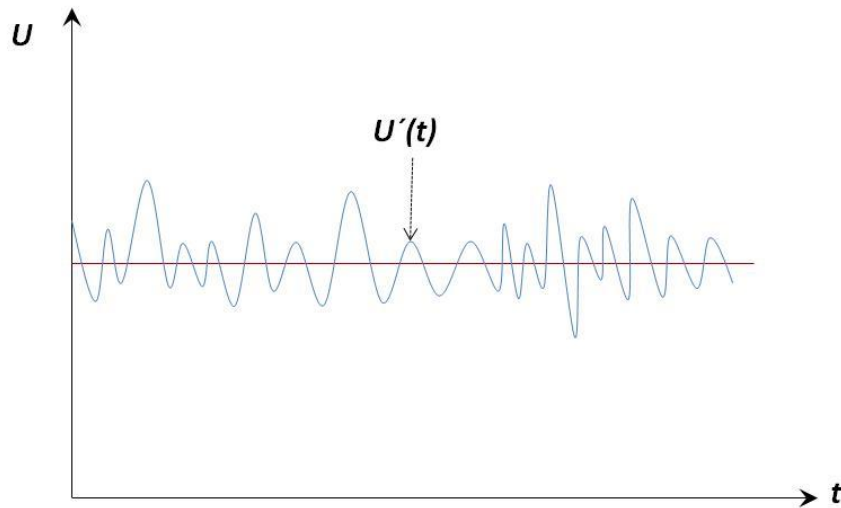
Figure 5.1 Fluctuations of velocity over time, adapted from Tu et al. (2007)

Therefore to use the conservation equation, the velocity variable can be considered like a steady state value of $\bar{u}$ with a moving component $u'(t)$, we have Equation 5-8.

$$u(t) = \bar{u} + u'(t) \ .$$

<div align="right">**Equation 5-8**</div>

A turbulence model is necessary to solve the governing equations which accounts for the fluctuations on velocity over time. Several turbulence models exist, the most popular ones appear to be (Sumer, 2013):

- Algebraic models, Mixing-Length model
- Turbulence-energy equations, k-ε and k-ω
- Simulation models, Direct Numerical Simulations (DNS), Large Eddy Simulations (LES) and Detached Eddy Simulations (DES)

Algebraic models are the simplest, where the Reynolds stress is expressed as the product of turbulence and viscosity and the mean strain rate. Turbulent viscosity is therefore computed in terms of mixing length (Sumer, 2013).

Turbulence-energy equation models express Reynolds stress as the product of turbulence viscosity and mean strain rate, where turbulence viscosity is computed in terms of turbulence kinetic energy (Sumer, 2013).

Finally we have the models which address turbulence directly. Direct Numerical Simulation (DNS) computes a direct time dependant solution of the Navier-Stokes equations, while Large Eddy Simulation (LES) aims to average the Navier-Stokes equation over a defined, generally small, volume. At the moment, these models are the most advanced and required relatively large computer power (Sumer, 2013). DNS, is the most accurate method and directly solves the transport equations during a numerical discretization. In other words, it completely solves the turbulence in the flow without making averages or assumptions on solutions. This tends to be highly computational expensive, and for that reason another option for problems showing high Reynolds numbers or when high levels of accuracy are required is the LES, which calculates large eddies exactly but deals with small eddies by approximations, thus saving computational resources (Tu et al., 2007).

The k-ε model

The k-ε model, which is the one used for the majority of CFD analysis in this thesis, is a practical process for cases in which accurate information about turbulence in a system is required, yet detailed information about every specific eddy on the flow is not necessary (Tu et al., 2007).

This model focuses on developing equations to accommodate the turbulent quantity k and the dissipation rate of turbulent energy ε. This can be described as Equation 5-9 and Equation 5-10.

$$k = \frac{1}{2}\left(\overline{u_i'}\,\overline{u_i'}\right)$$

Equation 5-9

$$\varepsilon = vT\overline{\left(\frac{\partial u_i'}{\partial x_j}\right)\left(\frac{\partial u_i'}{\partial x_j}\right)}$$

Equation 5-10

Where $i,j = 1,2,3$. From here a local turbulent equation can be defined as Equation 5-11

$$\mu T = \frac{C\mu\rho k^2}{\varepsilon}$$

Equation 5-11

With the turbulent viscosity given by

$$vT = \frac{\mu T}{\rho}$$

Finally, the differential transport equations required for the standard k-ε model are:

$$\frac{\partial k}{\partial t} + u\frac{\partial k}{\partial x} + v\frac{\partial k}{\partial y} = \frac{\partial}{\partial x}\left(\frac{vT}{\sigma k}\frac{\partial k}{\partial x}\right) + \frac{\partial}{\partial y}\left(\frac{vT}{\sigma k}\frac{\partial k}{\partial y}\right) + P - D$$

$$\frac{\partial \varepsilon}{\partial t} + u\frac{\partial \varepsilon}{\partial x} + v\frac{\partial \varepsilon}{\partial y} = \frac{\partial}{\partial x}\left(\frac{vT}{\sigma \varepsilon}\frac{\partial \varepsilon}{\partial x}\right) + \frac{\partial}{\partial y}\left(\frac{vT}{\sigma \varepsilon}\frac{\partial \varepsilon}{\partial y}\right) + \frac{\varepsilon}{k}(C_{\varepsilon 1}P - C_{\varepsilon 2}D)$$

With P defined by:

$$P = 2vT\left[\left(\frac{\partial u}{\partial x}\right)^2 + \left(\frac{\partial v}{\partial y}\right)^2\right] + vT\left(\frac{\partial u}{\partial y} + \frac{\partial v}{\partial x}\right)^2$$

These set of equations contain five constants as follows: $C\mu = 0.09$, $\sigma k = 1.0$, $\sigma \varepsilon = 1.3$, $C_{\varepsilon 1} = 1.44$, and $C_{\varepsilon 2} = 1.92$, to summarise, the dissipation of ε is large, where the production of k is large (Tu et al., 2007).

The k-ω model

There are two basic equations in this model, one is for k which is the turbulent kinetic energy, and one for ω which is the specific dissipation of turbulent energy (Sumer, 2013).

Where k is

$$k = \frac{1}{2}(\overline{u_i'u_i'})$$

And ω is

$$\omega = \frac{\varepsilon}{k\beta^*}$$

Here ε is the dissipation of turbulent kinetic energy, and is expressed as

$$\varepsilon = vT \overline{\left(\frac{\partial u'_i}{\partial x_k}\right)\left(\frac{\partial u'_i}{\partial x_k}\right)}$$

<div align="right">**Equation 5-18**</div>

The turbulent kinetic energy (k) is defined per Equation 5-19

$$\frac{\partial pk}{\partial t} + \frac{\partial p\bar{u}_j k}{\partial x_j} - \frac{\partial}{\partial x_j}\left[(\mu + \sigma_k \mu_t)\frac{\partial k}{\partial x_j}\right] = \tau_{ij}\frac{\partial \bar{u}_i}{\partial x_j} - \beta^* \rho \kappa \omega$$

<div align="right">**Equation 5-19**</div>

While ω is defined per Equation 5-20

$$\frac{\partial p\omega}{\partial t} + \frac{\partial p\bar{u}_j \omega}{\partial x_j} - \frac{\partial}{\partial x_j}\left[(\mu + \sigma_\omega \mu_t)\frac{\partial \omega}{\partial x_j}\right] = \frac{\gamma}{v_t}\tau_{ij}\frac{\partial \bar{u}_i}{\partial x_j} - \beta\rho\omega^2 + 2\rho(1 - F_1)\frac{\sigma_{\omega 2}}{\omega}\frac{\partial k}{\partial x_j}\frac{\partial \omega}{\partial x_j}$$

<div align="right">**Equation 5-20**</div>

With the values of the model constants being:

$$\sigma_k = F_1\sigma_{k1}(1 - F_1)\sigma_{k2}$$

<div align="right">**Equation 5-21**</div>

$$\sigma_\omega = F_1\sigma_{\omega 1}(1 - F_1)\sigma_{\omega 2}$$

<div align="right">**Equation 5-22**</div>

$$\gamma = F_1\gamma_1(1 - F_1)\gamma_2$$

<div align="right">**Equation 5-23**</div>

$$\beta = F_1\beta_1(1 - F_1)\beta_2$$

<div align="right">**Equation 5-24**</div>

Which for inner (wall) regions have values of: $\beta_1 = 0.075$, $\beta^* = 0.09$, $\gamma_1 = 0.567$, $\sigma_{k1} = 0.85$, and $\sigma_{\omega 1} = 0.5$. And for the outer region: $\beta_2 = 0.0828$, $\beta^* = 0.09$, $\gamma_2 = 0.463$, $\sigma_{k2} = 1.0$, and $\sigma_{\omega 2} = 0.856$.

The k-ω solves for kinetic energy and turbulent frequency, this model appears to be more accurate for flows close to a wall, and with low Reynolds number.

5.2.3 Meshing

When using CFD it is necessary to subdivide the domain volume under analysis into a finite number of discrete volume cells where the transport equations will be solved. The meshing process is rather important as it affects the accuracy of the CFD results and the solving time of the model. A fine grid will better capture the qualities of the flow and other governing equations included in the model, as in this case the DO irradiation.
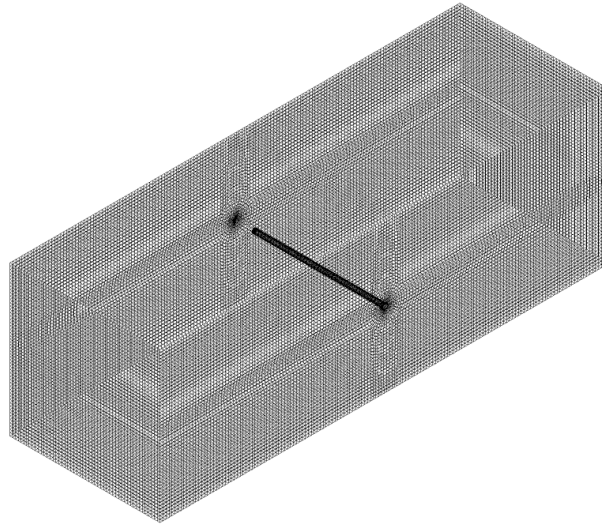
Figure 5.2 Mesh of a 3d model for CFD use.

Meshing is a subject on itself, and as such it is important to understand basic terminology.

Mesh topology refers to the structure of the mesh. There are various types of mesh topologies such as:

Structured mesh: Simple and regular geometry, the mesh is composed of orthogonal 90° cells (Figure 5.3). These type of meshes tend to ease the flow solving process, as the connectivity between cells is rather simple, although in some cases it might be hard to fit this type of structure into complex geometries (Tu et al., 2007).
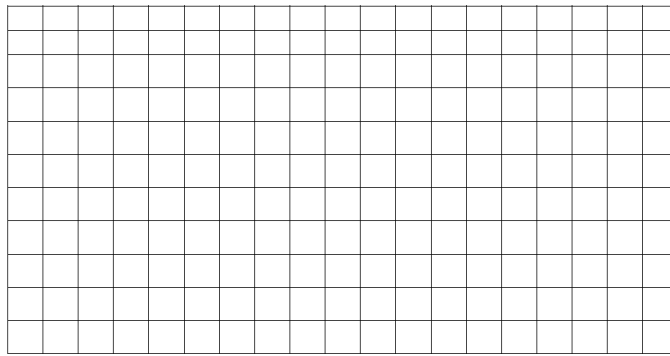
Figure 5.3 Structured mesh.

Unstructured mesh: This is when cells are allowed to assemble freely, with most cells in the shape of triangles or tetrahedrons (Figure 5.4). They are especially useful when dealing with non-standard geometries. The disadvantage of this type of meshing is that calculation might required more computational power as neighbouring cells are not well defined and more complex solution algorithms might be required (Tu et al., 2007).
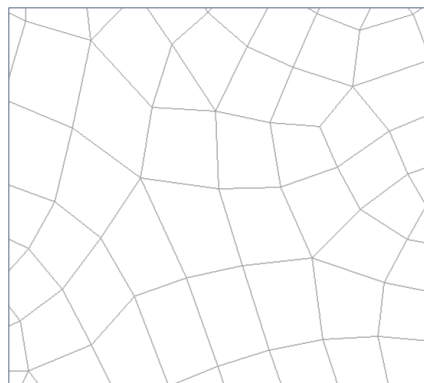
Figure 5.4 Unstructured mesh.

Block structure: A third approach is to have combinations of cells, in what is called block structures. In this type of meshing, a certain part of the domain volume is meshed in a specific manner, i.e. structured mesh while other parts are meshed in a manner which accommodates better the specific geometry i.e. unstructured mesh. In this manner, geometries within the domain volume can be solved easier with less computational resources, while focusing resources in other more complex geometries within the domain (Tu et al., 2007).
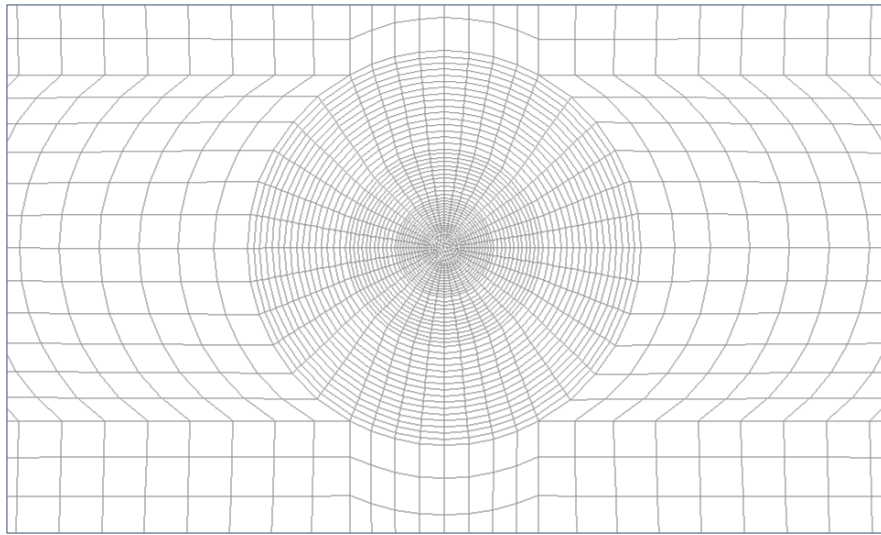
Figure 5.5 Block structured mesh.

The accuracy and time taken to solve a CFD model is directly dependant on the quality of the mesh, therefore a good mesh is essential to obtain the best results.

5.3 EPA experimental test series.

The US Environmental Protection Agency (EPA) ran a series of lab test on various in-duct UV air sterilisation systems known as *"Biological Inactivation Efficiency by HVAC In-Duct Ultraviolet Light Systems"* (EPA, 2006a, EPA, 2006b, EPA, 2006c). The purpose of these tests was to measure their efficacy and efficiency at sterilising microorganisms and were based on earlier tests standards developed by VanOsdell and Foarde (2002).

The CFD model developed in this thesis was validated by comparison with results from three EPA test (Figure 5.6):

- EPA 600/R-06/050, which used a device entailing a single 53 cm mercury lamp located perpendicular to the air flow,
- EPA 600/R-06/051 which compromises a device using four 53 cm long UV lamps located perpendicular to the airflow and evenly distributed over the height of the duct
- EPA 600/R-06/055 which uses a system of 8 UV lamps each one of 41.4 cm in length installed perpendicular to the airflow in two arrays of four lamps along the height of the duct.
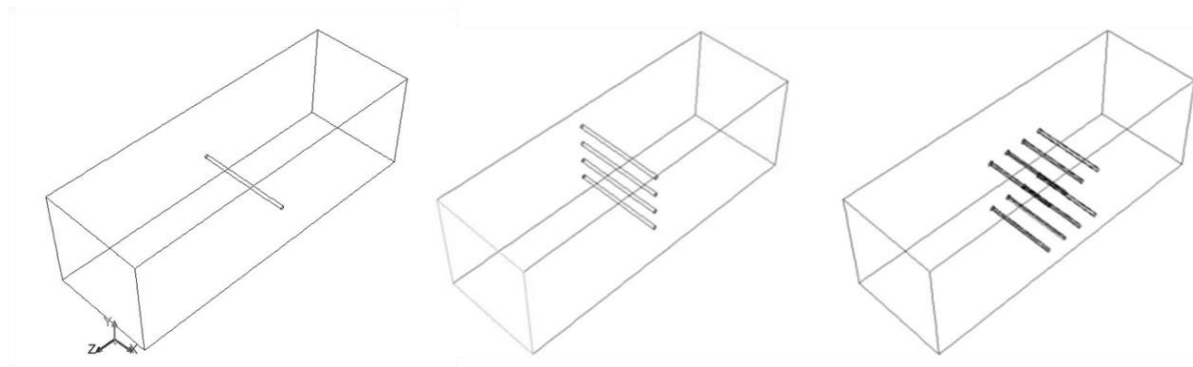
Figure 5.6 Geometry from left to right for the EPA 600/R-06/050, EPA 600/R-06/051 and EPA 600/R-06/055

The EPA tests were conducted on devices available on the market, and show increasingly complex lamp geometry. The lamp and UV systems specifications are listed in Table 5-1.

Table 5-1 EPA tests specifications.

Spec	600/R-06/050	600/R-06/051	600/R-06/055
Number of lamps	1	4	8
Lamp power	58 Watts	25 Watts	60 Watts
Lamp UVC power	19 Watts	8.5 Watts	18 Watts
Total system power	58 Watts	100 Watts	480 Watts
Total system UV power	19 Watts	34 Watts	144 Watts
Lamp length	53.3 cm	53.82 cm	61 cm
Lamp diameter	1.9 cm T6	1.9 cm T6	1.9 cm T6
Duct	61 cm x 61 cm	61 cm x 61 cm	61 cm x 61 cm
Duct length	7.83 m	7.83 m	7.83 m
Duct wall Emissivity	0.75-0.85-1.0	0.75-0.85-1.0	0.75-0.85-1.0
Duct wall Reflectivity	25%-15%-0%	25%-15%-0%	25%-15%-0%
Duct wall refractive index	1	1	1

The EPA experimental tests were conducted using two bacteria (*Bacillus atrophaeus* and *Serratia Marcescens*) and one virus (MS2 Bacteriophage), nebulised and aerosolized into an enclosed ducting ventilation test unit (Figure 5.7). The description of the tests, included in the EPA reports, state that the microorganisms were suspended in a fluid composed of salts and peptone and for the case of *S. marcescens* antifoam. This was aerosolised at 15 PSI using a collision nebuliser and injected into the test duct. Bioaerosol samples were taken before and after the UV device by the means of liquid impingers (Figure 5.7), and these samples were incubated and counted to quantify the efficacy of the UV sterilization system by the fraction of survival of microorganisms. Full details of the experimental methods adopted by EPA are given in the reports (EPA, 2006a, 2006b, 2006).
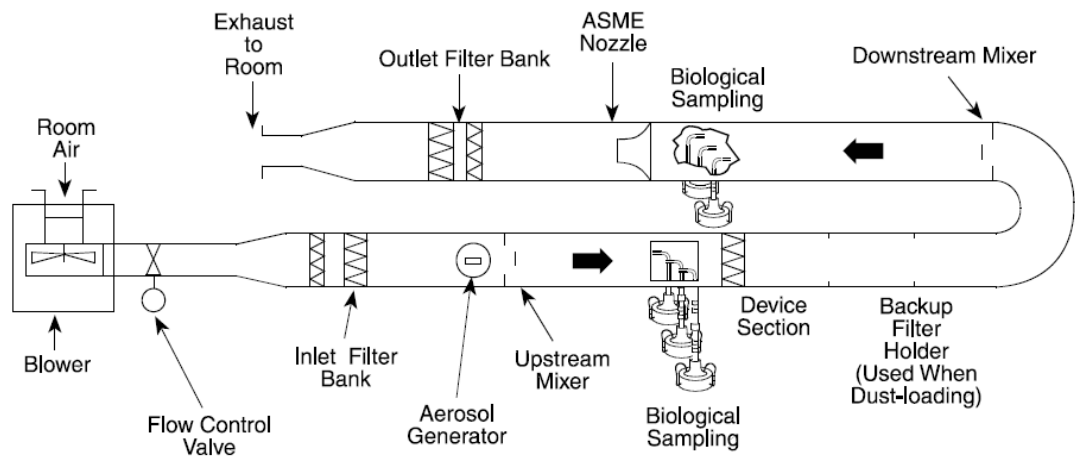
Figure 5.7 Schematic of test duct as shown in EPA tests.

In each case the EPA calculated the average UV dose delivered by the device using the single stage decay model (reviewed in Chapter 3). Experimental results in the test report were expressed in terms of microbiological inactivation or "kill" (1-survival), and a calculated mean dose was obtained with Equation 5-25 (explained in Chapter 3).

$$S = e^{-kD}$$

<div align="right">Equation 5-25</div>

5.3.1 CFD Model Development

CFD models of the EPA tests described above were carried using Fluent (ANSYS v13.0). The geometry of the UV chamber was based on details reported by EPA (Kowalski, 2009a, EPA, 2006a, EPA, 2006b, EPA, 2006c)., consisting of a duct area of 0.61 x 0.61 m and a duct length of 1.83 m. The airflow was developed in a duct with the same face area with a length of 6 m, and then incorporated at the inlet of the 1.83 m UV chamber as a developed velocity profile A structured mesh refined close to the lamps was defined using the ANSYS meshing module; the quality of the mesh is discussed in section 5.3.2 (Figure 5.8).
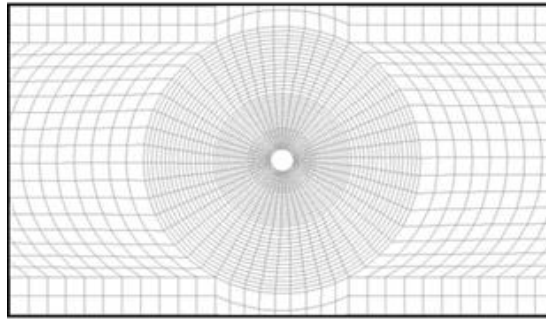
Figure 5.8 CFD modelled geometry for the single lamp case showing an example mesh around the lamp.

The materials assumed in the simulation were air as fluid and stainless steel as solid walls. All properties remained as standard, except for the absorption coefficient (α_c) and refractive index(n) of stainless steel which were adjusted to fit the wavelength of sterilisation UV light (253.7 nm) with values of 99,338,898 m^{-1} and 1 respectively (Chapter 4.5.4) (Karlsson and Ribbing, 1982). Originally stainless steel should have a diffusive wall reflectivity of 35% (Kowalski, 2009a), however reflectivity inside the UV chamber was not measured nor specified in the EPA reports. A different combination of material, dirt or dust could have impact on the wall reflectivity, therefore the CFD models were run at three values of diffusive wall reflectivity 25% (emissivity=0.75), 15% (emissivity=0.85) and 0% (emissivity=1), it was found that the latter (15% diffusive wall reflectivity) better approached the values reported by the EPA. Irradiation was based on the power and geometry stated in the EPA reports (Table 5-1). Flow was assumed to be steady and isothermal in all cases, with turbulence approximated through the k-ε model with standard wall functions. Boundary conditions were set as indicated in Table 5-2.

Table 5-2 CFD Model Boundary Conditions.

Zone	Property	600/R-06/050	600/R-06/051	600/R-06/055
Inlet	Velocity magnitude (m.s^{-1})	2.5*	2.5*	2.5*
	Turbulent intensity (%)	10	10	10
	Hydraulic diameter (m)	0.61	0.61	0.61
Walls	No slip	-	-	-
	Diffuse fraction	1	1	1
	emissivity	1.0, 0.85, 0.75	1.0, 0.85, 0.75	1.0, 0.85, 0.75
UV lamps	Direct irradiation (W.m^{-2})	0	0	0
	Diffuse irradiation (W.m^{-2})	597.2 per lamp*	294.17 per lamp*	494.36 per lamp*

*Data taken from EPA reports.

The solution methods used were SIMPLE scheme (Semi-Implicit Method for Pressure-Linked Equations) for pressure-velocity coupling, while the spatial discretization used the Least Square Cells Based Solution for gradient, Second order discretization solution for pressure, and Second Order Upwind for momentum, turbulent kinetic energy, turbulent dissipation rate, energy and discrete ordinates; calculations were run for approximately 3000 iterations with a convergence criteria of 10^{-6} on residuals .

5.3.2 Discrete Random Walk

Once a converged flow field had been obtained, Lagrangian particle model with Discrete Random Walk (eddy lifetime model) was used to simulate airborne microorganisms carried by the flow (King et al., 2013). The turbulent dispersion of particles can be predicted by stochastic tracking models (random walk), which considers the effect of instantaneous turbulent velocity fluctuation of the particle trajectory.

During a turbulent flow the CFD code (ANSYS) predicts the trajectory of particles using the average fluid phase velocity ($\bar{u}$), moreover, the code allows to introduce the values of fluctuating gas (u').

$$u = \bar{u} + u'$$

Equation 5-26

Then the code predicts the particle turbulent dispersion by integrating the trajectory equation for each individual particle. A number of tries, representing the number of times a particle will be injected to represent its final path, is assigned to each particle and in this manner the random effect of turbulence is included on the particle dispersion. Moreover, the Discrete Random Walk (DRW) includes a time scale constant to solve at discrete constant functions of time.

The number of particles injected in the system is defined by the number of cells at the surface area, in this case one particle stream is released from each cell at the inlet, in average each simulation accounted between 10,000 to 13,000 particle tracks.

The parameters of the Random Walk simulation included using particles with physical characteristics of water liquid droplets, diameter distribution ranging from 3×10^{-8} to 3×10^{-6} m (0.03 micros to 3 microns) divided along 20 number of diameters with a spread factor of 3.5, injected by surface at the inlet of the CFD models as described in Chapter 4.5.5, and using a DRW tracking method with an assigned number of tries value of 3 and a time scale constant of 0.15, the particle injection was made over 500 steps.

Results of the airflow development are shown in Figure 5.26. The flow developed evenly towards the centre of the duct until reaching the lamp located at Z 0.915 m (centre of the 1.83 m UV chamber).
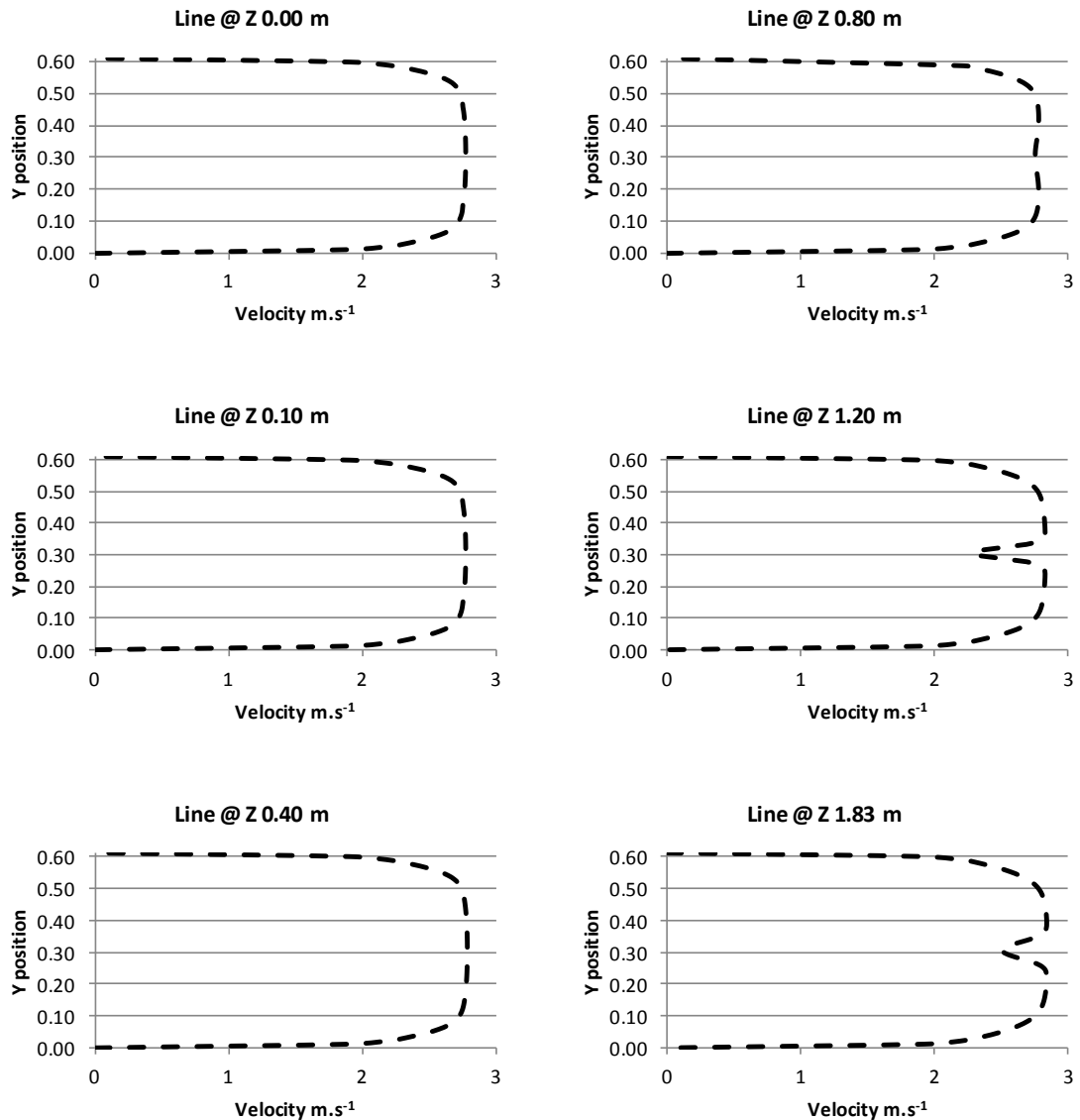
Figure 5.9 Airflow profiles along the duct length (z) for the single lamp CFD model EPA 600/R-06/050.

5.3.3 Mesh Quality

Mesh independency tests were carried for the single lamp (EPA 600/R-06/050) CFD model. The calculation was run for three different mesh sizes containing 100,000 160,000 and 280,000 elements respectively. Flow profiles were taken at six different points within the duct at the UV system section. The total volume average velocity and pressure were consistent between the three models, and in each case the average UV dose at the end of the domain was calculated using the arithmetic mean of the dose for all the particle tracks. All three models were run at

25% diffusive wall reflectivity (0.75 emissivity) and yielded similar values of average UV dose in a range of 12.137 to 12.271 J.m^{-2} (Table 5-3).

Table 5-3 Calculated UV Dose for the Three mesh sizes for the EPA 600/R-06/050 CFD Models.

Model	Average Dose J/m^2	Average velocity (m/s)	Average pressure (Pa)
100 k mesh	12.228	2.500	0.117
160 k mesh	12.234	2.509	0.117
280 k mesh	12.271	2.487	0.135

The velocity profiles of the three models appear to be relatively identical with minimal differences at the end of the duct (Z 1.83m) (Figure Figure 5.10).
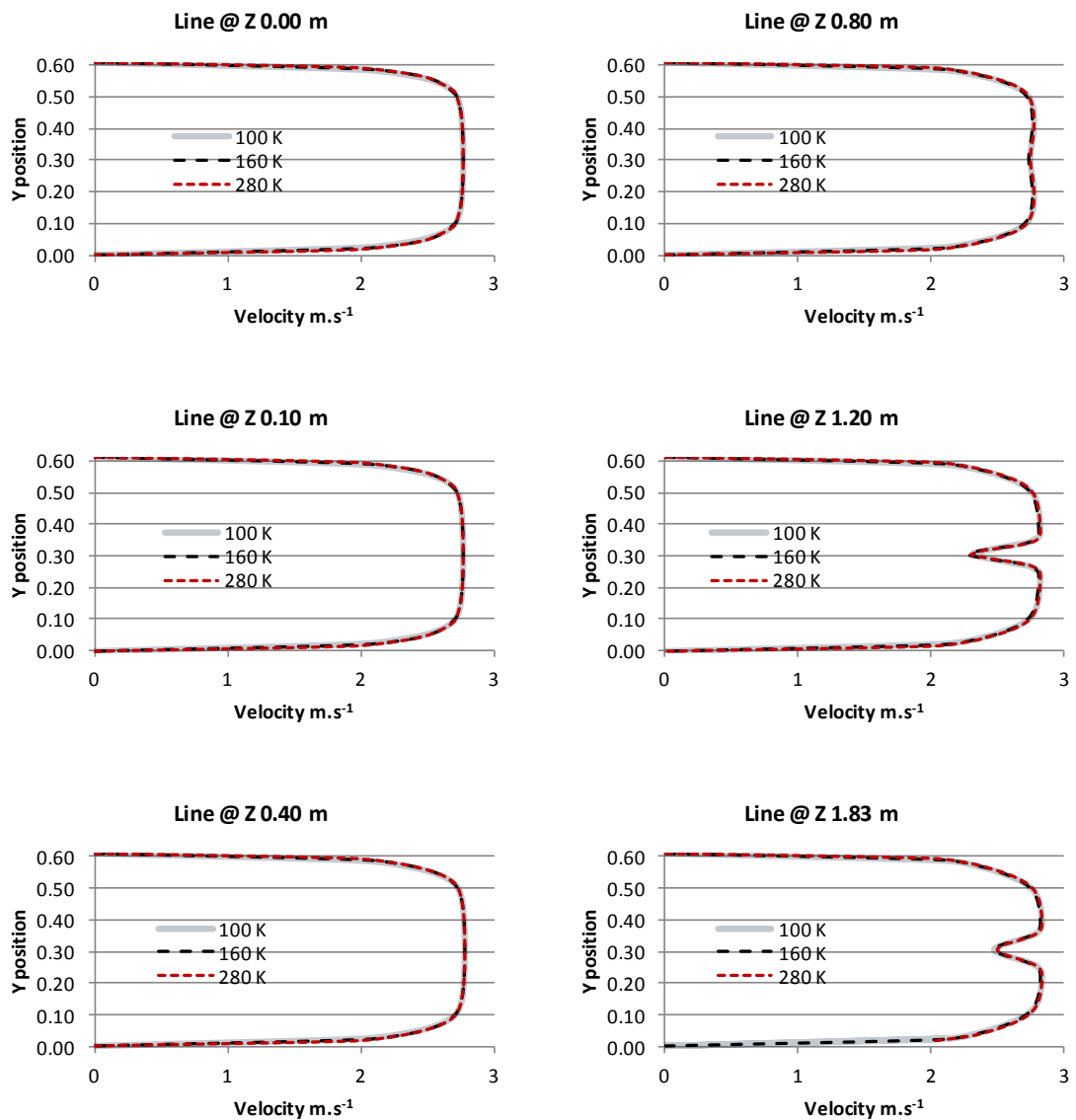
Figure 5.10 Velocity profile for the 100,000 160,000 and 280,000 element size CFD models.

When comparing pressures, there appears to be minimal differences of less than 0.05 Pascal between the models (Figure 5.11).
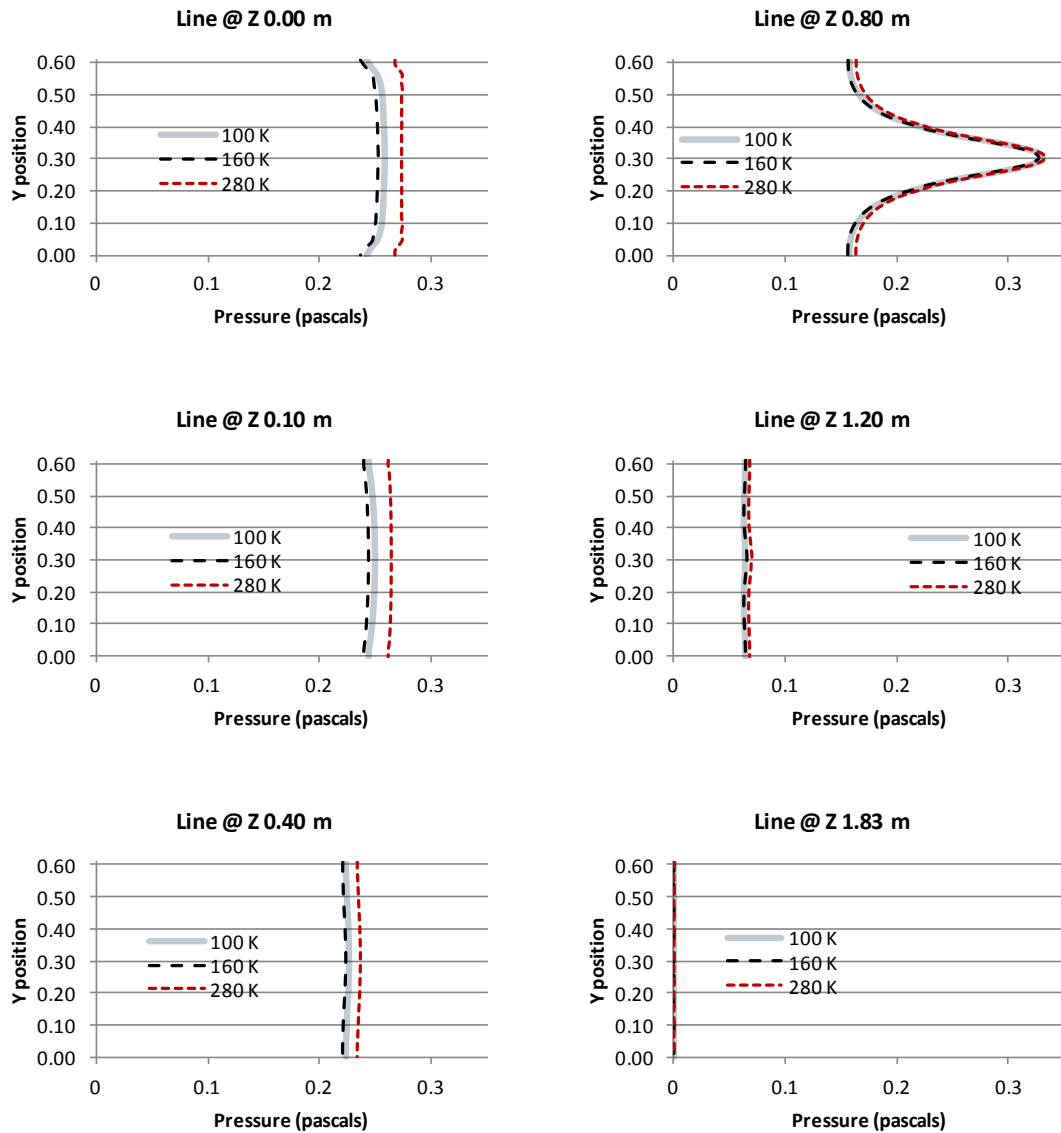
Figure 5.11 Pressure profile for the 100,000 160,000 and 280,000 element size CFD models.

Finally to check on mesh independency, the turbulent kinetic energy (k) (Figure 5.12), dissipation rate (ε) (Figure 5.13) and the Reynolds number (Figure 5.14) were compared for the three cases. These parameters also showed three virtually equal profiles, confirming mesh independency.
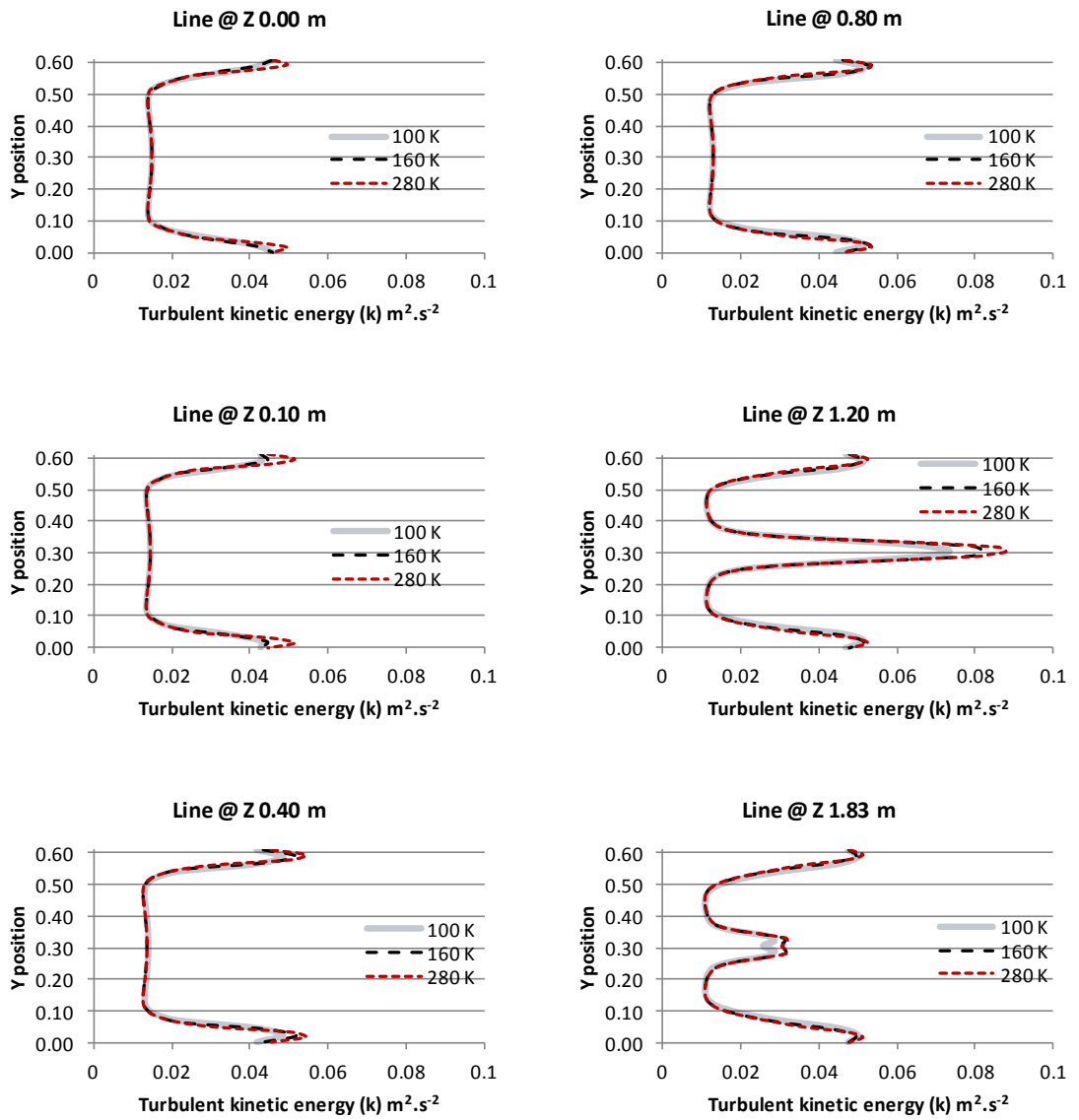
Figure 5.12 Turbulent kinetic energy (k) profile for the 100,000 160,000 and 280,000 element size CFD models.
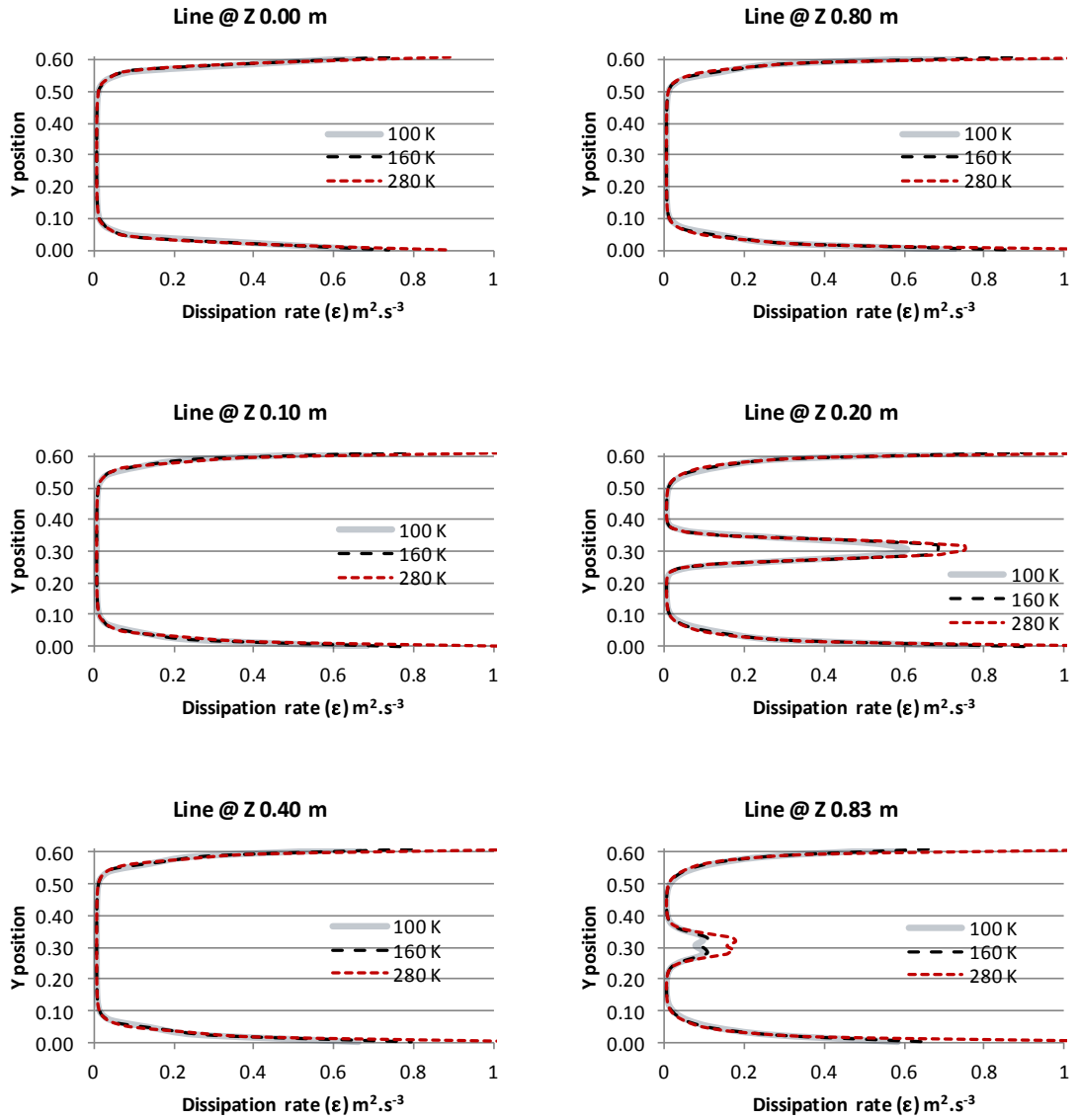
Figure 5.13 Dissipation rate (ε) profile for the 100,000 160,000 and 280,000 element size CFD models.
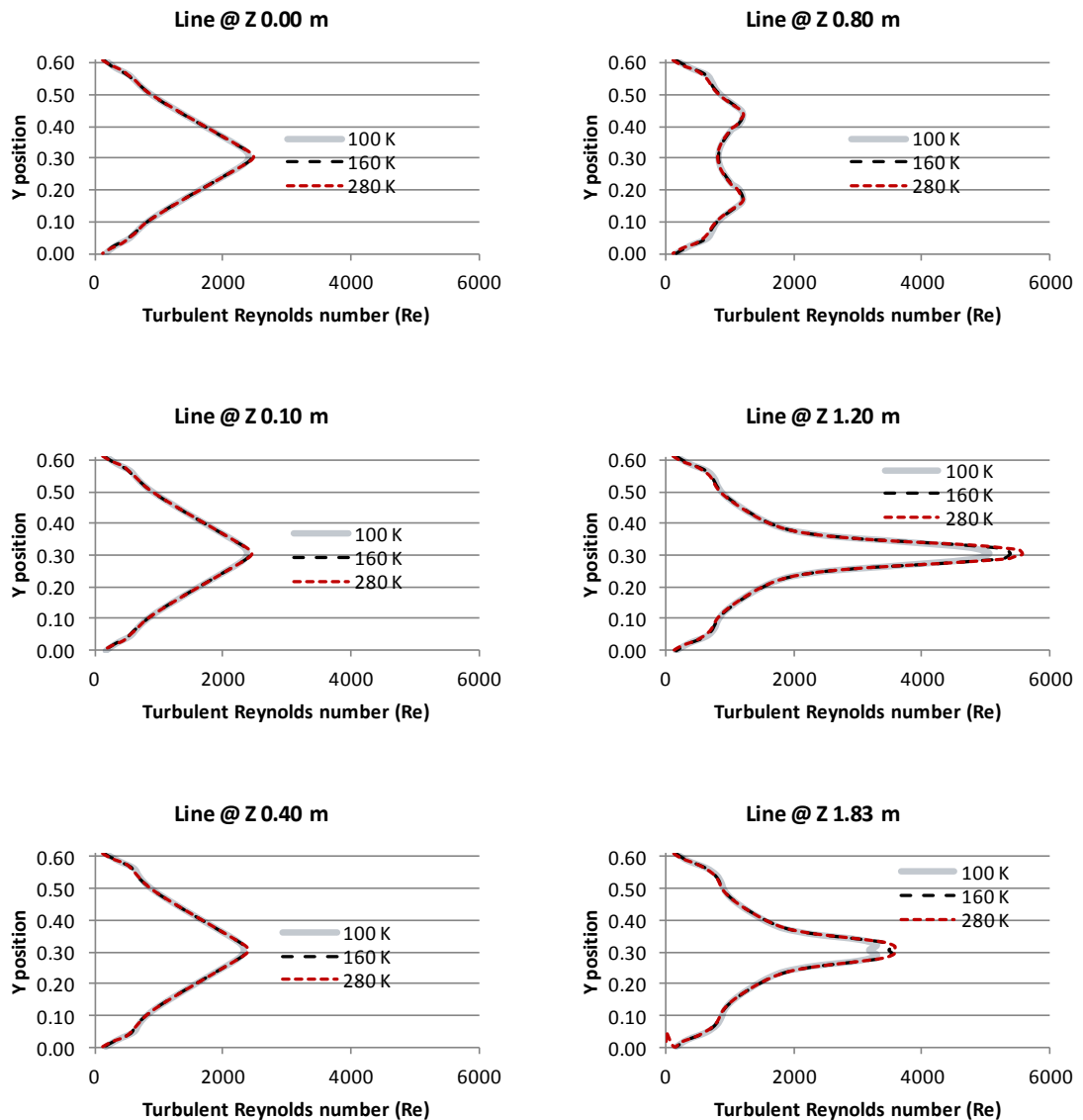
Figure 5.14 Reynolds number (Re) profile for the 100,000 160,000 and 280,000 element size CFD models.

Although the behaviour of the three mesh sizes are similar, the 280,000 mesh is able to better capture the subtleties of the airflow pattern, and for these reasons this mesh model is used in further calculations.

The other two models, EPA 600/R-06/051 and EPA 600/R-06/055, used the same element size as the 280,000 mesh of the EPA 600/R-06/050 CFD model.

5.3.4 CFD calculated inactivation performance.

All three EPA test reports measured microbiological kill rate of *B. atrophaeus*, *S. marcescens* and MS2 Bacteriophage, then determined UV dose via calculation from the UV susceptibility of *B. atrophaeus*. In the case of the CFD model, UV dose is directly calculated from the trajectory of

the simulated microorganism through the calculated UV field, then inactivation is determined. Both approaches depend on appropriate data for microorganism susceptibility (Chapter 3). Table 5-4 shows the EPA reported kill rates for the three different systems.

Table 5-4 EPA reported microorganisms kill rates.

EPA Microorganism kill rate	600/R-06/050	600/R-06/051	600/R-06/055
S. Marcesens	99%	99.8%	99.9%
MS2	39%	46%	82%
B. atrophaeus	4%	0%	40%

The UV susceptibility of *S. marcescens* in air has been extensively tested as shown in Chapter 3.4.11, and both Fletcher et al. (2003) and Lai et al. (2004) suggests a single stage decay model is appropriate. Both calculated a susceptibility constant of 0.92 $m^2.J^{-1}$ to 0.939 $m^2.J^{-1}$, yet this is higher than the value of 0.445 $m^2.J^{-1}$ reported in Sharp (1940). For the case of MS2 Bacteriophage, Walker et al. (2007) reported values of k=0.038 $m^2.J^{-1}$ for 32-50% relative humidity and k=0.048 $m^2.J^{-1}$ for 74-82% relative humidity. For the next microorganism under analysis, *Bacillus atrophaeus,* the susceptibility value used by EPA (2006a) is said to be k=0.016 $m^2.J^{-1}$. The RTI study by VanOsdell and Foarde (2002) reported the susceptibility of *B. subtilis* spores to be 0.02 $m^2.J^{-1}$. As discussed in Chapter 3.4.1, *B. subtilis* spores do not follow a first order decay model and are better represented with a shoulder (n) in its decay model (Kowalski, 2009a, Nicholson and Galeano, 2003). Ke et al. (2009) reported susceptibility values for *B. subtilis* spores to be 0.017 $m^2.J^{-1}$ with a shoulder (n) of 3 for relative humidity levels of 50 to 60% and 0.014 $m^2.J^{-1}$ with a shoulder (n) of 2 for relative humidity levels of 70 to 83% (Chapter 3.5.2).

The EPA calculated the average UV dose of the systems by regression of the kill rate of *B. atrophaeus* spores using a microorganism susceptibility constant of 0.016 $m^2.J^{-1}$ (EPA, 2006). Table 5-5 shows a comparison of the average UV dose reported by the EPA tests, the UV dose calculated by Kowalski (2009a) and those calculated by CFD modelling at 0%, 15% and 25% wall reflectivities.

Table 5-5 Average UV dose calculated by EPA, Kowalski and current CFD studies, and the EPA reported UV dose.

	600/R-06/050 J.m^{-2}	600/R-06/051 J.m.^{-2}	600/R-06/055 J.m.^{-2}
EPA reported average UV dose	2.47	2.95	31.80
Kowalski reported average UV dose	10	18	73
This study CFD 0% wall reflectivity average UV dose	9.22	15.52	58.27
This study CFD 15% wall reflectivity average UV dose	10.97	18.45	70.19
This study CFD 25% wall reflectivity average UV dose	12.27	20.63	79.76

Kowalski (2009a) calculated UV dose and the CFD calculated UV dose at 15% reflectivity are quite similar, however slight differences are present. The reasons for the difference between the EPA, Kowalski and CFD results from the current study are various. Kowalski (2009) calculated a dose of 10 J.m^{-2} for the EPA 600/R-06/050, 18 J.m^{-2} for the EPA 600/R-06/051 and 73 J.m^{-2} for the EPA 600/R-06/055; however he did not consider a fully developed airflow, and did not account for airflow patterns and particle trajectories within the system. The CFD models here presented used a developed airflow in a duct of 6 m long prior to the entering the UV chamber of 1.83 m long and considered trajectories and the 3D UV irradiance field. Another issue is the reflectivity within the duct, the EPA did not report the reflectivity of the material, and for that reason Kowalski (2009a) assumed a 25% diffusive wall reflectivity as such value better approached the EPA result, for the CFD model 0%, 15% and 25% diffusive wall reflectivity values were used in the analysis, finding that results at 15% reflectivity matched both, the calculated UV doses reported by Kowalski (2009a) and the kill rates reported by EPA (EPA, 2006a, EPA, 2006b, EPA, 2006c). The susceptibility values of *B. subtillis* spores used by EPA for the calculation of the systems UV dose is one of the main reasons on the difference in calculated performance. The EPA calculated performance by regression of kill rate of *B. subtillis* spores, while Kowalski (2009) and the CFD study calculated average UV dose of the system to then calculate sterilisation performance. This combined with the natural variation found in microbial tests can be the reason for the slight differences on results. Nevertheless the CFD models were successful on reproducing experimental results with more than 90% accuracy.

The performance kill rate of CFD models were calculated using a range of UV susceptibilities as for each microorganism as reported in Chapter 3. For *S. marcescens* it was used an average kill rate obtained from the susceptibilities reported by Fletcher et al. (2003) at 48% relative humidity (RH), Sharp (1940) and Lai et al. (2004) at 68% RH. For the MS2 Bacteriophage is was used an average of the susceptibilities reported by Walker and Ko (2007) at 32-50% RH and 74-85% RH.

The kill rate of *B. atrophaeus* spores was calculated using the single stage with shoulder model with an average UV susceptibility obtained from the reports of VanOsdell and Foarde (2002) and Ke et al. (2009) at 50-60% RH and 70-83% RH.

Table 5-6 EPA 600/R-06/050 CFD Calculated Performance against test results using 0%, 15% and 25% wall reflectivity.

Reference values	Microorganism	RH %	*n value	K m²·J⁻¹	EPA Test Kill rate	CFD 0%R 9.22 J.m⁻² Kill rate	CFD 15%R 10.97 J.m⁻² Kill rate	CFD 25%R 12.27 J.m⁻² Kill rate
Fletcher 2003	*S. marcescens*	48	-	0.939	99%	99.82%	99.96%	99.98%
Sharp 1940		Low	-	0.445		96.20%	98.26%	98.65%
Lai 2004		68	-	0.920		99.79%	99.96%	99.98%
Average		-	-	*0.662*		***99.03%***	***99.71%***	***99.89%***
Walker 2007	MS2 Bacteriophage	32-50	-	0.038	39%	28.45%	33.03%	36.63%
Walker 2007		74-85	-	0.048		34.28%	39.54%	43.63%
Average		-	-	*0.043*		***31.44%***	***36.38%***	***40.24%***
VanOsdell 2002	*B. subtillis* (*B. atrophaeus*)	-	-	0.020	4%	16.36%	19.22%	21.53%
Ke et al. 2009		50-60	3	0.017		0.43%	0.62%	0.81%
Ke et al. 2009		70-83	2	0.014		1.61%	2.15%	2.65%
Average		-	1.66	*0.017*		***4.18%***	***5.36%***	***6.40%***

*N value= shoulder

In the case of the single lamp model, the kill rate of *S. marcescens* is matched by all three wall reflectivities, this is due to the relatively high UV susceptibility of the microorganism. However, as the UV susceptibility of MS2 Bacteriophage and *B. subtillis* is stronger, differences in results are more evident. MS2 Bacteriophage appears to be better represented by the results at 15% reflectivity, and B. atrophaeus is better represented by results at 0% reflectivity. In general it seems that 15% diffusive wall reflectivity better reflects the EPA lab results, showing no difference on the kill rate of *S. marcescens*, and only 2.62% difference in the kill rate of MS2 Bacteriophage and 1.36% difference in the kill rate of *B. subtillis* spores. Now for the EPA 600/R-06/051 showing a 4 lamps system, the results are relatively similar, however in this case the model without reflectivity seems closer to EPA reported results, nevertheless the results of the 15% diffusive wall reflectivity are not far from those reported by EPA (Table 5-7).

Table 5-7 EPA 600/R-06/051 CFD Calculated Performance against test results using 0%, 15% and 25% wall reflectivity.

Reference values	Microorganism	RH %	*n value	K m².J⁻¹	EPA Test Kill rate	CFD 0%R 15.52 J.m⁻² Kill rate	CFD 15%R 18.45 J.m⁻² Kill rate	CFD 25%R 20.63 J.m⁻² Kill rate
Fletcher 2003		48	-	0.939		99.99%	100%	100%
Sharp 1940	*S. marcescens*	Low	-	0.445	**99.9%**	99.70%	99.92%	99.95%
Lai 2004		68	-	0.920		99.99%	100%	100%
Average		-	-	*0.662*		***99.96%***	***100%***	***100%***
Walker 2007	MS2 Bacteriophage	32-50	-	0.038		43.99%	49.90%	53.72%
Walker 2007		74-85	-	0.048	**46.0%**	51.77%	58.10%	62.06%
Average		-	-	*0.043*		***48.03%***	***54.19%***	***58.03%***
VanOsdell 2002		-	-	0.020		26.47%	30.67%	33.55%
Ke et al. 2009	*B. subtillis* (*B. atrophaeus*)	50-60	3	0.017	**0.0%**	1.39%	2.10%	2.78%
Ke et al. 2009		70-83	2	0.014		3.94%	5.30%	6.43%
Average		-	1.66	*0.017*		***8.95%***	***11.41%***	***13.31%***

*N value= shoulder

It can be seen in Table 5-7 that the EPA 600/R-06/051 test reported a 0.00% kill rate on *B. atrophaeus*, while the CFD model predicts 8.95%, 11.41% and 13.31%. It is thought that this value of 0.00% is an error in the experimental data as a higher UV power for the four lamps model (34 Watts) than the single lamp model (19 Watts) should result in a higher kill rate. It is also worth commenting on the results for *S. marcescens*, as they show very close comparison between CFD and experiments for all three lamp configurations. However, *S. marcescens* is highly susceptible to UV light, and any UV dose over 10 J.m⁻² would result in a 99.99% kill rate. Therefore it is not a good reference microorganism to conduct UV dose calculations or experimental assessments for duct mounted installations.

Finally, the EPA 600/R-06/055 which consisted of a complex geometry of 8 lamps showed the following results (Table 5-8).

Table 5-8 EPA 600/R-06/055 CFD Calculated Performance against test results using 0%, 15% and 25% diffusive wall reflectivity.

Reference values	Microorganism	RH %	*n value	K m².J⁻¹	EPA Test Kill rate	CFD 0%R 58.27 J.m⁻² Kill rate	CFD 15%R 70.19 J.m⁻² Kill rate	CFD 25%R 79.76 J.m⁻² Kill rate
Fletcher 2003		48	-	0.939		100%	100%	100%
Sharp 1940	*S. marcescens*	Low	-	0.445	**99.9%**	100%	100%	100%
Lai 2004		68	-	0.920		100%	100%	100%
Average		-	-	0.662		***100%***	***100%***	***100%***
Walker 2007	MS2 Bacteriophage	32-50	-	0.038		87.95%	92.13%	94.57%
Walker 2007		74-85	-	0.048	**82.0%**	92.94%	95.83%	97.41%
Average		-	-	*0.043*		***90.79%***	***94.28%***	***96.26%***
VanOsdell 2002		-	-	0.020		67.83%	74.43%	78.92%
Ke et al. 2009	*B. subtillis* (*B. atrophaeus*)	50-60	3	0.017	**40.0%**	24.81%	33.34%	40.34%
Ke et al. 2009		70-83	2	0.014		30.81%	38.57%	44.70%
Average		-	1.66	*0.017*		***45.53%***	***53.95%***	***60.14%***

*N value= shoulder

It can be seen from Table 5-6, Table 5-7 and Table 5-8 that there is considerable variation in the calculated inactivation of *B. atrophaeus* from the CFD model depending on the susceptibility constant and whether single stage or shoulder decay model is used. This is of paramount importance if measured inactivation rates are used to calculate UV dose by biodosimetry regression, as done by the EPA test, and explains why the reported UV dose calculated from the EPA tests is lower than that determined by the CFD analysis.

The EPA test 600/R-06/050, 600/R-06/051 and 600/R-06/055 rated the performance of the systems by regression of the kill rate of *B. atrophaeus* in single stage decay at the susceptibility value of 0.016 $m^2.J^{-1}$ (EPA, 2006). If the EPA stated UV dose value is used to calculate the inactivation rate of the other tested microorganisms *S. marcescens* and MS2 Bacteriophage, using the average susceptibility constants as given in Table 5-6, we would obtain the results as shown in Table 5-9.

Table 5-9 Calculated kill rates using EPA Tests stated UV dose.

Microorganism	EPA	EPA Dose J.m^{-2}	Susceptibility reference	EPA Test measured kill rate	EPA Dose Calculated kill rate
B. atrophaeus *S. marcescens* MS2 Bacteriophage	600/R-06/050	2.47	Average	4.0% 99.0% 39.0%	2.20 % 90.16% 10.07%
B. atrophaeus *S. marcescens* MS2 Bacteriophage	600/R-06/051	2.95	Average	0.0% 99.0% 46.0%	0.66% 85.81% 11.91%
B. atrophaeus *S. marcescens* MS2 Bacteriophage	600/R-06/055	31.80	Average	40.0% 99.9% 82.0%	56.0% 100% 95.66%

The UV dose delivered by an enclosed UV system working under normal constant operation should remain constant as it is function of the physical and irradiation parameters of the system only. Therefore when calculating the UV dose of a system by regression of biodosimetry test results, the calculated dose of the system should remain constant independently of the microorganism used; if it is different, then it is an indication that the microorganism decay model used for the calculation is wrong.

The UV dose calculated by the EPA by regression of the kill rate of *B. atrophaeus* spores (EPA, 2006a, EPA, 2006b, EPA, 2006c) was wrong as it assumed a single stage decay curve, and did not account for its shoulder. This resulted on an under calculation of the UV dose of the system. It was shown that the average UV dose calculated by CFD modelling for each system achieved the kill rate performances for each microorganism as reported by the EPA, and at the same time

matched the calculated UV doses reported by Kowalski (2009a). Moreover, the reasons for the differences in results were also explained.

5.3.5 Multi-susceptibility

The UV susceptibility of a microorganism, being a biological parameter presents a considerable amount of variation as expressed in Chapter 3. Even the same microorganisms can present variations in susceptibility due differences between strains (Fletcher, 2004). Some microorganisms might behave in a rather standardise manner, and show a UV susceptibility that is somewhat stable with changes and does not result in significant effects in UV sterilisation performance, such as in the case for *M. bovis* (Peccia and Hernandez, 2004). Others, as in the case of *B. atrophaeus* present large changes in susceptibility that can affect the performance of a system in a significant manner.

Prior research dealt with variations in susceptibility by averaging a single value (Kowalski, 2009a). Without the use of single particle tracking, multi-susceptibility analysis would be impossible and the performance of a system would be given by either its average UV dose, or the calculated sterilisation rate of a single microorganism.

CFD modelling benefits from the ability to calculate representative particle trajectories (scalars) independently and treat them as microorganisms with their own susceptibility constant. Therefore it is possible to assign a randomised susceptibility value to each particle, normally distributed within a certain range, to observe the performance of a UV system. Previous research showed the performance based on the kill rate of a specific pathogen individually, as the average UV dose was calculated as a surface integral and could not account for particle trajectories (Kowalski et al., 2001). By using a multi-susceptibility technique it is possible to determine the reliability of the system based on the standard deviation of its performance.

To calculate microbial decay due to UV irradiation it is necessary to know the microorganism received UV dose (D) and the microorganism UV susceptibility (k) which as it was explained in Chapter 3, can vary over a given range for each microorganism, thus it is common practice to use the average UV susceptibility value, and to use the average UV dose of the system to calculate microbial decay (chapter 3). However, the use of computational fluid dynamics allow us to calculate the specific microorganism decay (or kill rate) for each scalar, and to obtain the average microbial decay of the system by accounting for each scalar. Moreover, it is possible to modify the UV susceptibility value (K) in the calculation of each scalar. This gives the flexibility to use a band range of susceptibility values, which appears to be a more realistic alternative for

the microbial decay calculation, than using the average UV susceptibility of a microorganism family.

To compare the CFD results directly to the EPA tests, each microorganism was independently simulated with a suitable range of susceptibilities. Each CFD simulation tracked in average 10,000 scalars, at the end of the duct each scalar reported the UV irradiation dose (D) received as it passed through the system. For each scalar, the dose received remained constant while the UV susceptibility was modified randomly over an assigned range of susceptibilities, simulating the range of UV susceptibilities reported by each microorganism. For example, in the case of *B. subtilis* the susceptibility ranged from $0.014 - 0.020$ m^2.J^{-1} with shoulder values ranging from 1 to 3. The average UV dose of the system was then calculated. This same iteration, of leaving the scalar UV dose constant and modifying the assigned UV susceptibility, was run over 100 times for each UV system to calculate its average performance in a monte-carlo style calculation (Table 5-10).

Table 5-10 Multi-susceptibility performance.

Microorganism	EPA	EPA Test measured kill rate	M-S kill rate 0% R	M-S kill rate 15% R	M-S kill rate 25% R
S. marcescens[*]		99.0%	99.53%	99.57%	99.81%
MS2 Bacteriophage[**]	600/R-06/050	39.0%	31.41%	36.34%	40.21%
B. atrophaeus[***]		4.0%	3.77%	4.74%	5.59%
S. marcescens[*]		99.0%	99.98%	99.99%	99.99%
MS2 Bacteriophage[**]	600/R-06/051	46.0%	47.98%	54.13%	58.03%
B. atrophaeus[***]		0.0%	7.63%	8.47%	11.18%
S. marcescens[*]		99.9%	100%	100%	100%
MS2 Bacteriophage[**]	600/R-06/055	82.0%	90.68%	94.18%	96.17%
B. atrophaeus[***]		40.0%	40.28%	48.63%	54.98%

M-S=Multi-Susceptibility
*MS2 Bacteriophage – k=0.038-0.048 m^2.J^{-1}
**S. marcescens – k=0.430 – 0.920 m^2.J^{-1}
***B. subtillis – k= 0.014 - 0.020 m^2.J^{-1} with a shoulder n=1.33

5.3.6 UV dose distribution within a duct

CFD analysis can help to visualise important data which otherwise would be impossible to capture on a biodosimetry test. While the average UV dose for the single lamp model at 15% diffusive wall reflectivity and 25% diffusive wall reflectivity is calculated at 10.82 J.m^{-2} and 12.27 J.m^{-2} respectively, not all particles received the same amount of UV dose. In this case the CFD model is able to show the variation of UV dose within the system. Figure 5.15 shows the dose distribution received by particles at the end of the duct. The mode UV dose is somewhere located at 9 J.m^{-2} for the 15% diffusive wall reflectivity model and 10 J.m^{-2} for the 25% diffusive wall reflectivity, where the peak of %particles is. This is lower than the average UV dose of the

system which appears to be increased by a small number of particles receiving a very high dose. This means that a large population (56% population for the 15% diffusive wall reflectivity and 62% population for the 25% diffusive wall reflectivity) receive less than the average dose.

EPA 600/R-06/050
15% Reflectivity - Average UV dose 10.97 J.m⁻²

EPA 600/R-06/050
25% Reflectivity - Average UV dose 12.27 J.m⁻²
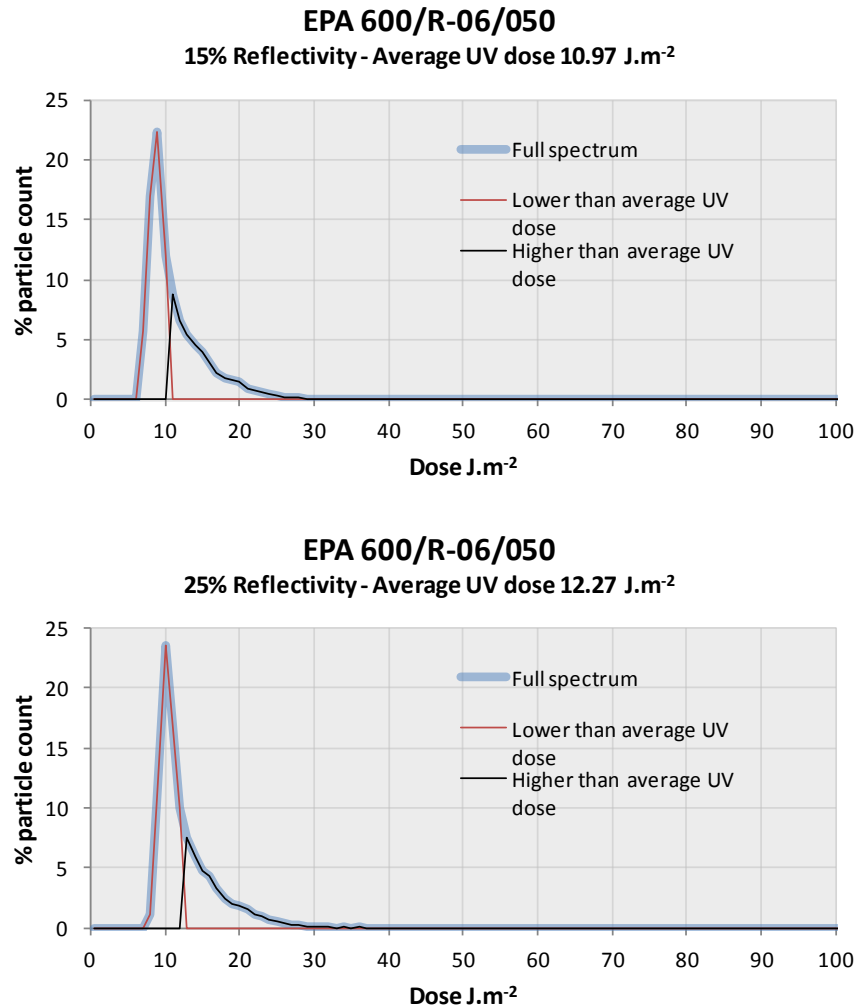
Figure 5.15 Dose distributions by particle track at the end of the duct for the EPA 600/R-06/050.

In reference to Figure 5.15, the ideal distribution would be a single sharp peak of particles all receiving the required UV dose; particles receiving less are underexposed and those receiving more UV dose than necessary can be translated as waste of resources. Figure 5.16 shows the end of the duct and the lamp location in relation with areas of the duct where particles received the average UV dose of the system or more. It can be seen a tall sharp peak before the point of average UV dose of the system, this peak represents the particles passing on top and below the UV lamp. The dose distribution of the single lamp system is relatively narrow, meaning that most particles received a similar UV dose, this can be seen by the standard deviation of the UV dose received by a particle, which in this case if of 4.40 J.m⁻².
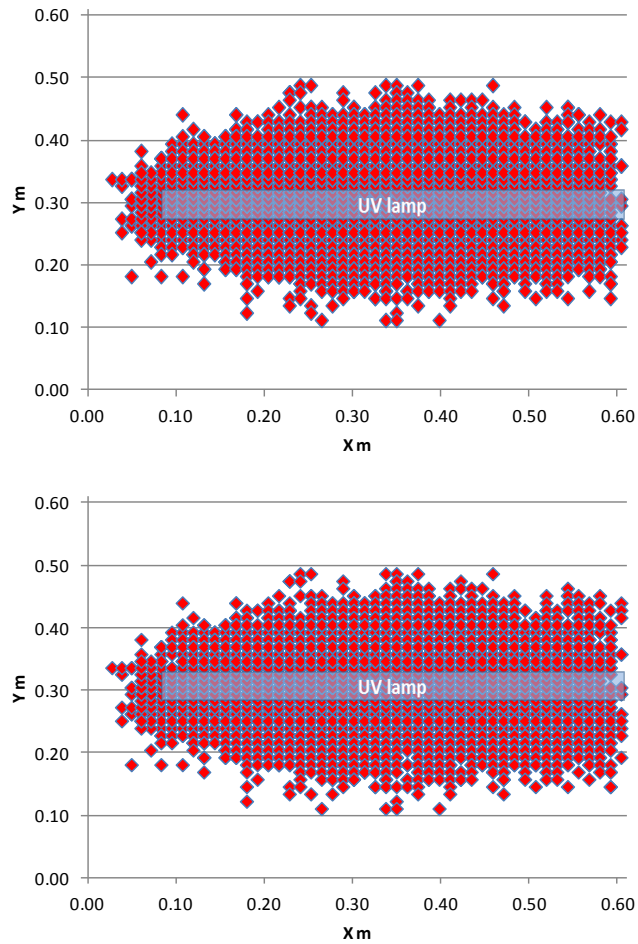
Figure 5.16 Cross section of the EPA 600/R-06/050 duct at 15% diffusive wall reflectivity (top) and 25% diffusive wall reflectivity (bottom) showing lamp position and location of particles receiving the average UV dose or more.

Each point on the plots in Figures 5.15 to 5.17 represents one of the simulated particle locations. An interesting insight to see how reflectivity affects the performance of a system is to see how the area of UV dose coverage changes at a specific UV dose. In this case Figure 5.17 shows how the UV dose coverage changes for particles receiving 10 J.m^{-2} when a 15% diffusive wall reflectivity or 25% diffusive wall reflectivity is present in the duct.
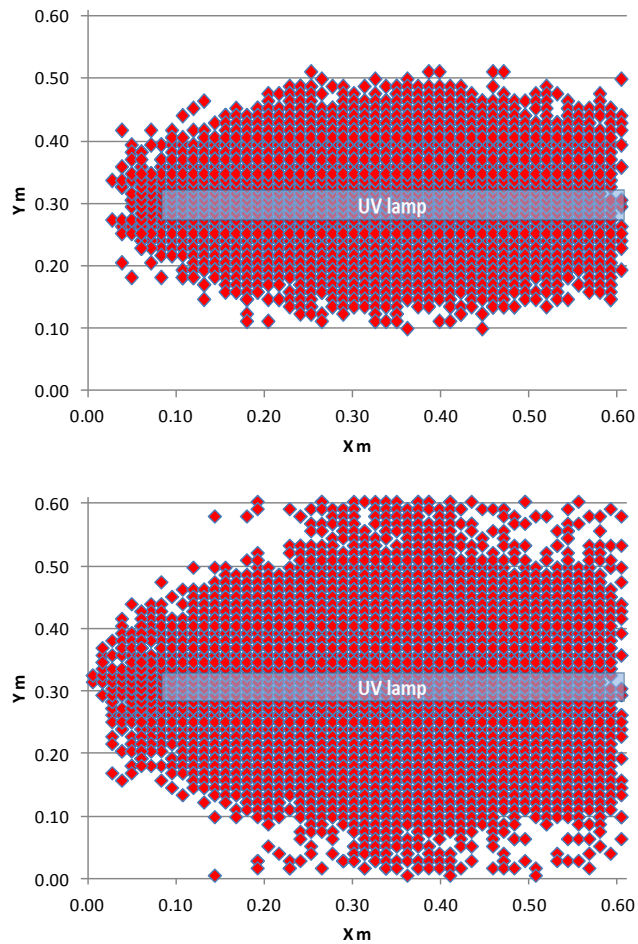
Figure 5.17 Area of UV dose coverage above 10 J.m^{-2} for a 15% (top) and 25% (bottom) diffusive wall reflectivity for the EPA 600/R-06/050.

It can be seen in Figure 5.16 how the area of coverage improves for 25% diffusive wall reflectivity and now it extends closer to the walls. Figure 5.18 shows the areas where particles received less than the average UV dose of the system. In this case the area was filtered for a 10 J.m^{-2} UV dose. The results indicate that duct corners have the lowest average irradiation values, with particles here receiving the lowest dose, while those that pass close to the lamp generally have higher than the average dose. This highlights the impact of lamp location and configuration, and the need to improve dose distribution while reducing energy consumption.
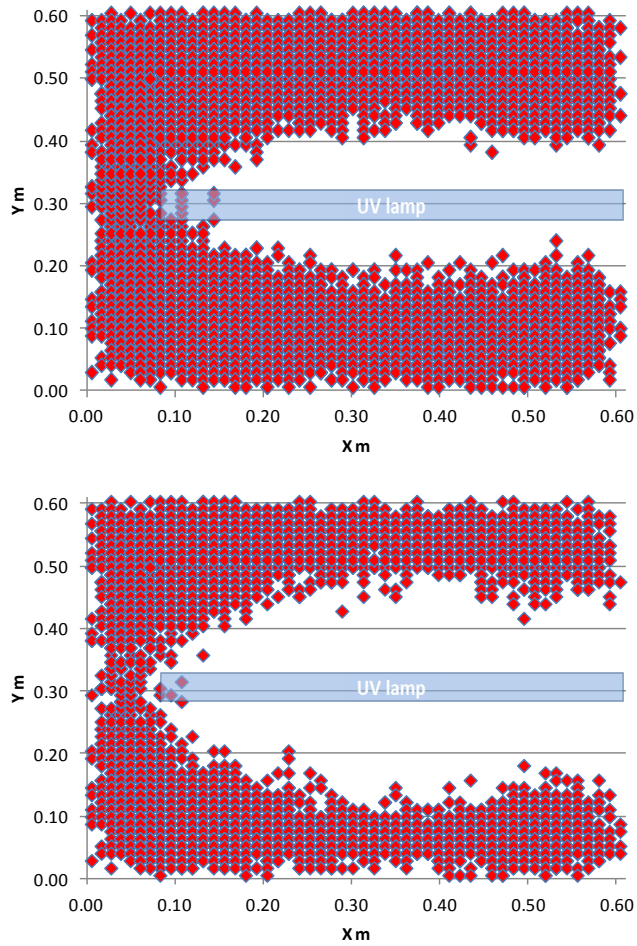
Figure 5.18 Cross section of the EPA 600/R-06/050 duct at 15% reflectivity (top) and 25% reflectivity (bottom) showing lamp position and location of particles receiving less than 10 J.m^{-2}.

Figure 5.19 shows the dose distribution for the case with four lamps evenly distributed over the height of the duct. The results show a double peaked distribution, with 50% of particles receiving the average UV dose or more.

EPA 600/R-06/051
Average UV dose 18.45 J.m^{-2}

EPA 600/R-06/051
Average UV dose 20.17 J.m^{-2}
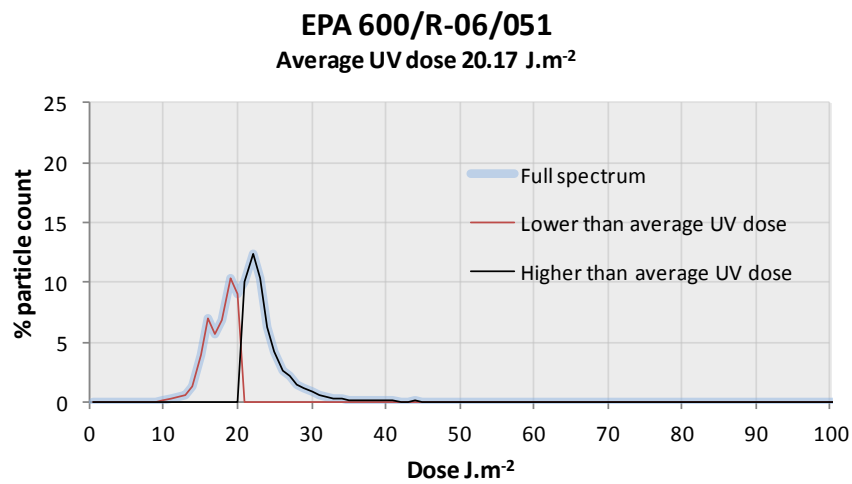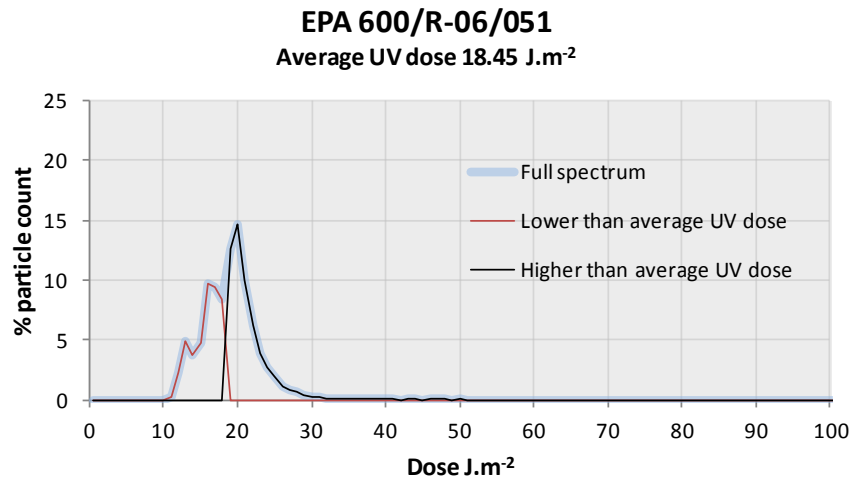
Figure 5.19 Dose distributions for EPA 600/R-06/051 at 15% reflectivity (top) and 25% reflectivity (bottom).

The dose distribution for the EPA/R-06/051 is relatively narrow, and almost 50% of particles receive the average UV dose or more. This is an indication of an even distribution across the face of the duct. Regarding the coverage of this design, it can be seen on Figure 5.20 how the four lamps distributed across the height of the duct delivered a more evenly distributed UV dose. The standard deviation of the dose received by the particles was of 3.87 J.m^{-2}.
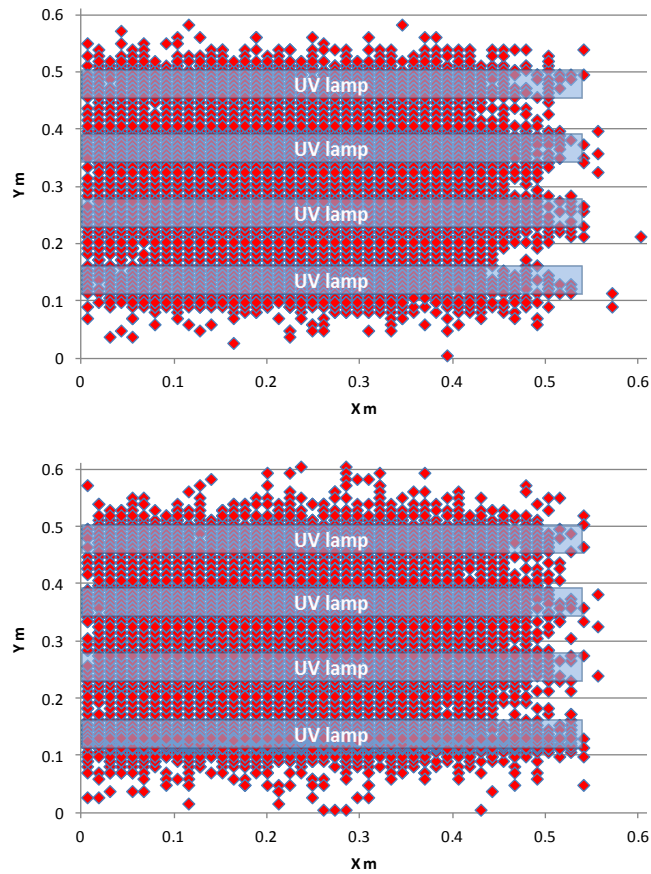
Figure 5.20 Cross section of the EPA 600/R-06/051 duct at 15% reflectivity (top) and 25% reflectivity (bottom) showing lamp position and location of particles receiving the average UV dose or more.

However, if we filter results to show particles receiving less than 15 J.m^{-2} it can be seen that the end corners of the duct, where there is a free space between the end of the lamps and the duct walls is the most compromised (Figure 5.21). This situation becomes more apparent when there is only 15% diffusive wall reflectivity. Figure 5.21 shows how an increase in reflectivity improves the UV dose area coverage of the system.
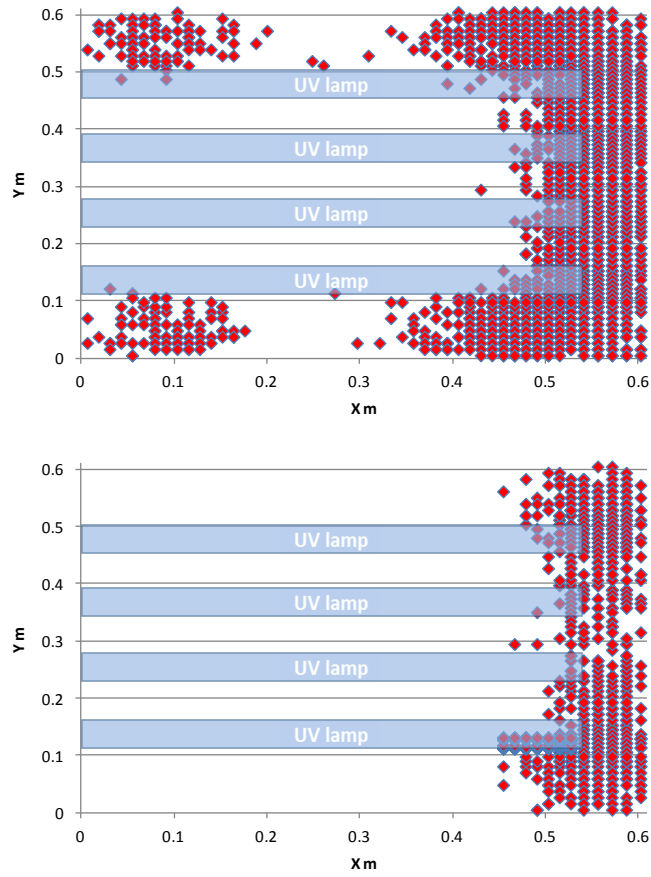
Figure 5.21 Cross section of the EPA 600/R-06/051 duct at 15% reflectivity (top) and 25% reflectivity (bottom) showing lamp position and location of particles receiving less than 15 J.m^{-2}.

When the wall reflectivity was increased from 15% to 25%, the particles receiving less than 15 J.m^{-2} were reduced, and were only presented at the end side of the lamps and close to the walls. This exemplifies the impact reflectivity can have on an in-duct system.

EPA 600/R-06/055
Average UV dose 70.19 J.m^{-2}
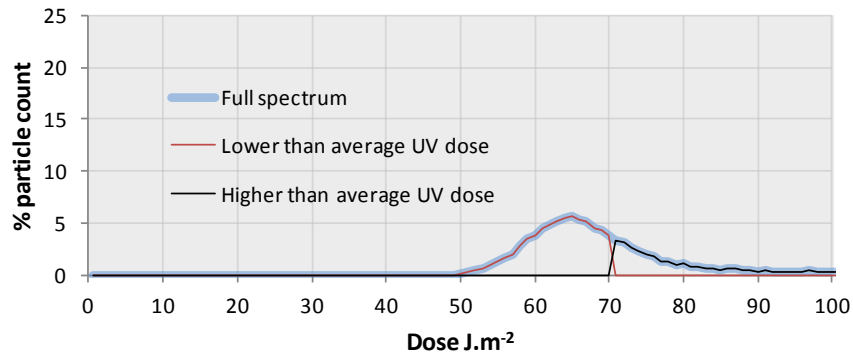
EPA 600/R-06/055
Average UV dose 79.76 J.m^{-2}
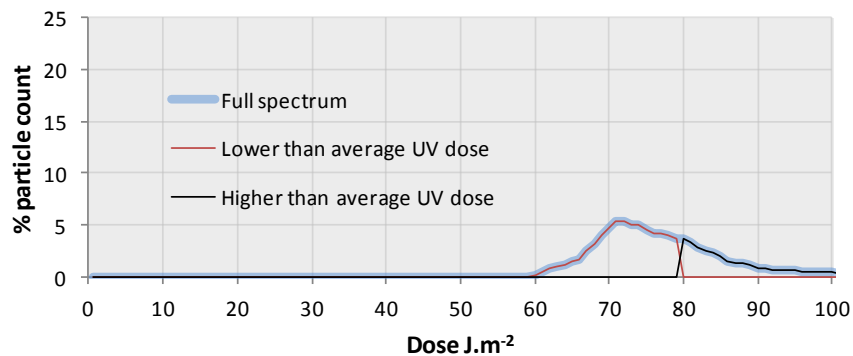
Figure 5.22 Dose distributions for EPA 600/R-06/055 at 15% reflectivity (top) and 25% reflectivity (bottom).

Figure 5.22 presents the eight lamp model, which shows a wider dose distribution, with only 37% of particles receiving the average UV dose or more. This broadened dose distribution is a sign of uneven irradiation distribution, as there is a considerably difference between the minimum and maximum dose received by a particle, this is also reflected in the standard deviation of the UV dose received by particles which for this system is of 14.87 J.m^{-2}. With this configuration, it can be seen that only the areas around the lamps appear to be covered with the average UV dose or more (Figure 5.23).
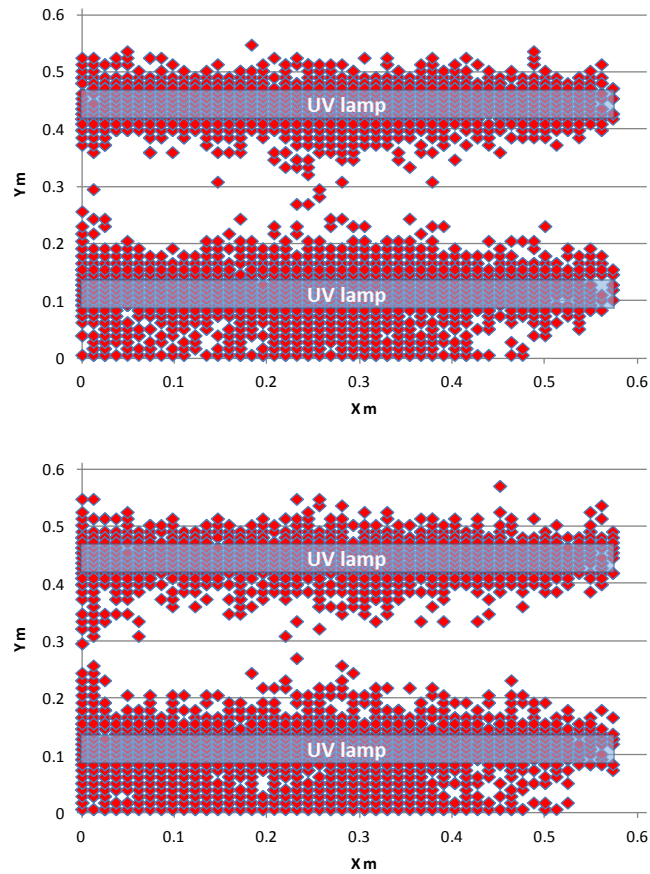
Figure 5.23 Cross section of the EPA 600/R-06/055 duct at 15% reflectivity (top) and 25% reflectivity (bottom) showing lamp position and location of particles receiving the average UV dose or more..

Currently, due to the number of variations in designs and specifications, as yet there is no parameter to measure efficiency of these types of UV systems.

5.3.7 Contours of Irradiation

The effect of the lamp location on UV irradiation of the system can be further assessed by looking at contours of irradiation. Figure 5.23 shows contour plots at five locations in the duct for the single lamp model. One striking aspect of the irradiation pattern is how rapidly the irradiation power decays as the distance from the lamp increases (as seen in Chapter 4 Figure 4.9 of lamp irradiation power). For such reasons it was impossible to use the same UV power scale when portraying the irradiation in various planes along the duct, as using a global scale would rendered the irradiation at inlet and outlet unnoticeable compared with that at the centre of the lamp (Figure 5.24).
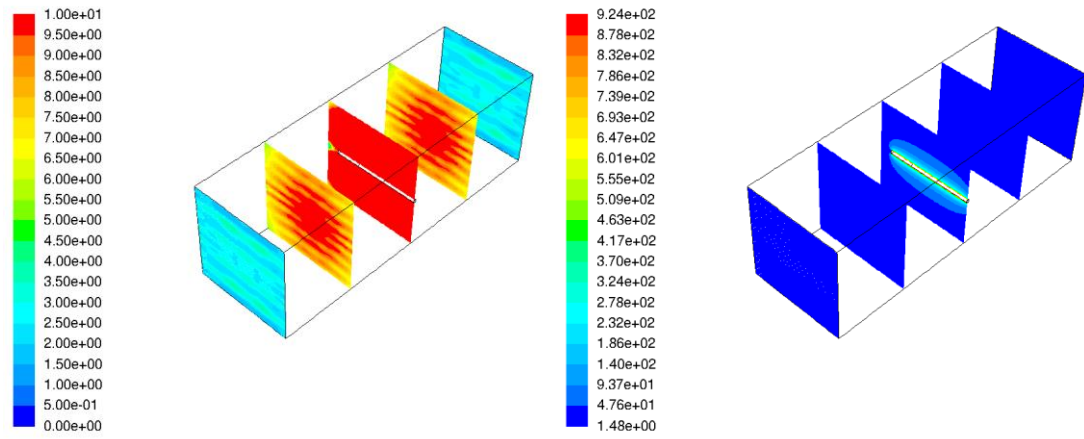
Figure 5.24 Contours of irradiation. Left) scaled from 0 to 10 W.m^{-2}. Right) scaled globally based on highest irradiation value Watts.

There was no noticeable difference in irradiance between the planes at the inlet (Figure 5.25A) and outlet (Figure 5.25B), and between the planes located between outlet and lamp (Figure 5.25C), and between inlet and lamp (Figure 5.25D). The low irradiation seen at the corners of the duct is more noticeable in section C and D of Figure 5.25, it can be appreciated lower irradiation levels at the left corners as the lamp is stacked to the right of the duct wall.
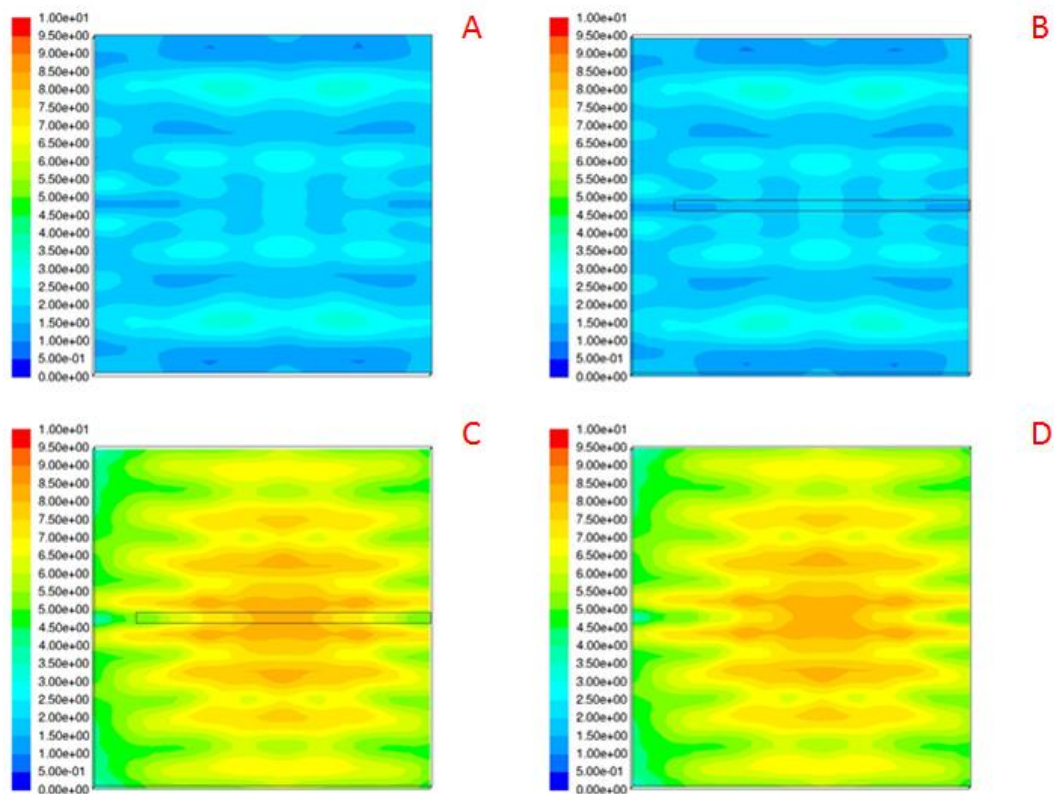
Figure 5.25 UV irradiation contours. A) Inlet, B) Outlet), C) between outlet and lamp, D) between inlet and lamp.

For the EPA 600/R-06/051 the irradiation contours show how the duct is being better covered with UV light, although again it is evident that corners are areas of low irradiation. Figure 5.26 shows how rapidly irradiation decays as the distance from the source increases; the planes here shown are 0.4575m separated between each other.
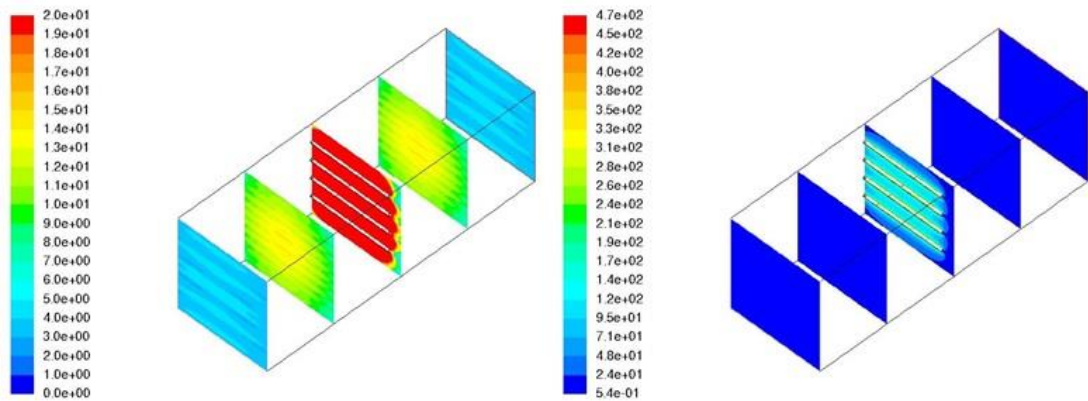
Figure 5.26 Contours of irradiation EPA 600/R-06/051. Left) scaled from 0 to 20 W.m⁻², Right) scaled globally based on highest irradiation value Watts.

A closer look at the contour surfaces reveals how lamp position, in this case four lamps located at equal distances along the height of the duct, distributes the irradiation. This has a direct impact on the particle dose distribution (Figure 5.19).
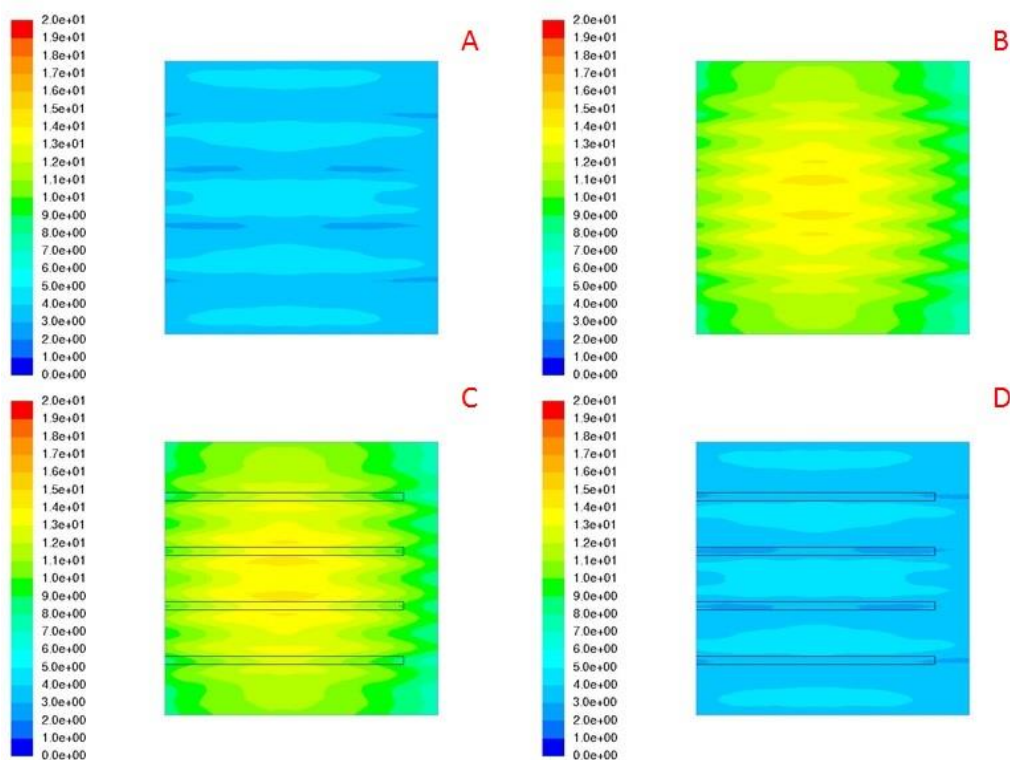
Figure 5.27 UV irradiation contours EPA 600/R-06/051. A) Inlet, B) between inlet and lamps, C) between lamp and outlet, D) Outlet.

The EPA 600/R-06/055 with eight lamps shows how the irradiation is differently distributed due to lamp locations (Figure 5.28). Having lamps located along the length of the duct as well as the height help to distribute the UV field in direction of the airflow.
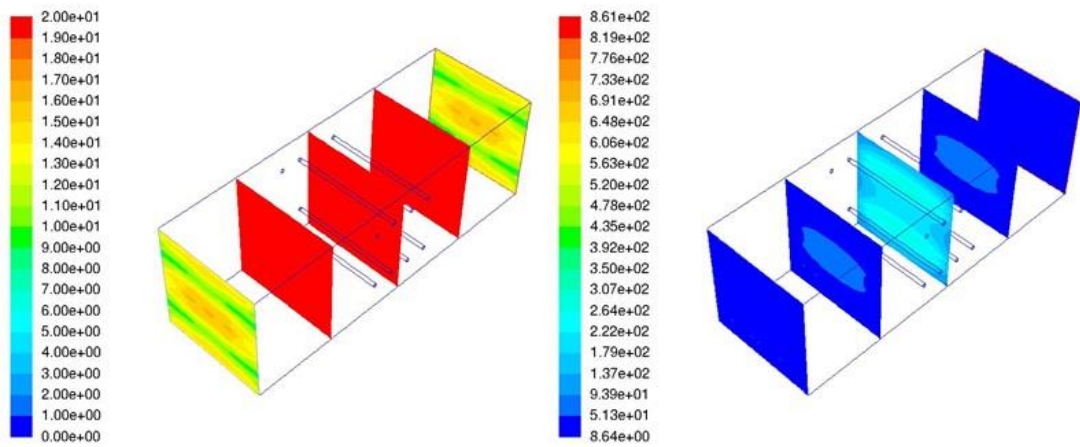
Figure 5.28 Contours of irradiation EPA 600/R-06/055. Left) scaled from 0 to 20 Watts, Right) scaled globally based on highest irradiation value Watts.

With this lamp configuration, it is still noticeable that areas towards the end of the lamps and the corners of the duct contain the lowest irradiation values (Figure 5.29).
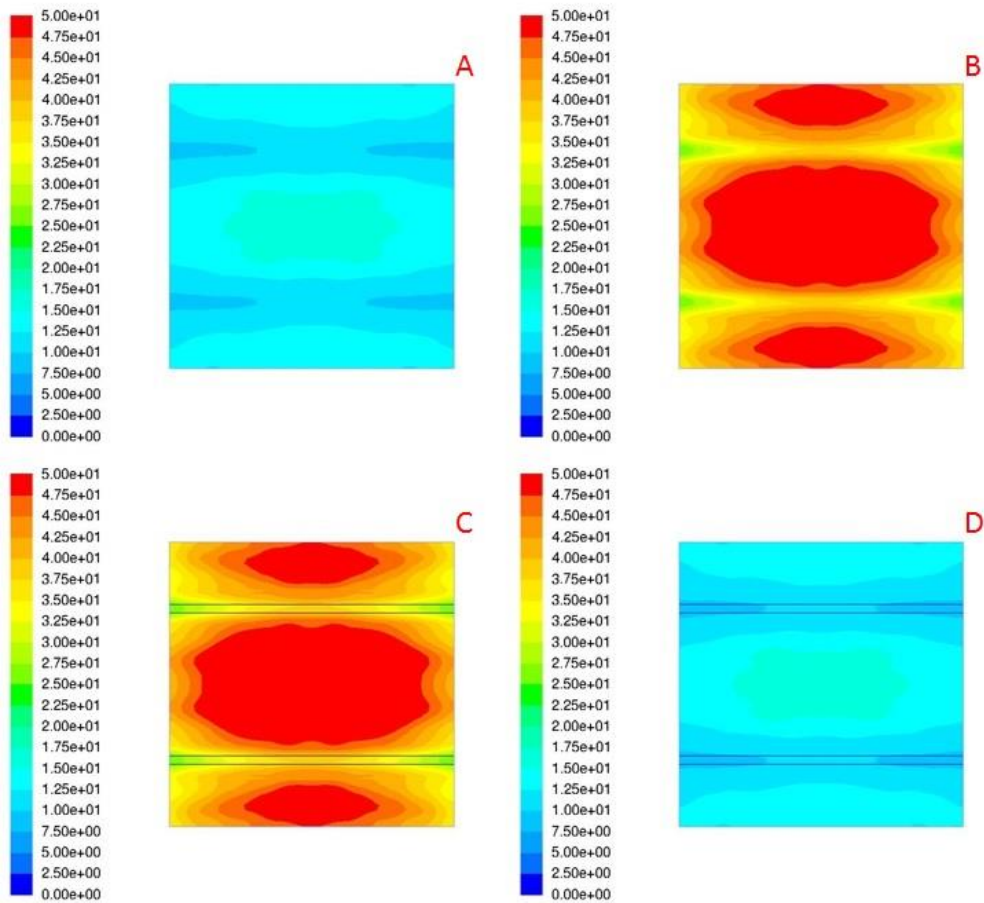
Figure 5.29 UV irradiation contours EPA 600/R-06/055. A) Inlet, B) between inlet and lamps, C) between lamp and outlet, D) Outlet.

Another aspect for consideration is the distribution of the irradiation along the length of the duct, while the EPA 600/R-06/051 distributes the lamps along the height of the duct, the EPA 600/R-06/055 does it along the length of the duct, therefore covering a longer distance (Figure 5.30).
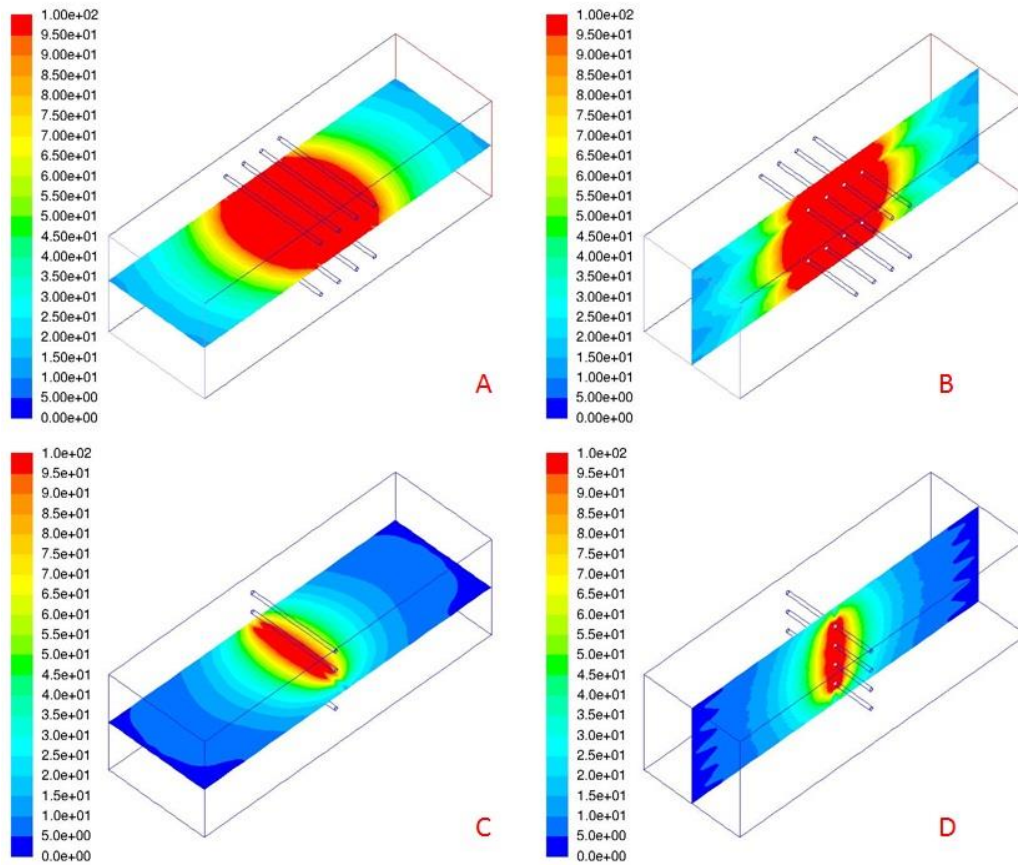
Figure 5.30 Irradiation along the duct length at 100 watts scale for the EPA 600/R-06/051 and EPA 600/R-06/055.

When comparing all the cases, it is difficult to define under what parameter to measure efficiency in performance. For example if performance is measured by dose distribution we have that the more even the UV dose distribution, the more efficient the system is. However a broad dose distribution, like the one of the EPA 600/R-06/055 (Figure 5.22) suffers on performance due to the large variation in UV dose received by particles, meaning that a great number of particles will receive less or more than the average UV dose of the system. Both of these are potentially a waste of energy, as higher than required UV dosage will not bring further improvement in performance, and less than required UV dosage will not achieve the required sterilisation goals. Moreover the real performance will be masked by the average UV dose of the system.

Results for the EPA 600/R-06/050 (single lamp system) show that 62.23% of particles received less than the average dose of the system, similar values were observed for the EPA 600/R-06/055 (eight lamps system) where 62% of particles received less than the average dose of the system. In the case of the EPA 600/R-06/051 (four lamp system), shows that only 45% of particles received less than the average dose. Moreover, it appears that the spread of the UV dose distribution, and the standard deviation of the UV dose received by particles, can be used

to evaluate the quality of the irradiation distribution of the system, the more even the irradiation, the lower the standard deviation of the system. A good design should consist of a single sharp peak located at the centre of the system average dose.

These results show the impact of lamp position on the distribution of UV irradiation within a duct, and its subsequent impact on sterilisation performance. This will be further discussed in Chapter 6.

5.4 Conclusions.

Section 5.3 compares CFD modelling of three in duct UV systems with published experimental data and demonstrates that CFD models are a viable method of predicting performance and supporting system design. DO models in CFD modeling appear to be a reliable technique for the calculation of UV field, UV dose and microorganism kill rate within in-duct UV sterilization systems. Good comparison is seen between CFD calculated inactivation, EPA (2006a, 2006b, 2006c) test results, and previously published average UV dose calculations (Kowalski, 2009a).

The results of section 5.3.3 highlight important considerations in selecting appropriate test microorganisms for performance assessments. *B. subtillis* and *B. atrophaeus* present a shoulder on their decay curve. The results show that not accounting for such a shoulder when calculating UV dose by regression from microbiological tests may result in an under calculation of the UV system dosage. The results also indicate that *S. marcescens* is not a good reference microorganism for the calculation of a system UV dosage as it has a high susceptibility to UV and any dose over 10 J.m^{-2} will result in kill rates of 99.99% regardless of system design. The results also confirmed what was discussed in Chapter 3, the limitations of current UV susceptibility data in the literature. While there are a good number of studies that report susceptibility data, there is a considerable amount of variability between studies which depends on test conditions and the particular strain of a microorganism species. A more comprehensive database of UV susceptibility of microorganisms that includes the full spectrum of the microorganism decay is required for accurate calculation of the UV power demands for the sterilization of air. This is the case for performance assessment through modelling or experimental approaches.

System design and the method of evaluation are shown to have a significant effect on the energy efficiency and sterilization efficacy of a UV installation. Calculating UV dose by regression from biodosimetry tests using the wrong microorganism decay model or incorrect UV susceptibility values will result in miscalculation of UV dosage. This in turn can lead to underpowered systems in which the sterilization efficiency would be compromised or overpowered UV systems

resulting in a waste of energy and excessive capital and maintenance costs. Furthermore the average dose delivered by a system may be a poor representation of its performance. The average UV dose and kill rate data at 15% diffusive wall reflectivity compares well between experiments and CFD models, differences might be due to variations on airflow and or wattage during the operation of the system on the real life experiment, nevertheless the approximations made by CFD analysis appear to be reliable enough for design purposes.

The CFD analysis showed that more than half particles received less than the average calculated dose for the EPA 600/R-06/050 and EPA 600/R-06/055 This indicates a poor design with both under performance and excess energy use apparent within the same device. Only in the case of the EPA 600/R-06/051 54% of particles received the average UV dose or more.

Section 5.3.5 and 5.3.6 showed how lamp position has an impact on UV performance. Extrapolating this, it means that particle trajectories have an impact on performance, therefore airflow patterns are paramount parameters for sterilisation efficiency. Hence, the performance of a system is not static; it will present variation depending on the particle trajectories.

Section 5.3.4 saw the introduction of a novel multi-susceptibility performance calculation, with results showing good agreement with experimental data, as opposed to prior calculations where the kill rate of a specific pathogen was considered individually with a single susceptibility value and the average UV dose was calculated as a surface integral and could not account for particle trajectories.

CFD analysis is capable of identifying variability in dose distribution that otherwise would be impossible to identify by a biodosimetry test. Initial simulations with four and eight lamp configurations show the benefit of positioning lamps to create a more even UV irradiation field and hence UV dose in the system. The standard deviation of the UV dose distribution appears to be a good quantitative parameter to measure the quality of an even irradiation distribution, the lower the standard deviation, the more even the irradiation distribution within the duct.

Finally, this chapter validated the CFD model to be used in future analysis, highlights the need for a reliable data set of microorganism UV susceptibility values in air, evaluated dose distribution among injected particles and demonstrated the importance of system design, moreover it is shown that within a given design, in this case a single lamp system, a significant number of particles receive a dose that is different than the average. Chapter 6 will focus on lamp position and the impact of dose distribution.

Chapter 6. In-Duct UV system design parameterisation.

6.1 Introduction.

This chapter applies the use of CFD analysis to consider how the position of a UV lamp in a duct influences the performance.

Section 6.2 presents a parameterisation study to analyse the impact of lamp position on sterilisation performance within a duct, by studying a system with a lamp located in seven different positions, results suggest that turbulence does not directly affects the final average UV dose of the system, and that airflow patterns will have a bigger impact.

Section 6.5 shows a comparison of a lamp located perpendicular to the airflow against a lamp located parallel to the airflow, and how UV irradiation and UV dosage is affect in the system, and concludes that for a single lamp system, lamps located parallel to the airflow perform better than a lamp located perpendicular to the airflow.

6.2 Parametric study methodology.

The first study of this chapter is a steady state CFD simulations (ANSYS) used to model the irradiation field and UV dose of an induct system of 0.61 m x 0.61 m duct, 1.83 m long with a constant airflow of 2.5 m.s^{-1} in line with the models provided by Kowalski (2009b), and assuming to contain a UV lamp 53.3 cm long with a diameter of 1.9 cm (T6) producing 19 W of UV power located at seven different positions (Table 6-1).

Table 6-1 System configuration.

Configuration	Z position	Y position
L1H1	230 mm	205 mm
L1H3	230 mm	405 mm
L2H1	915 mm	205 mm
L2H2	915 mm	305 mm
L2H3	915 mm	405 mm
L3H1	1600 mm	205 mm
L3H3	1600 mm	405 mm

The lamps were located perpendicular to the airflow at three different position over the height of the duct and at three different distances from the inlet of the duct as shown in Figure 6.1.
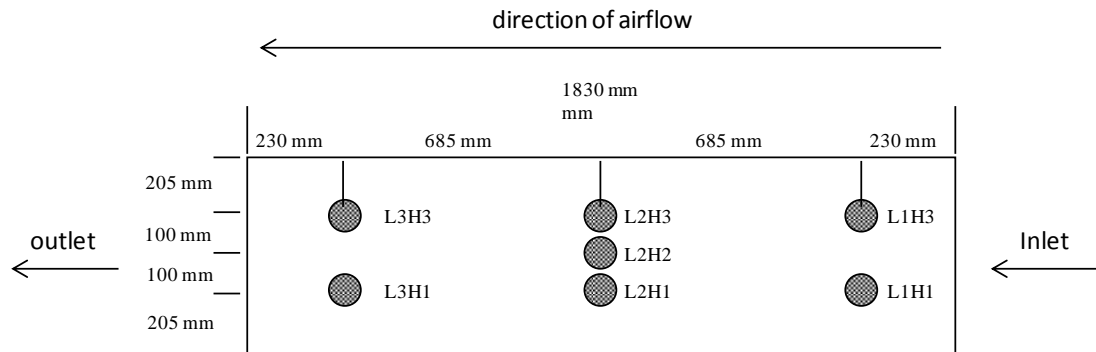
Figure 6.1 Lamp configuration schematics.

Both the mesh and the boundary conditions were as described in Chapter 5. The CFD models contained between 280,000 to 330,000 cells depending on lamp configuration. The UV field produced by the lamp was defined using the discrete ordinates method described in Chapter 4. The airflow was developed in model of a 6 m long duct with the same face area (0.61m x 0.61m x 6m), and the flow profile was then inserted at the inlet of the UV chamber (1.83 m long duct). Once a solution for the flow field was converged, particles were injected using a discrete random walk Lagrangian model to simulate microorganisms within the flow (King et al., 2013). On average 10,500 scalars with physical characteristics of water liquid droplets with diameter ranging from 3×10^{-8} to 3×10^{-6} m (0.03 microns to 3 microns) were injected by surface at the inlet. A user defined function, adapted from Ho (2009b), was employed to determine the cumulative UV dose (J.m^{-2}) received by each particle as it passed through the UV field by a trapezoidal rule to approximate the integral (as described in Chapter 5). The model was validated at the configuration L2H2 against the EPA test report 600/R-06/050 (Chapter 5). The performances of the different configurations were then systematically compared in order to find the lamp location with the highest sterilisation rate.

With the use of CFD it was possible to track airflow patterns, identify the areas with the lowest and maximum air velocities, the irradiation volume created by the UV lamp and the effect of diffuse reflectivity from the walls. This allowed for the calculation of each particle received UV dose, path travelled, residence time, and outlet coordinates (X and Y coordinate within the duct). Moreover, the use of the DO method to model irradiation allowed for the inclusion of reflectivity (emissivity) on the walls of the duct. With this information it was possible to value the average system UV dose, and the impact of airflow patterns, UV irradiation volumes created at different lamp position within the system and the reflectivity of the walls.

6.3 Influence of lamp position and duct reflectivity.

Lamp position has impacts on turbulence and UV irradiation within the system, and more importantly, duct reflectivity increased the irradiation area and the average UV dose of the system. The following sections consider how these parameters impact on the performance of a UV system.

6.3.1 Particle dose distribution

The Figure 6.2 shows average UV dose measured at the end of the duct for each lamp position. In each case the value is calculated by averaging the dose received by the particles injected into the system (described in Chapter 5). The performance of the induct UV system varied according to lamp configuration, with differences accounting for up to 20% in some cases (i.e. when comparing average UV dose of L2H2 vs. L3H3). It can be seen how the distribution changes according to lamp configuration, with lamps located at L2 (centre of duct) showing the highest average dose, followed by lamps on L1 (beginning of duct) and then lamps at L3 (end of duct).
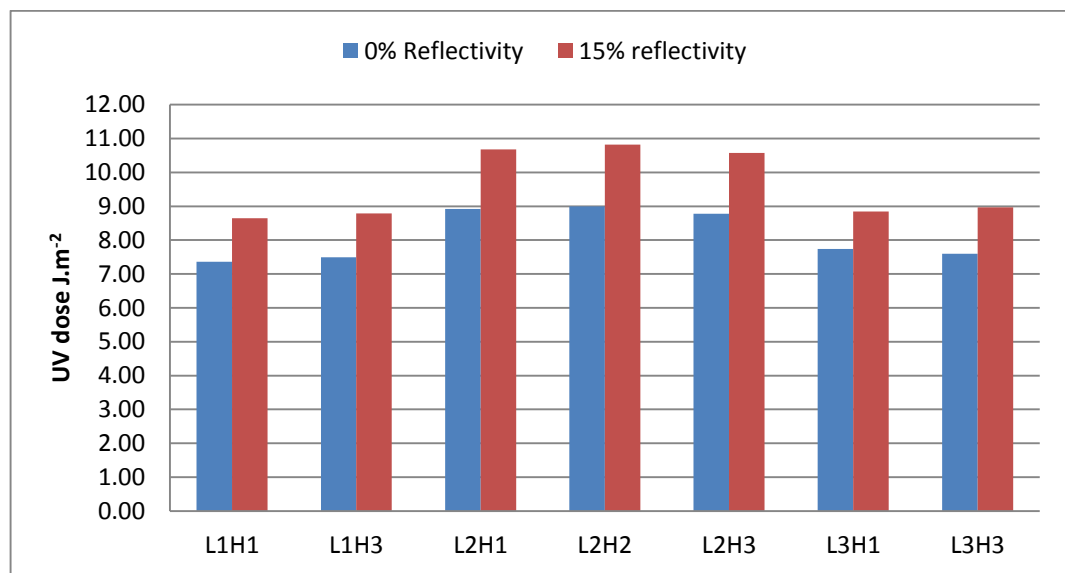
Figure 6.2 Average UV dose by lamp configuration and reflectivity.

The average UV dose of the system was influenced most significantly by the position of the lamp along the length of the duct (*Z* axis), while changes of the lamp position along the height of the duct (*Y* axis) resulted in minimal or irrelevant impacts in performance. In both cases, at 0% and 15% diffuse wall reflectivity, the best performances were achieved when the lamp was located at the centre of the *Z* axis within the duct (L2), and the highest performance was achieved when the lamp was located at the centre of both *Z* and *Y* axis (L2H2).

The particle dose distribution at the end of the duct, presented in Figure 6.3, reveals that lamps located at L1H1 and L1H3 show almost the same dose spectrum. Indeed both configurations show the same average UV dosage, at 0% reflectivity of 7.81 J.m^{-2}, and at 15% reflectivity the performance of the system increased to 9.14 J.m^{-2} for both L1H1 and L1H3.
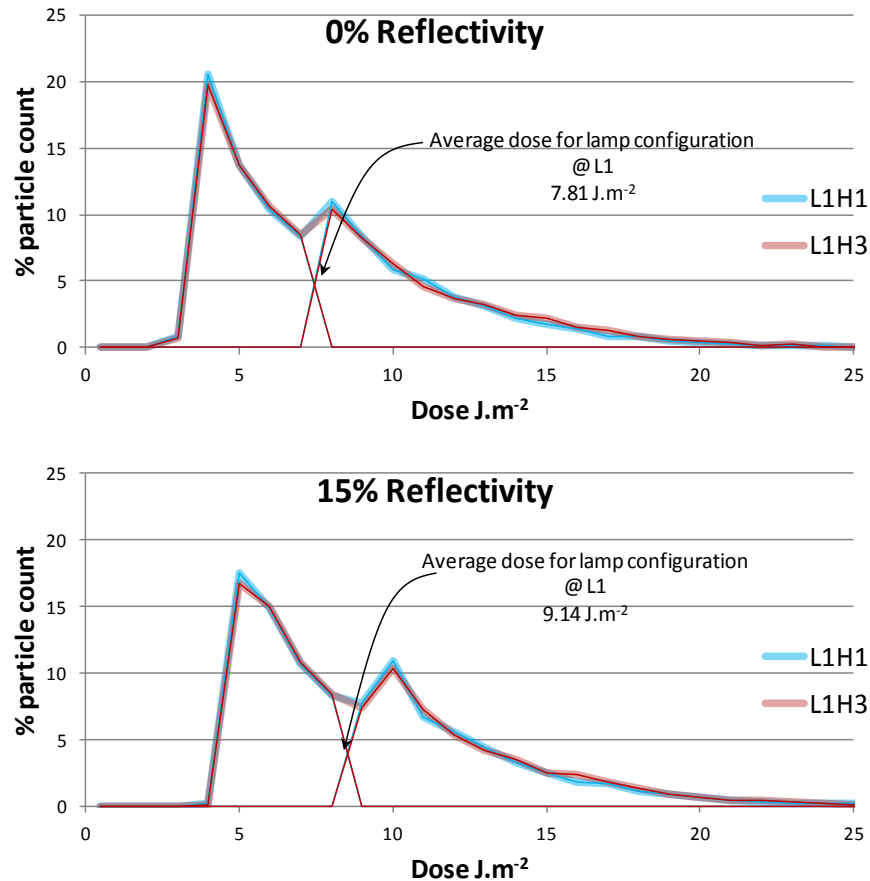
Figure 6.3 UV dose distribution for configurations at L1.

In the case of lamps in the L2 position, the dose spectrum for L2H1 and L2H3 is very similar with an average UV dose ranging from 8.96 J.m^{-2} to 9.16 J.m^{-2} and slightly different to the case of L2H2 at 0% reflectivity with an average UV dose of 9.22 J.m^{-2}. However, when the material has a diffuse wall reflectivity of 15%, the average UV dose of the three configurations evens out, and stays between 10.74 J.m^{-2} and 10.97 J.m^{-2}. Such small differences in average UV dose of less than 1 joule might be insignificant when translated into sterilisation performance, and more importantly, when translating these results to a real operational system, the difference might be insignificant.
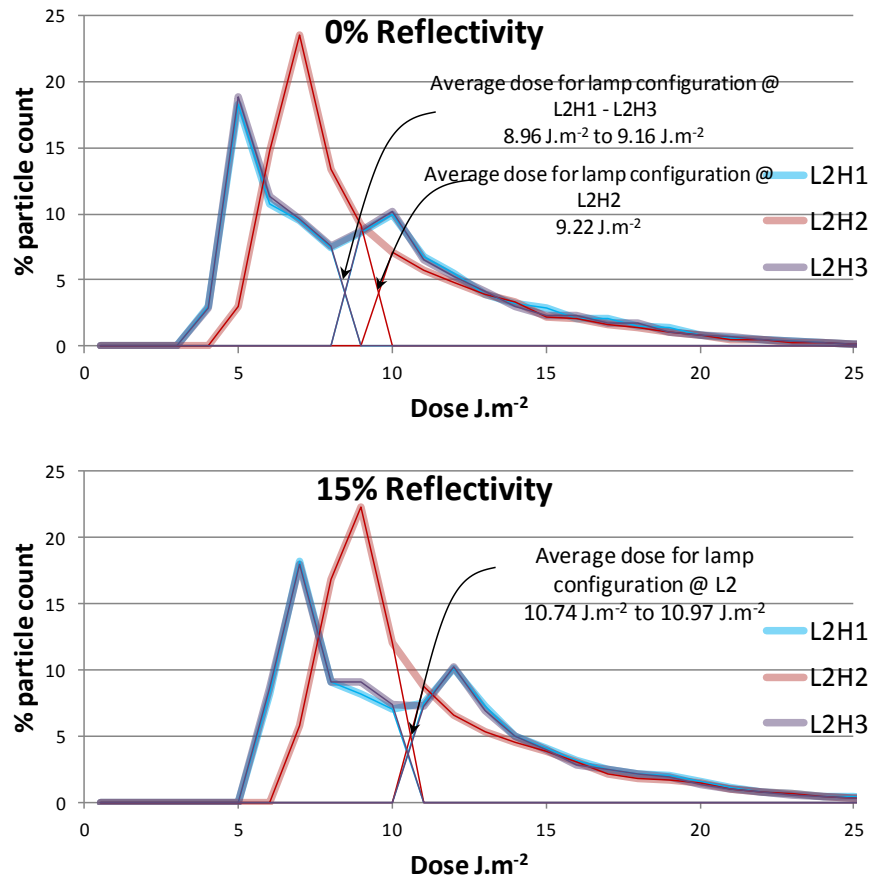
Figure 6.4 UV dose distribution for configurations at L2.

Lamps located at L1 (beginning of the duct) performed slightly better than lamps located at L3 (end of the duct), lamps located at L3 show an average UV dose of 7.60 J.m^{-2} to 7.73 J.m^{-2} at 0% wall reflectivity while lamps at L1 showed 7.81 J.m^{-2}, at 15% wall reflectivity L3 showed 8.86 J.m^{-2} to 9.0 J.m^{-2} while L1 performed at 9.14 J.m^{-2} (Figure 6.5).

There was a slight difference in performance between L1 and L3, although their position is symmetrical within the UV chamber, lamps at L1 performed marginally better than lamps located at L3. However; as previously stated, differences in performance of less than 1 joule might not be relevant in real operational conditions.
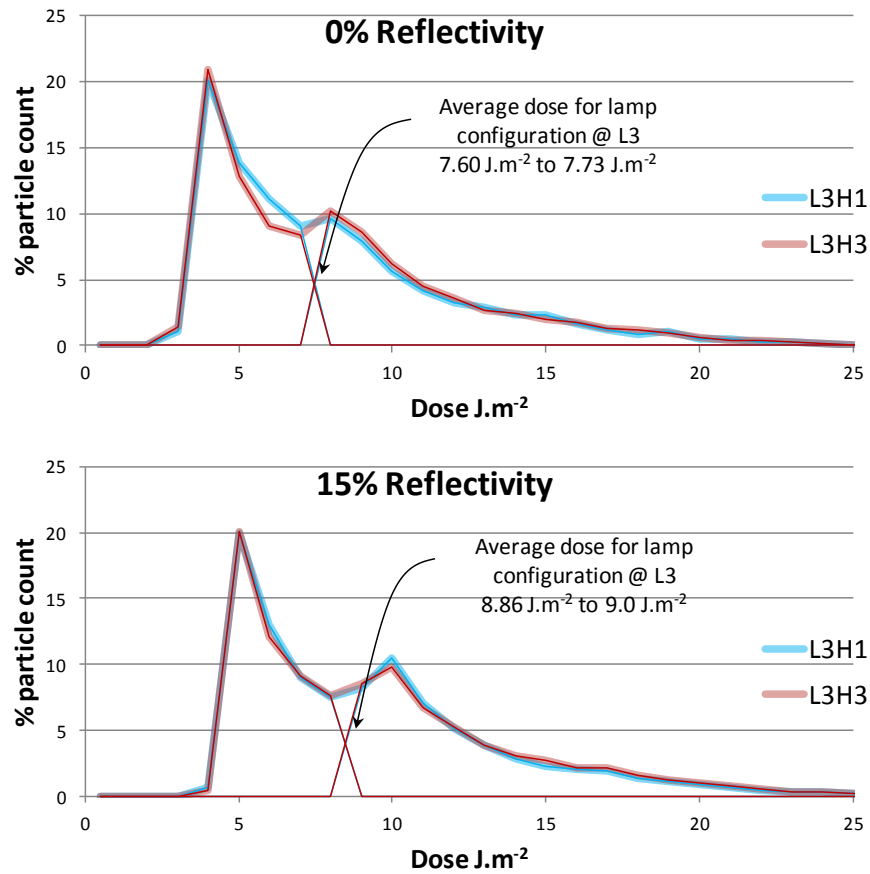
Figure 6.5 UV dose distribution for configurations at L3.

Table 6-2 shows the difference in performance at 0% diffuse wall reflectivity expressed in percentage of efficiency. It can be seen how lamp configuration at L2H2 is in average 20% higher than those at L1 and L3 and just marginally better than the other two configuration at L2 (L2H1 and L2H2). The configuration at L2H1 was the second highest, with an average performance 18% higher than those at L1 and L3, followed by the configuration at L2H3 with an average performance 15% higher than those at L1 and L3.

Table 6-2 UV dose performance comparison matrix at 0% reflectivity.

0% R	UV dose J.m⁻²	0% R						
		L1H1	L1H3	L2H1	L2H2	L2H3	L3H1	L3H3
		7.81	7.80	9.16	9.22	8.96	7.73	7.60
L1H1	7.81	0.00%	0.14%	-17.27%	-18.04%	-14.71%	1.04%	2.70%
L1H3	7.80	-0.14%	0.00%	-17.44%	-18.21%	-14.87%	0.90%	2.56%
L2H1	9.16	14.73%	14.85%	0.00%	-0.66%	2.18%	15.61%	17.03%
L2H2	9.22	15.28%	15.40%	0.65%	0.00%	2.82%	16.16%	17.57%
L2H3	8.96	12.82%	12.95%	-2.23%	-2.90%	0.00%	13.73%	15.18%
L3H1	7.73	-1.05%	-0.91%	-18.50%	-19.28%	-15.91%	0.00%	1.68%
L3H3	7.60	-2.78%	-2.63%	-20.53%	-21.32%	-17.89%	-1.71%	0.00%

Results expressed in percentage of performance

At 15% reflectivity, results are not much different. Nevertheless, one notable variation is the increase in performance in L2H1 and L2H3, now being closer to that of L2H2. This is due to the effect of diffuse wall reflectivity, which in this case helped in the distribution of the average UV dose, reducing the impact of lamp position in the "Y" axis even further in configurations at L2. As it can be seen, the difference between L1H1 and L1H3 was of just 0.1%, differences in performance at configuration in L2 accounted for no more than 2.12% and configurations at L3 the difference in performance was of merely 1.60%. Such small differences would be insignificant in a real operational installation.

The performance of the system is virtually unaffected by the lamp location across the height of the duct.

Table 6-3 UV dose performance comparison matrix at 15% reflectivity.

15% R	UV dose J.m⁻²	15% R						
		L1H1	L1H3	L2H1	L2H2	L2H3	L3H1	L3H3
		9.14	9.13	10.94	10.97	10.74	9.00	8.86
L1H1	9.14	0.00%	0.11%	-19.67%	-19.94%	-17.45%	1.58%	3.13%
L1H3	9.13	-0.11%	0.00%	-19.80%	-20.07%	-17.58%	1.47%	3.02%
L2H1	10.94	16.44%	16.53%	0.00%	-0.23%	1.89%	17.75%	19.05%
L2H2	10.97	16.63%	16.72%	0.23%	0.00%	2.12%	17.94%	19.23%
L2H3	10.74	14.86%	14.95%	-1.89%	-2.12%	0.00%	16.20%	17.52%
L3H1	9.00	-1.60%	-1.49%	-21.58%	-21.86%	-19.33%	0.00%	1.60%
L3H3	8.86	-3.23%	-3.12%	-23.53%	-23.81%	-21.24%	-1.60%	0.00%

Results expressed in percentage of performance

The direct comparison of the UV dose performance of the system at 15% reflectivity is in average 15% greater than that at 0% wall reflectivity e.g. when comparing L2H2 at 15% reflectivity against L2H2 at 0% reflectivity (Table 6-4).

Table 6-4 Performance comparison matrix of 15% reflectivity vs 0% reflectivity.

		0% R						
		L1H1	L1H3	L2H1	L2H2	L2H3	L3H1	L3H3
15% R	**UV dose J.m^{-2}**	7.81	7.80	9.16	9.22	8.96	7.73	7.60
L1H1	9.14	14.56%	14.68%	-0.20%	-0.85%	1.99%	15.45%	16.87%
L1H3	9.13	14.47%	14.59%	-0.31%	-0.96%	1.88%	15.35%	16.78%
L2H1	10.94	28.60%	28.70%	16.27%	15.72%	18.10%	29.34%	30.53%
L2H2	10.97	28.76%	28.86%	16.46%	15.91%	18.29%	29.50%	30.69%
L2H3	10.74	27.25%	27.35%	14.69%	14.13%	16.55%	28.01%	29.22%
L3H1	9.00	13.19%	13.31%	-1.80%	-2.47%	0.42%	14.09%	15.54%
L3H3	8.86	11.80%	11.92%	-3.43%	-4.11%	-1.17%	12.71%	14.18%

Results expressed in percentage of performance

In relation to the area coverage of the various lamp configurations, Figure 6.6, Figure 6.7 and Figure 6.8 show the area where particles receive 10 J.m^{-2} or more (this dose is merely representative and is used only for the purpose of direct comparison between designs). The effect of reflectivity is evident in all three figures showing how the area coverage is improved and particles close to the wall now receive irradiation.
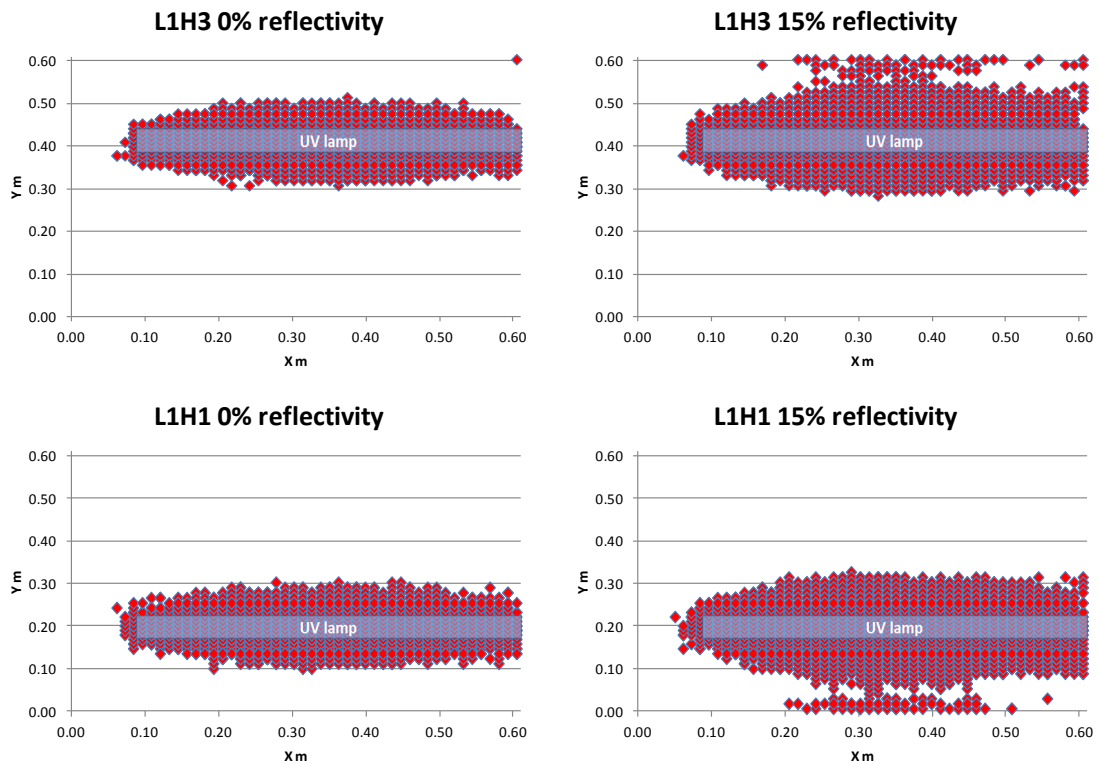
Figure 6.6 Cross section at the outlet of the L1H1 and L1H3 lamp configuration at 0% and 15% diffuse wall reflectivity showing lamp position and location of particles receiving the UV dose of 10 J.m^{-2} more.

Particle dose and area coverage of the configurations at L1H1 and L1H3 is almost identical with the only difference being that one is located at bottom while the latter on the top of the duct, it appears as if lamp position in the *Y* axis did not have any considerable effect.
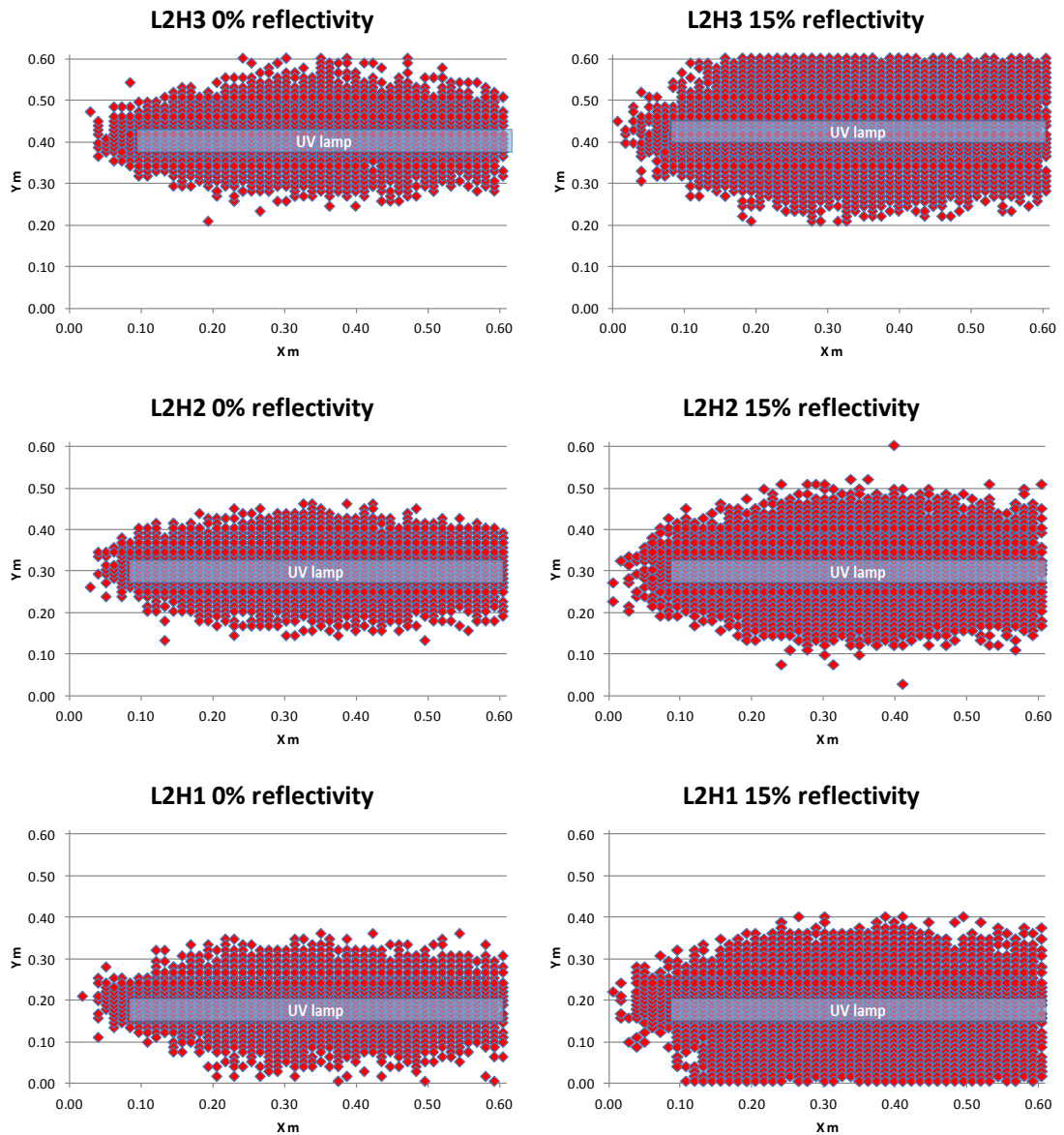
Figure 6.7 Cross section at the outlet of the L2H1, L2H2 and L2H3 lamp configuration at 0% and 15% diffuse wall reflectivity showing lamp position and location of particles receiving the UV dose of 10 J.m^{-2} more.

For lamps located at the L2 position, the central lamp at L2H2 shows a slightly bigger area of coverage; it appears that lamps located close to the walls do not allow for the full development of the UV dose area coverage as seen in L2H1 and L2H3.
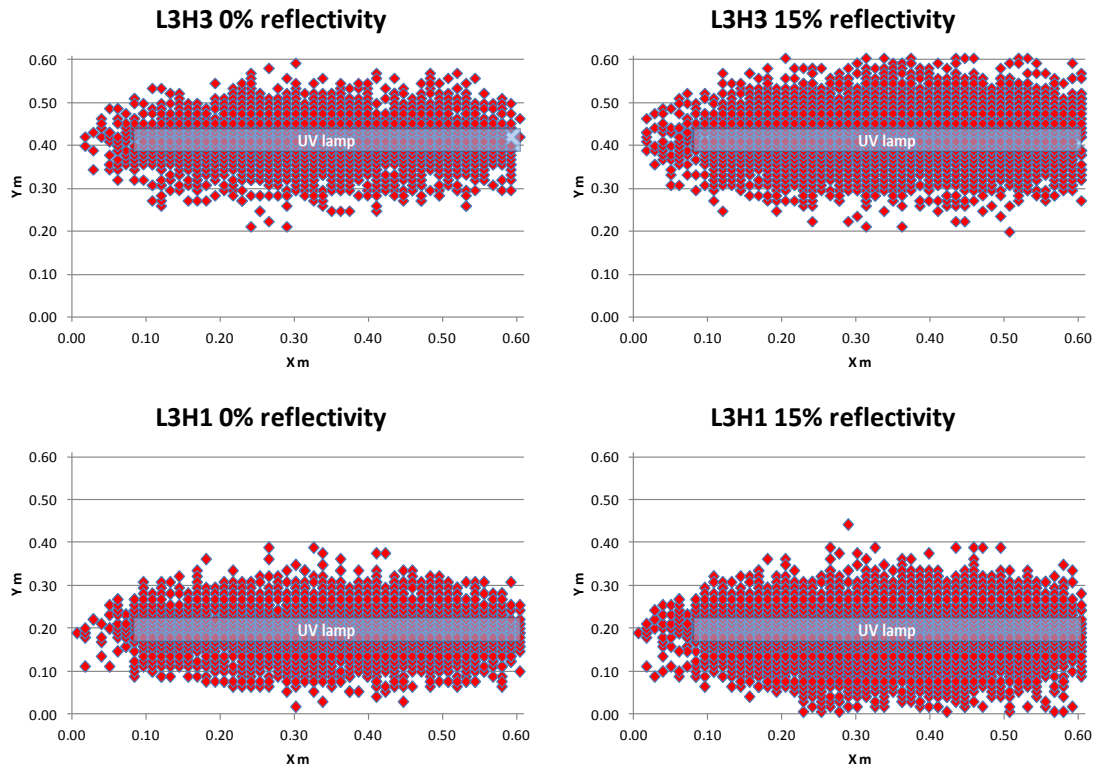
Figure 6.8 Cross section at the outlet of the L3H1 and L3H3 lamp configuration at 0% and 15% diffuse wall reflectivity showing lamp position and location of particles receiving the UV dose of 10 J.m^{-2} more.

Lamps at L3H1 and L3H3 showed similar area coverage, with the only difference being that one being located at the bottom and the other at the top.

6.4 Impact of airflow patterns.

Airflow patterns and turbulence are defined by the lamp position within the system, which in turn, impact its performance; it was found that turbulence do not show a direct correlation with UV dose, however it appears that airflow patterns impact in the sterilisation performance of the system. The following section reviews the impact of turbulence and airflow patterns.

6.4.1 Velocity profile

The contours of velocity show us that the airflow velocity reduces just after the lamp, and close to the walls, creating an area (volume) where particles travel relatively slower in comparison with other areas of the duct.
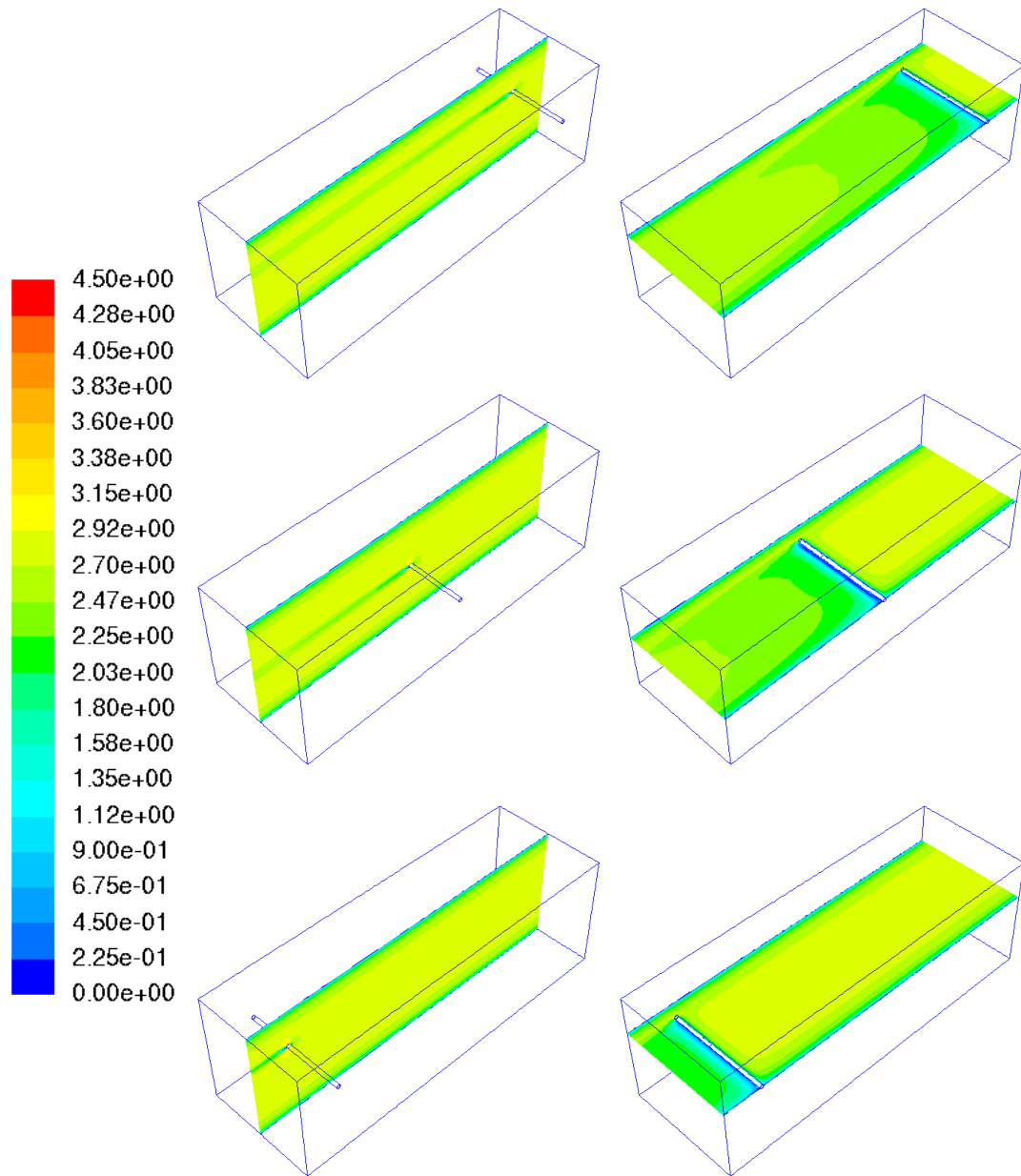
Figure 6.9 Contours of velocity (m.s^{-1}) for L1H2 (top), L2H2 (centre) and L3H3 (bottom).

6.4.2 Turbulent kinetic energy (k)

The models were run using the K-ε turbulence model (explained in Chapter 5), which is just one of the many turbulence models available (e.g. RNS, LES etc). In the case of these studies, turbulence modeling is just a possible representation of the turbulence behaviour within the system. Due to the lack of airflow data, it is impossible to validate a turbulence model. Nonetheless, as all the designs were analysed under the same turbulence model, the results work as direct comparison between them. Moreover it is not the intention of this research to analyse turbulence models, there is literature information available on the topic (Liu et al., 2007,

Chang and Young, 2007, Liu, 2004), however, results from this research can lead to the study of turbulence on in-duct UVC system as future work.

The mean kinetic energy per unit mass is associated with eddies in a turbulent flow, plotting its contours within the in-duct systems can give us notice of where turbulence is created. In general, all single lamp configuration show little change in kinetic energy apart from the area after the lamp.

Configuration at L1 show little changes on kinetic energy whether lamps are located at top (L1H3) or bottom (L1H1) within the duct .Again, configuration at L2 show little change on the turbulent kinetic energy confirming that lamp location in the Y axis has little impact on turbulence in the system. Lamps located at L3 show a turbulent kinetic energy contour which has not developed entirely.
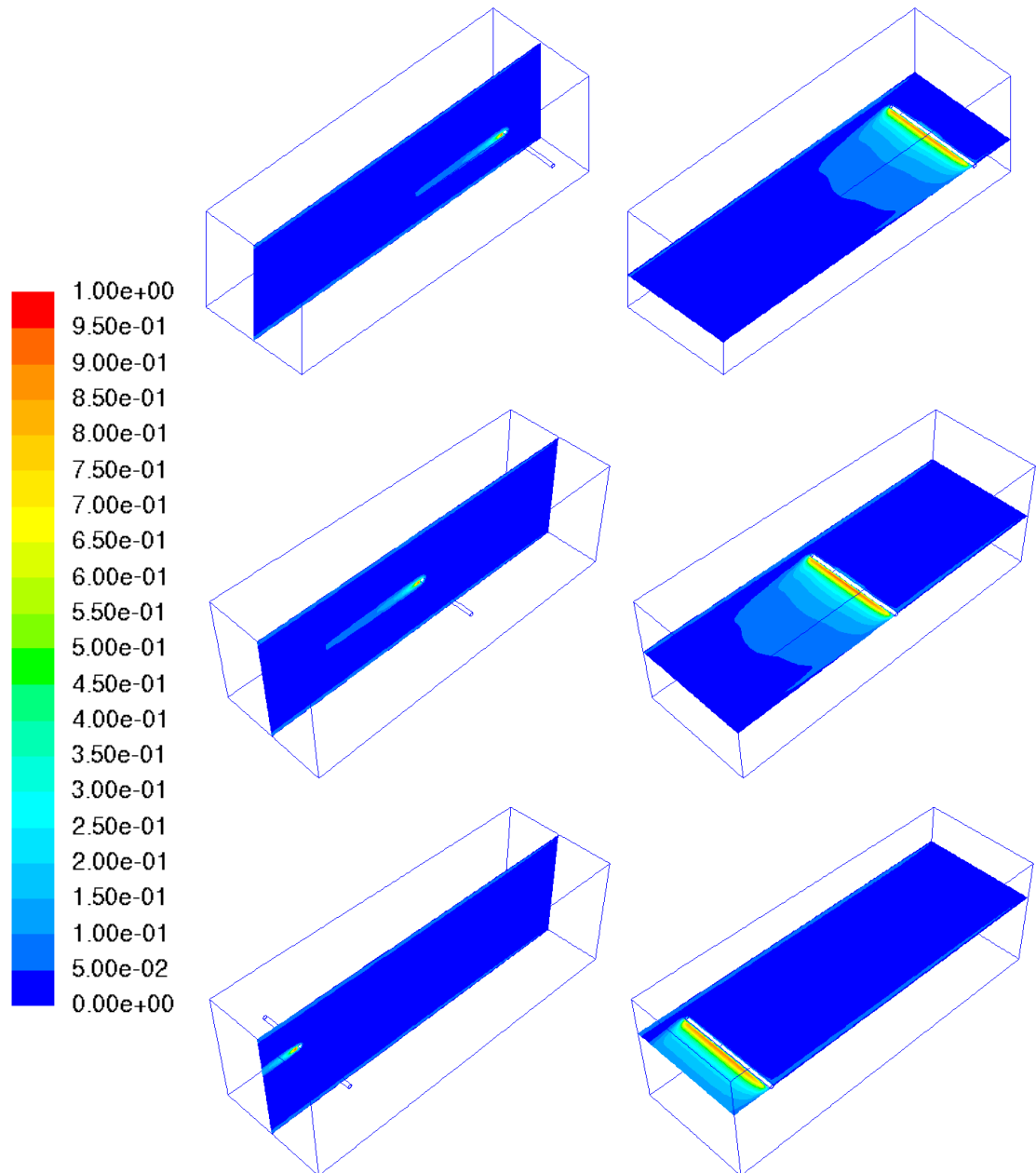
Figure 6.10 Contours of turbulent kinetic energy (K) m^2.s^{-2} for L1H1 (top), L2H2 (centre) and L3H3 (bottom).

6.4.3 Turbulence intensity

The following figures show the percentage of turbulence intensity within the system, in general, for all three configurations it can be seen how turbulence intensifies after the UV lamp and close to the walls (Figure 6.11). Again, for lamp located at L3, turbulence was not allowed to develop and just a small area after the lamp presented intensified turbulence.
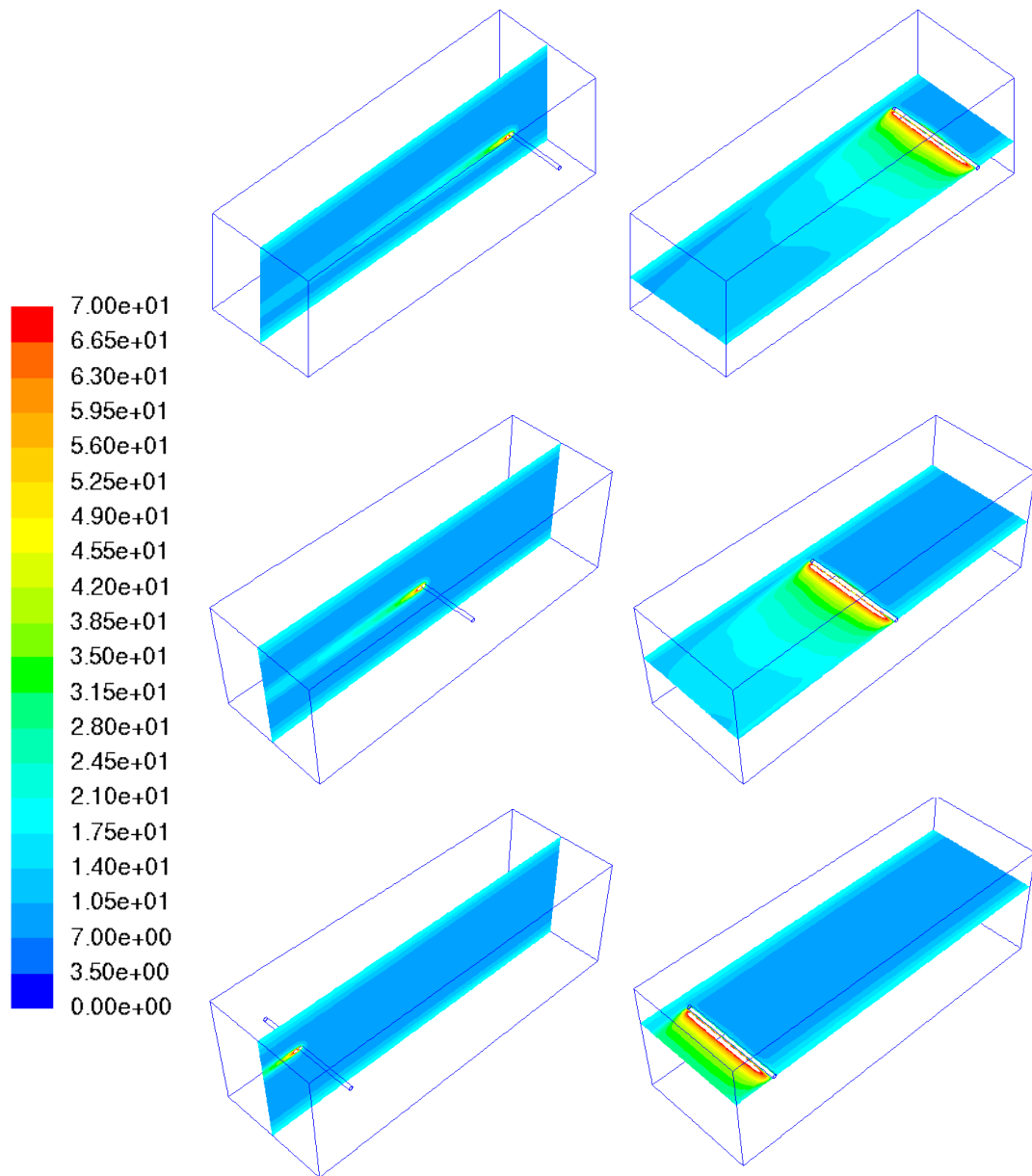
Figure 6.11 Contours of turbulence intensity % for L1H1 (top), L2H2 (centre) and L3H3 (bottom).

6.4.4 Turbulent Reynolds number

Turbulent Reynolds number (Re_y) is defined by Equation 6-1:

$$Re_y \equiv \frac{\rho y \sqrt{k}}{\mu}$$

<div align="right">

Equation 6-1

</div>

In which y is the normal distance to the wall at the cell centre, ρ is the density of the fluid, k is the turbulent kinetic energy and μ is the dynamic viscosity. As explained in Chapter 5.1.2, the Reynolds number is the ratio of the force of inertia over the force of friction, and is a direct

indicator of the type of flow, laminar or turbulent, of the system. It is assumed that a region is fully turbulent when Re_y is greater than 200 (total value) (ANSYS, 2011).

The contours of turbulent Reynolds number for lamps located at L1 was almost identical with the only difference being that one is located at the bottom (L1H1) while the other is located at the top of the duct (L1H3).For lamps located at L2, the position L2H2 showed a high turbulent Reynolds number at the centre just after the lamp in both planes (Figure 6.12). The lamps located at L3 do not allowed for a fully developed contour of turbulent Reynolds number.
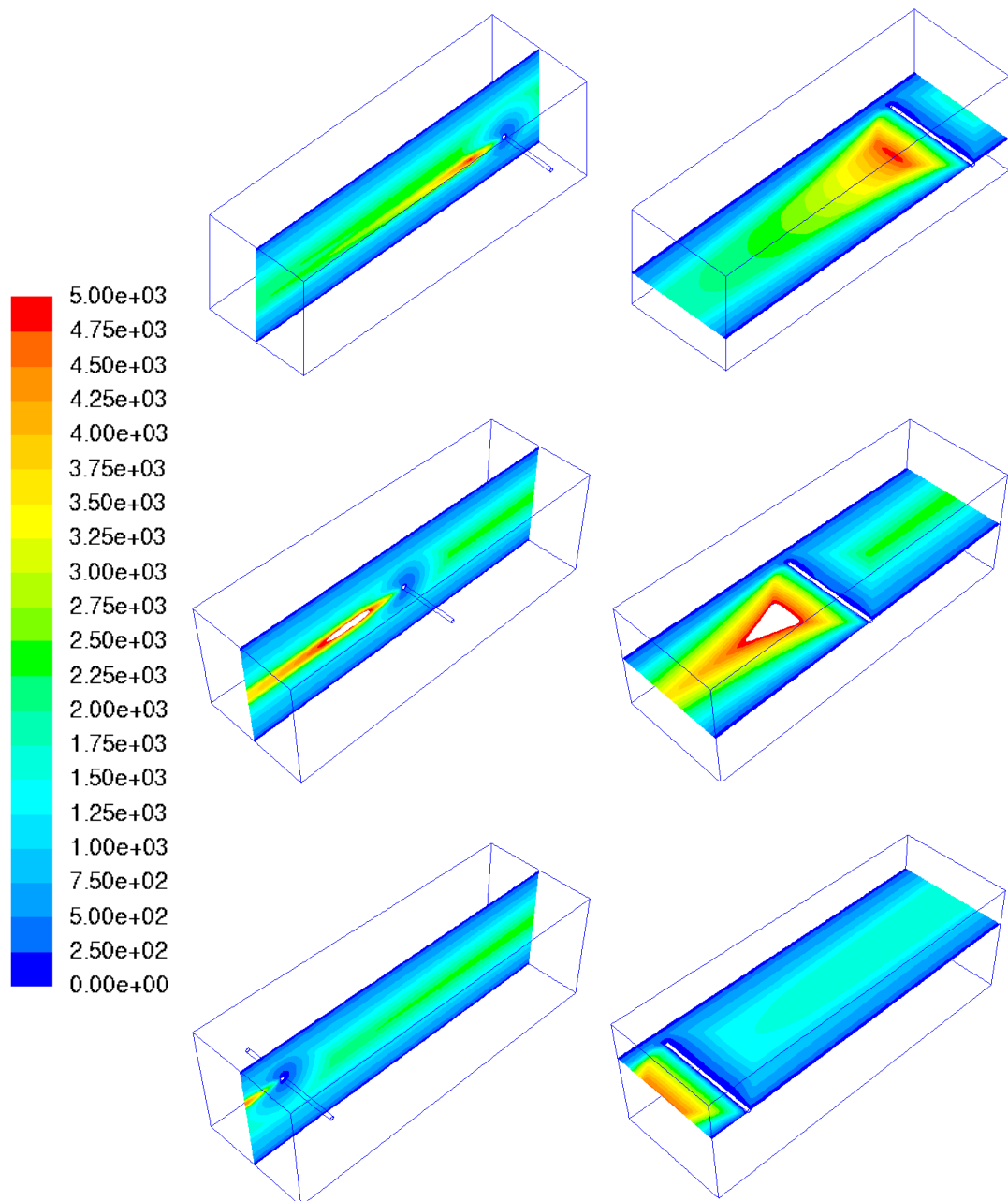
Figure 6.12 Contours of turbulent Reynolds number (Re_y) for L1H1 (top), L2H2 (centre) and L3H3 (bottom).

6.4.5 Irradiation profile

The irradiation profile shows how the UV light covers the volume within the duct, it can be seen how in the cases of L1 and L3, irradiation is stopped by the limits of the duct (beginning and end of duct). More importantly, it can be seen how the walls receive the lowest irradiation values on the scale.
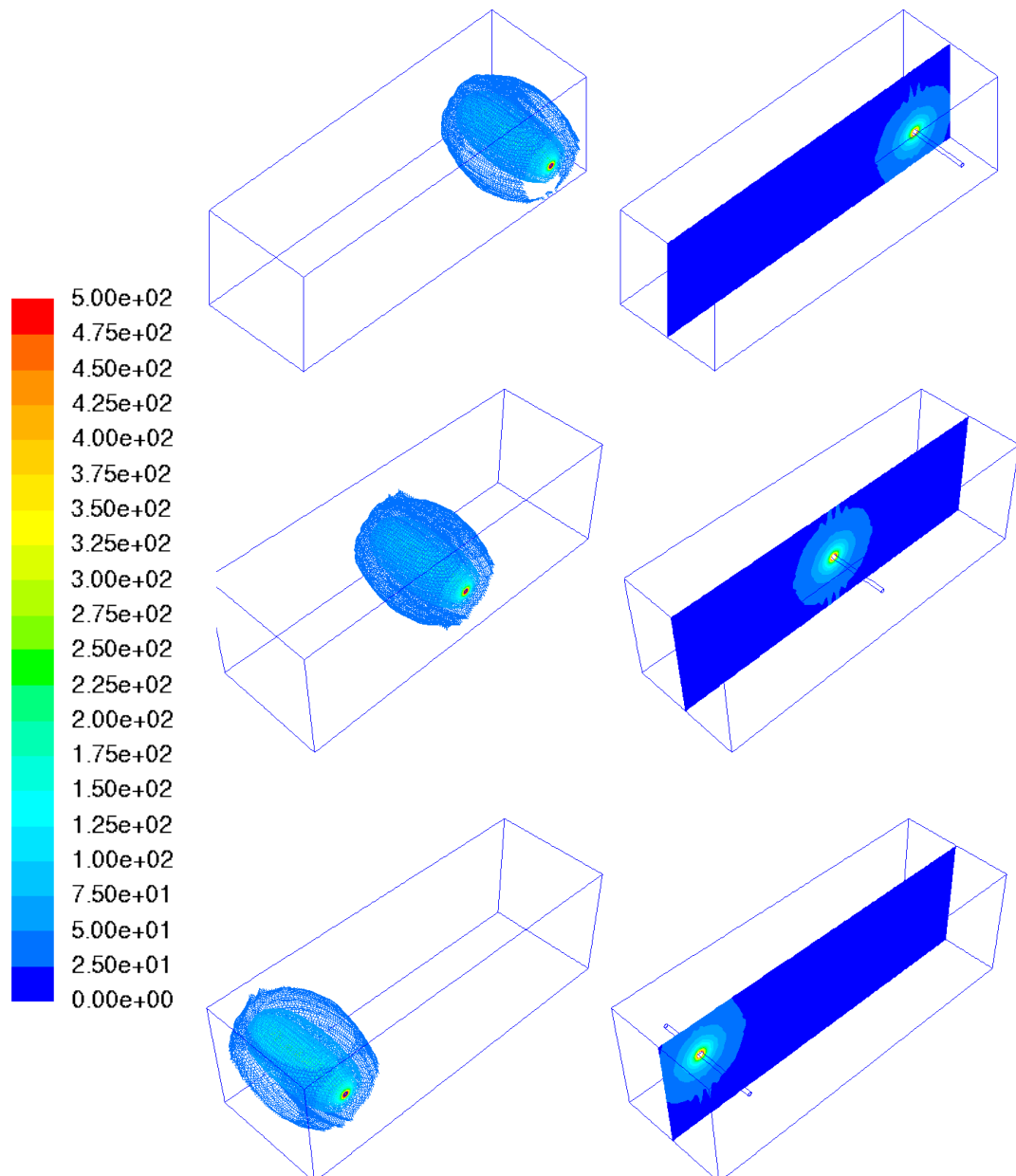
Figure 6.13 Contours of Irradiation (W.m^{-2}) for L2H1 (top), L2H2 (centre) and L2H3 (bottom).

The irradiation profile at L1 and L3 show how the irradiation is not allowed to develop as it is stopped by the walls. Lamps located at L2 do not have the obstruction of the front and rear

ends, and just suffer from the top and bottom walls at L2H1 and L2H3, while L2H2 is allowed to develop the irradiation profile in all directions (Figure 6.13).

6.4.6 Turbulence, Irradiation and UV dose

The sterilisation performance depends on UV irradiation, contact time of UV irradiation with the microorganism and the susceptibility of the specific microorganism. Average irradiation is the only parameter which shows a direct correlation with UV dose when lamps are positioned perpendicular to the airflow (Figure 6.14). However this is not the only parameter that defines average UV dose performance (as it will be seen in section 6.6). Table 6-5 shows the volume-weighted average (VA) value for % turbulence, turbulent Reynolds number (Re_y), velocity and irradiation.

Table 6-5 UV dose, turbulence and velocity.

	15% Reflectivity UV dose J.m^{-2}	0% Reflectivity UV dose J.m^{-2}	VA Turbulence %	VA Re_y	VA Vel m.s^{-1}	VA Irradiation w.m^{-2}
L1H1	9.14	7.81	12.79	900.90	2.50	12.49
L1H3	9.13	7.80	12.79	901.90	2.50	12.50
L2H1	10.94	9.16	12.61	876.54	2.50	14.77
L2H2	10.97	9.22	12.64	882.59	2.50	15.13
L2H3	10.74	8.96	12.58	874.42	2.50	14.78
L3H1	9.00	7.73	12.30	832.46	2.50	12.17
L3H3	8.86	7.60	12.26	830.47	2.50	12.17

VA= Volume-weighted Average
Re_y= turbulence Reynolds number

The VA was calculated as the summation of the product of the field variable (e.g. % turbulence, Re_y, velocity) and cell volume, by the total volume (ANSYS, 2011) (Equation 6-2).

$$\frac{1}{V}\int \emptyset dV = \sum_{i=1}^{n} \emptyset_i |V_i|$$

Equation 6-2

Lamps located at L1 (beginning of the duct) performed marginally better than lamps located at L3 (end of the duct), it was also noted that configurations at L1 carried higher turbulence (turbulence % and the turbulence Reynolds number) than configurations at L3 and L2, however the VA irradiation was higher for the lamps at L2 with L2H2 giving them the highest average UV dose (Equation 6-2). It was found that the only value that showed a direct correlation with the average UV dose of the system was the VA irradiation (R^2=0.995) (Figure 6.14).
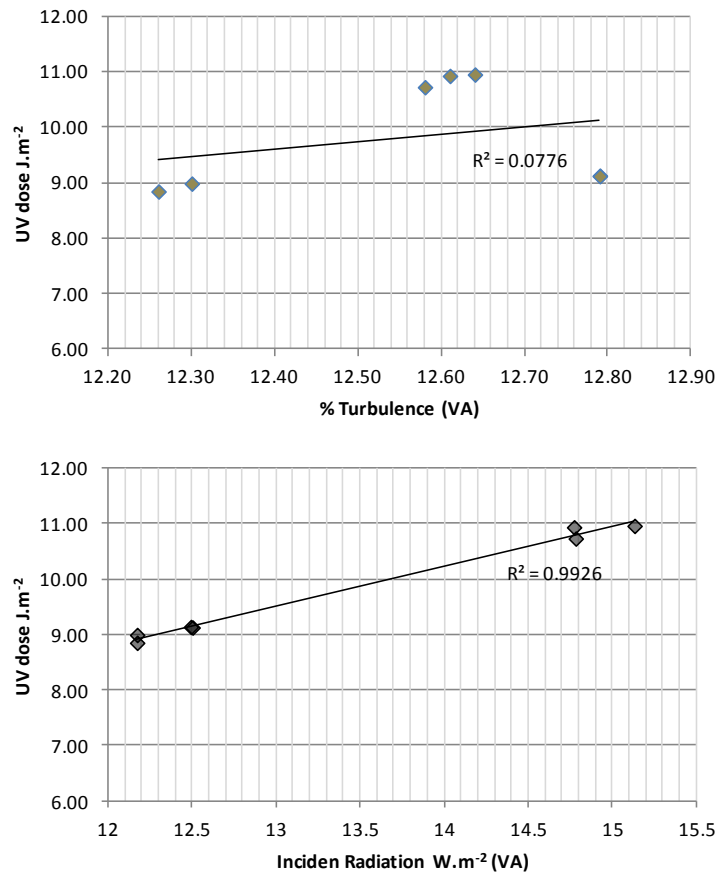
Figure 6.14 Correlation graph of UV dose vs % Turbulence (top) and incident Radiation (bottom) for the 15% reflection system.

In the case of turbulence, lamps at L1 showed the highest turbulence of all configurations, even higher than those at L2, nevertheless, lamps at L2 showed the highest VA irradiation of all configurations. Lamps located at L3 showed the lowest turbulence and VA irradiation which in turn was reflected as the lowest performance (in average UV dose) of all configurations. In the case of L2H1 and L2H3 VA irradiation was almost identical, while turbulence was greater for the L2H1 configuration, and also this configuration had a slightly higher average UV dose (10.94 J.m^{-2} at 15% reflectivity and 9.16 J.m^{-2} at 0% reflectivity) over the L2H3 configuration (10.74 J.m^{-2} at 15% reflectivity and 8.96 J.m^{-2} at 0% reflectivity).
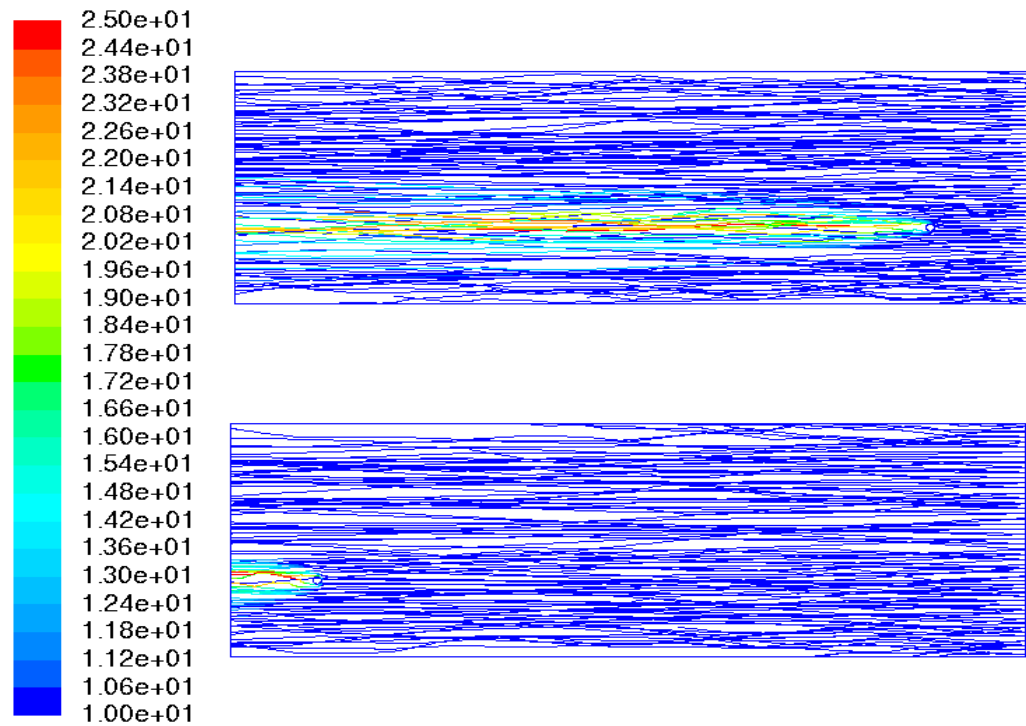
Figure 6.15 UV dose (J.m⁻²) received by particles at L1H1 (top) and L1H3 (bottom), flow moves from right to left.

The effect of UV irradiation in the airflow can be seen in Figure 6.15, where a high UV dose stream is visible just after the lamp in the L1H1 configuration (top) as opposed to the L3H1 where the stream is small and does not develops entirely. At the end the difference in average UV dose between lamps in L1 and L3 was of about 3%, which would be insignificant for a real operational system.

An interesting result from the analysis of turbulence was the finding that turbulence alone does not define the performance of the systems; instead it is a combination of the volume irradiation and the airflow patterns, which in turn can be influenced by turbulence.

6.4.7 Sterilisation performance

Variations in average UV dose do not translate directly to sterilisation performance i.e. in the case of the configuration L3H3 at 15% reflectivity (8.86 J.m⁻²) where the average UV dose was up to 20% lower than the average dose at L2H2 (10.97 J.m⁻²) the difference in sterilisation performance for a pathogen with a susceptibilities ranging from (k) of 0.038 m^2.J^{-1} to 0.048 m^2.J^{-1} (MS2 Bacteriophage) would be of 5.7% approximately i.e. 36.55% kill rate for L2H2 vs 30.9% kill rate for L3H3. This is due to the fact that sterilisation performance is linked to dose through an exponential relationship (as discussed in Chapter 4) (Equation 6-3).

$$S = e^{-k.D}$$

Where S = survival fraction, k = susceptibility factor of pathogen and D = average dose of the system.

Figure 6.16 shows the performance of the systems calculated using the monte-carlo multi-susceptibility method over 100 iteration (as described in chapter 5), assigning randomised susceptibility values ranging from 0.014 – 0.75 $m^2.J^{-1}$ to each particle. In all cases the standard deviation was of about 0.5% kill rate. Maximum kill rate value and minimum kill rate value found during the results are shown in the top and bottom outlier.
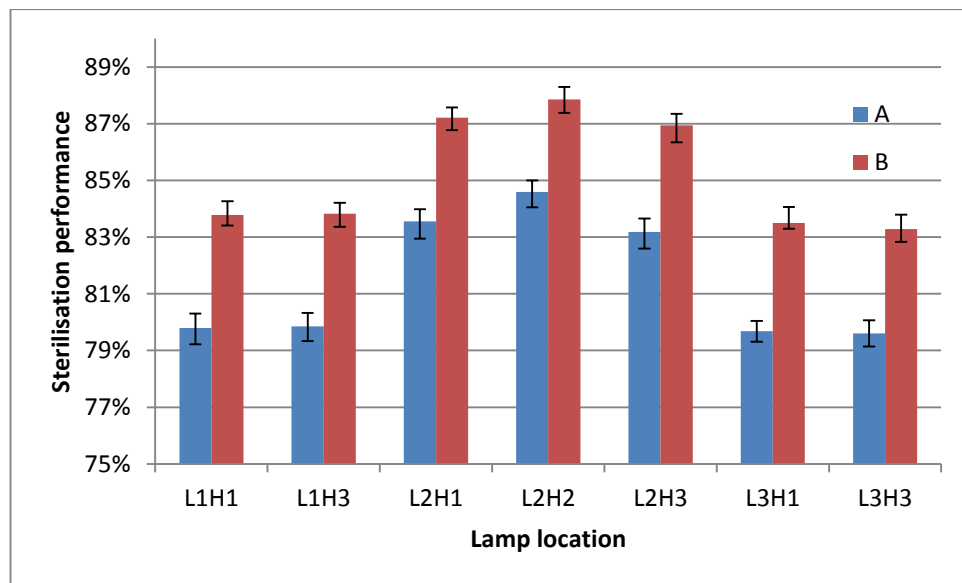
Figure 6.16 Average %kill rate for susceptibilities ranging from 0.014 - 0.75 $m^2.J^{-1}$. A) 0% reflectivity and B) 15% reflectivity, showing the maximum (top outlier bar), minimum (bottom outlier bar) and average value (main column).

The biggest difference in performance was found to be of about 5% in kill rate in both cases at 0% and 15% reflectivity, and it happened when comparing L2H2 against L3H3 (Table 6-6 and Table 6-7).

Table 6-6 Kill rate performance comparison matrix for UV susceptibilities ranging from 0.014 to 0.75 m².J⁻¹ at 0% reflectivity.

		0.014 - 0.75 m².J⁻¹ (k) at 0% R						
		L1H1	L1H3	L2H1	L2H2	L2H3	L3H1	L3H3
0% R	**%kill rate**	79.80%	79.85%	83.56%	84.60%	83.18%	79.68%	79.60%
L1H1	79.80%	0.00%	-0.05%	-3.76%	-4.80%	-3.38%	0.12%	0.20%
L1H3	79.85%	0.05%	0.00%	-3.71%	-4.75%	-3.33%	0.17%	0.25%
L2H1	83.56%	3.76%	3.71%	0.00%	-1.04%	0.38%	3.87%	3.96%
L2H2	84.60%	4.80%	4.75%	1.04%	0.00%	1.41%	4.91%	5.00%
L2H3	83.18%	3.38%	3.33%	-0.38%	-1.41%	0.00%	3.50%	3.58%
L3H1	79.68%	-0.12%	-0.17%	-3.87%	-4.91%	-3.50%	0.00%	0.08%
L3H3	79.60%	-0.20%	-0.25%	-3.96%	-5.00%	-3.58%	-0.08%	0.00%

Results expressed in percentage of performance

Increasing reflectivity within the system reduced the difference in performance between lamp configurations, as it can be seen; now the difference in performance between L2H2 and L3H3 is of 4.57% (Table 6-7).

Table 6-7 Kill rate performance comparison matrix for UV susceptibilities ranging from 0.014 to 0.75 m².J⁻¹ at 15% reflectivity

		0.014 - 0.75 m².J⁻¹ (k) at 15% R						
		L1H1	L1H3	L2H1	L2H2	L2H3	L3H1	L3H3
15% R	**%kill rate**	83.79%	83.82%	87.22%	87.86%	86.94%	83.50%	83.29%
L1H1	83.79%	0.00%	-0.03%	-3.43%	-4.07%	-3.15%	0.29%	0.50%
L1H3	83.82%	0.03%	0.00%	-3.40%	-4.04%	-3.12%	0.32%	0.53%
L2H1	87.22%	3.43%	3.40%	0.00%	-0.64%	0.28%	3.72%	3.93%
L2H2	87.86%	4.07%	4.04%	0.64%	0.00%	0.92%	4.36%	4.57%
L2H3	86.94%	3.15%	3.12%	-0.28%	-0.92%	0.00%	3.44%	3.65%
L3H1	83.50%	-0.29%	-0.32%	-3.72%	-4.36%	-3.44%	0.00%	0.21%
L3H3	83.29%	-0.50%	-0.53%	-3.93%	-4.57%	-3.65%	-0.21%	0.00%

Results expressed in percentage of performance

Lamps located at L2H2 at 0% reflectivity performed better than lamps located in L1 and L3 at 15% reflectivity, this highlights the impact of lamp position, as in this case lamp position had a bigger impact than reflectivity (Table 6-8).

Table 6-8 Kill rate performance comparison matrix for UV susceptibilities ranging from 0.014 to 0.75 m2.J-1 at 15% vs 0% reflectivity.

		0.014 - 0.75 m²·J⁻¹ (k) at 0% R						
		L1H1	L1H3	L2H1	L2H2	L2H3	L3H1	L3H3
15% R	**%kill rate**	79.80%	79.85%	83.56%	84.60%	83.18%	79.68%	79.60%
L1H1	83.79%	3.99%	3.94%	0.23%	-0.81%	0.61%	4.10%	4.19%
L1H3	83.82%	4.03%	3.97%	0.27%	-0.77%	0.64%	4.14%	4.22%
L2H1	87.22%	7.42%	7.37%	3.66%	2.63%	4.04%	7.54%	7.62%
L2H2	87.86%	8.06%	8.01%	4.30%	3.26%	4.68%	8.17%	8.26%
L2H3	86.94%	7.14%	7.09%	3.38%	2.34%	3.76%	7.26%	7.34%
L3H1	83.50%	3.70%	3.65%	-0.06%	-1.10%	0.32%	3.82%	3.90%
L3H3	83.29%	3.49%	3.44%	-0.27%	-1.31%	0.11%	3.61%	3.69%

Results expressed in percentage of performance

Reducing the susceptibility to a range of 0.014 m².J⁻¹ to 0.5 m².J⁻¹ amplifies the difference in performance of the system configurations.
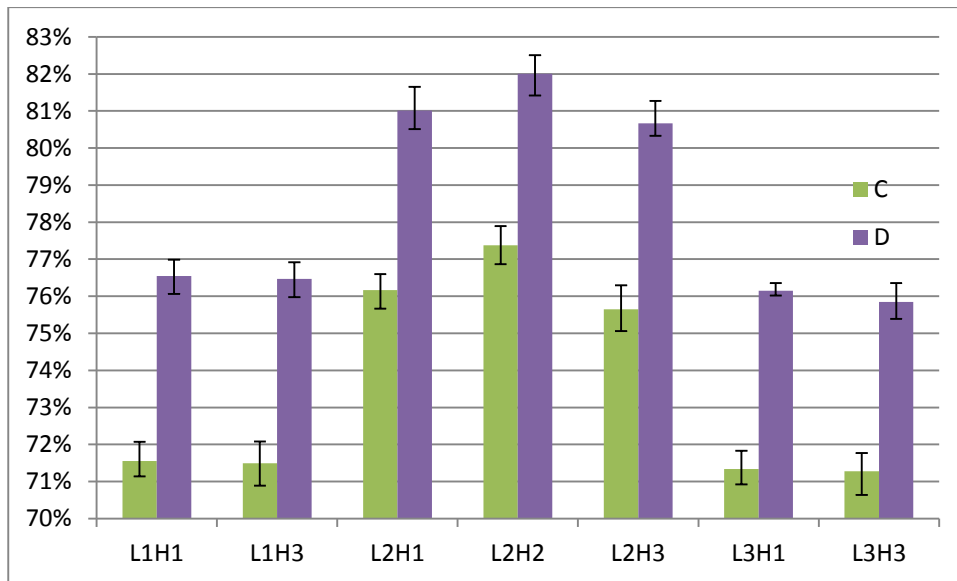
Figure 6.17 Average %kill rate for susceptibilities ranging from 0.014 - 0.5 m².J⁻¹. C) 0% reflectivity and D) 15% reflectivity.

When reducing the susceptibility, the difference between L2H2 and lamps located at L3 is in average of 6%, this is when reflectivity is at 0% (Table 6-9).

Table 6-9 Kill rate performance comparison matrix for UV susceptibilities ranging from 0.014 to 0.5 m².J⁻¹ at 0% reflectivity.

		0.014 - 0.5 m².J⁻¹ (k) at 0% R						
		L1H1	L1H3	L2H1	L2H2	L2H3	L3H1	L3H3
0% R	**%kill rate**	71.55%	71.49%	76.17%	77.38%	75.64%	71.34%	71.28%
L1H1	71.55%	0.00%	0.06%	-4.62%	-5.83%	-4.09%	0.21%	0.27%
L1H3	71.49%	-0.06%	0.00%	-4.68%	-5.89%	-4.15%	0.15%	0.21%
L2H1	76.17%	4.62%	4.68%	0.00%	-1.21%	0.52%	4.83%	4.89%
L2H2	77.38%	5.83%	5.89%	1.21%	0.00%	1.73%	6.04%	6.09%
L2H3	75.64%	4.09%	4.15%	-0.52%	-1.73%	0.00%	4.31%	4.36%
L3H1	71.34%	-0.21%	-0.15%	-4.83%	-6.04%	-4.31%	0.00%	0.05%
L3H3	71.28%	-0.27%	-0.21%	-4.89%	-6.09%	-4.36%	-0.05%	0.00%

Results expressed in percentage of performance

When reflectivity is increased to 15%, the difference in performance between the various configurations gets reduced (in average) (Table 6-10).

Table 6-10 Kill rate performance comparison matrix for UV susceptibilities ranging from 0.014 to 0.5 m².J⁻¹ at 15% reflectivity.

		0.014 - 0.5 m².J⁻¹ (k) at 15% R						
		L1H1	L1H3	L2H1	L2H2	L2H3	L3H1	L3H3
15% R	**%kill rate**	76.55%	76.47%	81.02%	82.01%	80.67%	76.15%	75.85%
L1H1	76.55%	0.00%	0.08%	-4.47%	-5.46%	-4.12%	0.40%	0.70%
L1H3	76.47%	-0.08%	0.00%	-4.55%	-5.54%	-4.20%	0.32%	0.62%
L2H1	81.02%	4.47%	4.55%	0.00%	-0.99%	0.34%	4.87%	5.17%
L2H2	82.01%	5.46%	5.54%	0.99%	0.00%	1.34%	5.86%	6.16%
L2H3	80.67%	4.12%	4.20%	-0.34%	-1.34%	0.00%	4.52%	4.82%
L3H1	76.15%	-0.40%	-0.32%	-4.87%	-5.86%	-4.52%	0.00%	0.30%
L3H3	75.85%	-0.70%	-0.62%	-5.17%	-6.16%	-4.82%	-0.30%	0.00%

Results expressed in percentage of performance

An interesting result is that In both cases at 0% and 15% reflectivity the variation in performance independently of the lamp configuration was minimal with standard deviations no greater than 0.6% over a set of 100 runs (monte-carlo analysis), this indicates that the reliability of the system is constant, and although the general performance of the system is affected by lamp position across the length of the duct, its reliability, meaning its capacity to keep a constant performance, is not.

The more resistant the microorganism is to UV light, the biggest the impact lamp configuration and reflectivity will have in sterilisation performance.

There was little impact on sterilisation performance due to lamp position across the height of the duct, e.g. L2H1 and L2H3 where the difference in average UV dose was of merely 2.12%

resulted in a difference in sterilisation performance of 0.38%, which is an insignificant difference in performance. In a real system installation, both systems will perform virtually identical. The tables of kill rate performance show us that lamps at L1 independently of position in Y performed virtually equal, and the same is for lamps at L2 and lamps at L3. Therefore, there was no real impact regarding the position of the lamp along the height of the duct.

The difference in performance between lamps in L2 and L3 was also virtually null, meaning that as lamp move away from the centre in either direction, their performance decreases at the same rate.

6.5 Alternative turbulence model k-ω.

The k-ε turbulence model (Chapter 5) is one of the most popularly used models, is not computationally expensive in comparison with other models, and generally valid for fully turbulent flows (as is the case of the UVC systems here analysed) (Tu et al., 2007). The K-ω (Chapter 5) is an alternative turbulence model that solves for kinetic energy and turbulence frequency (Sumer, 2013).

The first noticeable affectation of using an alternative turbulence model is the average UV dose of the system. While the k-ε calculated a UV dose of 10.965 $J.m^{-2}$ the k-ω calculated a slightly higher average UV dose of 11.264 $J.m^{-2}$, in reality such variation is minimal, of about 0.3 $J.m^{-2}$, and will not have any considerable affectation on performance.

EPA 600/R-06/050 k-ε
Average UV dose 10.965 J.m^{-2}
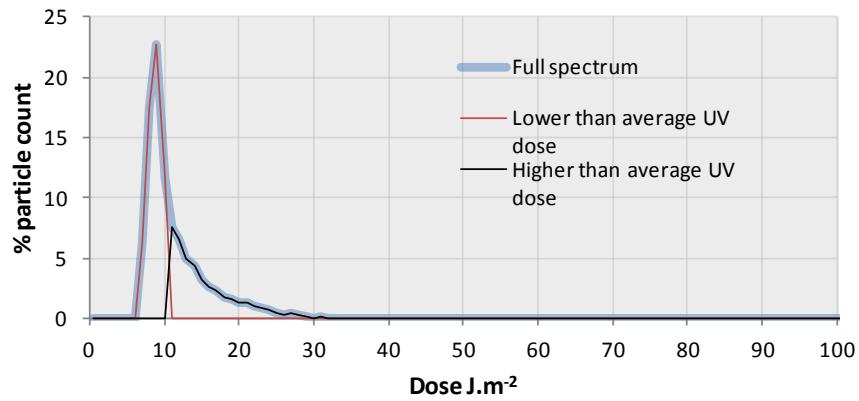
EPA 600/R-06/050 k-ω
Average UV dose 11.264 J.m^{-2}
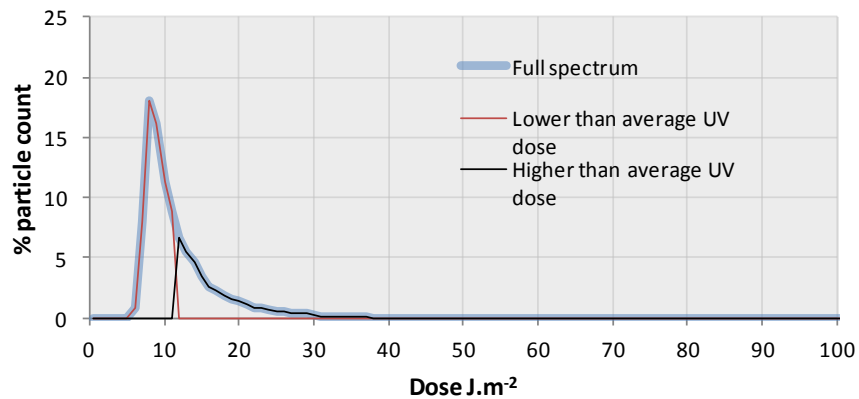
Figure 6.18 UV dose distribution for L2H2 at 15% diffuse wall reflectivity solved with the k-ε (top) and the k-ω (bottom) turbulence model.

The use of a different turbulence model also affected particle trajectories. Figure 6.18 shows the particles that received 10 J.m^{-2} or more at the outlet of the duct. In the case of the k-ω model, the particles appear to be spread covering a wider area, with a considerable amount of particles located close to the walls.
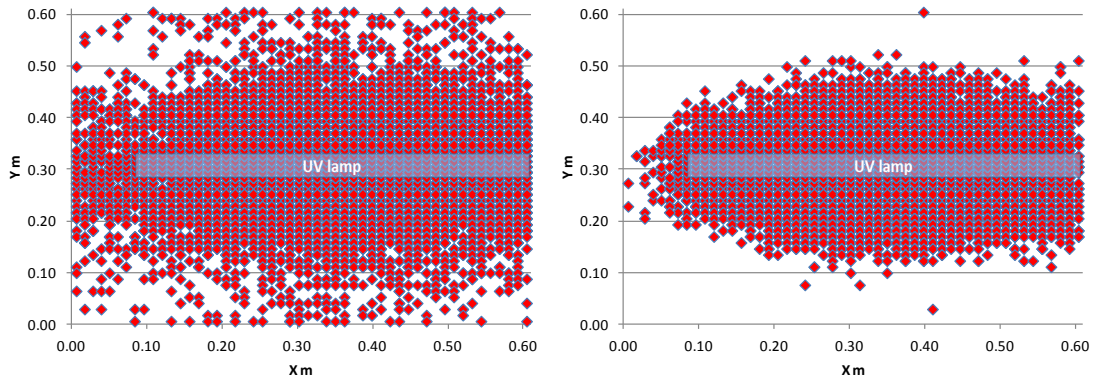
Figure 6.19 Cross section at the outlet of L2H2 solved with the k-ω (left) and k-ε (right) turbulence model at 15% diffuse wall reflectivity showing particles receiving the UV dose of 10 J.m^{-2} more.

In the same manner that particles trajectories are affected by the use of a turbulence mode, the residence time of particles is also influenced. While the k-ε calculated an average residence time of 0.69 m.s^{-1} the k-ω calculated 0.72 m.s^{-1} average residence time.
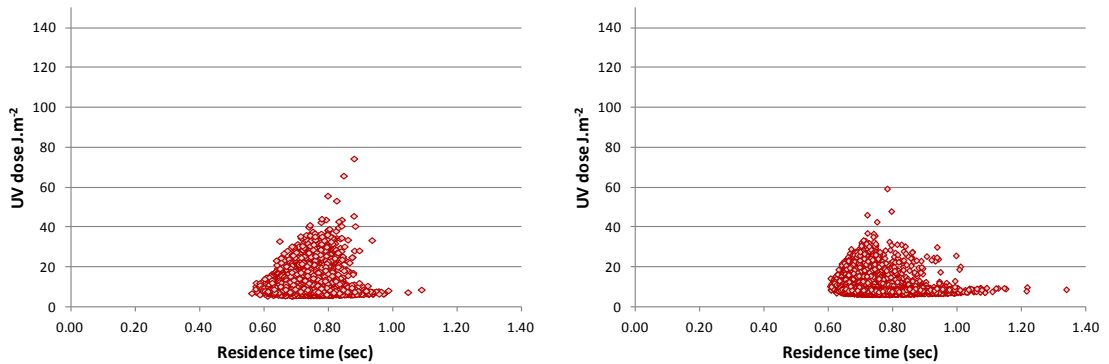
Figure 6.20 UV dose and Residence time of particles for L2H2 solved with k-ω (left) and k-ε (right) turbulence model.

When comparing the location of particles and the average UV dose they receive, we find that the results are relatively similar. Slight differences show that the k-ω model develops a more even particle distribution along the x axis, meaning that particles passing between the gap of the end of the lamp and the wall (in the x axis) receive a more even irradiation. While in the k-ε model is more evident the area after the lamp where particles receive less UV dose (located between x 0.00 and x 0.10 in the bottom left graph).
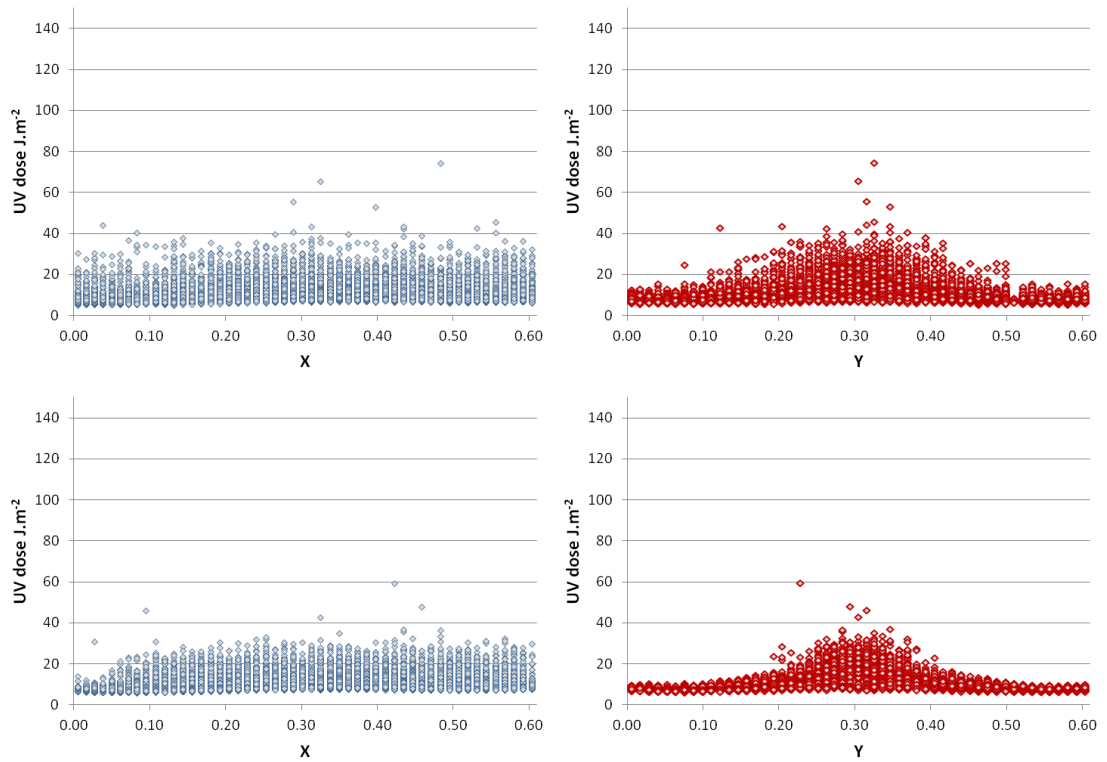
Figure 6.21 UV dose received by particles at X and Y coordinates at the end of the duct. L2H2 solved with the k-ω (top) and k-ε (bottom) turbulence model.

It appears as if the K-ω models captures the velocity profile in a more pronounced fashion, in the top image it can be seen the ellipse of the fully developed air velocity profile at the inlet of the system. Nevertheless, although the velocity profile appears slightly different when the system is solved using the k-ω turbulence, the average air velocity of the system remained the same at 2.50 m.s^{-1}.
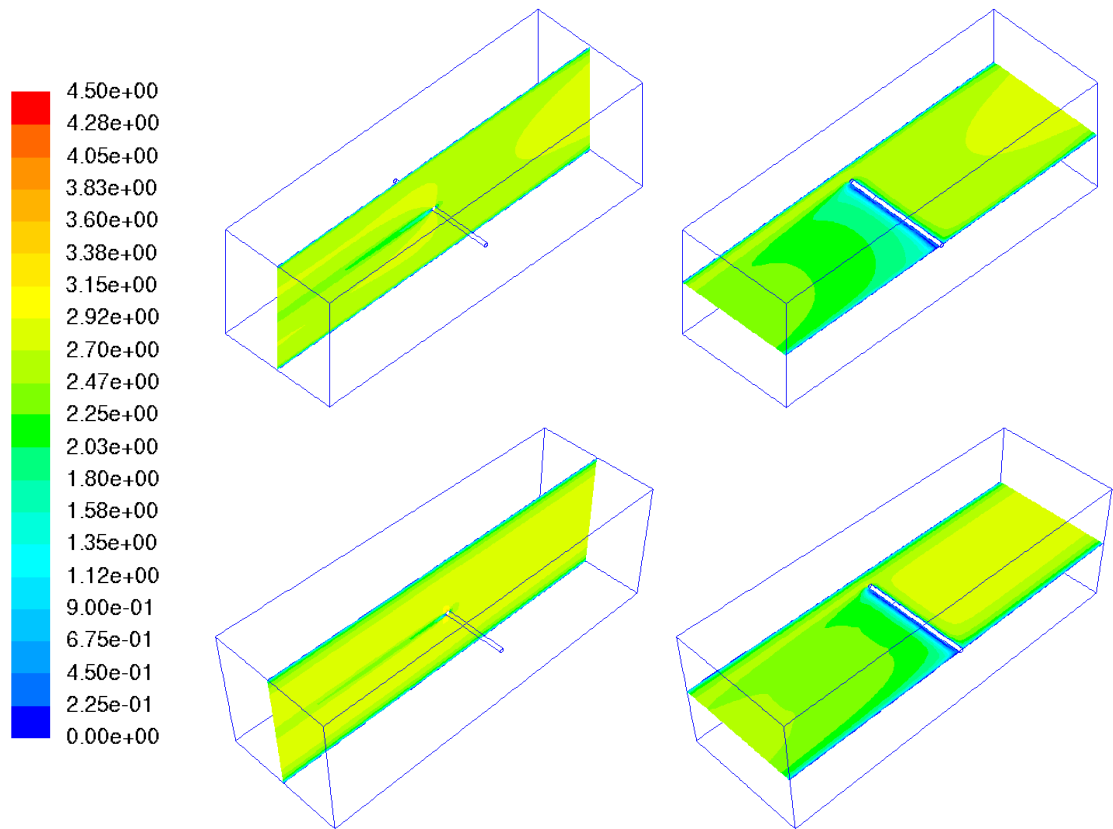
Figure 6.22 Contours of velocity (m.s^{-1}) for L2H2 solved with the K-ω (top) and K-ε (bottom) turbulence model.

The average volume kinetic energy of the system when solved with the k-ω turbulence model was calculated to be 0.0763 m^2.s^{-2} which is significantly greater than kinetic energy calculated with the K-ε model.
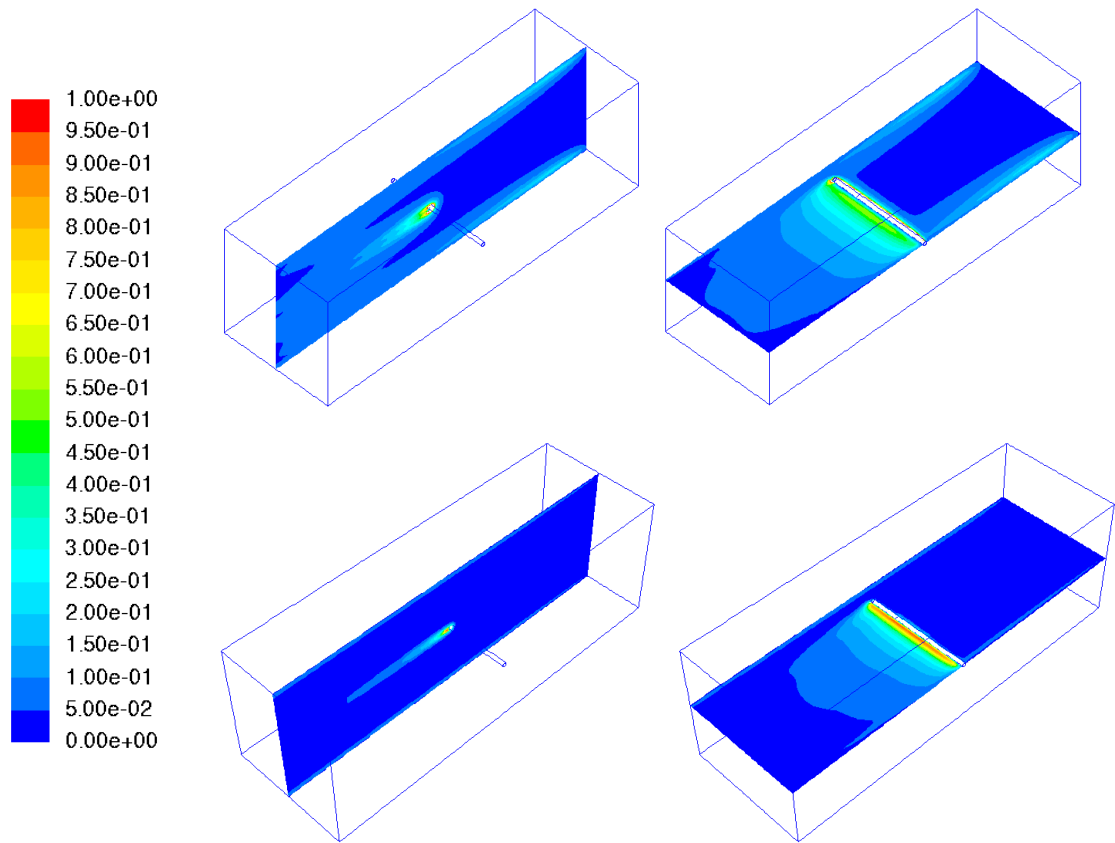
Figure 6.23 Contours of kinetic energy (K) m².s⁻² for L2H2 solved with the K-ω (top) and K-ε (bottom) turbulence model.

The volume average turbulence intensity of the system when solved with the k-ω turbulence model is of 21.63%, which is considerably higher than the value calculated when using the k-ε turbulence model (12.64%). It can be seen how the turbulence intensity is calculated to be greater before the UV lamp when solving with the k-ω model, while the k-ε did not developed turbulence before the UV lamp.
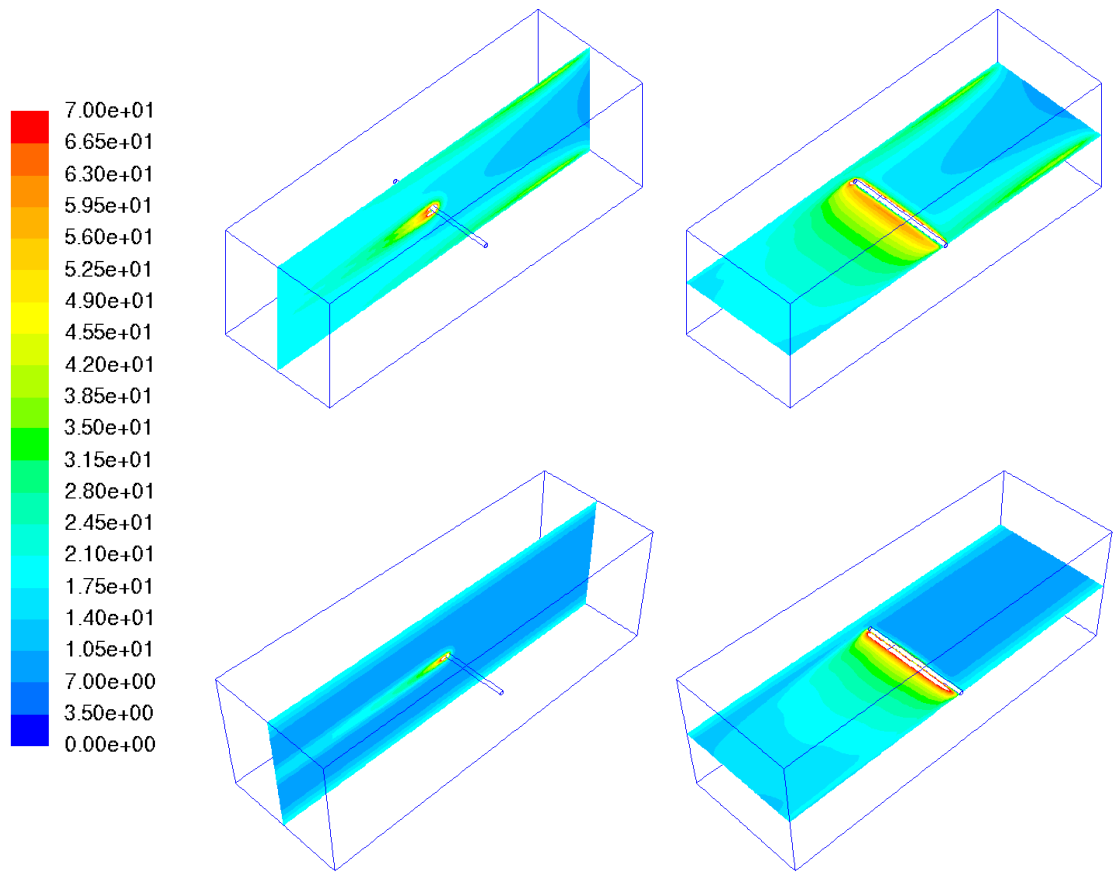
Figure 6.24 Contours of turbulence intensity % for L2H2 solved with the K-ω (top) and K-ε (bottom) turbulence model.

The volume average turbulence Reynolds number was also higher for the k-ω turbulence model which calculated to be 1593.99 as opposed to for the system.
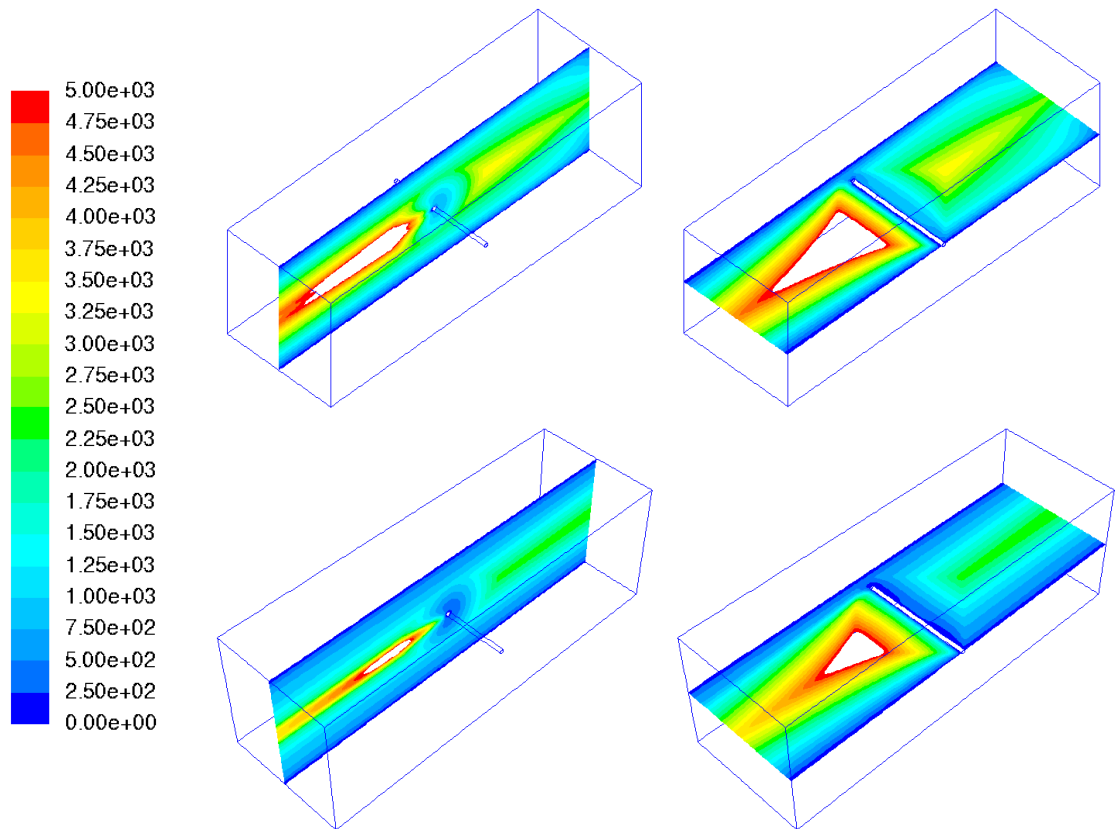
Figure 6.25 Contours of turbulent Reynolds number (Re_y) for L2H2 solved with the K-ω (top) and K-ε (bottom) turbulence model.

The volume average turbulence Reynolds number was also higher for the k-ω turbulence model which calculated 1593.99 for the system as opposed to 888.59 when using the k-ε model.

Albeit all the differences in turbulence results and velocity profiles, the performance of the system is relatively unaffected by the selection between k-ε and the k-ω turbulence model. For a theoretical microorganism with susceptibility ranging from 0.014 $m^2.J^{-1}$ (susceptibility of B. subtillis spores) to 0.75 $m^2.J^{-1}$ the k-ω has an average performance of 87.91% while the k-ε shows 87.86%, and for a susceptibility of 0.014 $m^2.J^{-1}$ to 0.50 $m^2.J^{-1}$ the performance is 82.08% and 82.01% respectively (Figure 6.26).
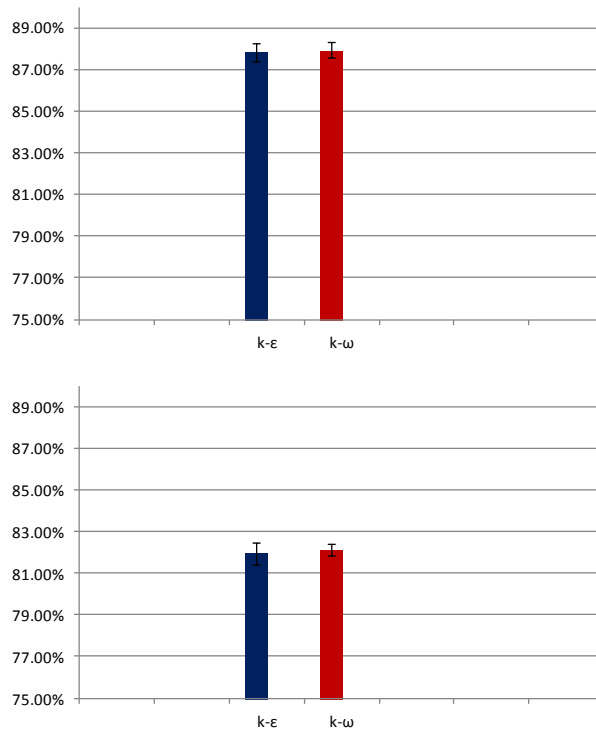
Figure 6.26 Sterilisation performance for range of susceptibilities 0.014 to 0.75 m².J⁻² (top) and 0.014 to 0.5 m².J⁻¹ (bottom).

In conclusion, the use of a different turbulence model (between k-ε and k-ω turbulence models) did not affect the calculation of performance of the system. The CFD models here presented used the k-ε model due to lower computational costs and faster solving times.

Table 6-11 Performance %kill rate comparison against specific microorganisms for the L2H2 solved with the k-ε and the k-ω turbulence model.

			% Kill rate	
Microorganism	K m².J⁻¹ Band width	Shoulder n width	k-ε	k-ω
B. Subtillis	0.014 - 0.020	1-3	4.85%	5.05%
E. coli	0.056 - 0.091	-	53.08%	53.58%
M. bovis BCG	0.170 - 0.360	-	90.94%	90.93%
M. tuberculosis	0.107 – 0.550	-	91.71%	91.72%
P. aeruginosa	0.412 - 0.530	-	98.50%	98.44%

6.6 Parallel lamp configuration.

In the previous models, lamps were located perpendicular to the airflow. This section explores how lamps are positioned within the duct, parallel or perpendicular to the airflow, and the impact on performance.

The configuration L2H2 at 15% reflectivity was modelled as parallel to the airflow (Figure 6.27) using the same lamp power, duct design and operation parameters as stated in section 6.3 of this chapter.

direction of airflow

1830 mm

L2H2 parallel

outlet   610 mm

Inlet
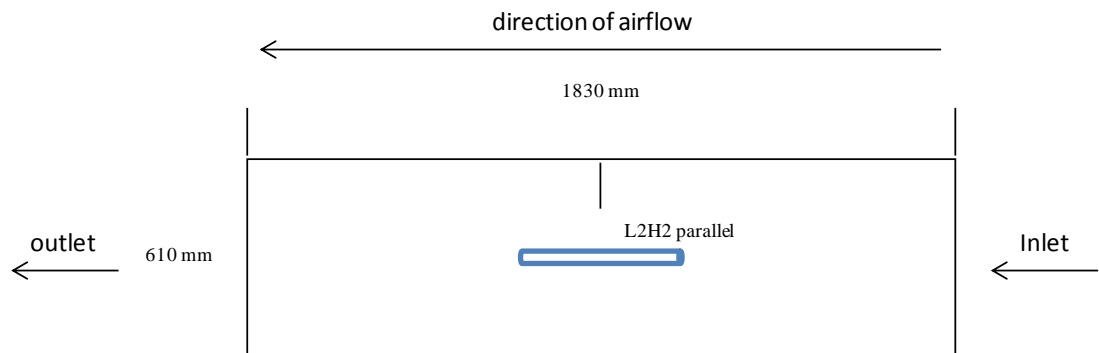
Figure 6.27 Lamp configuration schematics of L2H2 parallel.

6.6.1 Particle dose distribution comparison

The particle dose distribution of a lamp located parallel at the centre of the duct (L2H2 parallel) showed a peak at approximately 9 J.m^{-2} while the average UV dose of the system is of 17.36 J.m^{-2}, which is considerably higher (almost double) to that of the L2H2 perpendicular (10.97 J.m^{-2}) (Figure 6.28).

L2H2 parallel
Average UV dose 17.36 J.m^{-2}

L2H2 perpendicular
Average UV dose 10.97 J.m^{-2}
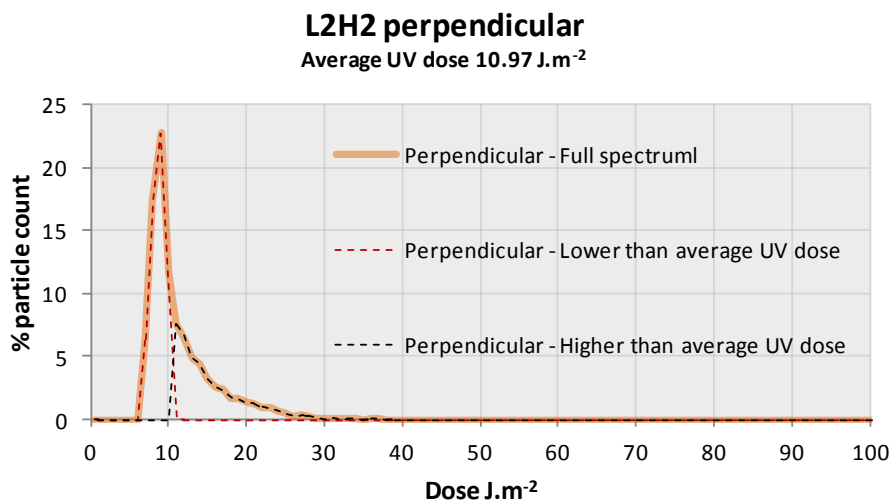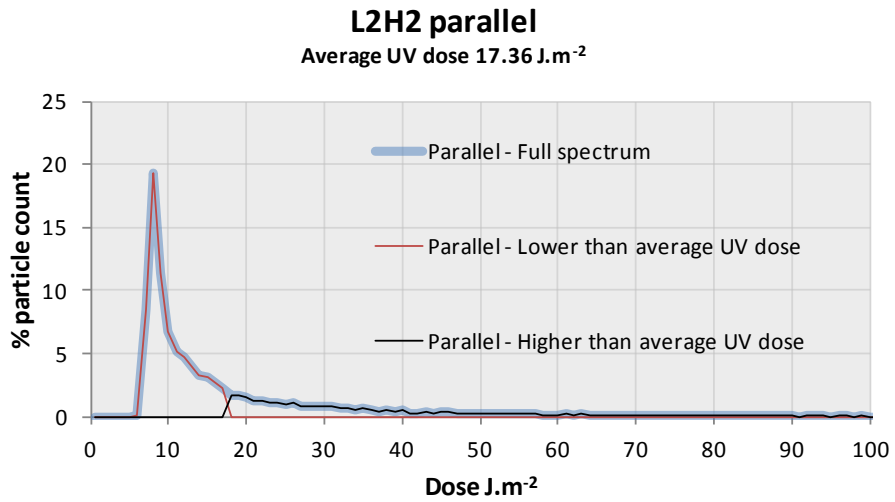
Figure 6.28 UV dose distribution for configuration L2H2 parallel vs perpendicular. Average UV dose at the crossing of lower and higher than average UV dose.

The particle dose distribution is very similar for both configurations (L2H2 parallel and L2H2 perpendicular), and the difference appears to be created by particles receiving high irradiation in the area close to the lamp when the lamp is positioned parallel to the airflow.

While the highest UV dose received by a particle in the L2H2 perpendicular configuration was of 60 J.m^{-2}, for the L2H2 parallel the highest UV dose received by a particle was more than 100 J.m^{-2}, with a few receiving up to 150 J.m^{-2}. This is to highlight how albeit lamp power inside the UV system remained constant, lamp position had a significant effect on the irradiation received by particles. This also shows one of the reasons why the average UV dose of the L2H2 parallel system is higher than that of the perpendicular configuration.
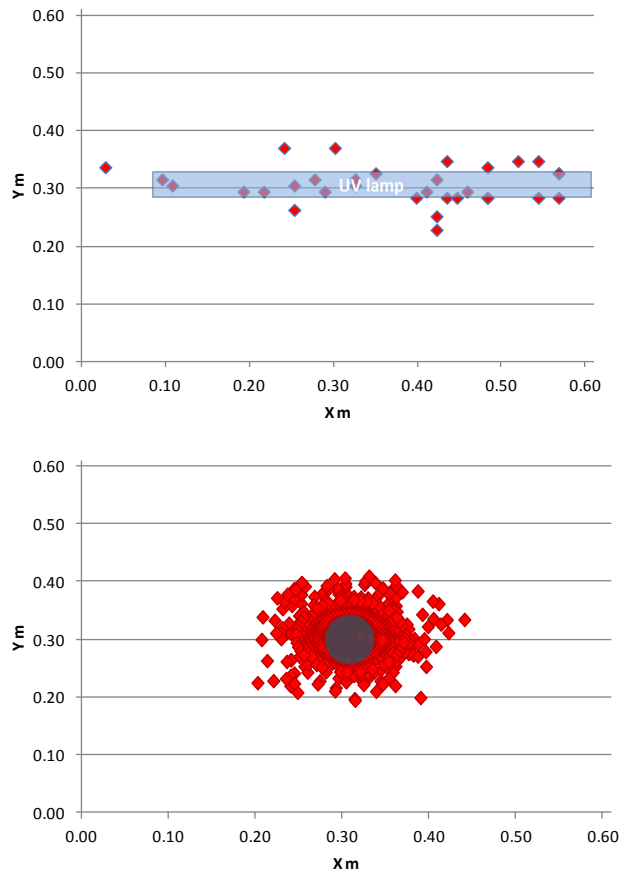
Figure 6.29 Cross section at the outlet of the L2H2 perpendicular (top) and L2H2 parallel (bottom) lamp configuration at 15% reflectivity showing lamp position and location of particles receiving the UV dose of 30 J.m^{-2} or more.

Particles passing close to the lamp receive higher UV irradiation, while just a few particles manage to receive the UV dose of 30J.m^{-2} or more for the perpendicular configuration, the parallel configuration allowed for many more particles to receive such UV dose or more, hence the average UV dose of the system is increased in the latter configuration.
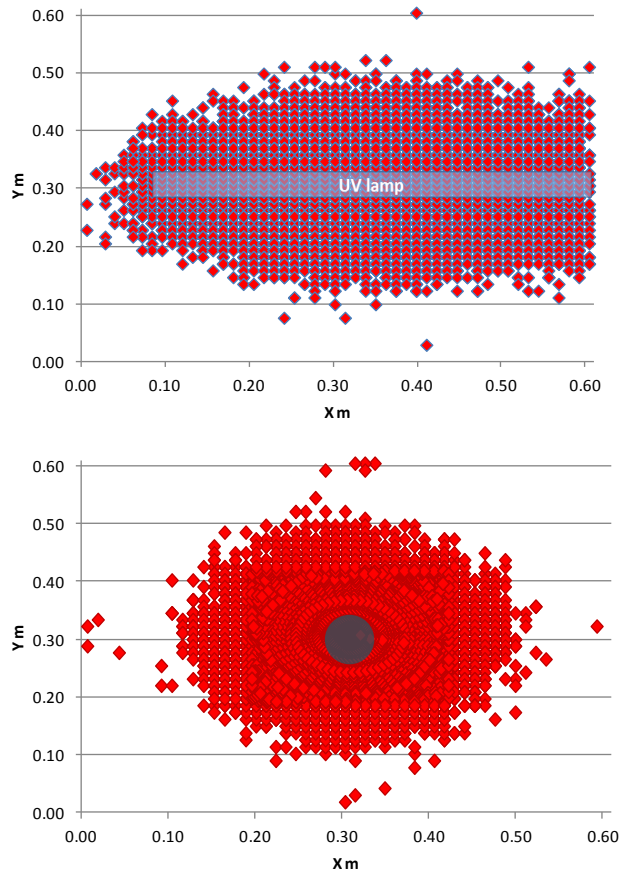
Figure 6.30 Cross section at the outlet of the L2H2 perpendicular (top) and L2H2 parallel (bottom) lamp configuration at 15% reflectivity showing lamp position and location of particles receiving the UV dose of 10 J.m^{-2} more.

Now, if we consider particles receiving just 10 J.m^{-2}, which was the representative dose used to compare area of coverage of the different lamp configurations earlier this chapter, it can be seen how the perpendicular configuration covers almost all the width of the duct (*X* axis) while the parallel configuration focuses the area of coverage at the centre of the duct (Figure 6.30).

The L2H2 parallel configuration had a higher average UV dose because it allowed a group of particles, those passing close to the lamp at the centre of the duct, to receive particularly high UV doses.

6.6.2 Sterilisation performance comparison

Perhaps, it is more interesting to analyse the calculated performance of the two systems at different susceptibilities. If we use a single number as susceptibilities e.g. 0.75 m^2.J^{-1}, 0.5 m^2.J^{-1} etc we would see that difference in performance is minimal between the two lamp configurations, and important changes would only be visible at susceptibilities of 0.1m^2.J^{-1} or less (Figure 6.31).
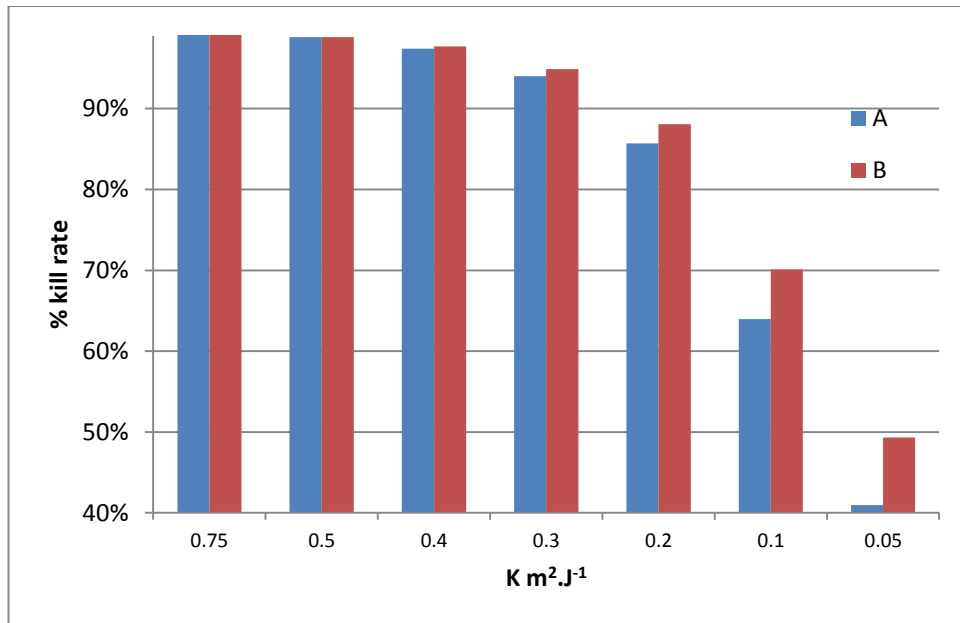
Figure 6.31 Performance kill rate of UV system L2H2 perpendicular (A) vs L2H2 Parallel (B) using static susceptibilities.

Nevertheless, we know from the research shown in Chapter 3 that microorganism do not have single number susceptibilities, instead the susceptibility of a microorganism consist of a range of values (minimum and maximum value) akin to a band width in the susceptibility spectrum, as such *E. coli* for example will have a susceptibility band width of $0.056 - 0.091$ m^2.J^{-1} at 70% RH depending on the particular strain and environmental conditions. If we would have the theoretical case in which the UV systems here presented would be injected with a group of microorganism with random susceptibilities normally distributed in a range from 0.014 m^2.J^{-1} (minimal susceptibility found for *B. subtillis* spores) to various maximum susceptibilities values (i.e. 0.75 m^2.J^{-1}, 0.5 m^2.J^{-1} etc), which is a more likely scenario in a real life installation, we would find that a) the average performance kill rate of the system is reduced and b) that the difference in performance between the systems becomes more evident (Figure 6.32).
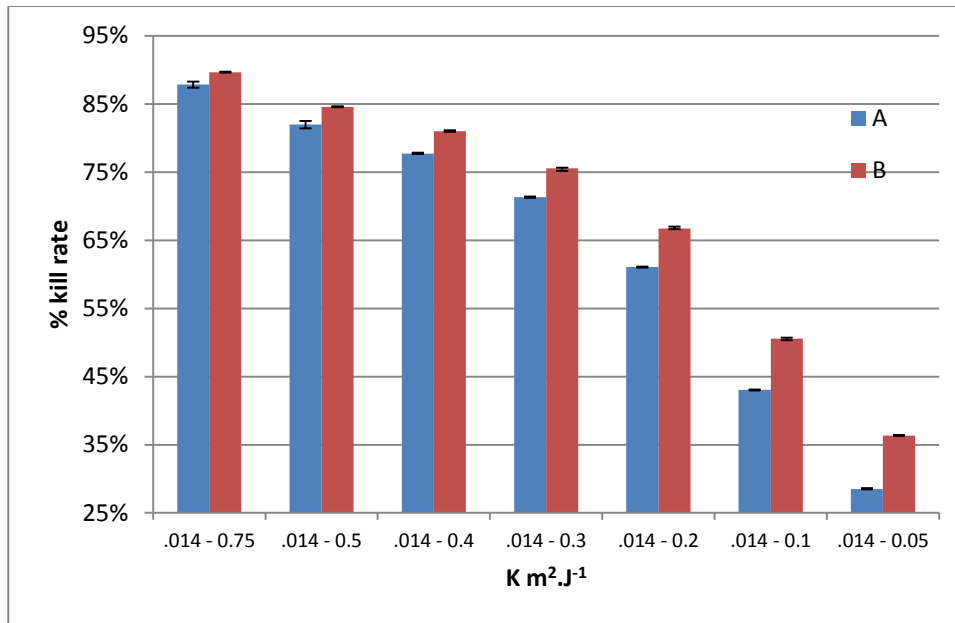
Figure 6.32 Performance kill rate of UV system L2H2 perpendicular (A) vs L2H2 Parallel (B) using band width susceptibilities (band ranges) showing the maximum (top outlier bar), minimum (bottom outlier bar) and average value (main column).

Table 6-12 shows the calculated kill rate for specific microorganism susceptibilities, to give an idea of how the two systems would compare in a real life installation

Table 6-12 Performance %kill rate against specific microorganisms.

Microorganism	K $m^2.J^{-1}$ Band width	Shoulder n width	% Kill rate L2H2 perpendicular	L2H2 parallel
B. Subtillis	0.014 - 0.020	1-3	4.85%	9.54%
E. coli	0.056 - 0.091	-	53.08%	60.55%
M. bovis BCG	0.170 - 0.360	-	90.94%	92.35%
M. tuberculosis	0.107 – 0.550	-	91.71%	93.03%
P. aeruginosa	0.412 - 0.530	-	98.50%	98.64%

6.6.3 Turbulence and Irradiation comparison

The lamp parallel to the airflow improved the average UV dose of the system, and reduced its turbulence. Nevertheless in a real operational installation, the parallel design will need mounting brackets which will affect its turbulence.

It is also of importance to note that the parallel system did not show a higher volume average irradiation and yet it showed a higher average UV dose, meaning that volume average irradiation of the system is not what defines its performance and its correlation with performance ceases when lamps are located at a different angle against the airflow e.g.

comparing volume irradiation of a lamp parallel to the airflow to a lamp perpendicular to the airflow. Instead, the performance of the system is a combination of irradiation and airflow patterns.
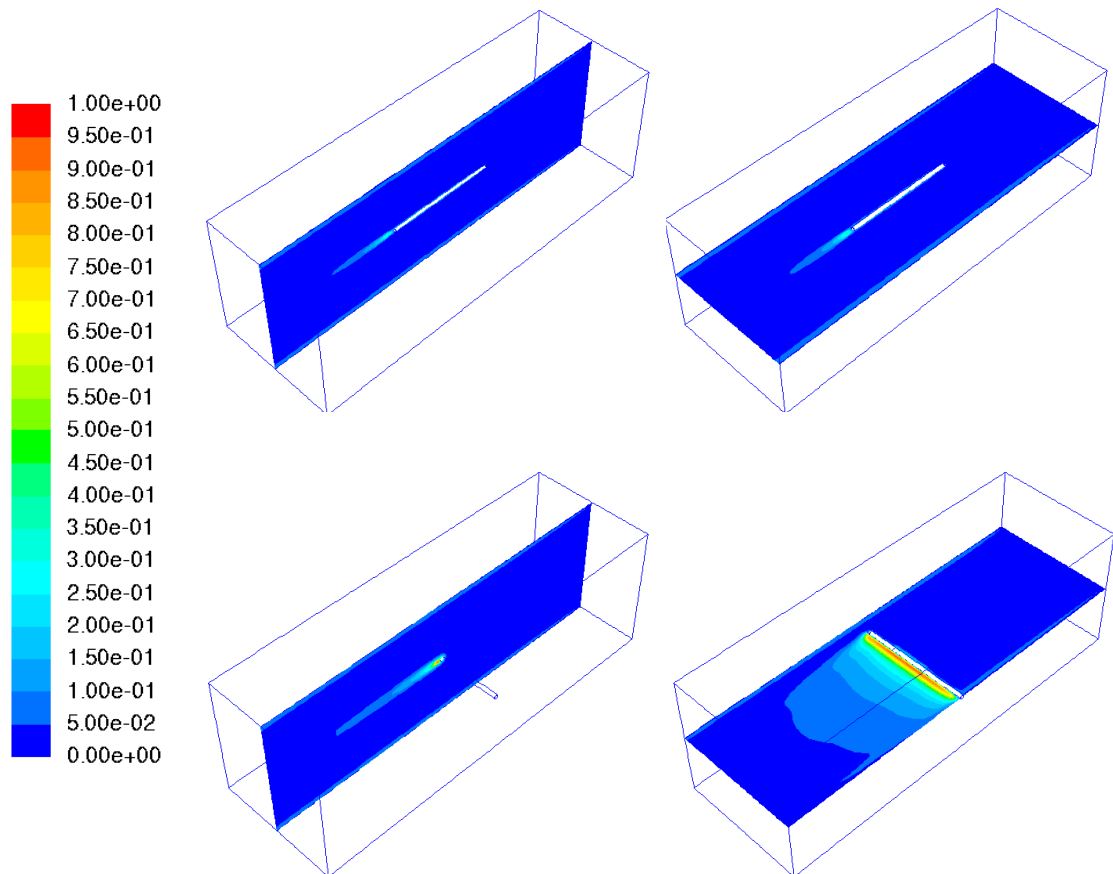
Figure 6.33 Contours of turbulent kinetic energy (K) m².s⁻² for L2H2 parallel (top) and L2H2 perpendicular (bottom).

The turbulent kinetic energy of the parallel lamp system is relatively low, as it can be seen the kinetic energy across the height and the width of the duct is reduced to a short stream located after the lamp, opposed to what happened when the lamps were located perpendicular to the airflow, where a stream of kinetic energy and turbulence is generated across the width of the duct.
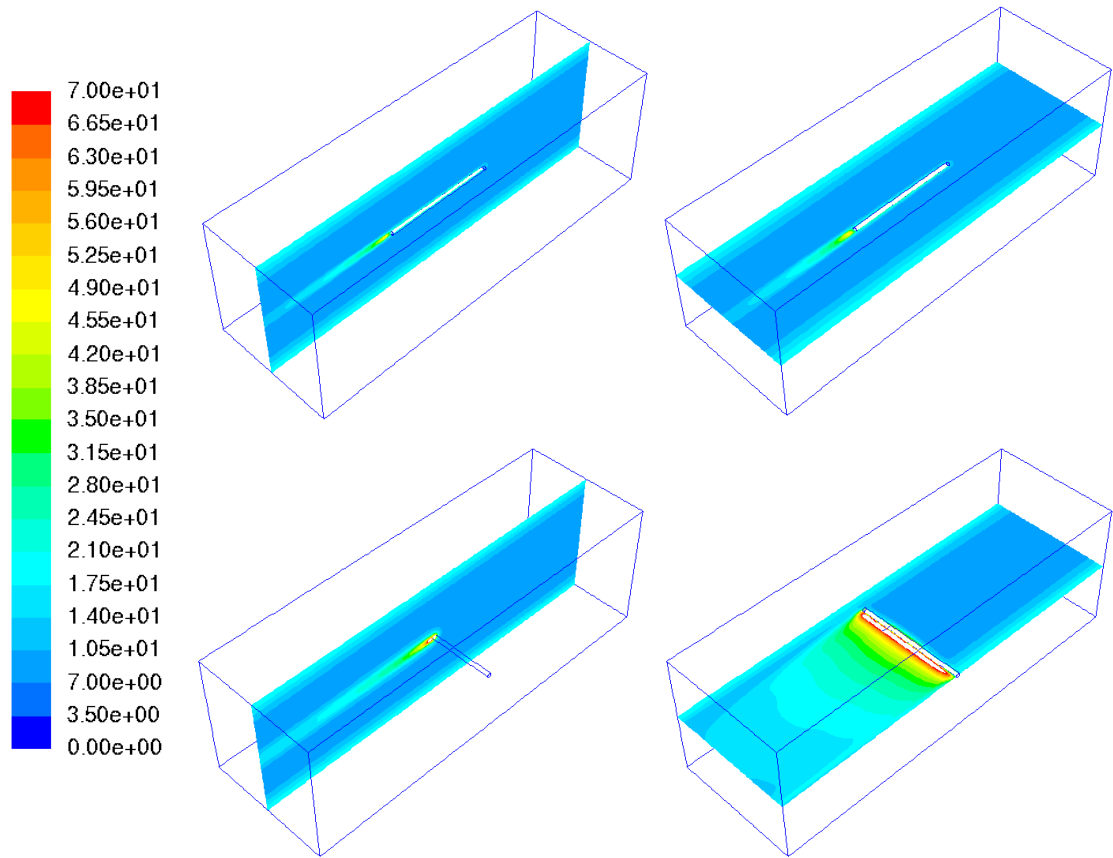
Figure 6.34 Contours of turbulence intensity % for L2H2 parallel (top) and L2H2 perpendicular (bottom).

The percentage of turbulent intensity was reduced with the lamp positioned parallel to the airflow; the volume average turbulence for the parallel lamp system was of 12.11% which is lower than in any of the perpendicular lamp design, reinforcing the evidence that turbulence can be either an advantage or a disadvantage for the effectiveness of the system performance (Chang and Young, 2007).
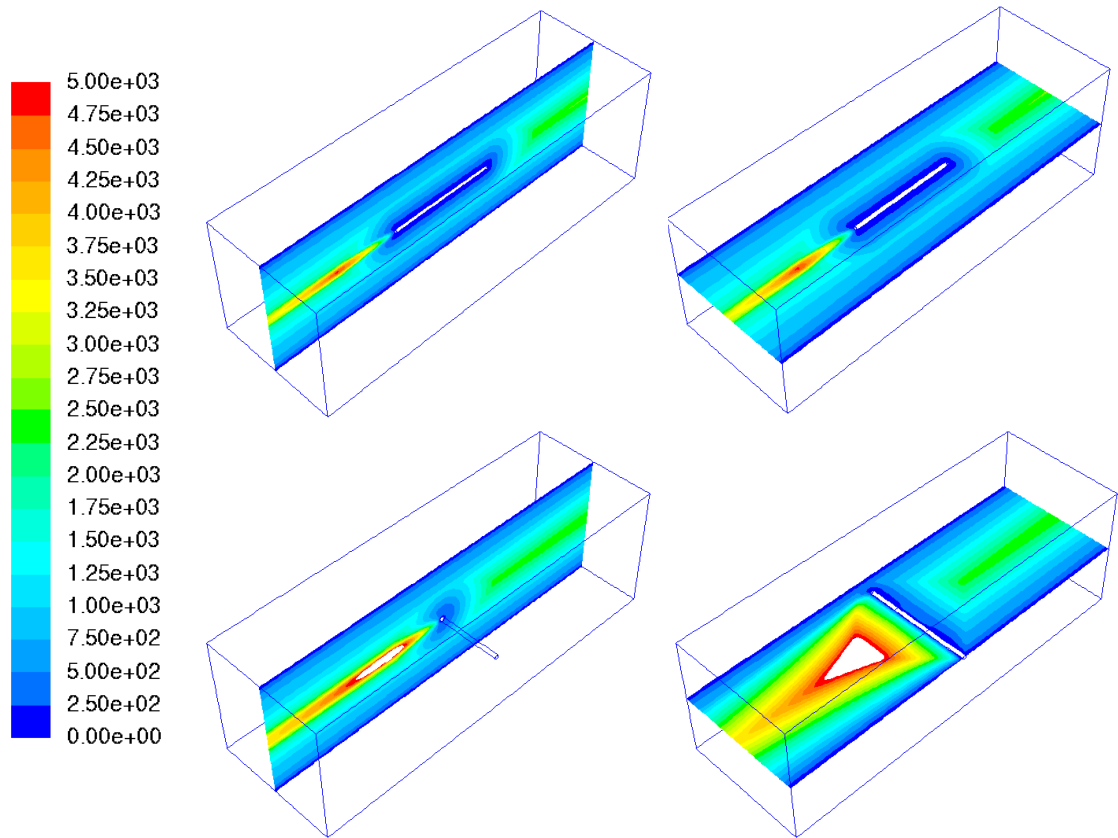
Figure 6.35 Contours of turbulent Reynolds number (Re_y) for L2H2 parallel (top) and L2H2 perpendicular (bottom).

The volume average turbulent Reynolds number for the L2H2 with lamps parallel to the airflow was the lowest if compared against the perpendicular lamp configurations.

The idea of low turbulence being beneficial for UVC sterilisation has been previously analysed by Chang and Young (2007), in a theoretical study they concluded that turbulence can either increase or decrease the sterilisation performance of a UV system. When $V^2 \gg 2KID$ the effectiveness of the UV system is increased, while for the case of $2KID \geq V^2$ the effectiveness is reduced. Where V is velocity, K is the microorganisms' susceptibility to UV, I is the irradiation and D is the longitudinal diffusion coefficient. Nevertheless, the study was a theoretical model and was not validated against physical or modelled data.
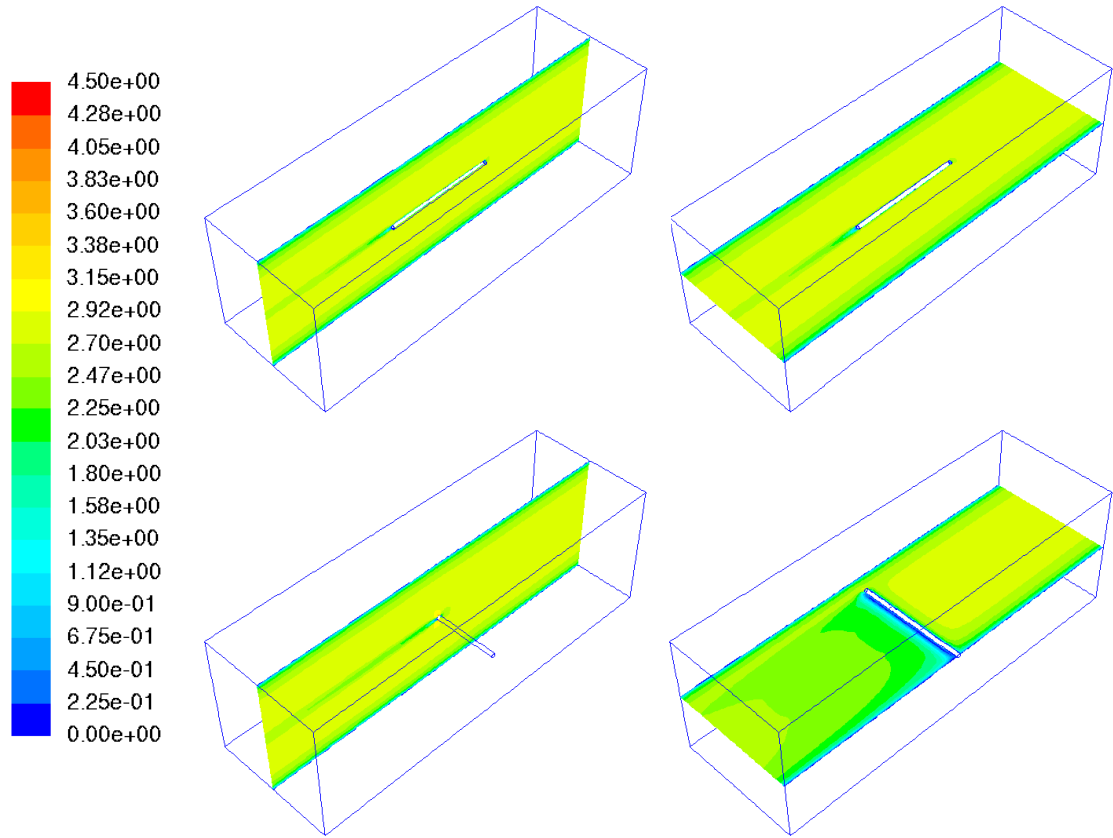
Figure 6.36 Contours of velocity (m.s^{-1}) for L2H2 parallel.

In regards to velocity, the parallel configuration showed to have higher velocities within the duct, hence shorter residence time of the particles injected in comparison with the lamps located perpendicular to the airflow. Nevertheless, it was also found that particles with the longest residence time were not the ones with the highest average UV dose; the highest UV dose was reached by particles within the average residence time which for the L2H2 parallel configuration was of 0.69 seconds while for the L2H2 perpendicular was of 0.71 seconds (Figure 6.37).
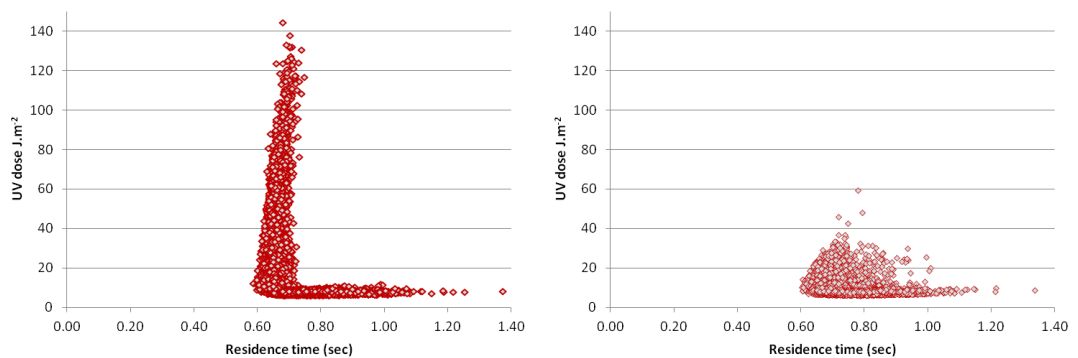
Figure 6.37 UV dose and Residence time of particles. L2H2 parallel (left) and L2H2 perpendicular (right).

Residence time did not have any correlation with the UV dose received by the particles, in fact the particles with the longest residence time were among the particles with the lowest UV dose, this means that although the particles spent longer times inside the UV chamber, they did it in areas of low UV irradiation, Figure 6.38 shows that particles located at the duct walls were the particles with the highest residence time, and as we know from the findings in section 6.3 and 6.4, the walls are the areas that receive the lowest irradiation.
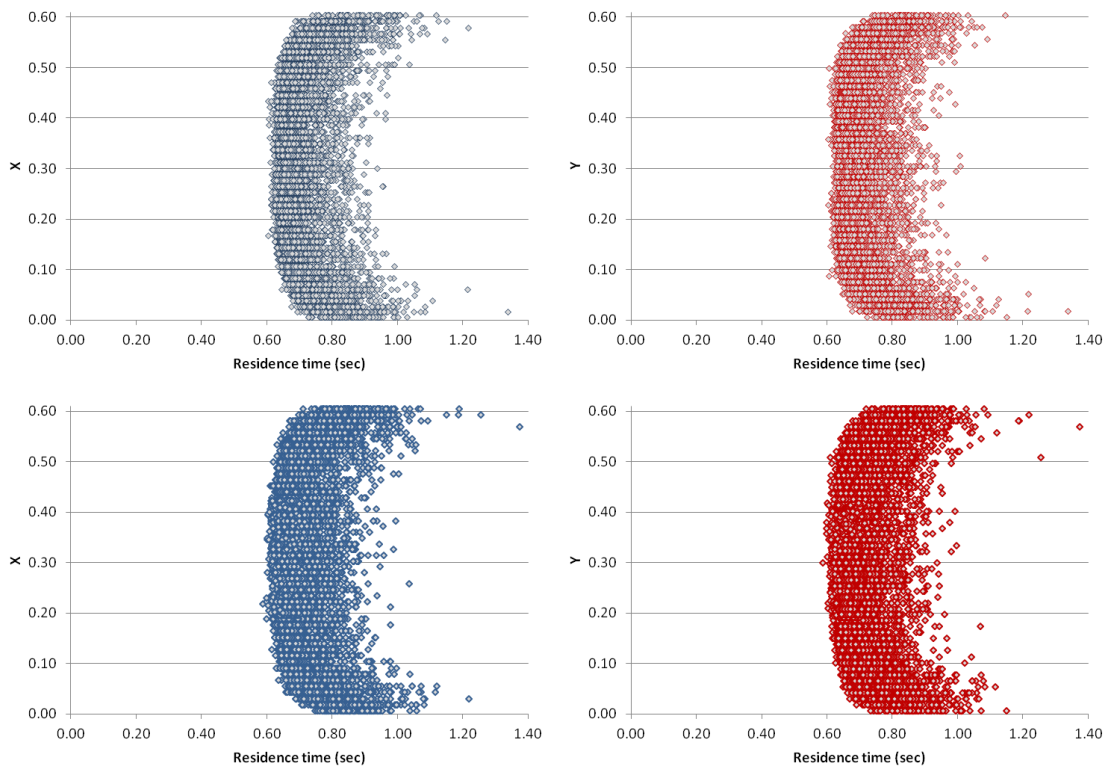
Figure 6.38 Residence time and particle position across the width (X) and height (Y) of the duct. L2H2 perpendicular (Top) and L2H2 parallel (bottom).

The particles that received the highest UV irradiations were the particles passing close to the lamp. For the L2H2 parallel system, as the lamp is located at the centre of both the X and Y planes, the particles receiving high irradiation where also located at the centre in both the X and Y position. For the L2H2 perpendicular configuration, where the lamp is located at the centre in the Y position but across in the X position, the particles receiving high irradiation where at the centre of the Y axis, while particles across the X axis received even irradiation (Figure 6.39).
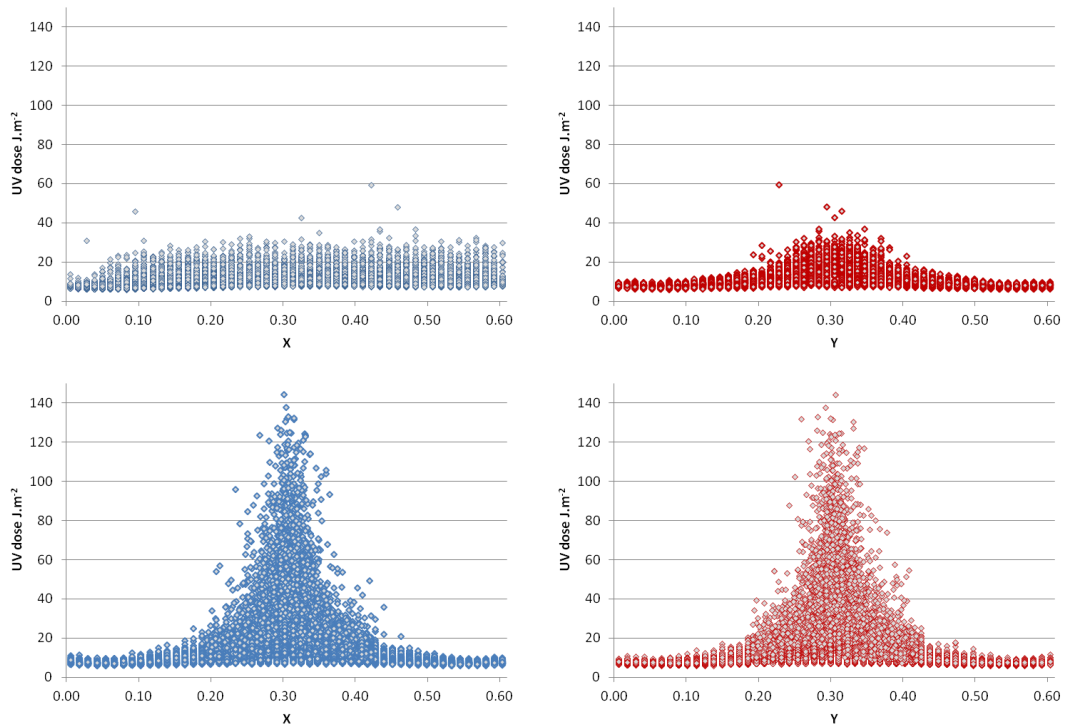
Figure 6.39 UV dose received by particles at X and Y coordinates at the end of the duct. L2H2 perpendicular (top) and L2H2 parallel (bottom).

The irradiation profiles in both cases developed symmetrically as the lamps are located at the centre, with the corner of the duct and the areas close to the wall receiving the lowest irradiation.
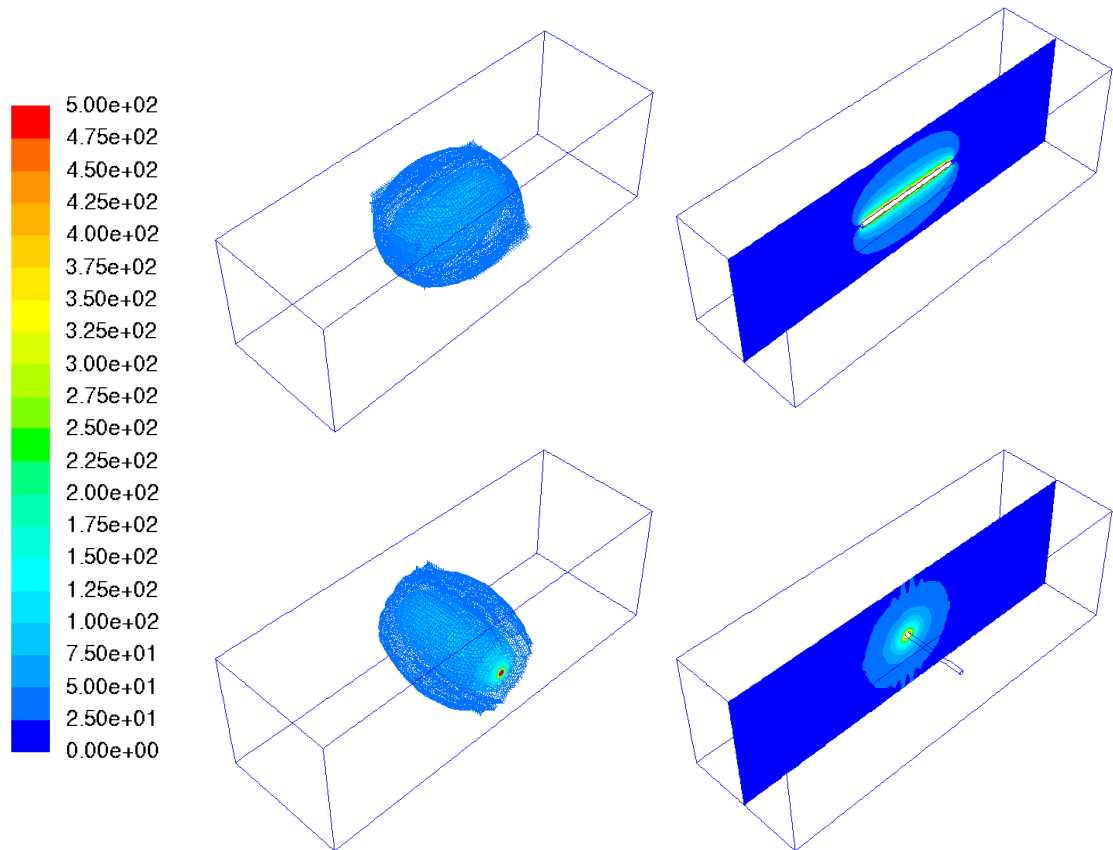
Figure 6.40 Contours of Irradiation (W.m^{-2}) for L2H2 parallel.

The particles receiving the maximum UV dose of the system where those passing in areas close to the lamp, while for the perpendicular system the maximum UV dose received by a particle was of 60 J.m^{-2} and most of particles did not exceeded 25 J.m^{-2}, for the parallel system particles received up to 160 J.m^{-2}. This difference in the particle received average UV dose made the parallel lamp configuration have a considerable higher UV dose standard deviation of 16.27 J.m^{-2} in comparison to that of the L2H2 perpendicular where the UV dose standard deviation was of only 4.39 J.m^{-2}. Meaning that in the parallel lamp configuration, some areas of the duct receive a considerably lower UV dose than the average of the system, while in the perpendicular lamp configuration even the areas receiving the lowest UV dose, the difference in comparison with the average of the system is not much.
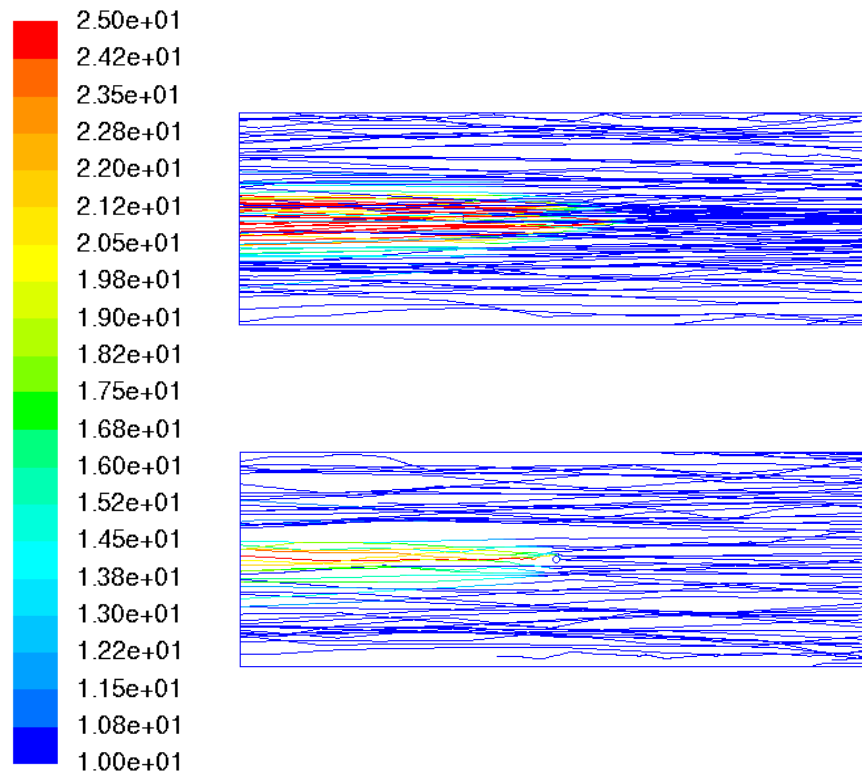
Figure 6.41 UV dose (J.m⁻²) received by particles at L2H2 parallel (top) and L2H2 perpendicular (bottom).

It appears that the average UV dose of the system was mostly influenced by particle trajectories i.e. the particles passing where the UV irradiation was at the highest. The more particles passing close to the lamp, the higher the UV dose of the system will be. The parallel system allowed for longer UV irradiation times at the centre of the duct, giving the system a better performance.

6.6.4 Summary of comparison results

UV systems with a single lamp positioned parallel to the airflow present a better performance than a UV system with a single lamp located perpendicular to the airflow.

The parallel to the airflow lamp system presented lower turbulence than the perpendicular lamp system. Nevertheless, the average UV dose of the parallel system was higher due to an extended high irradiation area located close to the UV lamp. Turbulence does not define performance of this particular UV sterilisation system.

Although particle dose distribution is relatively similar, in the parallel lamp configuration there are particles receiving considerably higher UV doses which in turn create a higher average UV dose for the system.

Although UV sterilisation depends on irradiation and contact time, the residence time of the particles was not directly related to performance, in fact the particles with the longest residence

time were among the particles with the lowest UV dose, and this was due to the fact that the longest residence time happened in areas of low irradiation.

The more particles passing close to the lamp, the better the performance of the system.

6.7 Conclusions.

The analysis shown in this Chapter suggest that the performance of the system was mainly influenced by lamps position across the length of the duct (Z axis) with the highest performance found at the centre of the length of the duct (L2H2). Lamp position across the height of the duct had no significant impact on performance.

Lamp position across the length of the duct can have an impact of up to 20% in average UV dose i.e. when comparing the performance of L2H2 against L3H3.

It appears that lamps located at the beginning of the duct perform slightly better than lamps located at the end of the duct. However, the difference in performance between lamps located at the beginning of the duct and the end of the duct was insignificant and might not have any significant impact in a real operational system.

As expected it was found that the difference in UV average dose between configurations does not directly translate to a difference in sterilisation performance. This is mainly due to the exponential relationship of UV dose with sterilisation performance. Moreover, the complete mechanisms and their impact in the sterilisation performance of a system are not yet fully understood.

Lamp configuration can have an impact as important as reflectivity, as it was shown, lamps located at L2H2 at 0% reflectivity performed better than lamps located at L3 at 15% reflectivity. Moreover, increasing reflectivity creates a more even irradiation distribution which in turn reduces the difference in performance between configuration.

The choice of turbulence model between k-ε and k-ω did not impact the calculation of the average UV dose of the system or its calculated sterilisation performance.

Lamps located parallel to the airflow appear to be more efficient than lamps located perpendicular to the airflow. The lamp positioned parallel to the airflow provided an average UV dose almost 70% higher than that of the lamp perpendicular to the airflow. Nevertheless, However, as the UV sterilisation performance is affected by a combination of the irradiation provided within the system and the airflow patterns and trajectories of it.

Particles passing close to the walls were the ones showing the longest residence time, and at the same time these were the particles receiving the lowest UV dose. This is due to the fact that end walls are the areas receiving the lowest UV irradiation.

Finally this chapter concludes that lamp position affects the performance of the system.

Chapter 7. CFD analysis of multi-lamp In-Duct UV systems and the impact of flow rate in performance.

7.1 Introduction.

This chapter builds on the study cases presented in chapters 5 and 6 to assess performance of realistic UV systems. The first study in this chapter aims to quantify the impact on performance of lamp position on a multi-lamp configuration.

The second study in this chapter considers the performance of a series of in-duct air sterilisation systems including the EPA 600/R-06/050, EPA 600/R-06/051 and the EPA 600/R-06/055 over a range of air flow rates, and identifies the relationship between average UV dose of a system and operational flow rates.

Finally this chapter introduces the notion of a performance efficiency constant (R') and a performance efficiency rating (PER), and revisits the results of earlier studies shown throughout the thesis.

7.2 Multi-lamp configuration performance.

The aim of this study is to quantify the impact of lamp position in a multi-lamp configuration system. Results from Chapter 6 shows that single lamp systems are not normally capable of providing sufficient UV coverage to achieve the levels of performance required for a thorough sterilisation. Moreover, many commercial UV sterilisation systems encompass more than one lamp.

Building from the insights revealed in the studies carried out in chapter 6, the following section focuses on the performance of six multi-lamp configuration set ups. Each multi-lamp configuration consisted of three lamps located at each of the three different lengths, L1 230 mm, L2 915 mm and L3 1600 mm from the inlet as shown in Chapter 6, but varying the position across the height of the duct. Table 7-1 and Figure 7.1 shows the lamp locations of the six configurations here analysed.

Table 7-1 Multi-lamp configuration.

Configuration	LH position 1	LH position 2	LH position 3
P01 – L1H4L2H2L3H4	L 230 mm, H 505 mm	L 915 mm, H 305 mm	L 1600 mm, H 505 mm
P02 – L1H4L2H2L3H0	L 230 mm, H 505 mm	L 915 mm, H 305 mm	L 1600 mm, H 105 mm
P03 – L1H4L2H4L3H4	L 230 mm, H 505 mm	L 915 mm, H 505 mm	L 1600 mm, H 505 mm
P04 – L1H2L2H2L3H2	L 230 mm, H 305 mm	L 915 mm, H 305 mm	L 1600 mm, H 305 mm
P05 – L1H4L1H2L1H0	L 230 mm, H 505 mm	L 230 mm, H 305 mm	L 230 mm, H 105 mm
P05 – L2H4L2H2L3H0	L 915 mm, H 505 mm	L 915 mm, H 305 mm	L 915 mm, H 105 mm

As was shown in Chapter 6, the performance of lamp position across the height of the duct is symmetrical from the centre i.e. L3H3 performs the same as L3H1. It would therefore be expected that P01 (L1H4L2H2L3H4) performs the same as P02 (L1H4L2H2L3H0), unless the irradiation distribution affects the performance of multi-lamp configuration systems. In case P03 (L1H4L2H4L3H4) all the lamps are located at the top of the duct and in P04 (L1H2L2H2L3H2), the lamps are all located at the centre. Finally we have the case of the three lamps in a row across the height of the duct at L1 P05 (L1H4L1H2L1H0) and three lamps across the height of the duct at L2 P06 (L2H4L2H2L2H0).
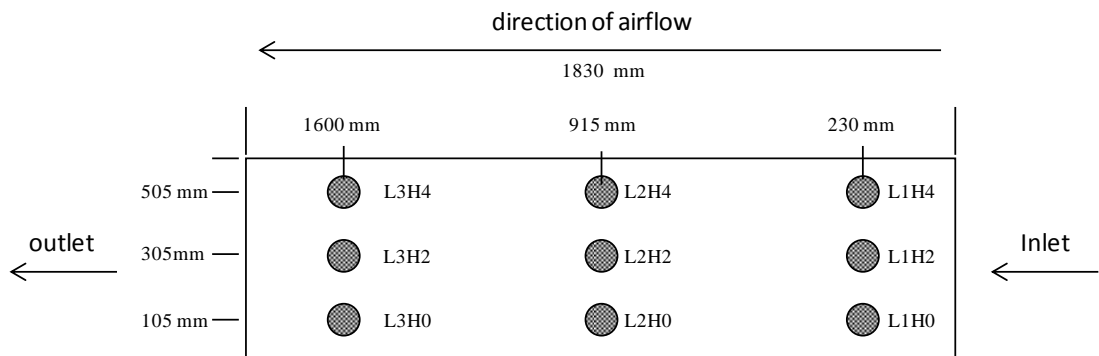
Figure 7.1 Lamp position diagram.

All CFD models were set up as described in Chapter 5.2.1, with materials being air as fluid and stainless steel as solid walls. The absorption coefficient (α_c) and refractive index(n) of stainless steel were adjusted to fit the wavelength of sterilisation UV light (253.7 nm) with values of 99,338,898 m^{-1} and 1 respectively (Chapter 4.5.4) (Karlsson and Ribbing, 1982). The diffusive wall reflectivity of stainless steel was set to 15% (emissivity=0.85), the irradiation was solved using the discrete ordinates method. The flow was assumed to be steady and isothermal in all cases, and the turbulence was approximated through the k-ε model with standard wall

functions. The mean velocity of the flow was set to 2.5 m.s^{-1} with the inlet profile as previously described.

P01 –L1H4L2H2L3H4   **P02 –L1H4L2H2L3H0**   **P03 –L1H4L2H4L3H4**

P04 –L1H2L2H2L3H2   **P05 –L1H4L1H2L1H0**   **P06 –L2H4L2H2L2H0**
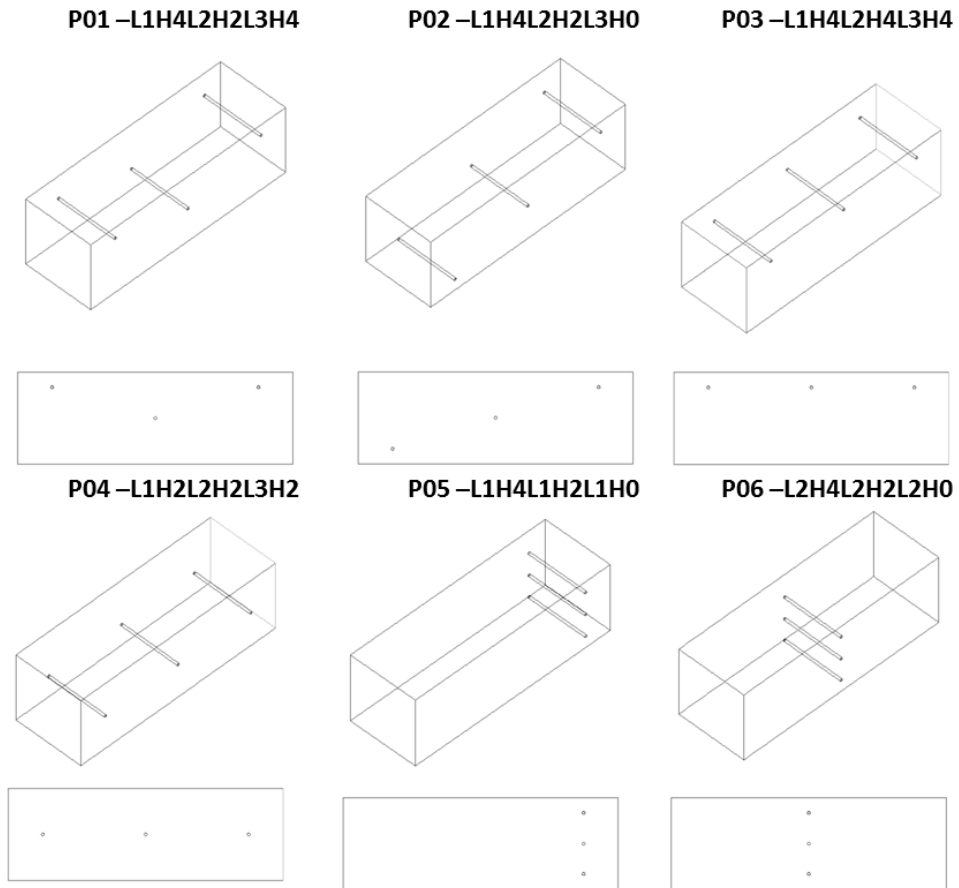
Figure 7.2 Multi-lamp configurations schematics.

7.2.1 Irradiation, velocity and turbulence

Each system had its own irradiation, velocity and turbulence profile, which in turn caused every system to have its very own UV dose distribution (which will be discussed in section 7.2.2) and sterilisation performance.
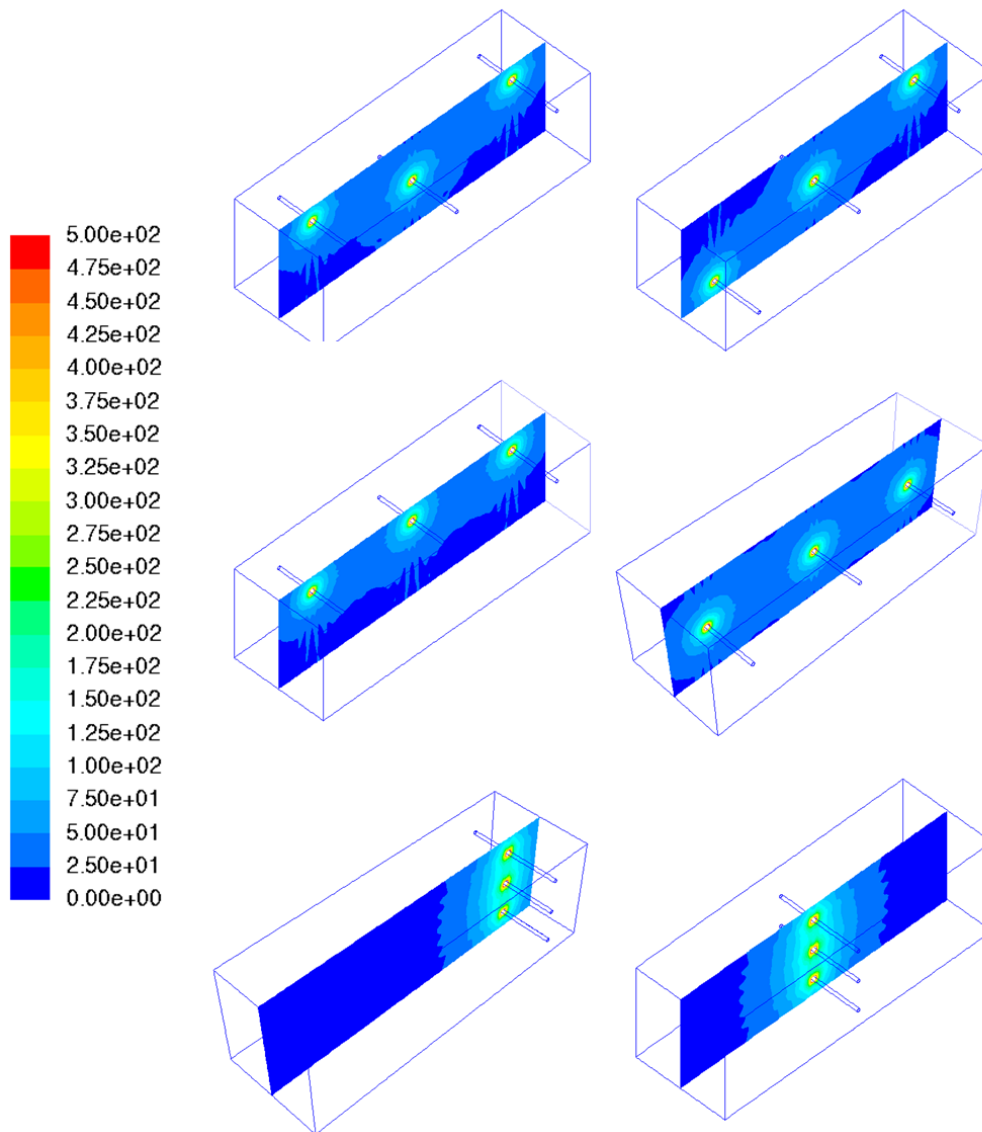
Figure 7.3 Multi-lamp systems irradiation profile in W.m^{-2}. P01 (top left), P02 (top right), P03 (centre left), P04 (centre right), P05 (bottom left) and P06 (bottom right).

The irradiation profiles in Figure 7.3 were filtered to show a maximum value of 500 W.m^{-2}, this is a representative value and its purpose is just to show a direct comparison between designs. From the irradiation profiles we can see that lamps located at the three different heights (H4, H2 and H0) as in the case of P02, P05 and P06 managed to cover the full area of the duct with an irradiation greater than 100 W.m^{-2}. In the system P05 (bottom left), it can be seen how the irradiation did not develop completely as the lamps are located at the beginning of the duct. The system P03 shows an irradiation profile with a low irradiation (less than 25 W.m^{-2}) at the bottom of the duct.
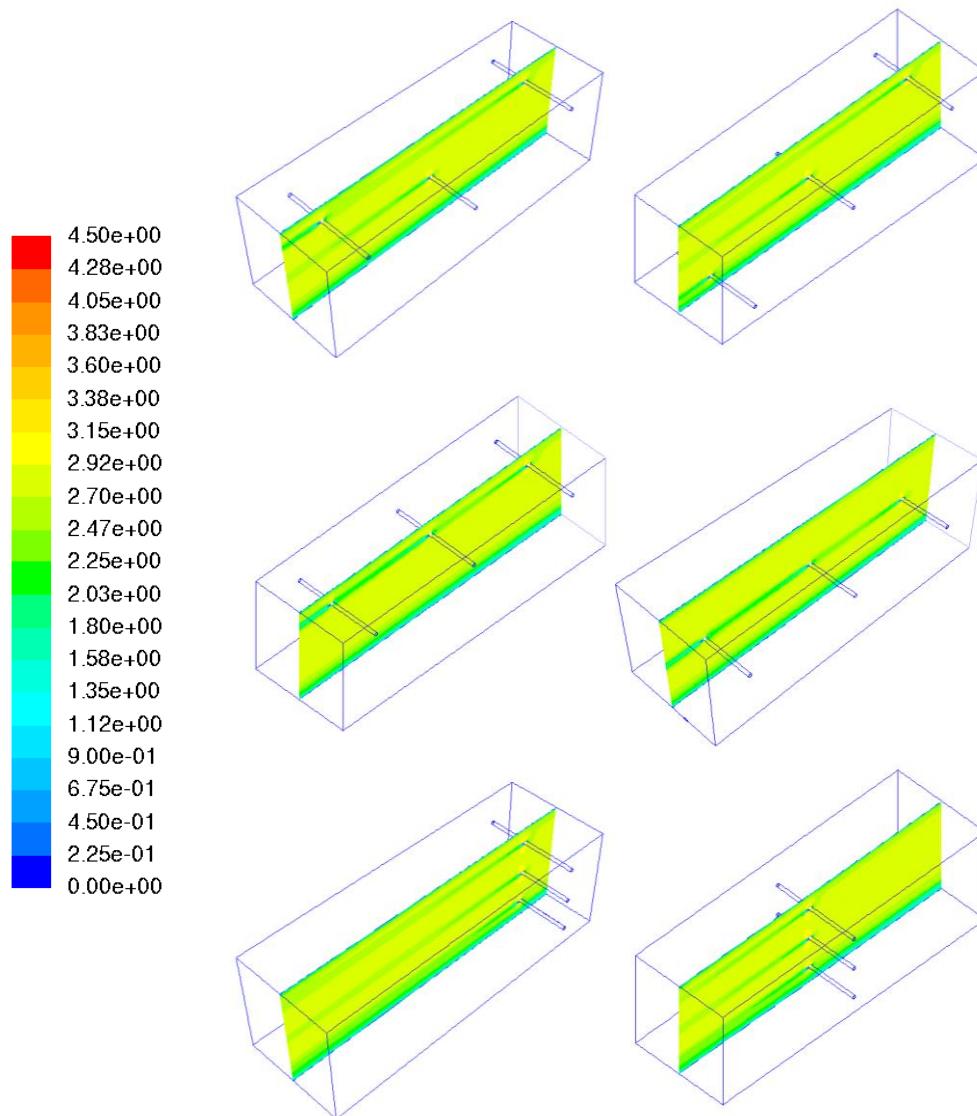
Figure 7.4 Multi-lamp systems velocity profile in m.s⁻¹. P01 (top left), P02 (top right), P03 (centre left), P04 (centre right), P05 (bottom left) and P06 (bottom right).

The velocity profile of the different systems, as shown in Figure 7.4, was not significantly affected by lamp position apart from the flow stream developed just after the lamp; however the average velocity remained the same between designs.
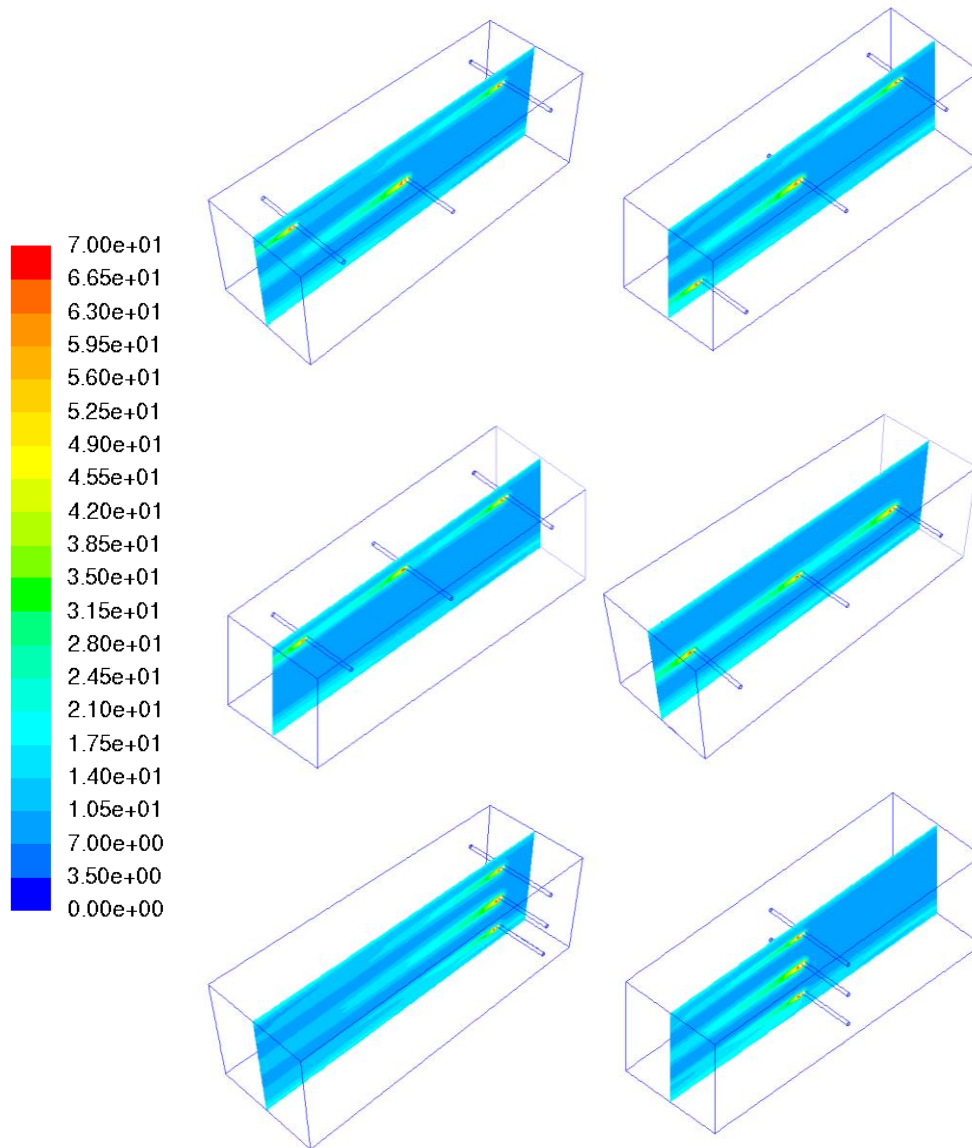
Figure 7.5 Multi-lamp systems turbulence intensity profile in percentage of turbulence. P01 (top left), P02 (top right), P03 (centre left), P04 (centre right), P05 (bottom left) and P06 (bottom right).

Again, the turbulence profile of the system, as seen in Figure 7.5 was not significantly affected by lamp position apart from the volume right after the UV lamp. The average turbulence intensity of the system remained constant between designs.

The irradiation profile appears to bear more impact on sterilisation performance than the velocity or turbulence profile of the system. The following section will explore the results on performance and dose distribution.

7.2.2 UV dose distribution.

The UV dose distributions for the six multi-lamp configurations are shown in Figure 7.6. Depending on lamp configuration, each system has its very own UV dose distribution spectrum.
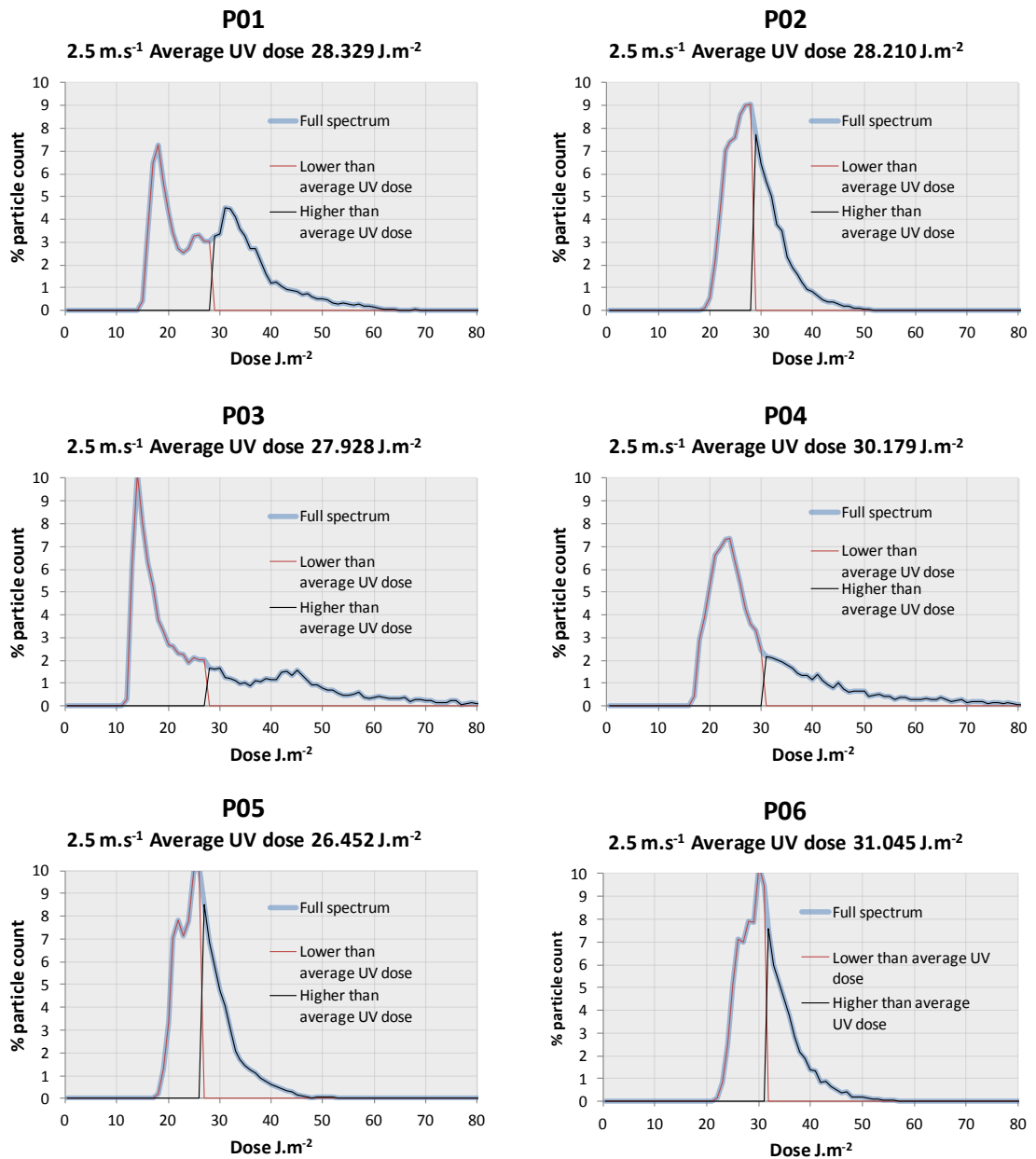
Figure 7.6 UV dose distribution for the different multi-lamp configurations.

From results it was found that lamp configuration affected the UV dose distribution of the system. For instance, it can be seen how having a configuration with a lamp at the centre and two lamps at the top, such as case P01, leads to a double peak pattern in the UV dose distribution. This means, that the dose distribution inside the duct is divided into two areas, an area where particles receive close to 20 $J.m^{-2}$ and an area where particles receive around 35 $J.m^{-2}$; in total the system has an average UV dose of 28.329 $J.m^{-2}$.

In the next case, P02, where the lamps are located at top, centre and bottom of the duct, it can be seen that the UV dose distribution has a sharp peak with the average UV dose almost at the centre of the peak. This means that most particles receive the same UV dose and the average UV dose of the system is calculated to be 28.210 $J.m^{-2}$.

For case P03, a system with three lamps located on the top row, the UV dose distribution shows a single tall peak, which is formed by all the particles passing under the lamps. Nevertheless the UV dose distribution gets widened by a small number of particles passing at the top of the duct were the three lamps are located and receiving high UV doses. The average UV dose of the P03 system is of 27.928 $J.m^{-2}$, the second lowest of all the configurations.

In case P04 where the three lamps are positioned in a centre row, this configuration showed a relatively higher average UV dose at 30.179 $J.m^{-2}$. The particle dose distribution is similar to that of case P03, with a single tall peak and a wide distribution. The key difference is that the distribution has been shifted to higher UV doses, which is the effect of having the lamps located at the centre of the duct in contrast to the lamps located at the top row. The tall peak on the dose distribution is formed by the particles passing at the top and bottom of the duct where no lamps are present.

The last two multi-lamp configurations presented a row of lamps across the height of the duct. For system P05, with the three lamps at L1 (beginning of the duct), the results again showed a sharp tall peak, the sign of an even irradiation profile. Nevertheless, this set-up showed the lowest of all average UV dose at 26.452 $J.m^{-2}$.

Finally configuration P06, with all lamps at the centre of the duct showed the highest average UV dose at 31.045 $J.m^{-2}$, while keeping an even irradiation profile as indicated by the sharp peak on the UV dose distribution. The dose distribution of an evenly irradiated system tends to show a single sharp tall peak and a narrow spread.

The standard deviation of the dose distribution (UV std) appears to be a good indicator of the quality of the distribution of irradiation; the lower the standard deviation of the dose distribution, the more even the irradiation distribution within the duct. A low UV dose standard deviation means that difference between the particle receiving the lowest and the highest average UV dose is low, and thus most particles are receiving a similar amount of UV irradiation. Table 7-2 shows how systems P02, P05 and P06, which are the systems with the three lamps located at top, centre and bottom of the duct, giving a more even irradiation coverage, show the lowest standard deviation on the UV dose distribution. In the opposite case, the system P03, which had the three lamps at the top of the duct, had the biggest spread, showing the highest standard deviation.

Table 7-2 Standard deviation of the UV dose distribution for the multi-lamp systems.

Configuration	Average UV dose J.m^{-2}	UV std J.m^{-2}	UV std/Average UV dose
P01-L1H4L2H2L3H4	28.33	10.06	35%
P02-L1H4L2H2L3H0	28.21	5.39	19%
P03-L1H4L2H4L3H4	27.91	16.32	58%
P04-L1H2L2H2L3H2	30.18	12.60	41%
P05-L1H4L1H2L1H0	26.45	5.37	20%
P06-L2H4L2H2L2H0	31.05	5.45	17%

The average UV dose and the UV dose standard deviation of a system and its sterilisation performance are directly affected by the irradiation profile which in turn is defined by lamp position. An even irradiation profile would be expected to perform better, although as results show, this depends on the microorganism susceptibilities.

It is important to clarify the difference between average UV dose and sterilisation performance. The average UV dose is the mean UV dose received by all particles passing through the system. While the sterilisation performance is related to the rate at which a microorganisms decays while passing through the system. In such manner the average UV dose of a system depends on the lamp configuration and UV power, while the sterilisation performance depends on lamp configuration, UV power and microorganisms susceptibility to UV irradiation.

Put it another manner, the microorganisms' susceptibility refers to the amount of UVC irradiation the microorganisms can absorb before it is killed (or sterilised). If the microorganism is irradiated with more energy than what it can absorb, that over irradiated energy will be wasted as it will not have any further sterilisation effect i.e. a microorganisms cannot be killed (or sterilised) more than to the 100%.

From the six multi-lamp systems, case P06 with the three lamps distributed across the height and located at the centre of the duct showed the highest average UV dose, followed by P04 with the three lamps distributed at the centre row over the length of the duct, then P01 with one lamp at the centre in L2, and two lamps at the top in L1 and L3. Next in performance was system P02 with one lamp at the top one at the centre and one at the bottom, followed by P03 with the three lamps at the top row, and in last system P05 with the three lamps at the beginning of the duct, the low performance of the P05 can be related to the under developed irradiation profile shown in Figure 7.3.

All the systems had the same number of lamps and the same UV power, nevertheless they resulted in different average UV dose, and this is due to the CFD calculations implicitly accounting for irradiation distribution. The particles injected within the system received

different levels of UV dose, that in turn were a reflection of the irradiation distribution and particles trajectories within the duct. CFD modeling with the use of particle tracking is capable to measure the standard deviation of the UV dose distribution, which can be used as a direct parameter for the measuring of quality of irradiation distribution. Finite integral models such as the MPSS (Bolton, 2000), LSS (Liu et al., 2007)or the view factor (Kowalski et al., 2001) for the calculation of the average UV dose of a system are not capable of capturing this information as they average the UV irradiation within the system and do not account for particles trajectories.

Thus, in specific cases, a system with a lower average UV dose but with a more evenly distributed UV irradiation would perform better than a system of higher average UV dose but with a badly distributed irradiation profile. The average UV dose of a system accounts for the total UV power within, yet it is incapable of recognising how the irradiation is distributed as it averages the system as a whole.

The impact of the UVC irradiation distribution, which is the area of the duct covered with UV-C light and depends on the lamp configuration, can be seen on the resulting UV dose of particles at the end of the duct.
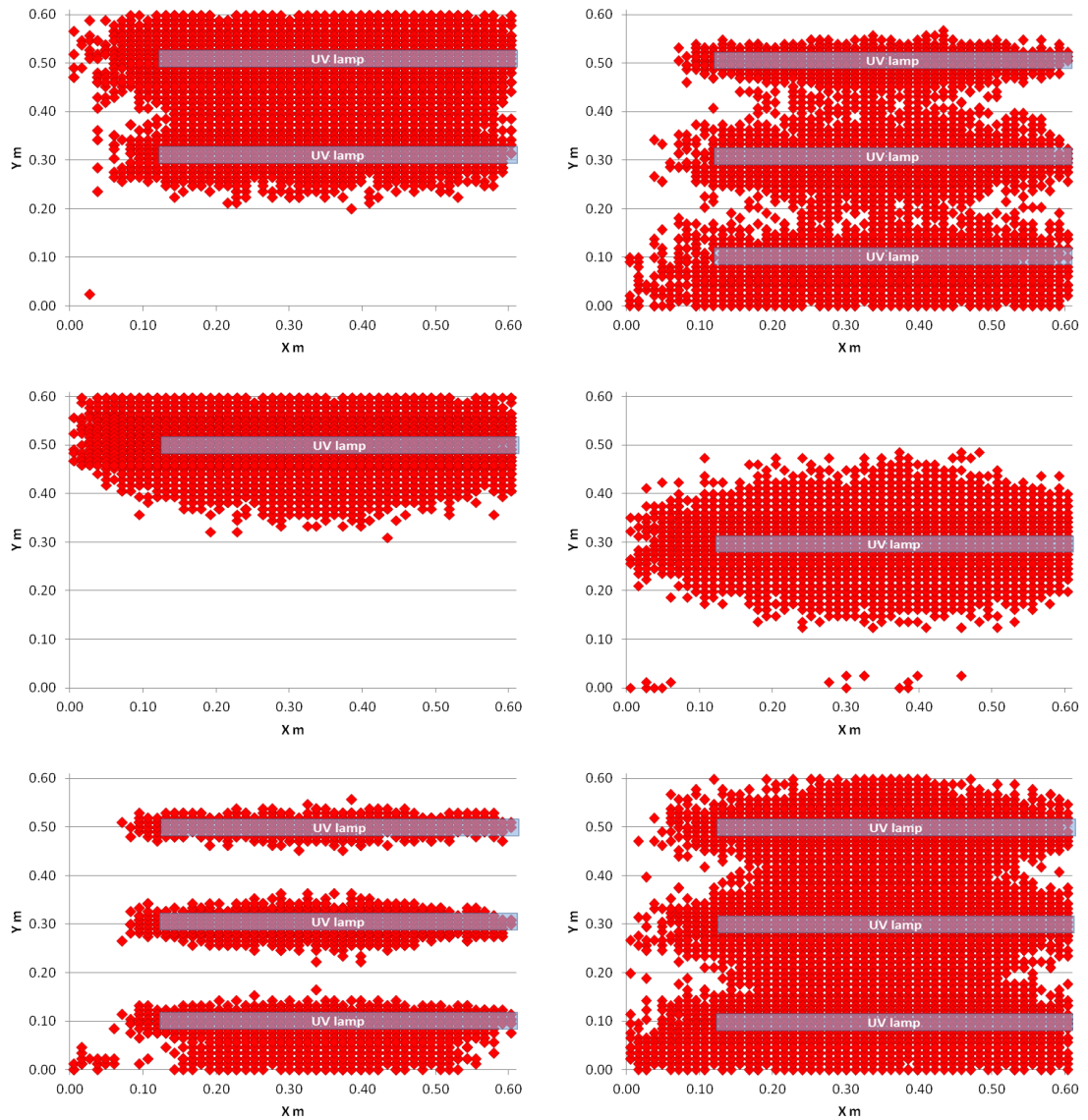
Figure 7.7 Particles receiving 28 J.m⁻² or more. P01 (top Left), P02 (top right), P03 (centre left), P04 (centre right), P05 (bottom left) and P06 (bottom right).

Figure 7.7 shows the particles that received 28 J.m⁻² or more at the end of the duct. The case P01 with lamps located at the top and centre row show an area of resulting UV dose focused around the lamps, leaving the lower part of the duct uncovered, this is what creates the double peak previously mentioned on the UV dose distribution, the low UV dose peak correspond to the bottom area of the duct while the high UV dose peak corresponds to the top area of the duct. The P02 shows a more even UV dose profile. This is due to the lamps being distributed top, centre and bottom of the duct. This even UV dose across the area of the duct is reflected on a single sharp peak with a narrow spread on the UV dose profile, meaning that most particles receive the same levels of UV dose. In the case of the P03 multi-lamp system, the UV dose concentrates at the top of the duct, leaving most of the duct uncovered, thus creating a single sharp peak on the UV dose distribution as most particles, passing below the UV lamps, receive similar amounts of UV dose, nevertheless this peak is far from the average UV dose of the

~ 200 ~

system, which has been skewed due to the amount of particles passing in at the top area of the duct, close to the three lamps, receiving high UVC irradiation. The P04 multi-lamp system with the three lamps at the centre row shows an area of UV dose concentrated on the centre of the duct. This creates a single sharp peak similar to the one of the P03 (with lamps located at the top) in the UV dose distribution of the system, however in this case the peak is shifted slightly to the right, showing higher UV doses. This system also presents a broad UV dose distribution, created by having the UV irradiation concentrated in a single area at the centre of the duct. The configurations P05 with the three lamps evenly distributed across the height of the duct located at the beginning of it, showed a small area of coverage in the area close to the lamps. As we gathered from the average UV dose results, this system showed the lowest average UV dose as well as the smallest area of coverage; this appears to be the result of having the lamps located at the beginning of the duct. Finally the multi-lamp set-up used on P06, with the three lamps located across the height and in the centre of the duct showed the biggest area coverage as well as the highest average UV dose.

The UV irradiation profile has a direct impact on the performance of the system, and its effects will be analysed in the following sections.

7.2.3 Average UV-dose and Sterilisation performance.

Table 7-3 exemplifies how at high susceptibility values, a more evenly distributed UV irradiation brings better performance than a system with higher average UV dose but worse irradiation distribution. For example system P02 with lamps at top, centre and bottom and UV dose standard deviation of 5.39 $J.m^{-2}$ performs better than system P04 with all lamps located at the centre row and with a UV dose standard deviation of 12.60 $J.m^{-2}$ at high microorganism susceptibilities. However at low susceptibilities, of 0.05 $m^2.J^{-1}$ or less, similar to those shown by spores and fungi (Fletcher et al., 2003), the system with the highest average UV dose, in this case P04, performs better as highly resistant microorganisms are capable of absorbing more UVC irradiation before being sterilised, thus avoiding any waste of energy for the system.

Table 7-3 Multi-susceptibility performance of the different systems at various susceptibility ranges.

Configuration	%kill rate for susceptibility ranges in $m^2.J^{-1}$					
	0.014 – 0.75	0.014 – 0.50	0.014 – 0.30	0.014 – 0.10	0.014 – 0.05	0.014 – 0.02
P01	96.22	94.24	90.25	72.31	55.97	37.28
P02	96.60	94.88	91.28	73.98	57.14	37.77
P03	95.23	92.78	87.88	68.44	52.86	35.57
P04	96.49	94.64	90.93	73.72	57.62	38.82
P05	96.26	94.39	90.40	72.08	54.92	35.90
P06	97.06	95.51	92.42	76.74	60.54	40.68

The reason for the P02 performing better than the P04 at high susceptibility values is due to an over performance effect, where the microorganisms receive UV doses higher than those required for high levels of sterilisation. The irradiation profile leads to kill rates around 99.9%, concentrated in a small area, whereas other areas of the duct, which have not been evenly irradiated, receive lower UVC doses that produce low kill rates, thus reducing the performance of the system overall.

To exemplify this, Figure 7.8 shows a comparison of the sterilisation levels for systems P02 and P04, first showing the areas were a microorganism representative of *E. coli* at 50% RH with a relatively mild UVC susceptibility ranging from 0.160 – 0.182 $m^2.J^{-1}$ are sterilised to 99.9% and then showing areas where the sterilisation levels are of 99% and over.
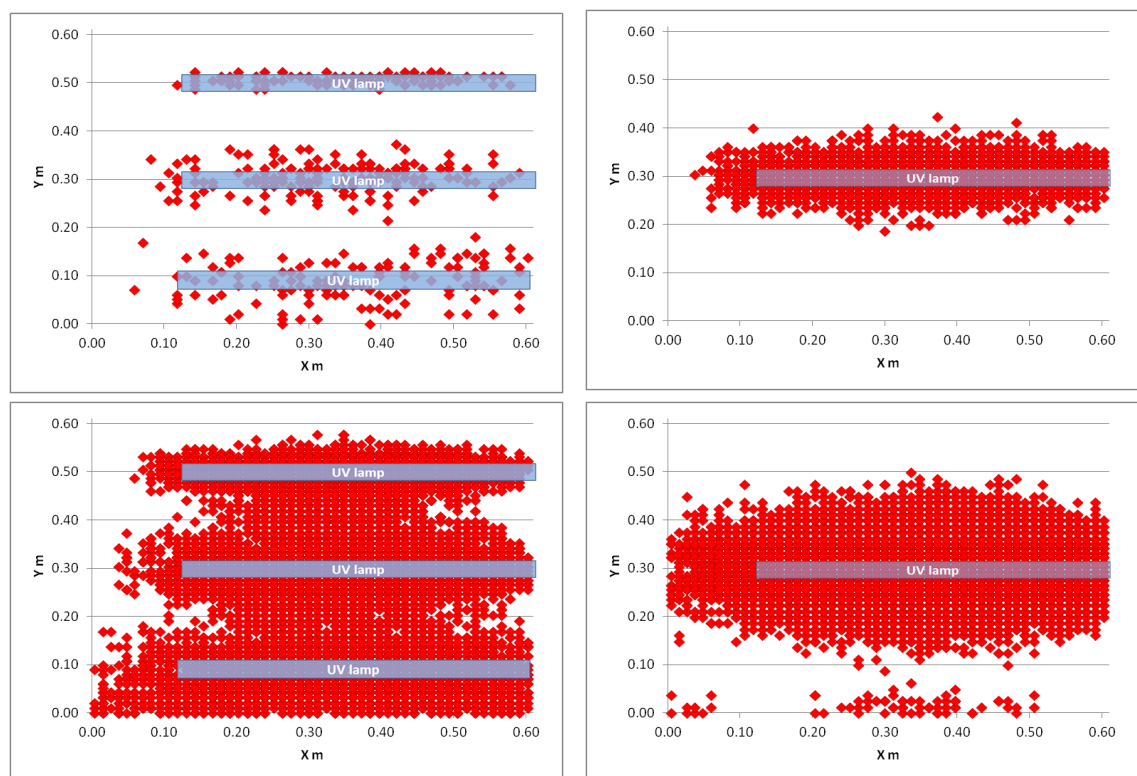
Figure 7.8 *E. coli* particles receiving over 99.9% sterilisation for the system P02 (top left) and P04 (top right) and *E. coli* particles receiving over 99% sterilisation levels for the P02 (bottom left) and the P04 (bottom right).

The system P04, which showed a higher average UV dose than system P02, managed to sterilise up to 16% of the microorganism population to a 99.9% while P02 only managed to give such sterilisation level to 2.98% of the microorganism population. As can be seen on the top row of Figure 7.8, system P04 concentrated the sterilisation performance at the centre of the duct, where the three lamps were located. However, when we look at the microorganism population that managed to be sterilised to the 99% the results are significantly different. Now system P02 managed to sterilise over 53% of the microorganism population to 99%, while system P04

reached 99% kill for 43% of the microorganism population. This is the effect of over performance. System P02 concentrated the irradiation in a small area, microorganism passing through the area managed to get high levels of sterilisation. However, areas further away from the lamp remained less covered, and in the case of system P04, where the irradiation was better distributed across the duct, microorganism received a more even UV dose overall, and managed to cover a bigger area although at a lower sterilisation rate.

Table 7-4 Multi-lamp configuration performance, UV dose standard deviation and %kill rate against specific microorganisms.

Microorganism	K $m^2.J^{-1}$ Band width	Shoulder n width	P01	P02	P03	P04	P05	P06
			UV std $J.m^{-2}$					
			10.06	5.39	16.32	12.60	5.37	5.45
			% Kill rate					
B. Subtillis	0.014 - 0.020	1-3	17.15	17.04	17.00	18.56	15.50	19.20
M. tuberculosis	0.029 - 0.056	1-4	24.71	24.21	24.02	26.82	21.36	31.57
E. coli	0.056 - 0.091	-	84.01	86.08	79.51	85.30	84.24	88.61
M. bovis BCG	0.170 - 0.360	-	99.45	99.76	98.65	99.62	99.67	99.87
P. aeruginosa	0.412 - 0.530	-	99.99	100	99.94	100	100	100

The over performance effect is reduced on highly resistant microorganism such as *B. subtillis* spores (0.014 $m^2.J^{-1}$ – 0.020 $m^2.J^{-1}$) and *M. tuberculosis* (0.029 $m^2.J^{-1}$ – 0.056 $m^2.J^{-1}$ and shoulder of 4). In these cases the system with the highest average UV dose will indeed perform better. However when dealing with more susceptible microorganisms e.g. *P. aeruginosa* (0.412 $m^2.J^{-1}$ – 0.530 $m^2.J^{-1}$) or *S. marcescens* (0.430 $m^2.J^{-1}$ – 0.920 $m^2.J^{-1}$) the system with a better UV dose distribution, e.g. P02, will perform better (as seen in Table 7-4). There appears to be a threshold of relating to the UV susceptibility of the microorganism and when a system with the highest average UV dose or the lowest UV dose standard deviation (better UV irradiation profile) performs better, however at the moment the parameters to define such threshold are not know, and might be a case for further research.

Although in most cases there were only marginal differences in performance, the benefits of an evenly distributed irradiation and/or lamps located at the centre of the duct, either in a single row across the length (P04), or across the height of the duct (P06) were explained. Such marginal differences in performance would not have a considerable impact on a real life installation where the parameters of operation will be under constant variability e.g. airflow volumes, lamp UV power and/or performance. Nevertheless, it was shown that the best performance was achieved when lamps provided a more evenly distributed irradiation. Moreover, the standard deviation of the UV dose distribution appears to be a reliable parameter to measure the quality of the irradiation distribution.

7.3 Performance constant and the impact of airflow rate.

The performance of a system can be measured in at least three different ways. A biodosimetry study, involves the use of an enclosed lab facility where an in-duct UV system is installed in a ventilation system and microorganisms are injected with the purpose of measuring kill rates. This in turn can be transformed into average UV dose of the system using suitable assumptions about microorganism susceptibility, as shown in Chapter 5 with the EPA series (EPA, 2006a, EPA, 2006b, EPA, 2006c, VanOsdell and Foarde, 2002). The second option is to calculate mathematically the average UV dose of the system using knowledge about the UV lamps. This can be done by finite integrals as in the case of the MPSS (Bolton, 2000), LSS (Liu et al., 2007) or the View factor (Kowalski et al., 2001) as explained in Chapter 4. The third option is by finite integral calculation with the use of CFD models and the injection of scalars to track particle trajectories and the received UV dose (Gilkeson and Noakes, 2013, Ho, 2009b, Ho, 2009a) as applied in Chapter 5 and Chapter 6 of this thesis. All of these tools require complex modelling or are expensive or resource intensive if a series of measurements at various airflows are carried with the purpose of mapping the performance of a system.

It is known that the performance of an in-duct UV system is in direct relation with the airflow. Therefore if we are capable of quantifying such a relationship, it would be possible to map the performance of an in-duct UV air sterilisation system based on a single measurement point, i.e. by knowing the average UV dose of a system at a given airflow.

With the purpose of identifying and quantifying the relationship between the average UV dose and the airflow of an in-duct UV system, a series of CFD models were run at various air velocities (airflow flow rates $m^3.s^{-1}$) of 0.5 $m.s^{-1}$ (0.19 $m^3.s^{-1}$), 1.0 $m.s^{-1}$ (0.37 $m^3.s^{-1}$), 2.0 $m.s^{-1}$ (0.74 $m^3.s^{-1}$), 2.5 $m.s^{-1}$ (0.93 $m^3.s^{-1}$), 3.0 $m.s^{-1}$ (1.12 $m^3.s^{-1}$) and 4.0 $m.s^{-1}$ (1.49 $m^3.s^{-1}$). The models were run using the Discrete Ordinates method (DO) to model UV irradiation, and the K-ε turbulence model to solve the flow (as described in Chapter 5), the average UV dose of the system was calculated by particle injection following the methodology explained in Chapter 5. In total 8 systems were run for the configurations listed in Table 7-5. Diagrams of the various systems can be found in Appendix A.

Table 7-5 CFD model parameters.

Spec	600/R-06/050	600/R-06/051	600/R-06/055	L2H2 parallel	P01	P02	P03	P04
Number of lamps	1	4	8	1	3	3	3	3
Lamp power watts	58	25	60	58	58	58	58	58
Lamp UVC power watts	19	8.5	18	19	19	19	19	19
Total system power	58	100	480	58	174	174	174	174
Total system UV power	19	34	144	19	57	57	57	57
Lamp length cm	53.3	53.82	61	53.3	53.3	53.3	53.3	53.3
Lamp diameter	1.9 cm T6	1.9 cm T6	1.9 cm T6	1.9 cm T6	1.9 cm T6	1.9 cm T6	1.9 cm T6	1.9 cm T6
Duct size	61 cm x 61 cm	61 cm x 61 cm	61 cm x 61 cm	61 cm x 61 cm	61 cm x 61 cm	61 cm x 61 cm	61 cm x 61 cm	61 cm x 61 cm
Duct length	7.83 m	7.83 m	7.83 m	7.83 m	7.83 m	7.83 m	7.83 m	7.83 m
Duct wall Emissivity	0.85	0.85	0.85	0.85	0.85	0.85	0.85	0.85
Duct wall Reflectivity	15%	15%	15%	15%	15%	15%	15%	15%
Duct wall refractive index	1	1	1	1	1	1	1	1

7.3.1 Average UV dose and particle residence time.

Each system showed its very own residence time-UV dose "blueprint". This can be seen in the figures below.
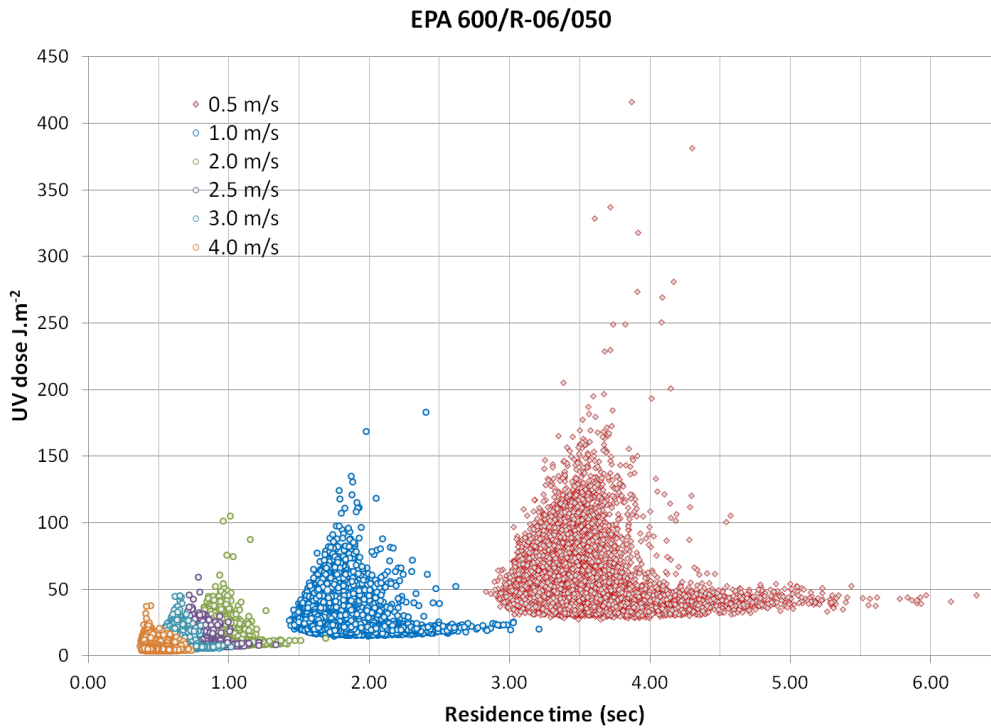
Figure 7.9 Particle residence time and UV dose for EPA 600/R-06/050 at six airflow rates.

Figure 7.9 shows the particles received UV dose and residence time distribution for the EPA 600/R-06/050, it can be seen how the particles with the longest residence time ranked among the particles with the lowest received UV dose. This is due to the fact that the longest residence time within the system was achieved by particles passing close to the walls, hence far away from the source of UV irradiation. As the air velocity increased, the magnitude of the UV dose received by each particle changed. Nevertheless the distribution remained relatively constant.
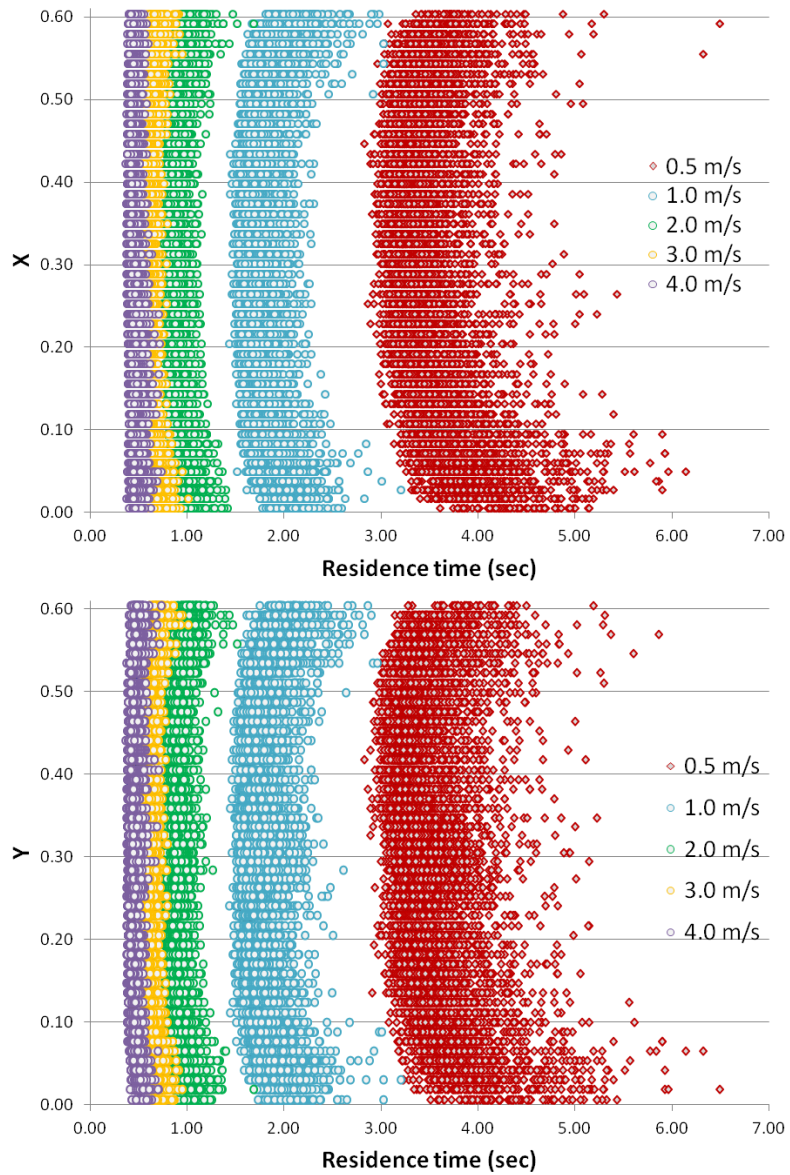
Figure 7.10 Particle residence time and position at the outlet for the EPA 600/R-06/050.

Figure 7.10 shows the areas in the X and Y position of particles at the outlet and their residence time for the EPA 600/R-06/050. It can be seen how lamps at the walls (0.00 and 0.61), in both X and Y section of the duct, shows the longest residence time. This is the effect of a fully developed flow, where the velocity concentrates at the centre of the duct.
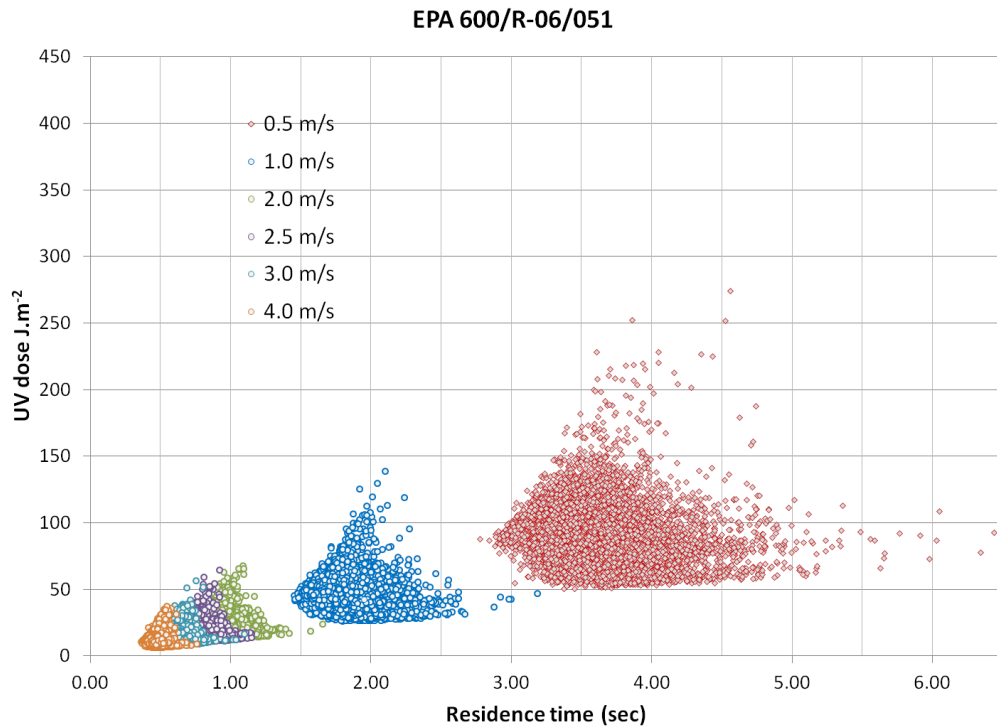
Figure 7.11 Particle residence time and UV dose for EPA 600/R-06/051 at six airflow rates.

The EPA 600/R-06/055 (Figure 7.11) behaved closely similar to the single lamp system, with most particles sharing similar UV dose and residence time. Again, as the velocity increased the magnitude of UV dose received by particle changed, however the distribution remains constant.
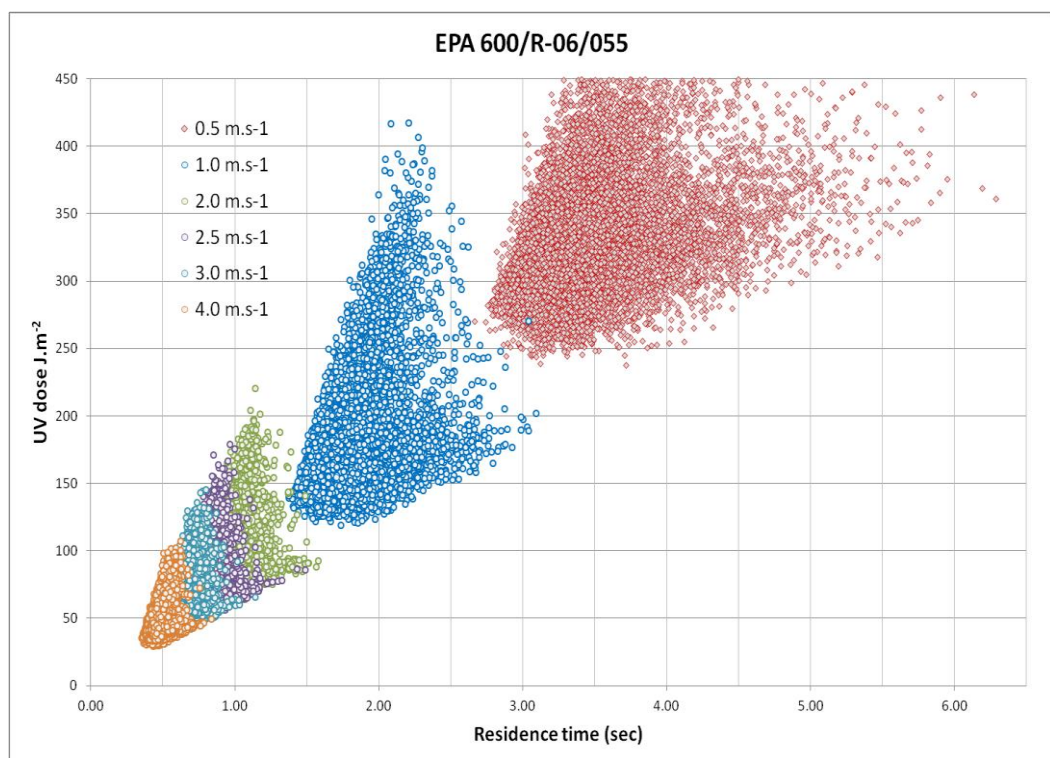
Figure 7.12 Particle residence time and UV dose for EPA 600/R-06/055 at six airflow rates.

The EPA 600/R-06/055 (Figure 7.12) showed a very distinctive distribution, in this case the particles with the longest residence time managed to rank considerably high on the UV dose received. This could be due to the lamps being located at the walls (top and bottom), as seen by the air velocity profiles (section 7.2.1), close to the walls is where particles show the lowest velocity. By now it is evident that independently of the lamp configuration, the distribution of particle residence time and average UV dose remains constant although at different magnitudes as the air velocity changes within the system.
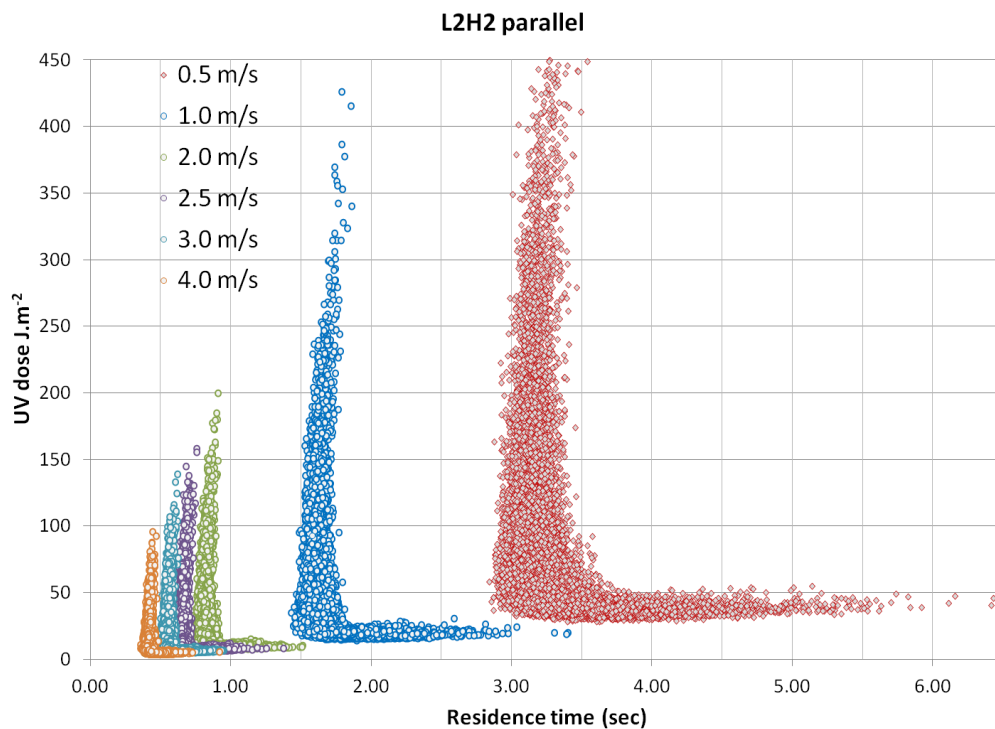
Figure 7.13 Particle residence time and UV dose for L2H2 parallel at six airflow rates.

Figure 7.13 shows how positioning the lamp parallel to the airflow resulted in a very distinctive UV dose and residence time distribution forming an L shape. The residence time of the particles did not affect much the UV dose they received. The particles with the shortest and the particles with the longest residence time received a very similar UV dose. A distinctive aspect of this distribution is the difference in magnitude between the particles that received the lowest and the highest UV dose. Meaning that within the system there are areas which concentrate high UVC irradiation as well as areas with considerably low UVC irradiation.
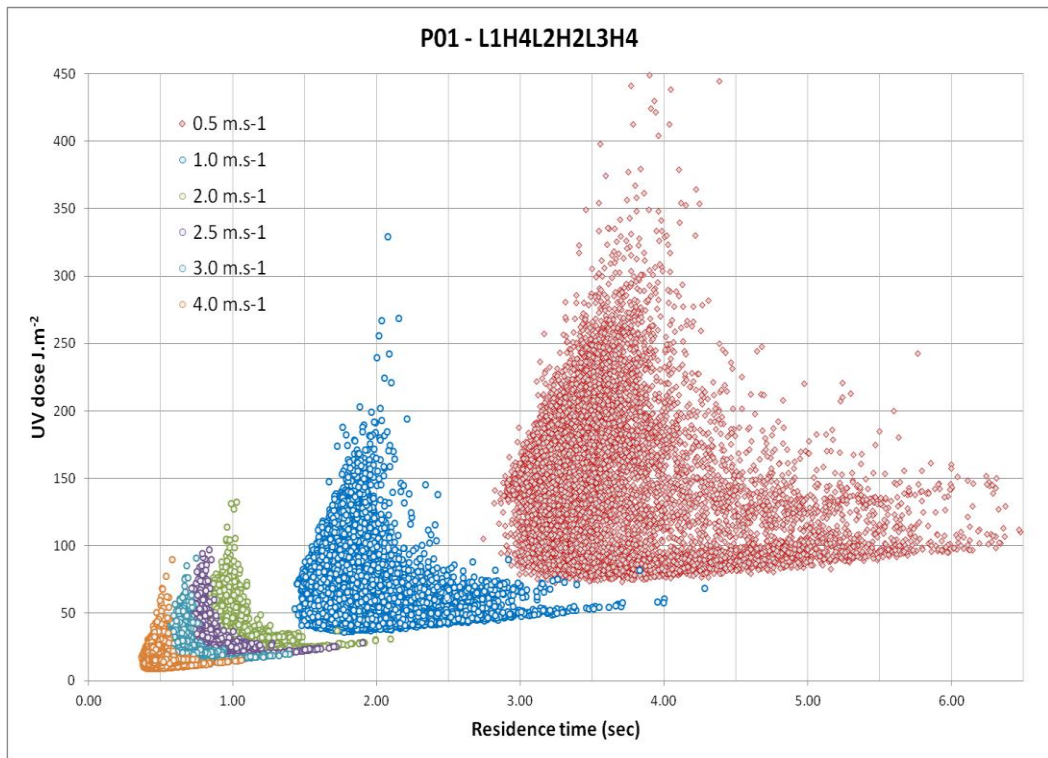
Figure 7.14 Particle residence time and UV dose for system P01 at six airflow rates.

The system P01, shown in Figure 7.14, which had two lamps at the top row, and one lamp at the centre shows a distribution similar to that of the EPA 600/R-06/050 and EPA 600/R-06-051.
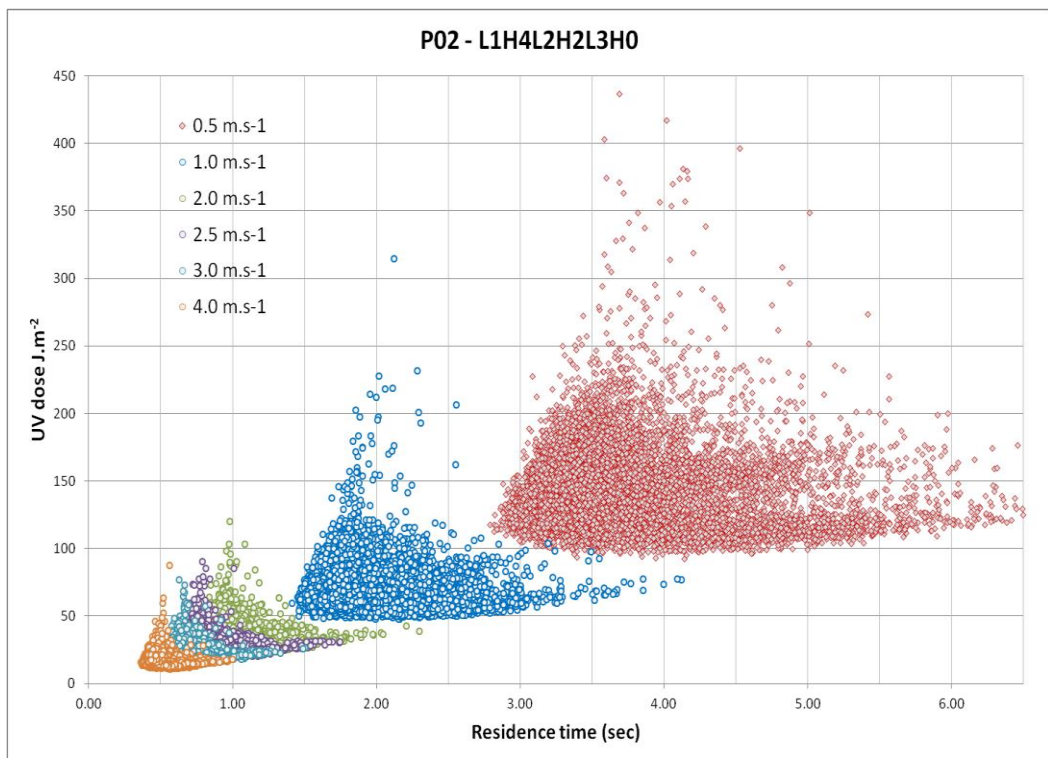
Figure 7.15 Particle residence time and UV dose for system P02 at six airflow rates.

Figure 7.15 of the systems P02, with the lamps located top, centre and bottom, showed a slightly more compact residence time and UV dose distribution blueprint. This system saw the lowest difference in magnitude between the particles receiving the lowest and the highest UV dose, the opposite case of the L2H2 parallel system. This means that most of the system was covered with a similar UVC irradiation.
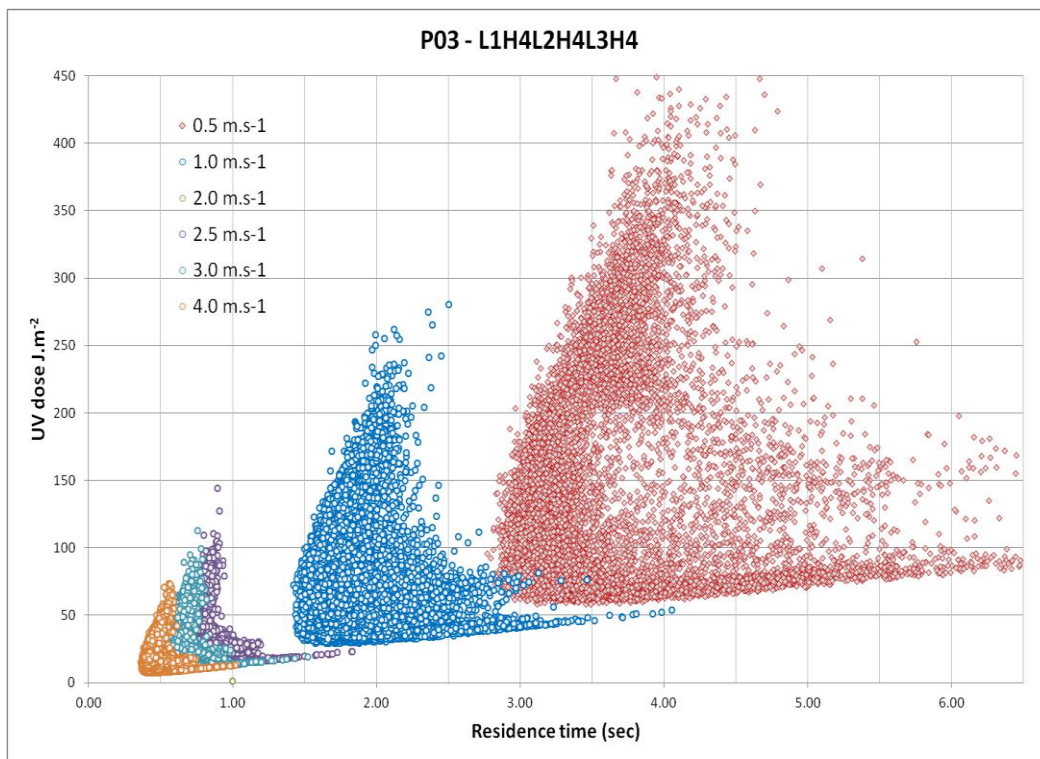
Figure 7.16 Particle residence time and UV dose for system P03 at six airflow rates.

The system P03, as shown in Figure 7.16, with the three lamps at the top, developed an L type particle UV dose- residence time distribution. Again, this is given by having the irradiation concentrating in a single area within the duct, while other areas remain uncovered.
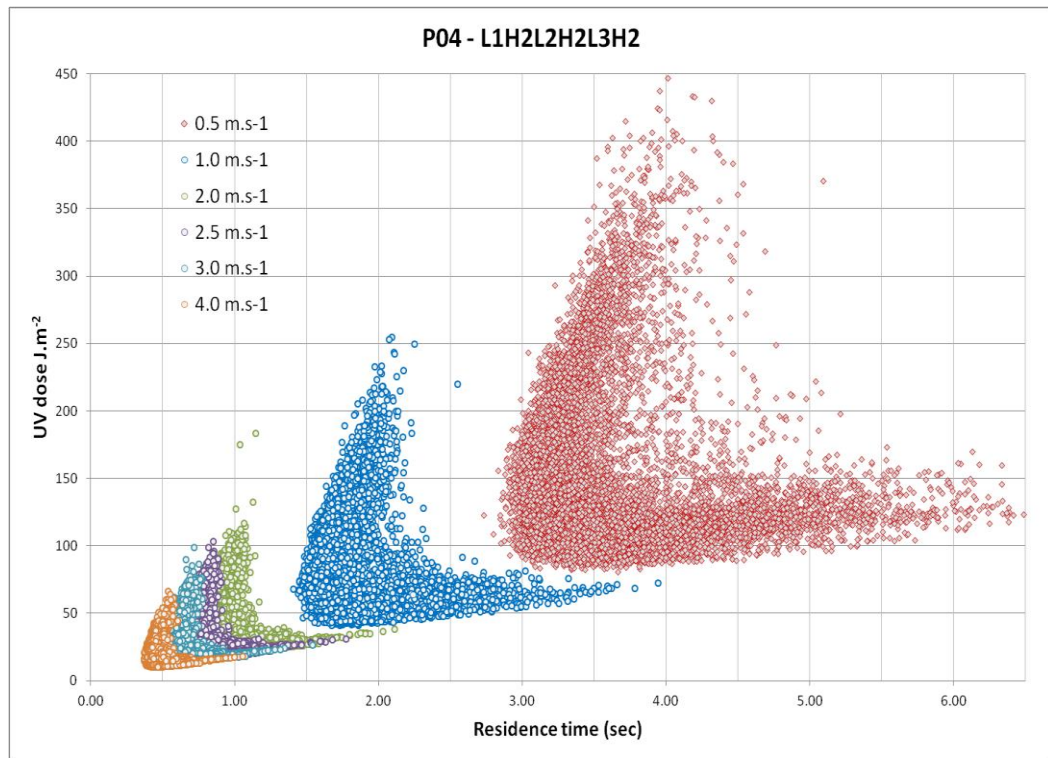
Figure 7.17 Particle residence time and UV dose for system P04 at six airflow rates.

Finally, Figure 7.17 shows the system P04 with lamps located in a row at the centre of the duct, again shows the L shape distribution, this is a distinctive distribution of an irradiation concentrating in a single area within the duct. A characteristic aspect of this distribution is the difference in received UV dose between the particle with the lowest and the highest received UV dose, the bigger the difference the worst the irradiation distribution of the system.

Most of the times, the particles with the highest UV dose settled within the average residence time for the system. Moreover, in most cases particles with the longest residence time ranked among the particles with the lowest UV dose. UV irradiation distribution is important to achieve higher average UV dose within the systems. Even if particles spend longer times within the system, if they do it in areas of low irradiation, their UV dose will remain low.

As it was shown airflow rate and hence air velocity at which a system operates directly affects the average UV dose of the system. However, independently of lamp configuration, airflow rates did not affect the particle trajectories within the system. Particles followed the same trajectories; just they did it at different speeds.

The distribution of the UV dose received by particles in relation to its residence time remained constant as the air flow rates changed; indeed the magnitude of the values were greater as the flow rates decreases, nevertheless the distribution remained constant.

7.3.2 Average UV dose and airflow.

The performance of the eight systems described above, run at five different air velocities, is shown in the Figure 7.18.
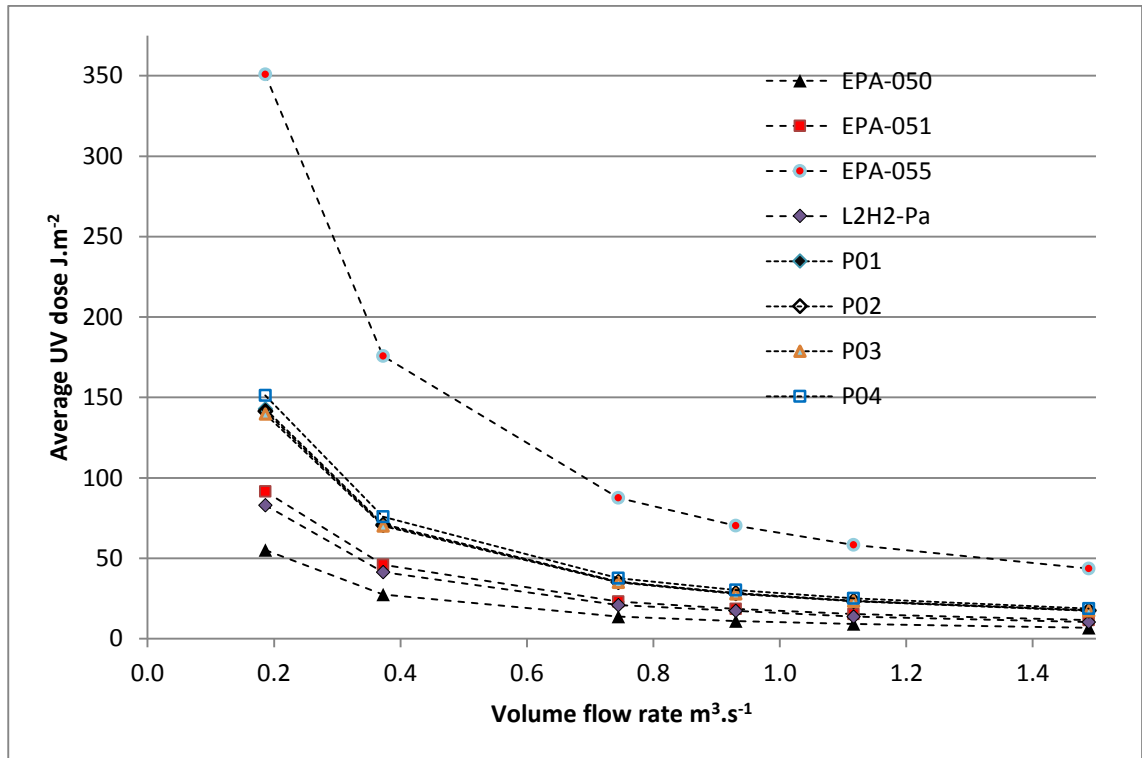
Figure 7.18 Average UV dose volume flow rate.

It can be seen that all the systems followed similar performance curves over the range of air flow rates. As the particle trajectories are not affected by airflow, and the average UV dose of the system is in direct relation with the airflow, it is possible to calculate the performance of a system over a range of airflows from a single data point by identifying the performance curve equation.

7.3.3 The introduction of the performance constant.

From the results shown through the CFD modelling of various systems at a range of air flow rates (Figure 7.18) it was found that the performance of the system can be described by a power law equation of the form:

$$D = RQ^{-\gamma}$$

Equation 7-1

Where D is the average UV dose of the system ($J.m^{-2}$), R is a performance constant expressed in W.m, Q is the air flow rate of the system ($m^3.s^{-1}$) and a constant γ is the exponential.

Table 7-6 Average UV dose and Performance constant R and γ for each systems.

System	Duct Area	Velocity m.s^{-1}	Air flow rate m^3.s^{-1}	Average UV dose J.m^{-2}	Performance constant R (W.m)	Exponential constant γ
EPA 600/R-06/050	0.3721	0.50	0.19	55.23	10.23	1.003
		1.00	0.37	27.53		
		2.00	0.74	13.79		
		2.50	0.93	10.96		
		3.00	1.12	9.15		
		4.00	1.49	6.87		
EPA 600/R-06/051	0.3721	0.50	0.19	91.52	17.20	0.995
		1.00	0.37	45.98		
		2.00	0.74	23.11		
		2.50	0.93	18.48		
		3.00	1.12	15.42		
		4.00	1.49	11.56		
EPA 600/R-06/055	0.3721	0.50	0.19	350.83	65.14	1.002
		1.00	0.37	175.74		
		2.00	0.74	87.56		
		2.50	0.93	70.23		
		3.00	1.12	58.28		
		4.00	1.49	43.66		
L2H2 parallel	0.3721	0.50	0.19	82.94	15.55	0.995
		1.00	0.37	41.48		
		2.00	0.74	20.89		
		2.50	0.93	17.36		
		3.00	1.12	13.79		
		4.00	1.49	10.37		
P01	0.3721	0.50	0.19	142.91	26.38	1.006
		1.00	0.37	71.20		
		2.00	0.74	35.43		
		2.50	0.93	28.33		
		3.00	1.12	23.56		
		4.00	1.49	17.67		
P02	0.3721	0.50	0.19	141.52	26.19	1.004
		1.00	0.37	70.74		
		2.00	0.74	35.18		
		2.50	0.93	28.21		
		3.00	1.12	23.45		
		4.00	1.49	17.55		
P03	0.3721	0.50	0.19	139.70	25.98	1.002
		1.00	0.37	70.17		
		2.00	0.74	35.03		
		2.50	0.93	27.93		
		3.00	1.12	23.24		
		4.00	1.49	17.40		
P04	0.3721	0.50	0.19	151.34	28.05	1.003
		1.00	0.37	75.77		
		2.00	0.74	37.70		
		2.50	0.93	30.18		
		3.00	1.12	25.12		
		4.00	1.49	18.80		

As seen in Table 7-6. The value of the ɣ constant is approximately equal to 1 in all systems. Thus for practical reasons Equation 7-1 can be re-arranged into Equation 7-2

$$D = \frac{R'}{Q}$$

Here R' represents the approximation of the performance constant R when ɣ is considered to be equal to 1.

Table 7-7 shows the performance constant R' calculated at various flow rates. In each case the difference in its value over the range of air flow rates was marginal and did not have a considerable effect on the final calculation of the average UV dose (D) during the use of Equation 7-2.

Table 7-7 Average UV dose and Performance constant R' at various airflows for the different systems.

System	Duct Area	Velocity m.s⁻¹	Air flow rate m³.s⁻¹	Average UV dose J.m⁻²	Performance constant R' (W.m)	Average R' (W.m)
EPA 600/R-06/050	0.3721	0.50	0.19	55.23	10.28	10.24
		1.00	0.37	27.53	10.24	
		2.00	0.74	13.79	10.26	
		2.50	0.93	10.96	10.20	
		3.00	1.12	9.15	10.22	
		4.00	1.49	6.87	10.23	
EPA 600/R-06/051	0.3721	0.50	0.19	91.52	17.03	17.16
		1.00	0.37	45.98	17.11	
		2.00	0.74	23.11	17.20	
		2.50	0.93	18.48	17.19	
		3.00	1.12	15.42	17.21	
		4.00	1.49	11.56	17.21	
EPA 600/R-06/055	0.3721	0.50	0.19	350.83	65.27	65.20
		1.00	0.37	175.74	65.39	
		2.00	0.74	87.56	65.16	
		2.50	0.93	70.23	65.33	
		3.00	1.12	58.28	65.06	
		4.00	1.49	43.66	64.98	
L2H2 parallel	0.3721	0.50	0.19	82.94	15.43	15.57
		1.00	0.37	41.48	15.44	
		2.00	0.74	20.89	15.54	
		2.50	0.93	17.36	16.15	
		3.00	1.12	13.79	15.40	
		4.00	1.49	10.37	15.44	
P01	0.3721	0.50	0.19	142.91	26.59	26.40
		1.00	0.37	71.20	26.49	
		2.00	0.74	35.43	26.36	
		2.50	0.93	28.33	26.35	
		3.00	1.12	23.56	26.30	
		4.00	1.49	17.67	26.30	

		0.50	0.19	141.52	26.33	
		1.00	0.37	70.74	26.32	
P02	0.3721	2.00	0.74	35.18	26.18	26.23
		2.50	0.93	28.21	26.24	
		3.00	1.12	23.45	26.18	
		4.00	1.49	17.55	26.12	
		0.50	0.19	139.70	25.99	
		1.00	0.37	70.17	26.11	
P03	0.3721	2.00	0.74	35.03	26.07	26.00
		2.50	0.93	27.93	25.98	
		3.00	1.12	23.24	25.95	
		4.00	1.49	17.40	25.90	
		0.50	0.19	151.34	28.16	
		1.00	0.37	75.77	28.19	
P04	0.3721	2.00	0.74	37.70	28.06	28.08
		2.50	0.93	30.18	28.07	
		3.00	1.12	25.12	28.04	
		4.00	1.49	18.80	27.99	

Therefore, with the use of the performance constant R' calculated at any given point of the performance curve, it is possible to calculate the average UV dose of the system at any given flow rate. Figure 7.19 shows a comparison of the CFD calculated average UV dose for the model EPA 600/R-06/050 and the average UV doses calculated with the average performance constant R'.
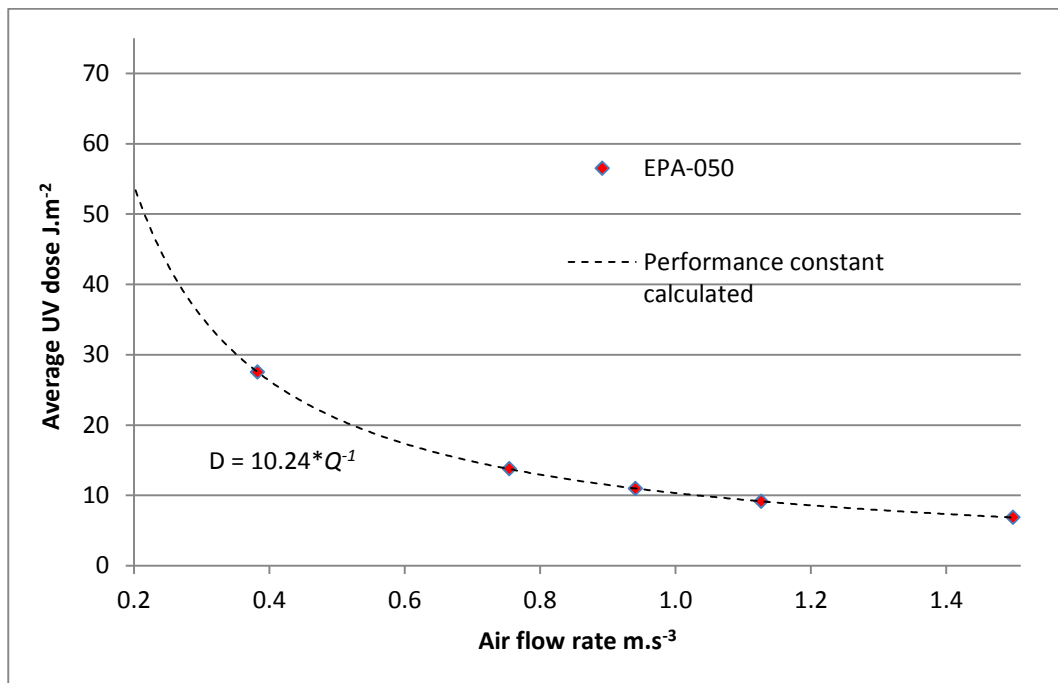
Figure 7.19 Average UV dose for the EPA 600/R-06/050 and performance curve calculated with the performance constant R'=10.24.

If the single decay sterilisation performance is given by Equation 7-3 (Chapter 3)

$$S = e^{-kD}$$

Equation 7-3

And for a single stage with shoulder is given by Equation 7-4 (Chapter 3)

$$S(t) = 1 - \left(1 - e^{-kD}\right)^n$$

Equation 7-4

Thus it is possible to rearrange Equation 7-3 to include the performance constant R' into Equation 7-5.

$$S = e^{\left(-\frac{kR'}{Q}\right)}$$

Equation 7-5

And to rearrange Equation 7-4 into Equation 7-6.

$$S(t) = 1 - \left(1 - e^{\left(-\frac{kR'}{Q}\right)}\right)^n$$

Equation 7-6

With these equations it is possible to approximate the sterilisation performance of a system against a specific microorganism, showing single stage decay and a single stage with shoulder, at any given airflow. However, the user must be aware that R' does not account for irradiation distribution, thus small variations on the calculation of performance will be expected, and these variations will be present in the calculation of performance of any method that does not account for irradiation distribution.

The following figures show a comparison of the sterilisation performance calculated by CFD, which takes direct account on irradiation distribution and particles trajectories, and the sterilisation performance calculated when using the performance constant R' with Equation 7-5 and Equation 7-6.
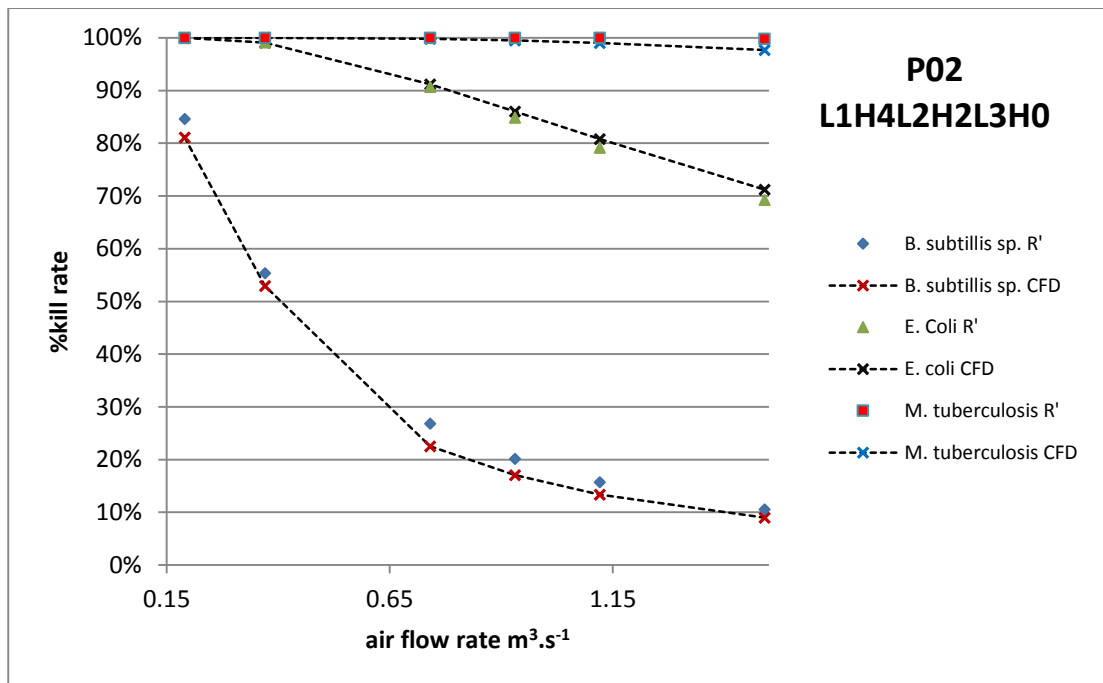
Figure 7.20 Kill rates for system P02 calculated by CFD and using the performance constant R'.

For the system P02, the difference between the kill rate calculated by CFD and using the performance constant R' was no more than 5% in any of the cases shown in Figure 7.20. In this case the system had an evenly distributed irradiation, with lamps being located top, centre and bottom of the duct.
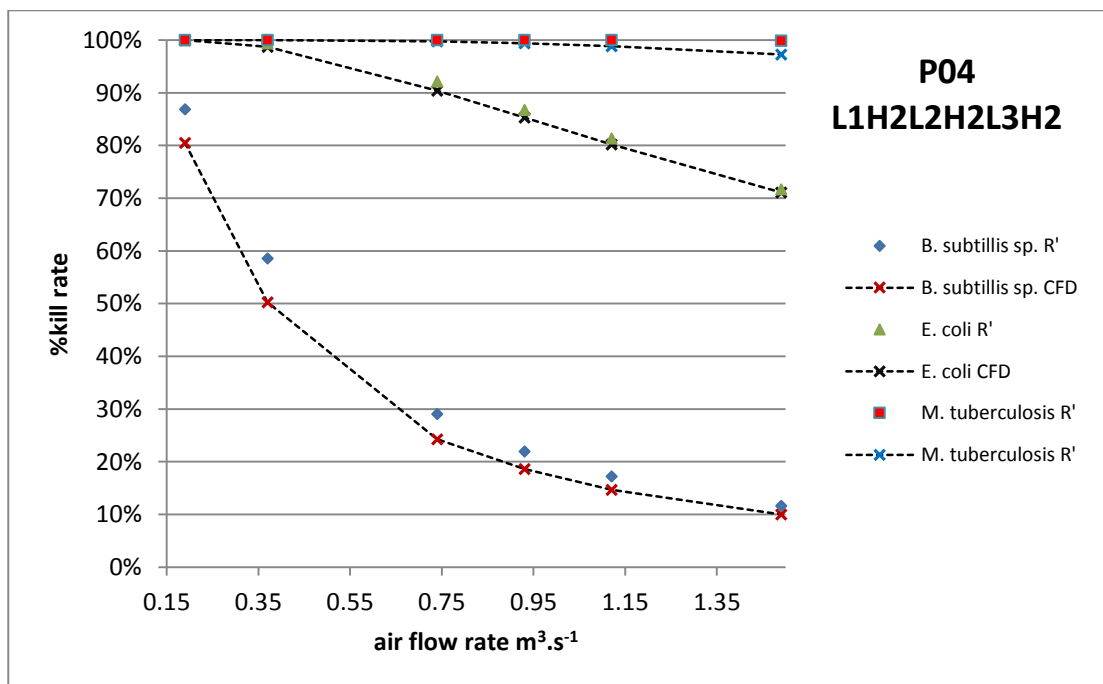
Figure 7.21 Kill rates for system P04 calculated by CFD and using the performance constant R'.

The system P04 shown in Figure 7.21, had all lamps located at the centre of the duct; this gave the system an irradiation field concentrated at the centre of the duct, and at the same time an average UV dose among the highest within the multi-lamp systems. In this case the difference in sterilisation performance calculated by CFD and using the R' was in average close to 5% for *B. subtillis* spores, which shows relatively low UV susceptibility plus a shoulder in its decay curve. In the other cases of *E. coli* and *M. tuberculosis*, which show a single stage decay curve, the difference in the calculation of performance between the two methods (CFD and R') was less than 1% in average.
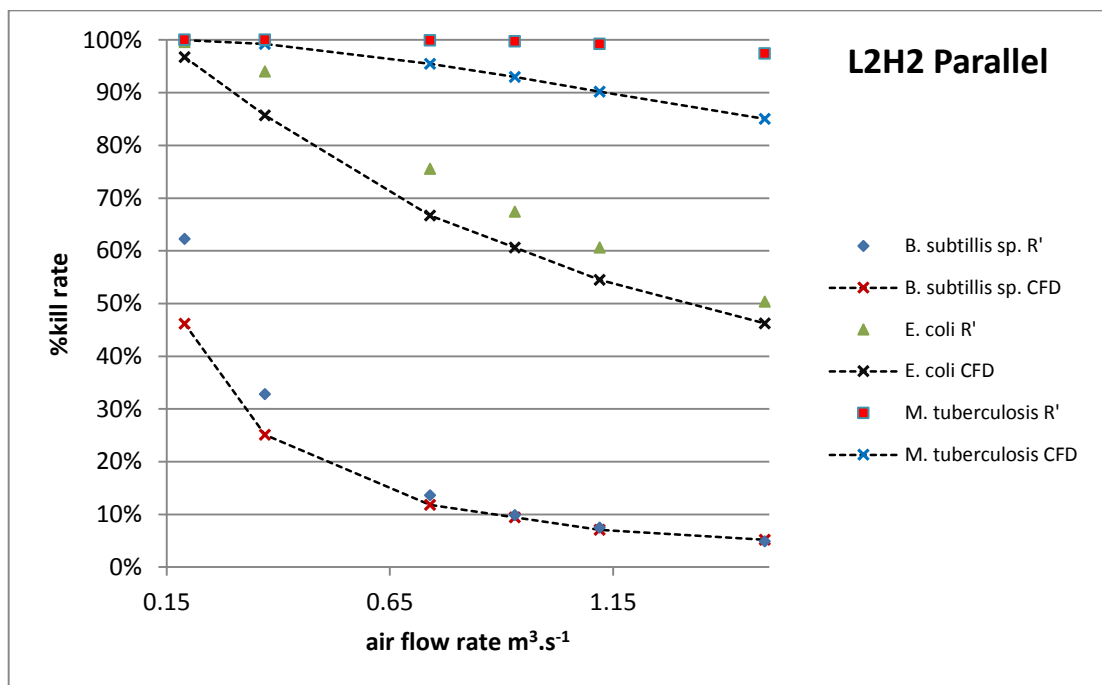
Figure 7.22 Kill rates for the L2H2 parallel system calculated by CFD and using the performance constant R'.

Figure 7.22 shows the system with a single lamp parallel to the airflow, which presented significant differences in the calculation of performance when using CFD or the performance constant R'. For the highly UVC resistant *B. subtillis* spores, at low air flows the difference in the calculated performance was of up to 15%, nevertheless at high air flow, the difference in the calculated performance was of less than 1%. For *E. coli* and *M. tuberculosis* the difference in the calculated performance between CFD and R' was up to 10% in some cases.

These differences happen due to the distribution of irradiation within system concentrating in a single area, thus creating the effect of over performance. This effect is more noticeable when the system deals with highly UVC susceptible microorganism, as the irradiation gets concentrated at the centre of the duct, microorganisms passing through this area receive considerably high UV doses, higher than those required for a 99.9% sterilisation, leaving all the

non absorbed energy as waste, unable to contribute to increase the sterilisation performance of the system. In these cases, the use of R' for the calculation of performance will over predict results. Nevertheless, against UVC resistant microorganisms such as *B. subtillis* spores, the high irradiation at the centre of the duct is not enough to reach the 99.9% sterilisation of the microorganism, avoiding the wastage of energy.

Although it is possible to use the performance constant R' to calculate the average UV dose of a system with relatively good accuracy, it still misses to fully account for the UV irradiation distribution of a system. The use of R' will tend to over predict the calculation of performance of a system designed with an uneven irradiation. Section 7.2 showed the CFD modelling of a set of multi-lamp configuration systems which had the same number of UV lamps and the same amount of UV power, and yet each system returned a different average UV dose. The only difference between the systems was the lamp position, and hence the irradiation distribution, which as it seems, the CFD calculation managed to account for. Data from biodosimetry tests or CFD modelling appear to implicitly account for an aspect of the UV irradiation distribution, thus reducing the error of the R' calculated sterilisation performance.

7.3.4 The introduction of the performance efficiency rating.

The performance constant can be used as a mean for direct comparison of sterilisation performance between systems. The higher the performance constant, the more sterilisation power the system has. Nevertheless, the efficiency of a system, meaning how good the system makes use of its UV power, is not shown by the performance constant R'.

While the air flow rate remains constant, the air velocity of a system can change depending on the system duct area. Therefore the performance constant should be used in relation to volume rate ($m^3.s^{-1}$) and not in relation to air velocity ($m.s^{-1}$).

By dividing the performance constant R' between the UV power of the system (E_{UV}) (Equation 7-7), a Performance Efficiency Rating (PER) can be calculated that can be used as an indicator for direct comparison of the efficiency of a system. In this approach the higher the number the better the system efficiency.

$$PER = \frac{R'}{E_{UV}}$$

Equation 7-7

By direct comparison of the performance efficiency rating, it is possible to evaluate designs and establish performance between lamp configurations.

Table 7-8 In-duct system performance constant.

System	Average Performance constant R' (W.m)	System total UV power (W)	Performance efficiency rating (PER)
EPA 600/R-06/050	10.24	19	0.54
EPA 600/R-06/051	17.15	34	0.50
EPA 600/R-06/055	65.20	144	0.45
L1H1	8.50	19	0.44
L1H3	8.49	19	0.44
L2H1	10.18	19	0.54
L2H2	10.20	19	0.54
L2H3	10.74	19	0.53
L3H1	9.00	19	0.44
L3H3	8.86	19	0.43
L2H2 parallel	15.40	19	0.81
P01-L1H4L2H2L3H4	26.40	57	0.46
P02-L1H4L2H2L3H1	26.23	57	0.46
P03-L1H4L2H4L3H4	25.00	57	0.45
P04-L1H2L2H2L3H2	28.08	57	0.49
P05-L1H4L1H2L1H0	26.45	57	0.43
P06-L2H4L2H2L2H0	31.05	57	0.51

As shown per Table 7-8, the performance efficiency rating (PER) for all the systems showing lamps perpendicular to the volume flow rate ranged between 0.45 and 0.54, with the highest value achieved when the lamps was located exactly at the centre of the system, as is the case of the EPA 600/R-06/050. This means that, at this position is where a lamp perpendicular to the airflow provides the highest UV dose for a system, and as lamps move from this position in either direction (up, down or along the length of the duct) their efficiency decreases, as it can be seen, none of the other systems with lamps perpendicular to the airflow managed to achieve this rating. In the case of the lamp positioned parallel to the airflow, the PER is of 0.81, meaning that this configuration manages to provide a higher UV dose within the system. Nevertheless this does not mean this configuration brings higher sterilisation performance, for that it is necessary to compare the performance constant R' of a system. The PER value of a system refers to how efficient is its lamp configuration, and how much of a UV dose is generated per UV watt input. PER is a rating on efficiency and not on performance.

The use of the system performance curve (Equation 7-2) and the introduction of the performance constant (R') can be a valuable tool for designers to map the performance of a system over a range of airflows with confident accuracy, compare sterilisation performance between design and their performance efficiency by using the PER.

An example of the use of PER can be done by comparing the system EPA 600/R-06/050 against the EPA 600/R-06/051. While the first system used only one lamp of 19 UVC watts located at the centre, the latter used four lamps of lower wattage, 8.5 UVC watts, located across the height of the duct, giving a total of 34 UVC watts for the system. The EPA 600/R-06/051 performed better as it had more UVC power, however it was less efficient showing a PER rating of 0.50 in comparison of that of the EPA 600/R-06/050 with a PER of 0.54. The single lamp system obtained more sterilisation performance per UV power input.

The use of the PER could help on the direct comparison of systems not through sterilisation performance, but on UVC efficiency, therefore helping on making more efficient system that will use lower UV power while providing better sterilisation performance. However, this PER value does not account for UV irradiation distribution, which also bears an impact on sterilisation performance. CFD calculations implicitly accounted for UV irradiation distribution in the calculated average UV dose of a system. However, it is important to clarify that the performance constant R', which is used to calculate the PER, does not fully reflects UV irradiation distribution and work is still required to account for it. Therefore future work should look for means to introduce a weighting system that accounts for irradiation distribution.

7.3.5 The use of the performance constant R' as a system rating value.

It is imperative the creation of a rating value that accurately assesses the performance of a UV air sterilisation system. In this manner, it would be easier for designers as well as for users to identify what are the capacities of an sterilisation system in question, or how to ask or request an specific performance. The performance constant R' has specific characteristics that could turn it an effective rating system for in-duct UV sterilisation systems.

Kowalski (2009a) and the IUVA (2005c) proposed the creation of an UV sterilisation rating system in the form of the URV (Ultraviolet rating value) (Chapter 1). The URV system classifies the performance of a UV sterilisation device in terms of the UV dose it produces. The rating is divided into 20 levels according to the UV dose ranges, the higher the rating the more UV dose the system produces. However, the UV dose of a system is a relation of the irradiation profile and the airflow rate of operation, therefore the URV value of a system would be variable depending on the operation parameters. This could be troublesome to use as a rating value, as it would need to be specified at what airflow did the system achieved certain URV value.

Table 7-9 URV rating values (Kowalski, 2009a).

URV	Dose J.m^{-2}	Mean dose J.m^{-2}	URV	Dose J.m-2	Mean dose J.m-2
1	0.01	0.055	14	30	35
2	0.1	0.15	15	40	45
3	0.2	0.25	16	50	55
4	0.3	0.4	17	60	70
5	0.5	0.63	18	80	90
6	0.75	0.88	19	100	150
7	1	1.25	20	200	250
8	1.5	2	21	300	350
9	2.5	3.75	22	400	450
10	5	7.5	23	500	750
11	10	12.5	24	1000	1500
12	15	17.5	25	2000	2500
13	20	25			

The performance constant R' is a specific performance of a system, and is not affected by airflow. Thus the system performance R´ remains constant independently of operation parameters.
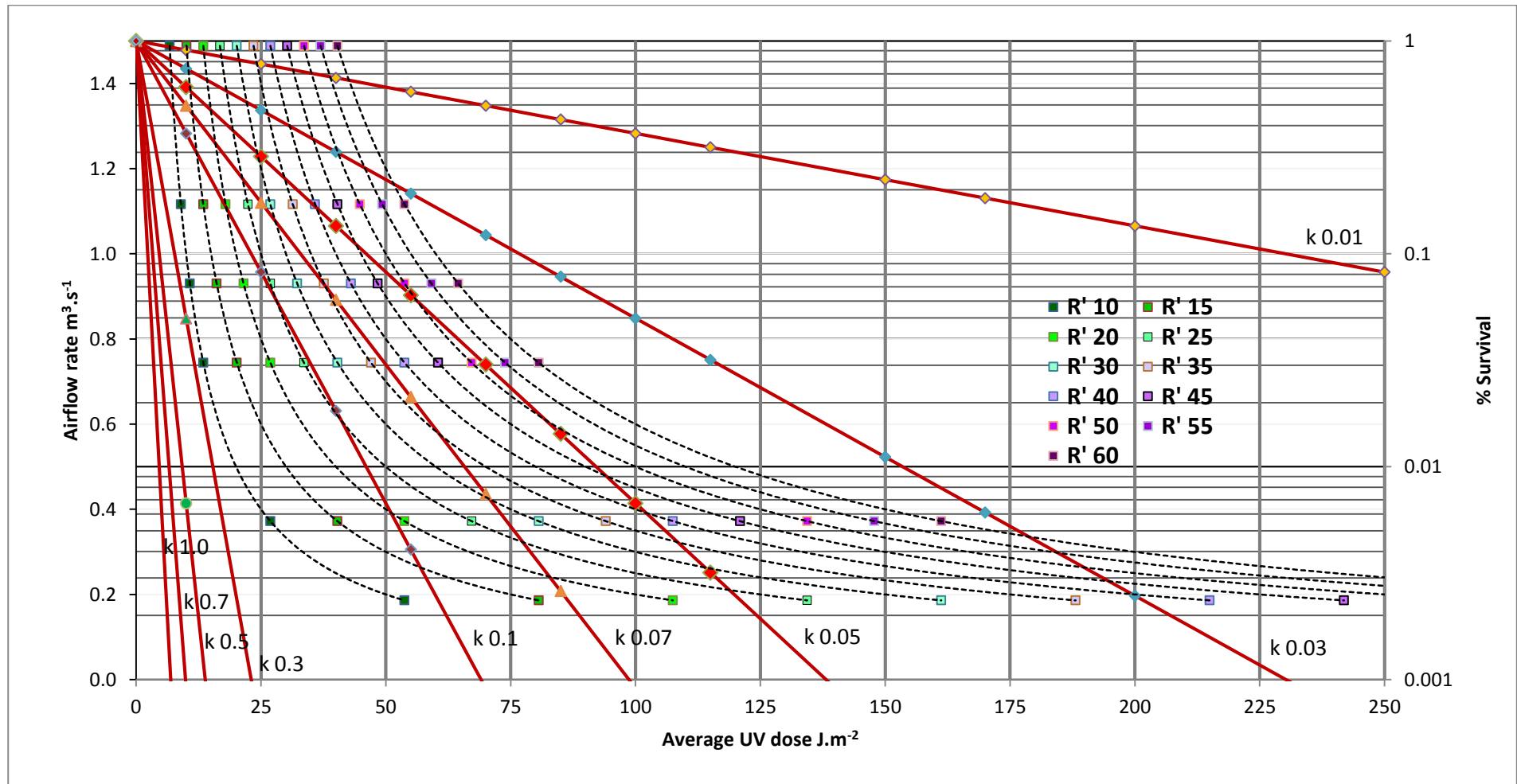
Figure 7.23 R' performance curve and single stage susceptibility decay (*k*).

UV air sterilisation systems can be rated by their performance constant R', and in this manner it would be possible to observe the sterilisation performance of the system against the ranges of microorganisms susceptibilities and airflow rates (Figure 7.23). It is also possible to size a system with the use of the R' performance curve as it is scalable. For example an R'10 system working at 0.2 $m^3.s^{-1}$ delivers an UV dose of 50 $J.m^{-2}$ approximately, and it can be seen that an R'20 system delivers exactly the double amount of UV dose when working at the same airflow rate (100 $J.m^{-2}$ working at 0.2 $m^3.s^{-1}$). The R' performance curve rating value not only does allows for direct comparison between system but also allows for the sizing of UV sterilisation systems and to effectively rate the sterilisation performance the systems will achieve.

7.4 Single lamp configuration, Applying the performance constant (R') and PER.

Applying the performance constant (R') to the lamp configuration study shown on Chapter 6 can disclose information otherwise difficult to appreciate.

Table 7-10 In-duct performance constant for the different lamp configurations as shown in Chapter 6.

System lamp position	Performance constant R' (W.m)	System total UV power (W)	Performance efficiency rating (PER)
L1H1	8.50	19	0.44
L1H3	8.49	19	0.44
L2H1	10.18	19	0.53
L2H2	10.20	19	0.53
L2H3	9.99	19	0.52
L3H1	8.37	19	0.44
L3H3	8.24	19	0.43
L2H2 parallel	15.40	19	0.81

The results of the performance curve for the various lamp positions as analysed in Chapter 6 are shown in Figure 7.24. The performance constant R' was calculated with the average UV dose of the system at the airflow velocity of 2.5 $m.s^{-1}$ (airflow rate 0.93 $m^3.s^{-1}$) using Equation 7-2. The highest PER value for perpendicular lamps was achieved by lamps located at L2, while lamps located at L1 and L3, which distance is symmetrical from the centre, showed relatively the same PER value of 0.44.
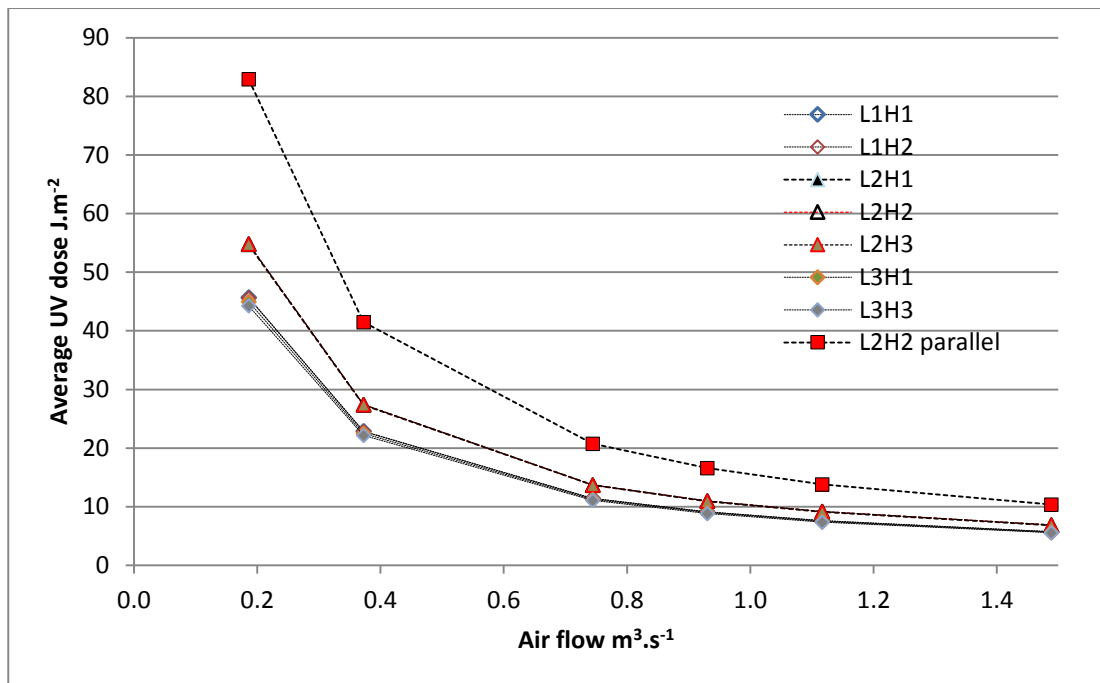
Figure 7.24 Average UV dose for lamps configuration shown in Chapter 6 as calculated with the use of the eprformance constant R.

The performance curves of the systems bring new insights on the impact of lamp position. For example now is evident that lamp position across the height of the duct did not have any considerable impact on the performance of the system and that lamps located at the centre of the duct, performed better than lamps located at the beginning (L1) or end (L3) of the duct. It is also evident that the performance of the lamps is symmetrical from the centre i.e. lamps at L1 performed the same as lamps at L3. As it can be seen on the two configurations at L1 and L3 fall under the same curve, with virtually no difference in performance (bottom black curve), then lamps located at L2 felt into the same curve of performance (red middle curve) independently of lamp position across the height of the duct.

By plotting the map of performance across a range of airflow we can see how small differences in average UV doses disclosed during the analysis at 2.5 m.s^{-1} (0.93 m^3.s^{-1}) increased as the airflows decreases.

Moreover the PER value, shown in Table 7-10, and the curve of performance shows that the lamp located parallel to the airflow was considerably more efficient than perpendicular lamp position (top dotted line). This is due to this configuration providing a higher UV dose to those particles passing close to the lamp.

7.5 Multi-Lamp configuration, performance constant and PER.

Figure 7.25 shows the performance of multi-lamp systems. The differences in performance of multi-lamp configurations are more significant when they operate at low air volumes. In contrast to the single lamp configuration, in which most lamp position perform similarly except for those located at the centre (L2), in the multi-lamp configuration, each system shows its very own performance curve.
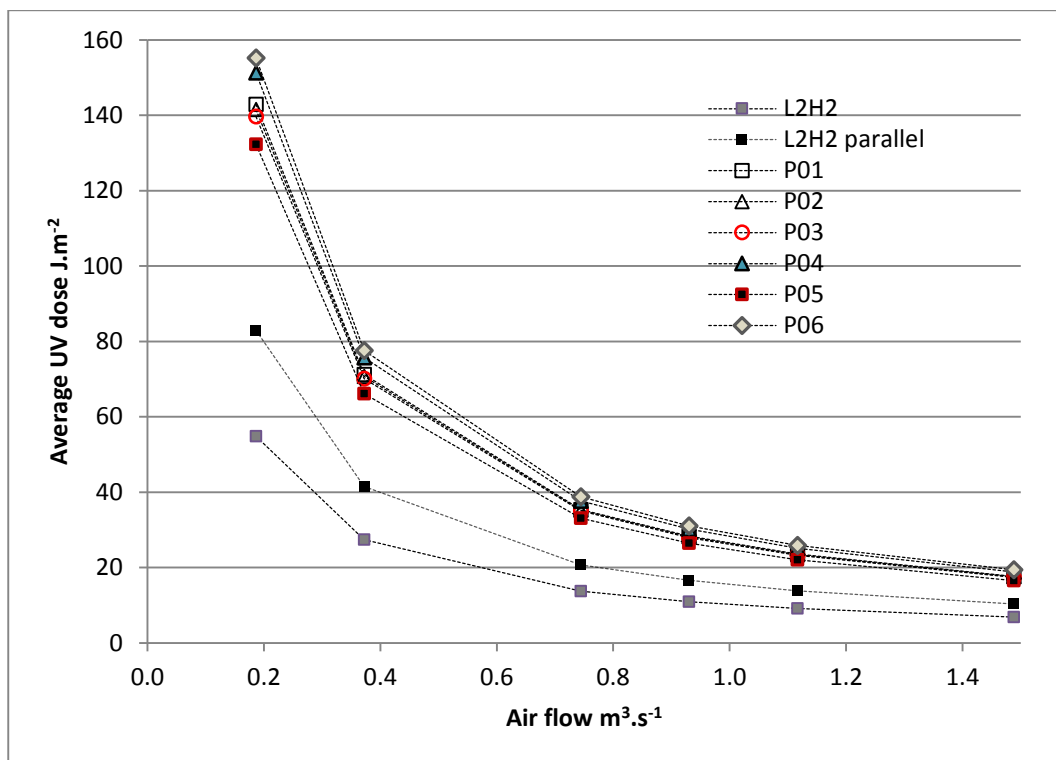
Figure 7.25 Performance comparison of multi-lamp configuration and single lamp configuration systems.

In general, tripling the UV power in the system increased the average UV dose by 2.5 to 3 times depending on the multi-lamp configuration i.e. L2H2 at 0.93 $m^3.s^{-1}$ performed at 10.97 $J.m^{-2}$, the multi-lamp system P06 with the three lamps at the centre working at the same airflow performed at 31.05 $J.m^{-2}$ (2.8 times the performance of L2H2) while the system P05 with the three lamps at the beginning of the duct performed at 26.45 $J.m^{-2}$ (2.4 times the performance of the L2H2). Increasing the UV power of the system, will bring almost the same increase on average UV dose, nevertheless there are certain recommendations that might help to improve the sterilisation performance.

Another finding coming from the analysis of the performance curve is that it appears that reducing the airflow of the system brings a better increase in sterilisation performance than increasing the UV power. E.g. a single lamp system like the L2H2 working at 0.31 $m^3.s^{-1}$ air flow

rate will perform better than a multi-lamp system of three times the power like the P06 configuration working at 0.93 $m^3.s^{-1}$ (three times the air flow rate), and the difference would be even more significant if the single lamp system is positioned parallel to the airflow.
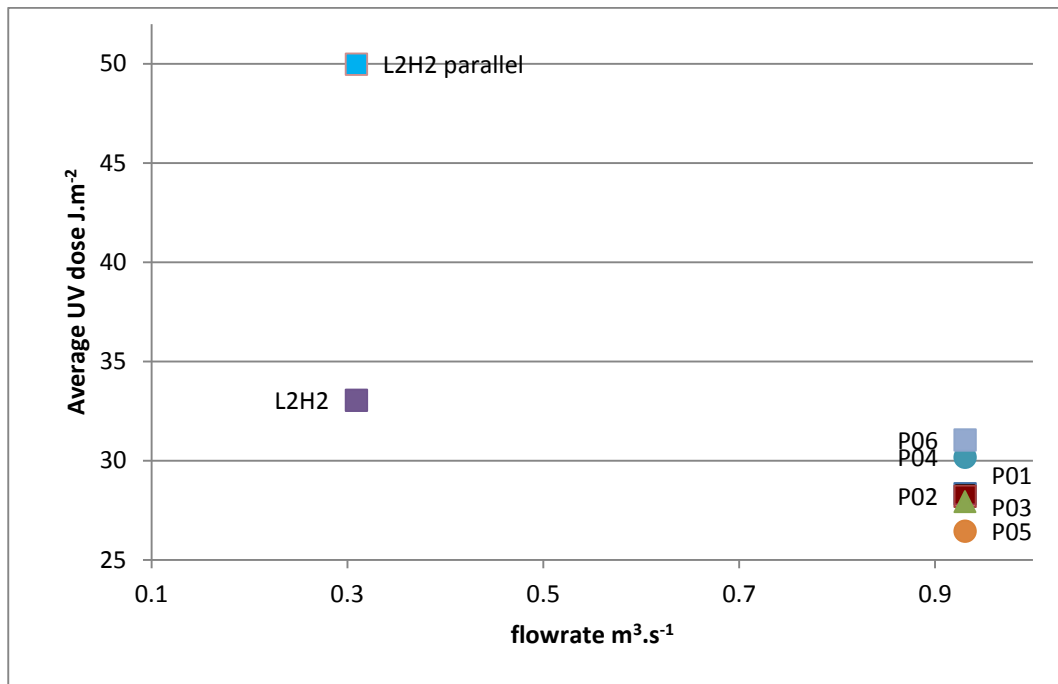
Figure 7.26 single lamp system at 0.31 $m^3.s^{-1}$, against a three-lamp system of at 0.93 $m^3.s^{-1}$.

7.6 Conclusions.

The first section of this chapter evaluated the performance of a set of multi-lamp systems. It was found that lamp position and irradiation distribution have a direct impact on the sterilisation performance of an in-duct UVC system (Section 7.2).

An even UVC irradiation across the face area of the duct can help to avoid sterilisation over-performance.

The system with the highest average UV dose will perform better against strongly resistant microorganism, such as *B. subtillis*; nevertheless, systems with a more evenly distributed UV irradiation can perform better against weak microorganisms even if they have a lower average UV dose.

The best performance was achieved by locating all the three lamps at the centre of the duct and distributed across the height of the duct.

The second part of this chapter analysed the performance of various in-duct UV sterilisation systems over a range of airflow rates. The results identified a relationship between the

operational airflow of a system and its average UV dose, introducing the concept of the performance constant (R') which enables users to calculate the performance curve of an in-duct UV sterilisation system out of a single data point.

Moreover, it was introduced the concept of the performance efficiency rating (PER) which makes use of the UV power of the system and the performance constant (R') that implicitly contains the duct area of the system, thus making possible the direct efficiency comparison between systems of different duct areas and UV power.

The performance constant R' allows for the direct comparison of performance between system, the higher the R' the better the average UV dose of the system. The performance Efficiency Rating (PER) allows for the direct comparison of efficiency of a system, the higher the PER the higher the efficiency of the system. Finally, the UV dose distribution standard deviation (UV std) allows for a direct comparison of the system irradiation distribution, the lower the UV std, the more evenly distributed the irradiation within the system.

It was also found that:

- The best sterilisation performance is achieved with lamps located at the centre of the duct.
- Multi-lamp system performed better with the lamps located at the centre of the duct in a single row across the height of the duct.
- The lowest performance for multi-lamp configurations was found when lamps were located at the beginning of the duct.
- Lamps parallel to the airflow appear to be almost twice as efficient, in average UV dose, than lamps perpendicular to the airflow.
- Reducing the airflow can bring better performance than increasing the UV power of a system.
- An evenly distributed irradiation profile improves the performance of a system.
- A higher average UV does not always results on higher sterilisation performance, as this also depends on irradiation distribution and microorganism susceptibility.
- The impact of irradiation distribution, in the form of over performance, gets increased when the system deals with highly UVC susceptible microorganisms such as *E. coli* or *P. aeruginosa*, and gets reduced when dealing with highly resistant UVC microorganisms such as *B. subtillis* spores or *M. tuberculosis*.

Finally, a set of design recommendations can be drafted out of the findings in this chapter that can be used to improve the sterilisation performance of in-duct systems.

Table 7-11 In-duct UV systems design recommendations.

Design recommendation
Locate lamps parallel to the airflow.
Locate lamps at the centre of the duct.
In Multi-lamp system, locate lamps at the centre of the duct in a single row across the height of the duct.
Avoid lamps at the beginning of the duct.
Leave a distance (1 metre) between lamp and the nearest duct elbow in both directions.
Distribute irradiation evenly across the face area of the duct.
Avoid single row of lamps at the top or bottom of the duct.
Whenever possible reduce operational air flow rates.

This chapter provided a tool for the calculation of performance of an induct UV system over a range or airflows in the form of the performance constant R', it also provided a method for the direct comparison of performance efficiency between designs by using the PER value.

Chapter 8. Conclusions.

8.1 Summary

The research presented here focused on the development and validation of a standard method for the modelling of in-duct UV air sterilisation systems with the use of computational fluid dynamics (CFD) and the application of the approach to evaluating the performance of different system designs.

Chapter 3 focused on the development of a set of reliable microorganism UV susceptibility curves, needed for the modelling and validation of UV air sterilisation systems, as outlined by Objective 1. A total 12 microorganism UV susceptibility curves were established by combining data from the published literature. The findings from this chapter are of help for the calculation, modeling and sizing of UV air sterilisation systems. The set of microorganism UV susceptibility curves here presented reduced and explained the variations in microorganisms UV susceptibility commonly found in literature and in most cases agreed in specific set of values that can be used as a baseline data for direct comparison of UV system performance.

Chapter 4 reviewed various UV irradiation modelling methods, and established the benefits of using the Discrete Ordinates (DO) method for the modelling of UV irradiation due to its ability to account for reflections, refractions, shadowing and particle trajectories when coupled with computational fluid dynamics (CFD) techniques. This satisfied the goal of the Objective 2. The DO method coupled with CFD techniques is a sophisticated and computational resource intensive process, however the current state of computational processing technologies allow for the use of these techniques in a reliable, efficient and functional manner.

The work and results presented on Chapter 5 match the goals set in the objective 3. The sterilisation performance of three UV in-duct air sterilisation systems previously tested by the EPA (EPA, 2006a, EPA, 2006b, EPA, 2006c) were reproduced with the use of CFD modeling and the DO method, finding good agreement with the EPA reported results, and validating the reliability of using CFD techniques to model the sterilisation performance of UV in-duct air sterilisation systems. Moreover, it was shown how the use of CFD techniques allowed for the calculation of particle trajectories, and the UV dose received by each particle, permitting to see details of the UV air sterilisation process that otherwise would have been unnoticed, such as the UV dose distribution of the system and the variability on the received UV dose by each particle. On a side note, this chapter also showed a comparison of the expected air sterilisation performance at three different reflectivity values of 0%, 15% and 25%, these findings are of

importance for the consideration of future designs, in which reflectivity can take a more dominant role to increase the sterilisation performance.

Chapter 6 showed how lamp position affected the sterilisation performance of an in-duct UV system, and found that lamps located at the centre of the duct provided the best sterilisation performance. In some cases the differences in average UV dose was of up to 20%. However, as it was explained the difference in the percentage of average UV dose does not translate directly into sterilisation performance due to the exponential relation between average UV dose and microorganisms' sterilisation i.e. 20% increase in average UV dose does not means 20% increase in microorganism kill rate. It was also found that lamps parallel to the airflow provide a higher average UV dose for the system, than a perpendicular lamp configuration; nevertheless the single lamp parallel configuration has a considerably higher UV dose standard deviation, meaning that the irradiation distribution within the system is not the best, leaving some areas of the duct with a highly concentrated UV dose, while other areas receive considerably lower UV doses. These findings relate to Objective 4.

Through Chapter 6 and Chapter 7 it was shown how the UV irradiation profile of a system i.e. how lamps are located within the in-duct system, affect the UV dose variability. Moreover, it was shown that UV dose variability, due to uneven irradiation profiles affects the performance of an UV air sterilisation system, and in some cases, a system with a better UV dose distribution can perform better than a system with a higher average UV dose. It was also shown how the standard deviation of the UV dose distribution could be used as a parameter to measure the quality of the UV irradiation profile, the lower the standard deviation the better the irradiation profile within the system. This satisfies the goal set in the Objective 5.

It was found that the performance of an in-duct air sterilisation system follows a power law decay in relation to the airflow, and it is possible to calculate the performance of a system at any given airflow with the use of a specific performance constant R' as explained in Chapter 7. It was shown that each system had its very own "blue print" of particles UV dose and residence time, which is defined by lamp position and the irradiation profile of a system.

The performance constant R' can be used as a performance rating for the direct comparison of average UV dose within systems, the higher the R' the higher the average UV dose of the system. When the performance constant R' is divided by the total UV power of the system, we obtain the Performance Efficiency rating (PER) of a system. The PER compares the UV power efficiency of a system, showing how well the UV power of the system is being employed. Finally it was shown that the quality of the UV irradiation distribution within the duct can be measured by the

standard deviation of the system UV dose distribution, the higher the lower the standard deviation, the better it is distributed the UV irradiation within the system. By using these three rating tools it is possible to compare a system on aspects of performance, energy efficiency and UV irradiation distribution. This addresses Objective 6.

Finally Chapter 7 finished with a set of recommendations for the design of in-duct UV air sterilisation systems, as set out by Objective 7.

The research described in this thesis can be used to model UV in-duct air sterilisation systems using CFD techniques in a systematic manner. Moreover, it lays the foundation to work on the optimisation of in-duct UV air sterilisation systems.

8.2 Future work.

There are a number of areas for future research to continue this work.

The current microorganism UV susceptibility curves are limited by available data and consistency between published experimental studies. Future work can focus on developing a standard test for quantifying the susceptibility of microorganisms to UV light in air that maps the full decay curve at various UV doses, identifies the microorganism decay type (single stage, double stage etc), and includes the impact of relative humidity in the microorganism susceptibility. This is a considerably time consuming exercise, for such reason, future work could focus on outlining key microorganisms where there is a greater need for data.

Chapter 4 and Chapter 5 explained the use of the DO method coupled with CFD techniques for the modelling of UV irradiation and the air sterilisation performance of in-duct systems. Nevertheless, it is known that air velocity and temperature directly affects the irradiation output of UV lamps (Lau, 2009, Philips, 2005). Future work should look to include the effect of air velocity and temperature on lamp irradiation power into the CFD modelling to achieve more accurate results.

It was established that a single lamp parallel to the airflow performs better than a single lamp perpendicular to the airflow. However there are still combinations at various angles that can be analysed to look for better performances. Chapter 7 also showed the modelling of multi-lamp systems of three UV lamps. Future work should look at the effect of increasing the number of UV lamps and lamp configurations on the performance of a UV system, and to determine the optimum number of UV lamps to be used on a specific duct area. For example, it would be of interest to asses if a multiple-parallel lamp configuration is capable of reducing the average UV

dose standard deviation present on the single lamp parallel configuration, hence making the systems more effective at sterilising air.

The CFD models here analysed only considered straight ducts, real life installations very often include 90∘ duct angles just before the in-duct UV system, therefore it is necessary to analyse the impact of such duct angles and other features on the airflow and hence the performance of an UV in-duct system. Future work can focus on optimisation studies like the most efficient duct area per UV power and the minimum duct length required for flow and irradiation development.

Beyond modelling the detail of the UV irradiation and air sterilisation process, it is also necessary to take the outcomes of this research, and apply them into a system level scale, to assess the energy and/or disinfection performance and benefits or problems over a period of time.

The work here presented laid the bases for a standard CFD modeling of in-duct UV air sterilisation systems. With this bases it will be possible for future studies to include the modeling of other technologies into the systems, for example the inclusion of fibrous filtrations (Fisk et al., 2002, Foarde and Hanley, 1999) or photocatalytic filtration with the use of TiO2 substrates (Sichel, 2009, Yang et al., 2007, Hodgson et al., 2005) into the sterilisation performance of in-duct UV air systems.

Appendix

Appendix-Table 1 EPA/R-06/050 specifications table.

Spec	600/R-06/050
Number of lamps	1
Lamp power watts	58
Lamp UVC power watts	19
Total system power	58
Total system UV power	19
Lamp length cm	53.3
Lamp diameter	1.9 cm T6
Duct size	61 cm x 61 cm
Duct length	7.83 m
Duct wall Emissivity	0.85
Duct wall Reflectivity	15%
Duct wall refractive index	1
Performance constant R'	10.20
PER	0.53
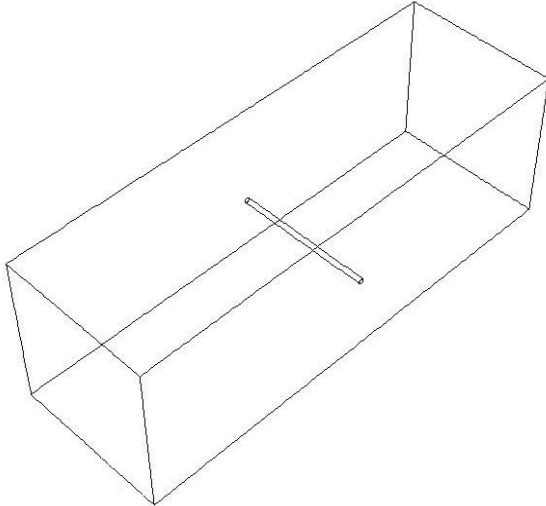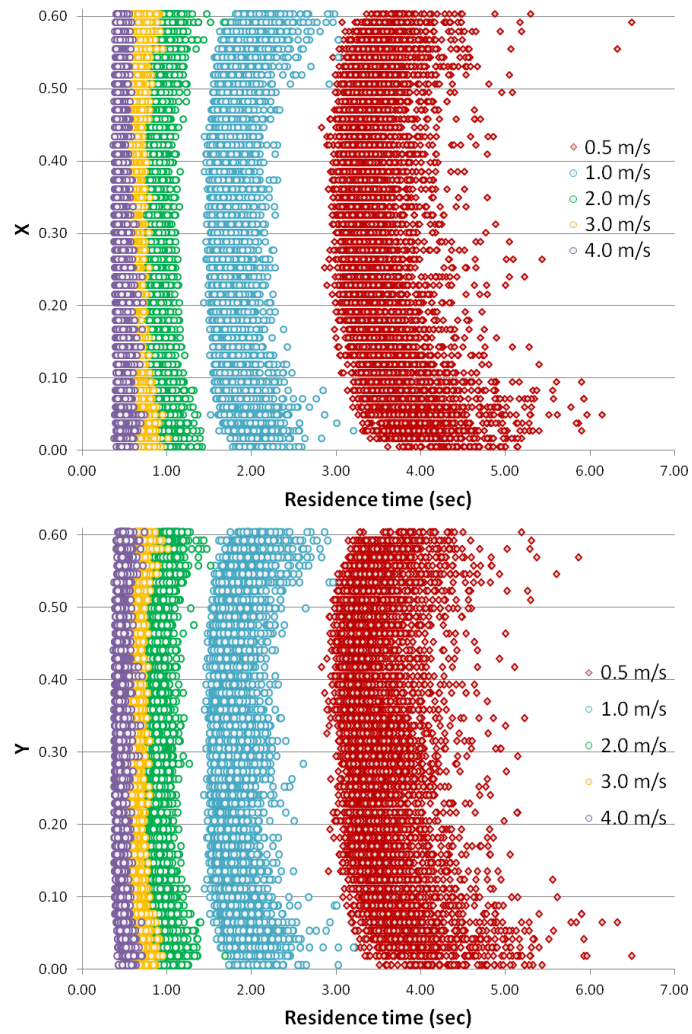
Appendix-Figure 1 Particle residence time and position at the outlet for the EPA 600/R-06/050.

Appendix-Table 2 EPA/R-06/051 specifications table.

Spec	600/R-06/051
Number of lamps	4
Lamp power watts	25
Lamp UVC power watts	8.5
Total system power	100
Total system UV power	34
Lamp length cm	53.82
Lamp diameter	1.9 cm T6
Duct size	61 cm x 61 cm
Duct length	7.83 m
Duct wall Emissivity	0.85
Duct wall Reflectivity	15%
Duct wall refractive index	1
Performance constant R'	17.18
PER	0.50
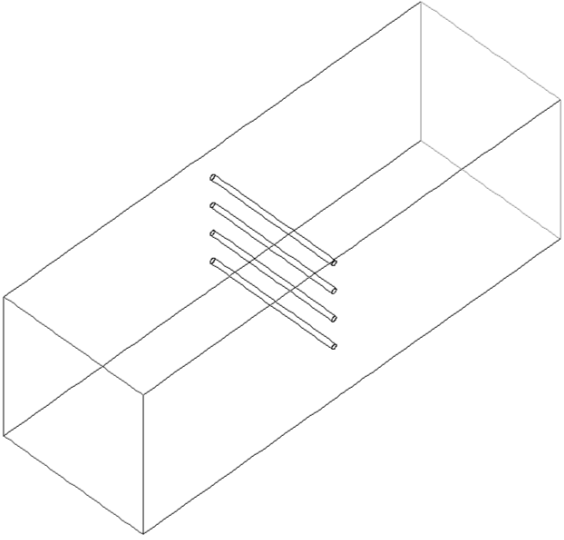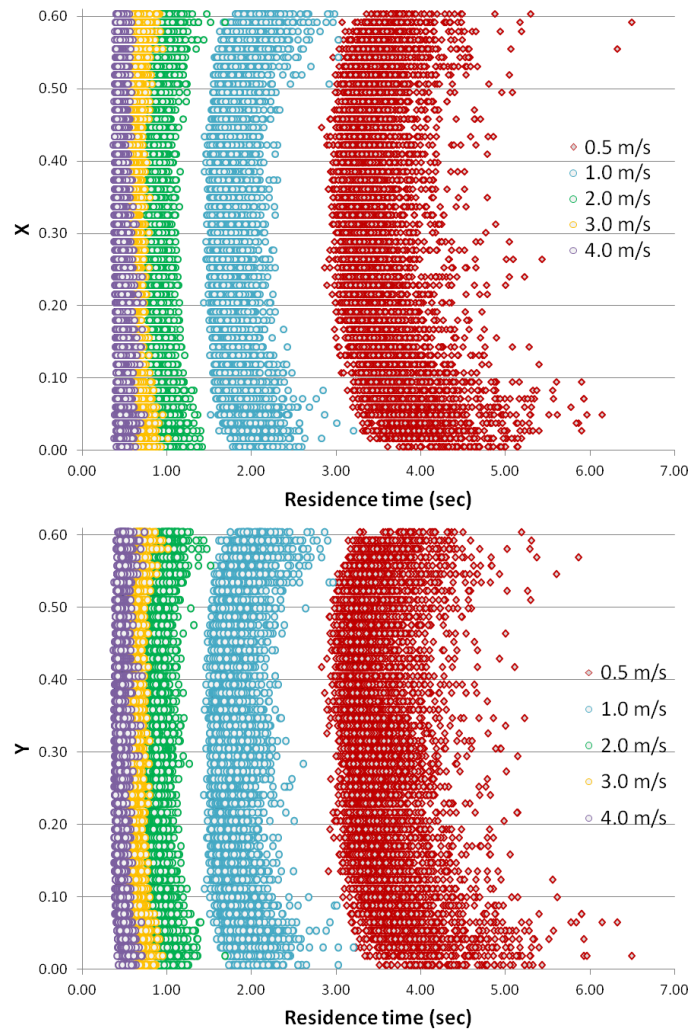
Appendix-Figure 2 Particle residence time and position at the outlet for the EPA 600/R-06/051.

Appendix-Table 3 EPA/R-06/055 specifications table.

Spec	600/R-06/055
Number of lamps	8
Lamp power watts	60
Lamp UVC power watts	18
Total system power	480
Total system UV power	144
Lamp length cm	61
Lamp diameter	1.9 cm T6
Duct size	61 cm x 61 cm
Duct length	7.83 m
Duct wall Emissivity	0.85
Duct wall Reflectivity	15%
Duct wall refractive index	1
Performance constant R'	65.20
PER	0.45
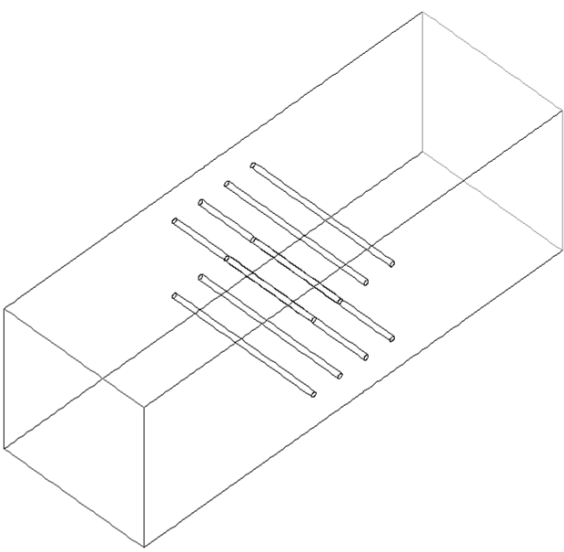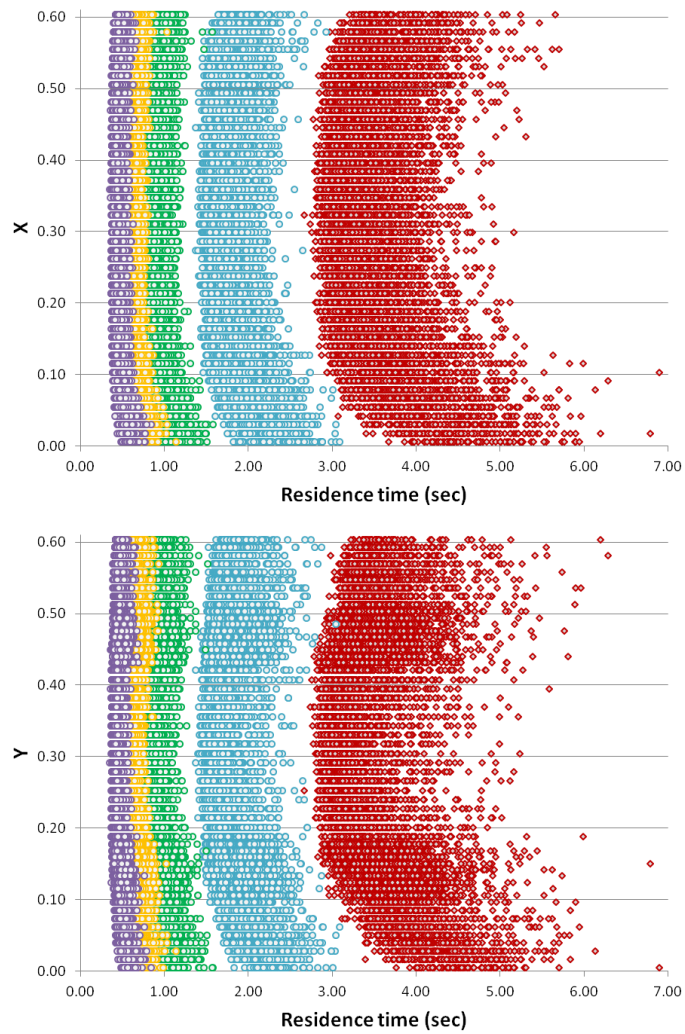
Appendix-Figure 3 Particle residence time and position at the outlet for the EPA 600/R-06/055.

Appendix-Table 4 L2H2 parallel specifications table.

Spec	L2H2 Parallel
Number of lamps	1
Lamp power watts	58
Lamp UVC power watts	19
Total system power	58
Total system UV power	19
Lamp length cm	53.3
Lamp diameter	1.9 cm T6
Duct size	61 cm x 61 cm
Duct length	7.83 m
Duct wall Emissivity	0.85
Duct wall Reflectivity	15%
Duct wall refractive index	1
Performance constant R'	15.40
PER	0.81
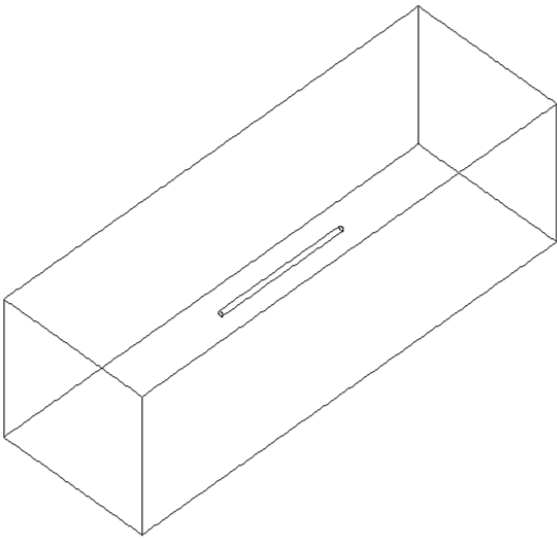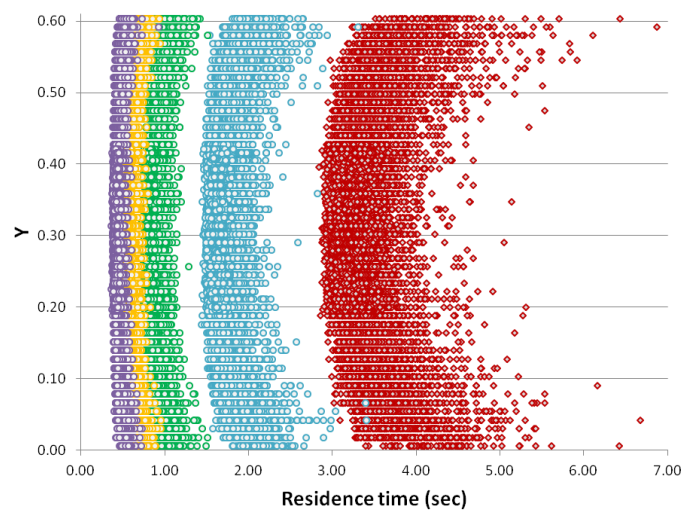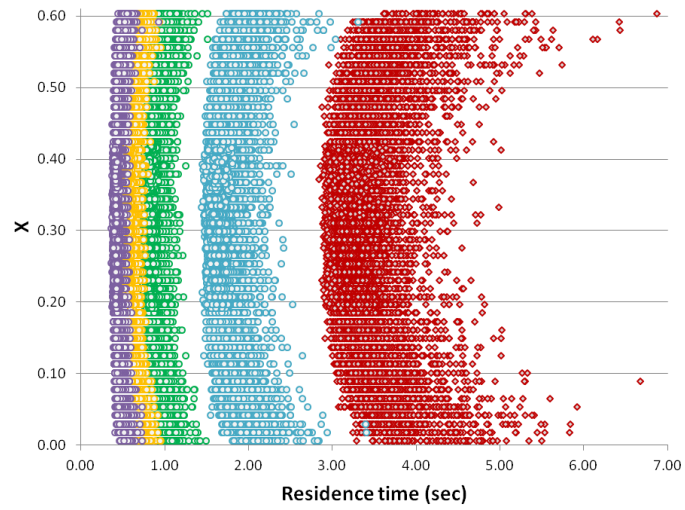
Appendix-Figure 4 Particle residence time and position at the outlet for the L2H2 parallel lamp configuration.

Appendix-Table 5 P01-L1H4L2H2L3H4 specifications table.

Spec	P01
Number of lamps	3
Lamp power watts	58
Lamp UVC power watts	19
Total system power	174
Total system UV power	57
Lamp length cm	53.3
Lamp diameter	1.9 cm T6
Duct size	61 cm x 61 cm
Duct length	7.83 m
Duct wall Emissivity	0.85
Duct wall Reflectivity	15%
Duct wall refractive index	1
Performance constant R'	26.40
PER	0.46

Appendix-Table 6 P02-L1H4L2H2L3H0 specifications table.

Spec	P02
Number of lamps	3
Lamp power watts	58
Lamp UVC power watts	19
Total system power	174
Total system UV power	57
Lamp length cm	53.3
Lamp diameter	1.9 cm T6
Duct size	61 cm x 61 cm
Duct length	7.83 m
Duct wall Emissivity	0.85
Duct wall Reflectivity	15%
Duct wall refractive index	1
Performance constant R'	26.23
PER	0.46

Appendix-Table 7 P03-L1H4L2H4L3H4 specifications table.

Spec	P03
Number of lamps	3
Lamp power watts	58
Lamp UVC power watts	19
Total system power	174
Total system UV power	57
Lamp length cm	53.3
Lamp diameter	1.9 cm T6
Duct size	61 cm x 61 cm
Duct length	7.83 m
Duct wall Emissivity	0.85
Duct wall Reflectivity	15%
Duct wall refractive index	1
Performance constant R'	25.09
PER	0.45
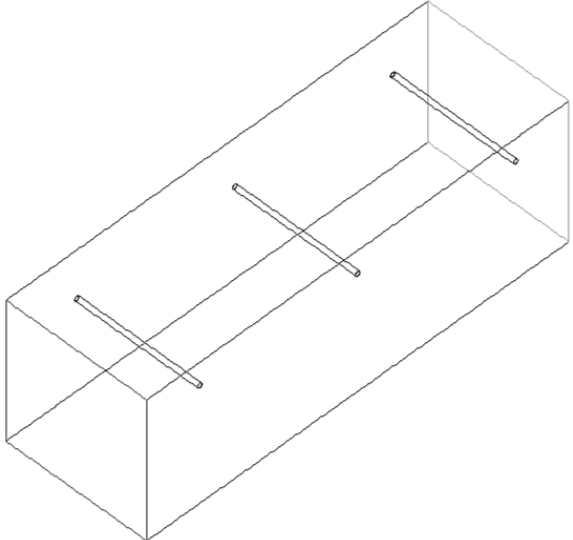
Appendix-Table 8 P04-L1H2L2H2L3H2 specifications table.

Spec	P04
Number of lamps	3
Lamp power watts	58
Lamp UVC power watts	19
Total system power	174
Total system UV power	57
Lamp length cm	53.3
Lamp diameter	1.9 cm T6
Duct size	61 cm x 61 cm
Duct length	7.83 m
Duct wall Emissivity	0.85
Duct wall Reflectivity	15%
Duct wall refractive index	1
Performance constant R'	28.08
PER	0.49
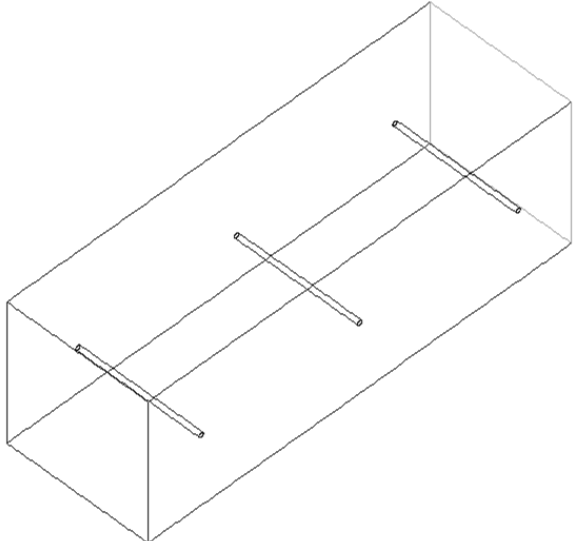
References

ABDALLAH, A. M., RASHID, M., ADROUB, S. A., ARNOUX, M., ALI, S. & SOOLINGEN, D. V. 2012. Complete Genome Sequence of Mycobacterium phlei Type Strain RIVM601174. *Journal of Bacteriology,* 194**,** 12.

ALFANO, O. M. & CASSANO, A. E. 2008. Photoreactor Modeling: Applications to Advanced Oxidation Processes. *International Journal of Chemical Reactor Engineering,* 6**,** 20.

ANSYS, I. 2009. *5.3.6 Discrete Ordinates (DO) Radiation Model Theory* [Online]. Available: https://www.sharcnet.ca/Software/Fluent12/html/th/node115.htm.

ANSYS, I. 2011. *ANSYS FLUENT Theory Guide*, ANSYS, Inc.

ASHRAE 2003. *ASHRAE HVAC Applications handbook,* Atlanta, GA.

ASHRAE 2007. *Chapter 7 Health Care Facilities*, ASHRAE.

ASHRAE 2008a. 3.3.6   ASHRAE Handbook Chapter 16: Ultraviolet lamp systems. American Society of Heating, Refrigeration and Air Conditioning.

ASHRAE 2008b. Air Cleaners for Particulate Contaminants. *ASHRAE Handbook - HVAC System and Equipment.*

ASHRAE 2009a. Chapter 11 Air Contaminants. *ASHRAE Applications Handbook***,** 22.

ASHRAE 2009b. Chapter 29 Industrial Gas Cleaning And Air Pollution Control. *ASHRAE Applications Handbook***,** 30.

ASHRAE 2011. *Chapter 60 Ultraviolet Air and Surface Treatment*.

BARKER, J., STEVENS, D. & BLOOMFIELD, S. F. 2001. Spread and prevention of some common viral infections in community facilities and domestic homes. *Journal of Applied Microbiology,* 91**,** 7-21.

BARTL, J. & BARANEK, M. 2004. Emissivity of aluminium and its importance for radiometric measurement. *Measurement of Physical Quantities,* 43**,** 3136.

BEEBE, J. M. 1959. Stability of disseminated aerosols of *Pasteurella tularensis* subjected to simulated solar radiations at various humidities. *J Bacteriol,* 78**,** 7.

BEEBE, J. M. & PIRSCH, G. W. 1958. Response of air-borne species of *Pasteurella* to artificial radiation simulating sunlight under different conditions of relative humidity. *Appl Microbiol,* 6**,** 12.

BEGGS, C. B. 2003. The Airborne Transmission of Infection in Hospital Buildings: Fact or Fiction? *Indoor and Built Environment,* 12**,** 9.

BEGGS, C. B., FLETCHER, L. A., SLEIGH, P. A., KERR, K. G. & NOAKES, C. An experimental method for determining the UV susceptibility of airborne microorganisms using an upper room UV field. Proceedings of the 2nd International Congress on Ultraviolet Technologies, 9-11 th July 2003 Vienna.

BEGGS, C. B., KERR, K. G., DONNELLY, J. K., SLEIGH, P. A., MARA, D. D. & CAIRNS, G. 2000. An engineering approach to the control of Mycobacterium tuberculosis and other airborne pathogens: a UK hospital based pilot study. *Transactions of the Royal Society of Tropical Medicine and Hygiene,* 94**,** 5.

BEGGS, C. B., NOAKES, C. J., SLEIGH, P. A., FLETCHER, L. A. & KERR, K. G. 2005. Methodology for determining the susceptibility of airborne microorganism to irradiation by an upper-room UVGI system. *Journal of Aerosol Science***,** 18.

BERNSTEIN, R. S., SORENSON, W. G., GARABRANT, D., REAUX, C. & TREITMAN, R. D. 1983. Exposures to Respirable, Airborne Penicillium from a Contaminated Ventilation System: Clinical, Environmental and Epidemiological Aspects. *American Industrial Hygiene Association,* 44**,** 9.

BLATCHLEY 1997. Numerical Modelling of UV Intensity: Application to Collimated-Beam Reactors and Continuous-Flow Systems. *Wat. Res.,* 31**,** 14.

BLATT, M. H. 2006. Avanced HVAC Systems for Improving Indoor Environmental Quality and Energy Performance of California K-12 Schools; Applications Guide for Off-the-Shelf Equipment for UVC Use. California Energy Commission.

BOLTON, J. R. 2000. Calculation of Ultraviolet Fluence Rate Distribution in an Annular Reactor: Significance of Refraction and Reflection. *Wat. Res.,* 34**,** 10.

BOLTON, J. R. 2001. *Ultraviolet Applications Handbook*.

BOLTON, J. R. & COTTON, C. A. 2001. *The ultraviolet Disinfection Handbook*, American Waterworks Association.

BOLTON PHOTOSCIENCE INC. 2011. *UVCalc Software* [Online]. Available: https://secure40.securewebsession.com/boltonuv.com/store/soft.php 2011].

BOSHOF, H. I. M., REED, M. B., ILL, C. E. B. & MIZRAHI, V. 2003. DnaE2 Polymerase Contributes to In Vivo Survival and the Emergence of Drug Resistance in Mycobacterium tuberculosis. *Cell,* 113**,** 11.

BRINKLE, J. T., SELVIN, S., HODGSON, A. T., FISK, W. J., MENDELL, M. J., KOSHLAND, C. P. & DAISEY, J. M. 1998. Development of New Volatile Organic Compound (VOC) Exposure Metrics and their Relationship to "Sick Building Syndrome" Symptoms. *Indoor air,* 8**,** 13.

BROWN, J. W., MANTE, S. & PASSON, T. J. 1996. Sick-building syndrome and building-related illness.(New and Emerging Pathogens, part 6). *Medical Laboratory Observer***,** 11.

BSI EN 1822-1:2009 2009. High efficiency air filters (EPA, HEPA and ULPA). *Part 1: Classification, performance testing, marking.*

CAMFIL FARR 2002. ASHRAE Testing for HVAC Air Filtration A Review of Standards 52.1-1992 & 52.2-1999. *Technical Services Bulletin.* Camfil Farr.

CAMFIL FARR. 2011. *Energy & Air quality rating* [Online]. Available: http://www.camfilfarr.com/Filter-technology/Energy-Savings/Energy--Air-quality-rating/ [Accessed August 2011].

CASARETT, A. 1968. *Radiation Biology,* Englewood, Prentice-Hall.

CASSANO, A. E., MARTIN, C. A., BRANDI, R. J. & ALFANO, O. M. 1995. Photoreactor Analysis and Design: Fundamentals and Applications. *Ind. Eng. Chem. Res,* 34**,** 47.

CAUL, E. O. 1994. Small round structured viruses: airborne transmission and hospital control. *The Lancet,* 343**,** 1240-1242.

CDC, C. F. D. C. A. P. 2011. *General Information. Escherichia coli (E. coli)* [Online]. Available: http://www.cdc.gov/ecoli/general/index.html [Accessed 09 December 2013].

COLLINS, F. M. 1971. Relative Susceptibility of Acid-Fast and Non-Acid-Fast Bacteria to Ultraviolet Light. *Applied and Environmental Microbiology,* 21**,** 3.

COOLEY, J., WONG, W., JUMPER, C. & STRAUS, D. 1998. Correlation between the prevalence of certain fungi and sick building syndrome. *Occupational and Environmental Medicine,* 55**,** 6.

CURTISA, L., CALIA, S., CONROYA, L., BAKERA, K., OUA, C.-H., HERSHOWB, R., NORLOCK-CRUZA, F. & SCHEFF, P. 2005. Aspergillus surveillance project at a large tertiary-care hospital. *Journal of Hospital Infection,* 59**,** 9.

CHANG, D. & YOUNG, C. 2007. Effect of turbulence on Ultraviolet Germicial Irradiation. *Journal of Architectural Engineering,* 13**,** 10.

CHANG, J., OSSOFF, S., LOBE, D., DORFMAN, M., DUMAIS, C., QUALLS, R. & JOHNSON, J. 1985. UV innactivation of pathogenic and indicator microorganisms. *Applied and Environmental Microbiology,* 49**,** 6.

CHICK, E. W., HUDNELL, A. B. & SHARP, D. G. 1963. Ultraviolet sensitivity of fungi associated with mycotic keratitis and other mycoses. *Sabouviad,* 2**,** 6.

DALY, B. B. 1992. *Woods Practical Guide to Fan Engineering*.

DAVID, H. L., JONES, W. D. & NEWMAN, C. M. 1971. Ultraviolet Light Inactivation and Photoreactivation in the Mycobacteria. *Infection and Immunity,* 4**,** 2.

DEPARTMENT OF HEALTH, D. 2008. Clean, safe care: Reducing infections and saving lives. NHS.

DURAN, J. E. 2010. *Development of a CFD-Based model for the simulation of immobilized photocatalytic reactors for water treatment.* PhD, The University of British Columbia.

ENGLAND, P. H. 2014. *Pseudomonas aeruginosa* [Online]. Available: http://www.hpa.org.uk/Topics/InfectiousDiseases/InfectionsAZ/PseudomonasAeruginosa/ [Accessed 08 March 2014].

EPA 1997. An Office Building Occupant's Guide to Indoor Air Quality. EPA.

EPA 2006a. EPA 600/R-06/050. Technology Evaluation Report. Biological Innactivation Efficiency by HVAC In-Duct Ultraviolet Light Systems. Dust Free Bio-Fighter 4Xtreme, model 21.

EPA 2006b. EPA 600/R-06/051 Biological Inactivation Efficiency by HVAC In-Duct Ultraviolet Light Systems Atlantic Ultraviolet Corporation Aerologic Model AD24-4. EPA.

EPA 2006c. EPA 600/R-06/055 Biological Innactivation Efficiency by HVAC In-Duct Ultraviolet Light Systems. Lumalier ADPL-60-8. EPA.

ESCOMBE, A. R., MOORE, D. A. J., GILMAN, R. H., NAVINCOPA, M., TICONA, E., MITCHELL, B., NOAKES, C., MARTINEZ, C., SHEEN, P., RAMIREZ, R., QUINO, W., GONZALEZ, A., FRIEDLAND, J. S. & EVANS, C. A. 2009. Upper-Room Ultraviolet Light and Negative Air Ionization to Prevent Tuberculosis Transmission. *PLoS MEDICINE,* 6**,** 12.

FINNEGAN, M. J., PICKERING, C. A. C. & BURGE, P. S. 1984. The sick building syndrome: prevalence studies. *British Medical Journal,* 289**,** 3.

FISK, W. J., FAULKNER, D., PALONEN, J. & SEPPANEN, O. 2002. Performance and Cost of Particle Air Filtration Technologies. *Indoor air,* 12**,** 12.

FLETCHER, L. A. 2004. The influence of relative humidity on the UV susceptibility of airborne gram negative bacteria. *IUVA News,* 6**,** 7.

FLETCHER, L. A., NOAKES, C. J. & BEGGS, C. B. The importance of Bioaerosols in Hospital Infections and the Potential for Control using Germicidal Ultraviolet Irradiation. Proceedings of the 1st seminar on Applied Aerobiology, 2004.

FLETCHER, L. A., NOAKES, C. J., BEGGS, C. B., SLEIGH, P. A. & KERR, K. G. 2003. The Ultraviolet Susceptibility of Aerolised Microorganisms and the Role of Photoreactivation. *Second international congress of the IUVA.* Vienna.

FOARDE, K., FRANKE, D., WEBBER, T., HANLEY, J. & OWEN, K. 2006. Biological Inactivation Efficiency by HVAC In-Duct Ultraviolet Light Systems: Steril-Aire, Inc. Model SE 1 VO with GTS 24 VO Emitter. *Technology Report.* EPA.

FOARDE, K. K. & HANLEY, J. T. 1999. Determine the efficacy of antimicrobial treatments of fibrous air filters. RTI.

FRITZE, D. & PUKALL, R. 2001. Reclassification of Bioindicator Strains Bacillus subtilis DSM 675 and Bacillus subtilis DSM 2277 as Bacillus atrophaeus. *International Journal of Systematic and Evolutionary Microbiology,* 51**,** 35-37.

GILKESON, C. A. & NOAKES, C. J. 2013. Applications of CFD Simulation to Predicting Upper-room UVGI. *Photochemistry and Photobiological*.

GILLIS, H. L. 1973. *Photoreactivation and ultraviolet inactivation of Mycobacteria in air.* MSc, Georgia Institute of Technology.

GOVAN, HUGHES & VANDAMME 1996. Burkholderia cepacia: medical, taxonomic and ecological issues. *J. Med. Microbiol,* 45**,** 13.

GRANGE, J. M., YATES, M. D. & KANTOR, I. N. D. 1996. Guidelines for speciation within the *Mycobacterium tuberculosis* complex. Second edition. World Health Organization.

GUSTAVSSON, J. 2000. Air Filters and IAQ. Camfil Farr.

GUTIERREZ, R. L., BOURGEOUS, K. N., SALVESON, A., MEIR, J. & SLATER, A. 2006. Microwave UV: A new wave of tertiary disinfection. *WEFTEC***,** 12.

HARSTAD, J., DECKER, H. M. & WEDUM, A. G. 1954. Use of ultraviolet irradiation in a room air conditioner for removal of bacteria. *Am Ind Hyg Assoc J,* 2**,** 4.

HEREAUS NOBLELIGHT 2007. Ultraviolet lamps for disinfection and oxidation.

HM GOVERNMENT 2011. Carbon Plan.

HO, C. K. 2009a. Evaluation of the reflection and refraction in simulations of UV disinfection using the discrete ordinates radiation model. *Water Science and Technology,* 59**,** 8.

HO, C. K. 2009b. Radiation Dose Modeling in Fluent. *WEF Disinfection 2009 Workshop: Modeling UV Disinfection using CFD.* University of North Carolina (UNC): Sandia National Laboratories.

HO, Y. S., ADROUB, S. A. & ALEISA, F. 2012. Complete Genome Sequence of *Mycobacterium fortuitum* subsp. *fortuitum* Type Strain DSM46621. *Journal of Bacteriology,* 194**,** 2.

HODGSON, A. T., DESTAILLATS, H., HOTCHI, T. & FISK, W. J. 2008. Benefits and technological challenges in the implementation of TiO2-based ultraviolet photocatalytic oxidation (UVPCO) air cleaners. *Indoor air 2008.* Copenhagen, Denmark.

HODGSON, A. T., SULLIVAN, D. P. & FISK, W. J. 2005. Parametric Evaluation of an Innovative Ultra-violet photocatalytic oxidation (UVPCO) air cleaning technology for indoor applications. Lawrence Berkeley National Laboratory.

IEA 2010. Energy Performance Certification of Buildings: A policy tool to improve energy efficiency. Paris: International Energy Agency.

IMOBERDORF, G. E., TAGHIPOUR, F. & MOHSENI, M. 2008. Radiation field modeling of multi-lamp, homogeneous photoreactors. *Journal of Photochemistry and Photobiology A: Chemistry,* 198**,** 10.

IRAZOQUI, H. A., CERDA, J. & CASSANO, A. E. 1973. Radiation Profiles in an Empty Annular Photoreactor with a Source of Finite Spatial Dimensions. *AIChE Journal,* 19**,** 8.

IRAZOQUI, H. A., CERDA, J. & CASSANO, A. E. 1976. The Radiation Field for the Point and Line Source Approximations and the Three-dimensional Source Models: Applications to Photoreactions. *The Chemical Engineering Journal,* 11**,** 11.

IUVA 2005a. General Guideline for UVGI Air and Surface Disinfection Systems. Ontario, Canada: International Ultraviolet Association.

IUVA 2005b. Guideline for the Design and Installation of UVGI In-duct Air Disinfection Systems in New Building Construction. International UV Association.

IUVA 2005c. Guideline for the Design and Installation of UVGI In-duct Air Disinfection Systems.: IUVA.

IUVA 2005d. Guideline for the Design and Installation of UVGI Unitary Recirculation and Air Disinfection Systems. IUVA.

IUVA 2005e. Medium Pressure and Low Pressure wave length spectrum.

JENSEN, M. M. 1964. Inactivation of airborne viruses by ultraviolet irradiation. *Applied Microbiology***,** 3.

KARLSSON, B. & RIBBING, C. G. 1982. Optical constants and spectral selectivity of stainless steel and its oxides. *Journal of Applied Physics,* 53**,** 6340-6346.

KE, Q. S., CRAIK, S. A., EL-DIN, M. G. & BOLTON, J. R. 2009. Development of a Protocol for the Determination of the Ultraviolet Sensitivity of Microorganisms Suspended in air. *Aerosol Science and Technology,* 43**,** 6.

KERR, J. H. & BARRET, T. L. 2010. Atypical Mycobacterial diseases. *Military Dermatology Text book.*

KETHLEY, T. 1979. Feasibility Study of Germicidal UV Lamps for Air Disinfection in Simulated Patient Care Rooms. San Francisco, Ca: American Public Health Association.

KIMA, K. Y. & KIM, C. N. 2006a. Airborne microbiological characteristics in public buildings of Korea. *Building and Environment,* 42**,** 9.

KIMA, K. Y. & KIM, C. N. 2006b. General of airborne bacteria and fungi identified in the public buildings regulated in Korea *In:* KOREA, G. O. A. B. A. F. I. I. T. P. B. R. I. (ed.).

KING, M. F., NOAKES, C. J., SLEIGH, P. A. & CAMARGO-VALERO, M. 2013. Bioaerosol Deposition in Single and Two-bed Hospital Rooms: A Numerical and Experimental Study. *Building and Environment,* 59**,** 11.

KO, G., FIRST, M. W. & BURGE, H. A. 2000. Influence of relative humidity on particle size and UV sensitivity of serratia marcescens and Mycobacterium bovis BCG aerosols. *Tubercle and lung disease,* 80**,** 12.

KOLLER, L. R. 1939. Bactericidal Effects of Ultraviolet Radiation Produced by Low Pressure Mercury Vapor Lamps. *Journal of Applied Physics,* 10**,** 624-630.

KOWALSKI, W. 2009a. *Ultraviolet Germicidal Irradiation Handbook*, Springer.

KOWALSKI, W. 2009b. Ultraviolet Germicidal Irradiation Handbook. 1 ed.: Springer.

KOWALSKI, W. J. 2003. *Immune building systems technology,* New York, Mc Graw Hill.

KOWALSKI, W. J. 2009c. Exposure limits for UV irradiation.

KOWALSKI, W. J. & BAHNFLETH, W. P. 2000a. Effective UVGI System Design Through Improved Modelling. *Transactions - American Society of Heating Refrigerating and Air Conditioning Engineers,* 106**,** 10.

KOWALSKI, W. J. & BAHNFLETH, W. P. 2000b. UVGI Design Basics for air and surface disinfection. *HPAC engineering***,** 10.

KOWALSKI, W. J., BAHNFLETH, W. P., WITHAM, D. L., SEVERIN, B. F. & WHITTAM, T. S. 2001. Mathematical Modelling of Ultraviolet Germicidal Irradiation for Air Disinfection. *Quantitative Microbiology,* 2**,** 22.

KUMARI, D. N. P., HAJI, T. C., KEER, V., HAWKEY, P. M., DUNCANSON, V. & FLOWER, E. 1998. Ventilation grilles as a potential source of methicillin-resistant Staphylococcus aureus causing an outbreak in an orthopaedic ward at a district general hospital *Journal of Hospital Infection,* 39**,** 7.

LAI, K., BURGE, H. A. & FIRST, M. 2004. Size and UV germicidal irradiation susceptibility of Serratia marcescens when aerosolized from different suspending media. *Applied and Environmental Microbiology,* 70**,** 8.

LAU, J. 2009. *Lamp and In-Duct Device Modelling For UVGI Systems Performance Prediction.* Doctor of Philosophy, The Pennsylvania State University.

LEE, B., BAHNFLETH, W. & AUER, K. Life-Cycle Cost Simulation of In-Duct Ultraviolet Germicidal Irradiation Systems. Proceedings of Building Simulation, 2009 Glasgow, Scotland.

LEEDS, U. O. 2010. *Fantastic and unique swimming pool* [Online]. Leeds. Available: http://sport.leeds.ac.uk/page.asp?section=64&sectionTitle=Swimming+Pool [Accessed 09 August 2011].

LI, C.-S. & KUO, Y.-M. 1992. AIRBORNE CHARACTERIZATION OF FUNGI INDOORS AND OUTDOORS. *Aerosol Sci,* 23**,** 4.

LIGHTSOURCES. 2009. *Products Data Sheets* [Online]. Available: http://www.germicidal.com/datasheets.php#ho [Accessed 25 November 2009 2009].

LIU, D. 2004. *Numerical simulation of UV Disinfection Reactors: Impact of Fluence Rate Distribution and Turbulence Modelling.* PhD, North Carolina State university.

LIU, D., WU, C., LINDEN, K. & JOEL, D. 2007. Numerical simulation of UV disinfection reactors: Evaluation of alternative turbulence models. *Applied Mathematical Modelling,* 31**,** 16.

LUCKIESH, M. 1946. *Applications of Germicidal, Erythemal and Infrared Energy*.

LUCKIESH, M., TAYLOR, A. H., T., K. & ET., L. 1949. Inactivation of molds by germicidal ultraviolet energy. *J Franklin Inst,* 248**,** 14.

MENDELL, M., FISK, W., KREISS, K., LEVIN, H., ALEXANDER, D., CAIN, W., GIRMAN, J., HINES, C., JENSEN, P., MILTON, D., REXROAT, L. & WALLINGFORD, K. 2002. Improving the Health of Workers in Indoor Environments: Priority Research Needs for a National Occupational Research Agenda. *Public Health Matters,* 92.

MENZIES, D. 1997. SPECIFIC ILLNESSES KNOWN OR SUSPECTED TO BE RELATED TO BUILDINGS.

MENZIES, D., PASZTOR, J., RAND, T. & BOURBEAU, J. 1999. Germicidal ultraviolet irradiation in air conditioning systems: effect on office worker health and wellbeing: a pilot study. *Occupational and Environmental Medicine,* 56**,** 6.

MENZIES, D., POPA, J., HANLEY, J. A., RAND, T. & MILTON, D. K. 2003. Effect of ultraviolet germicidal lights installed in office ventilation systems on workers' health and wellbeing: double-blind multiple crossover trial. *THE LANCET,* 362**,** 7.

MILLER, S. C. M., LIPUMA, J. J. & PARKE, J. L. 2002. Culture based and Non-Growth Dependent Detection of the Burkholderia cepacia complex in Soil Environments. *Applied and Environmental Microbiology,* 68**,** 9.

MILLER, S. L., LINNES, J. & LUONGO, J. 2013. Ultraviolet germicidal irradiation: future directions for air disinfection and building applications. *Photochemistry and photobiology,* 89**,** 777-781.

MUNAKATA, N. & RUPERT, C. 1975. Effects of DNA-polymerase-defective and recombination-deficient mutations on the ultraviolet sensitivity of Bacillus Subtillis spores. *Mutat Res,* 27**,** 13.

NAKAMURA, H. 1987. Sterilization efficacy of ultraviolet irradiation on microbial aerosols under dynamic airflow by experimental air conditioning systems. *Bull Tokyo Med Dent Univ,* 34**,** 16.

NAKAMURA, L. K. 1989. Taxonomic Relationship of Black-Pigmented Bacillus subtilis Strains and a Proposal for Bacillus atrophaeus sp. nov. *international journal of systematic Bacteriology,* 39**,** 295-300.

NATIONAL AUDIT OFFICE 2004. Improving patient care by reducing the risk of hospital acquired infection: A progress report. Ordered by the House of Commons.

NEIDLE, S. 1999. *Oxford Handbook of Nucleic Acid Structure,* New York, Oxford University Press.

NHS. 2008. *Smart Solutions For HCAI - Frequently Asked Questions* [Online]. 2008. Available: http://www.smartsolutionsforhcai.co.uk/faq.htm 2008].

NICHOLSON, W. L. & GALEANO, B. 2003. UV Resistance of Bacillus anthracis spores Revisited: Validation of Bacillus spores as UV Surrogates for Spores of B. anthracis Sterne. *Applied and Environmental Microbiology,* 69**,** 4.

NOAKES, C. J., BEGGS, C. B. & SLEIGH, P. A. 2004. Modelling the Performance of Upper Room Ultraviolet Germicidal Irradiation Devices in Ventilated Rooms: Comparison of Analytical and CFD Methods. *Indoor and Built Environment,* 13**,** 12.

NOAKES, C. J., FLETCHER, L. A., BEGGS, C. B., SLEIGH, P. A. & KERR, K. G. 2003. Development of a numerical model to simulate the biological inactivation of airborne microorganisms in the presence of ultraviolet light. *Journal of Aerosol Science,* 35**,** 19.

NTC, N. T. C. 2007. Tuberculosis Infection Control: A practical manial for preventing TB. San Francisco: The Francis J. Curry National Tuberculosis Center.

PAREEK, V. K. 2004. Light Intensity Distribution in a Phototcatalytics Reactor Using Finite Volume. *AIChE Journal,* 50**,** 16.

PASTUSZKA, J., PAW, U. K. T., LIS, D. O., WLAZLO, A. & UFIG, K. 1999. Bacterial and fungal aerosol in indoor environment in Upper Silesia, Poland. *Atmospheric Environment,* 34**,** 10.

PECCIA, J. & HERNANDEZ, M. 2001. Photoreactivation in Airborne *Mycobacterium parafortuitum*. *Applied and Environmental Microbiology,* 67**,** 8.

PECCIA, J. & HERNANDEZ, M. 2004. UV-Induced Inactivation Rates for Airborne *Mycobacterium bovis* BCG. *Journal of Occupational and Environmental Hygiene,* 1**,** 7.

PECCIA, J., WORTH, H. M., MILLER, S. & HERNANDEZ, M. 2001. Effects of relative humidity on the ultraviolet induced inactivation of airborne bacteria. *Aerosol Science and Technology,* 35**,** 13.

PERAL, J., DOMENECH, X. & OLLIS, D. F. 1997. Heterogeneous Photocatalysis for the purification, decontamination and deodorization of air. *J. Chem. Technol. Biotechnol***,** 23.

PEREZ, A. R. & MELLO, K. P. A. A.-D. 2000. SpoIIB Localizes to Active Sites of Septal Biogenesis and Spatially Regulates Septal Thinning during Engulfment in Bacillus subtilis. *Journal of Bacteriology,* 182**,** 12.

PHILIPS 2005. Effects of air temperature and air velocity on a model TUV36W-PLL.

PHILIPS 2007. UV Disinfection - Application Information. *In:* CATALOGUE, P. (ed.). Philips.

PRIVATE HEALTHCARE UK. 2005. *MRSA : Statistics in UK and Europe* [Online]. Private Healthcare UK. Available: http://www.privatehealth.co.uk/hospitaltreatment/treatment-abroad/mrsa-europe/ [Accessed 12 May 2008 2009].

PURCHAS, D. B. & SUTHERLAND, K. 2002. *Handbook of filter media*, Elsevier Science.

REDLICH, C. A., SPARER, J. & CULLEN, M. R. 1997. Sick-building syndrome. *The Lancet,* 349**,** 1013-1016.

RENTSCHLER, H. & NAGY, R. 1942. Bactericidal action of ultraviolet radiation on air-borne microorganisms. *Journal of Bacteriology,* 44**,** 85-94.

RILEY, R., WELLS, W., MILLS, C., NYKA, W. & MCLEAN, R. 1957. Air hygiene in tuberculosis: quantitative studies of infectivity and control in a pilot ward. *American review of tuberculosis,* 75**,** 420-431.

RILEY, R. L. 1961. AIRBORNE PULMONARY TUBERCULOSIS. *Bacteriological Reviews,* 25, 243-248.

RILEY, R. L. 1974. Airborne Infection. *The American Journal of Medicine,* 57**,** 10.

RILEY, R. L., KNIGHT, M. & MIDDLEBROOK, G. 1976. Ultraviolet susceptibility of *BCG* and virulent *tubercle bacilli*. *American Review of Respiratory Disease,* 113**,** 6.

ROSTRON, J. 1997. *Sick building syndrome : concepts, issues, and practice,* London, E & FN Spon.

RUTALA, W. A., KATZ, E. B., SHERERTZ, R. J. & JR, F. A. S. 1983. Environmental study of a methicillin-resistant Staphylococcus aureus epidemic in a burn unit. . *Journal of Clinical Microbiology,* 18**,** 6.

RYAN, K., RAY, C. G., AHMAD, N., DREW, W. L. & PLORDE, J. 2010. *Sherris Medical Microbiology*, McGraw Hill.

RYER, A. 1998. *Light Measurement Handbook,* Newbury, MA, International Light.

SAGRIPANTI, J.-L. & LYTLE, C. D. 2010. Sensitivity to ultraviolet radiation of Lassa, vaccinia, and Ebola viruses dried on surfaces. *Arch Virol,* 156**,** 6.

SCHAAL, K. P. 1991. Medical and microbiological problems arising from airborne infection in hospitals. *Journal of Hospital Infection,* 18**,** 9.

SGALARI, G., CAMERA-RODA, G. & SANTARELLI, F. 1998. Discrete Ordinate Method in the Analysis of Radiative Transfer in Photocatalytically Reacting Media. *Int. Comm. Heat Mass Transfer,* 25**,** 10.

SHARP, G. 1940. The effects of ultraviolet light on bacteria suspended in air. *Journal of Bacteriology,* 38**,** 535-547.

SHAUGHNESSY, R., LEVETIN, E. & ROGERS, C. 1999. The effects of UV-C on biological contamination of AHUs in a commercial office building: Preliminary results. *Indoor Environ,* 99**,** 8.

SICHEL, C. 2009. Potential fo advance oxidation processes (AOPs) in disinfection and simultaneous emerging contaminants removal: a review. *5th International Congress on UV technologies.* Amsterdam: IUVA.

SKOV, P., VALBJØRN, O. & PEDERSEN, B. 1990. Influence of indoor climate on the sick building syndrome in an office environment. The Danish Indoor Climate Study Group. *Scand J Work Environ Health,* 5**,** 9.

SUMER, B. M. 2013. Lecture Notes on Turbulence. DTU Mekanik, Section for Fluid Mechanics, Coastal & Maritime Engineering Building 403, 2800 Lyngby, Denmark, bms@mek.dtu.dk: Technical University of Denmark.

SUTHERLAND, K. 2007a. Chapter 7. Other types of separation equipment. *Filters and Filtration Handbook.* 5th edition ed.: Elsevier Science.

SUTHERLAND, K. 2007b. *Filters and Filtration Handbook*, Elsevier Science.

TANG, J. W., LI, Y., EAMES, I., CHAN, P. K. S. & RIDGWAY, G. L. 2006. Factors involved in the aerosol transmission of infections and control ventilation in healthcare premises. *Journal of Hospital Infection,* 64**,** 15.

TAYLOR, G. J. S., BANNISTER, G. C. & LEEMING, J. P. 1995. Wound Disinfection With Ultraviolet Radiation. *Journal of hospital infection,* 30**,** 9.

TEEUW, K. B., VANDENBROUCKE-GRAULS, C. M. & VERHOEF, J. 1994. Airborne gram-negative bacteria and endotoxin in sick building syndrome. A study in Dutch governmental office buildings. *Archives of Internal Medicine,* 154.

TOMPKINS, D. T., LAWNICKI, B. J., ZELTNER, W. A. & ANDERSON, M. A. 2005. Evaluation of Photocatalysis for Gas-Phase Air Cleaning - Part 1: Process, Technical, and Sizing Considerations. *American Society of Heating, Refrigerating and Air-Conditioning Engineers, Inc Transactions,* III**,** 24.

TROJAN. 2011. *Trojan to Supply Australia's Largest Ultraviolet (UV) Disinfection System* [Online]. Available: http://www.trojanuv.com/about/news?id=819 [Accessed 09 August 2011].

TRONVILLE, P. 2006. Global Standard for Filter Testing. *ASHRAE Journal,* 48**,** 5.

TU, J., YEOH, G. H. & LIU, C. 2007. *Computational Fluid Dynamics*, Butterworth-Heinemann.

UK GOVERNMENT 2008. Climate Change Act 2008. *In:* GOVERNMENT, U. (ed.).

UNIVERSAL, E. 2009. Aeguradoras pagan 5.8 mdp por virus H1N1. *El Universal.mx*.

VANOSDELL, D. & FOARDE, K. 2002. Defining the Effectiveness of UV lamps Installed in Circulating Air Ductwork. Arlington, VA: Air-Conditioning and Refrigeration Technology Institute (ARTI).

VERSTEEG, H. K. & MALALASEKERA, W. 2007. *An Introduction to Computer Fluid Dynamic: The Finite Volume Method,* Harlow, Prentice Hall.

W.M. HAYNES, E. 2011. *CRC Handbook of Chemistry and Physics,* Boca Raton, FL, CRC Press/Taylor and Francis.

WALKER, C. & KO, G. 2007. Effect of Ultraviolet Germicidal Irradiation on Viral Aerosols. *Environ Sci Technol,* 41**,** 16.

WANG, B., MORTAZAVI, R. & HAGHIGHAT, F. 2008. Evaluation of Modelling and Measurement Techniques of Ultraviolet Germicidal Irradiation Effectiveness - Towards the Design of Immune Buildings. *Indoor and Built Environment,* 18**,** 12.

WARGOCKI, P., WYON, D. P., BAIK, Y. K., CLAUSEN, G. & OLEFANGER, P. 1999. Perceived Air Quality, Sick Building Syndrome (SBS) Symptoms and Productivity in an Office with Two Different Pollution Loads. *Indoor air,* 9**,** 20.

WARGOCKI, P., WYON, D. P., JANUNSDELL, CLAUSEN, G. & OLEFANGER, P. 2000. The Effects of Outdoor Air Supply Rate in an Office on Perceived Air Quality, Sick Building Syndrome (SBS) Symptoms and Productivity. *Indoor air,* 10.

WEBB, S. J. 1970. Differential, Lethal and Mutagenic Action of 254 nm and 320-400nm Radiation on Semi-Dried Bacteria. *Photochemistry and Photobiology,* 12**,** 24.

WEINSTEIN, R. A., BRIDGES, C. B., KUEHNERT, M. J. & HALL, C. B. 2003. Transmission of influenza: implications for control in health care settings. *Clinical Infectious Diseases,* 37**,** 1094-1101.

WHO. 2005. *Indoor air pollution and health* [Online]. Available: http://www.who.int/mediacentre/factsheets/fs292/en/.

WHO 2007. Tuberculosis. World Health Organization.

WHO 2009a. Epidemic and Pandemic Alert and Response (EPR) - Influenza A(H1N1) - Update 41. World Health Organization.

WHO 2009b. Global Tuberculosis Control 2009. World Health Organization.

XU, PECCIA, J., FABIAN, P., MARTYNY, J. W., KEVIN, F., HERNANDEZ, M. & MILLER, S. 2003. Efficacy of ultraviolet germicidal irradiation of upper-room air inactivating airborne bacterial spores and mycobacteria in full-scale studies. *Atmospheric Environment***,** 15.

YANG, L., LIU, Z., SHI, J., ZHANG, Y., HU, H. & SHANGGUAN, W. 2007. Degradation of indoor gaseous formaldehyde by hybrid VUV and TiO2/UV processes. *Separation and Purification Technology,* 54**,** 8.

YOUNG, D. F., MUNSON, B. R., OKIISHI, T. H. & HUEBSCH, W. W. 2010. *A Brief Introduction to Fluid Mechanics*, Hoboken: Wiley.

YU, I. T. S., LI, Y., WONG, T. W., TAM, W., CHAN, A. T., LEE, J. H. W., LEUNG, D. Y. C. & HO, T. 2004. Evidence of Airborne Transmission of the Severe Acute Respiratory Syndrome Virus. *The NEW ENGLAND JOURNAL of MEDICINE,* 350**,** 9.